IMFUFA tekst

- I, OM OG MED MATEMATIK OG FYSIK

Rolling Resistance Modelling

From Functional Data Analysis to Asset Management System

Lasse G. Andersen

PhD Dissertation

nr. 503 - 2015

Roskilde University,
Department of Science, Systems and Models, IMFUFA
P.O. Box 260, DK - 4000 Roskilde
Tel: 4674 2263 Fax: 4674 3020

Rolling Resistance Modelling: From Functional Data Analysis to Asset Management System

By: Lasse Grinderslev Andersen

IMFUFA tekst nr. 503/ 2015 - 196 pages - ISSN: 0106-6242

The present thesis applied Functional Data Analysis (FDA) to empirical rolling resistance modelling. More specifically, the rolling resistance modelling concerned the relation between road macrotexture and rolling resistance. The guiding objective of the modelling efforts has been its potential use in strategic pavement management of an entire road network.

A new texture measure for road macrotexture called Texture Penetration Depth (TPA) have been developed with the intent of assessing rolling resistance from 2D road profiles. Two versions have been presented - a simple and a full version. The latter have been founded on methods from FDA.

TPA is distinguished by being based on fundamental principles of what causes macrotexture induced rolling resistance as opposed to, e.g., MPD which is constructed as a purely empirical measure that correlates with the old 'sand patch' texture measurement method. The intuitive foundation of the TPA measure enables a rather straightforward generalisation for 3D profiles which can accommodate the future generation of road profiling equipment.

The capability of the TPA measure, compared to MPD, has been tested on two kinds of rolling resistance data: (1) Rolling resistance data measured directly by a specially designed rolling resistance trailer developed by the Technical University of Gdansk in Poland and (2) data of coast-down experiments performed by Swedish Statens väg- och transportforskningsinstitut (VTI).
In addition, both TPA and MPD have been used together with a profile enveloping algorithm as a recent study showed that it significantly improved correlations. The results of (1) showed that TPA correlates significantly better than MPD i most cases. Especially, the simple TPA performed better. However, the data set is rather slim so further similar studies are needed before any definite conclusions can be drawn. Furthermore, the results of profile enveloping substantiated earlier findings that enveloping increases correlations for MPD as well as TPA in this case. The results of (2) showed that MPD and simple TPA performed equally well, but further investigations showed that the coast-down model's fit to data did not depend significantly on changes in macrotexture parameters. The explanation for this, it is argued, is that the contribution from macrotexture on the overall driving resistance, is small.

Finally, the application of FDA in large part of the data analysis and the TPA development is discussedIt is concluded that the use of FDA in connection with coast-down modelling has been fruitful. Moreover, FDA is a potential analysis tool for, e.g., trailer rolling resistance measurements. However, the amount of data in this work have been too small for this to be thoroughly demonstrated. On the other hand, the application of FDA in connection with TPA have been unnecessary and the advanced TPA have probably been over-engineered.

PhD thesis

ROLLING RESISTANCE MODELLING

From Functional Data Analysis to Asset Management System

Author:
Lasse G. ANDERSEN

Supervisors:
Jeppe DYRE & Jesper LARSEN

IMFUFA, Department of Science, Systems, and Models
Roskilde University, Denmark

Abstract in English

The present thesis applied Functional Data Analysis (FDA) to empirical rolling resistance modelling. More specifically, the rolling resistance modelling concerned the relation between road macrotexture and rolling resistance. The guiding objective of the modelling efforts has been its potential use in strategic pavement management of an entire road network.

A new texture measure for road macrotexture called Texture Penetration Depth (TPA) have been developed with the intent of assessing rolling resistance from 2D road profiles. Two versions have been presented - a simple and a full version. The latter have been founded on methods from FDA. TPA is distinguished by being based on fundamental principles of what causes macrotexture induced rolling resistance as opposed to, e.g., MPD which is constructed as a purely empirical measure that correlates with the old "sand patch" texture measurement method. The intuitive foundation of the TPA measure enables a rather straightforward generalisation for 3D profiles which can accommodate the future generation of road profiling equipment.

The capability of the TPA measure, compared to MPD, has been tested on two kinds of rolling resistance data: (1) Rolling resistance data measured directly by a specially designed rolling resistance trailer developed by the Technical University of Gdansk in Poland and (2) data of coast-down experiments performed by Swedish Statens väg- och transportforskningsinstitut (VTI). In addition, both TPA and MPD have been used together with a profile enveloping algorithm as a recent study showed that it significantly improved correlations.

The results of (1) showed that TPA correlates significantly better than MPD i most cases. Especially, the simple TPA performed better. However, the data set is rather slim so further similar studies are needed before any definite conclusions can be drawn. Furthermore, the results of profile enveloping substantiated earlier findings that enveloping increases correlations for MPD as well as TPA in this case. The results of (2) showed that MPD and simple TPA performed equally well, but further investigations showed that the coast-down model's fit to data did not depend significantly on changes in macrotexture parameters. The explanation for this, it is argued, is that the contribution from macrotexture on the overall driving resistance, is small.

Finally, the application of FDA in large part of the data analysis and the TPA development is discussed. It is concluded that the use of FDA in connection with coast-down modelling has been fruitful. Moreover, FDA is a potential analysis tool for, e.g., trailer rolling resistance measurements. However, the amount of data in this work have been too small for this to be thoroughly demonstrated. On the other hand, the application of FDA in connection with TPA have been unnecessary and the advanced TPA have probably been over-engineered.

Abstract in Danish

I denne afhandling forsøges Funktional Data Analyse (FDA) anvendt indenfor empirisk rulldemodstandsmodellering. Mere specifikt omhandler modelleringen sammenhængen mellem belægningers makrotekstur og rullemodstand. Det overordnede og ledende mål for modelleringen er, at det potentielt skal kunne anvendes inden for strategisk vejvedligehold af et helt vejnet.

Der er udviklet et nyt teksturmål for makrotekstur, kaldet "Texture Penetration Area" (TPA), med henblik på at estimere rullemodstand ud fra 2D vejprofiler. To udgaver af TPA bliver præsenteret - en simpel og en avanceret udgave. Sidstnævnte er baseret på metoder fra FDA. TPA udmærker sig ved at bygge på grundlæggende principper for, hvad der forårsager makroteksturinduceret rullemodstand i modsætning til klassiske teksturmål, som f.eks. MPD, der er konstrueret som en ren empirisk mål, der korrelerer med den gamle "sand patch" målemetode for tekstur. TPA målets intuitive grundlag gør det også muligt at generalisere det til 3D-profiler, hvilket imødekommer næste generation af måleudstyr.

TPA målets duelighed i forhold til MPD er testet på to typer af rullemodstandsdata: (1) rullemodstandsdata målt direkte vha. en speciel rullemodstandstrailer udviklet af Technical University of Gdansk i Polen og (2) data fra coast-down eksperimenter foretaget af Statens väg- och transportforskningsinstitut (VTI) i Sverige. Derudover er både TPA og MPD anvendt sammen med "profile enveloping", da dette har vist sig at forøge korrelationen mellem MPD i et nyligt studie. Resulterne af (1) viste, at TPA korrelerer mærkbart bedre end MPD i de fleste tilfælde. Dette gjaldt specielt den simple udgave af TPA. Det skal dog bemærkes, at da datagrundlaget er spinkelt, bør der foretages flere lignende undersøgelser, før der kan drages endelige konklusioner. Derudover blev resultaterne vedrørende enveloping eftervist for både MPD og TPA. Resultaterne af (2) viste, at MPD og den simple TPA klarede sig lige godt. Nærmere undersøgelser viste dog også, at coast-down modellens fit til data ikke afhang signifikant af ændringer i parametrene for makroteksturen. Begrundelsen for dette formodes at være makroteksturens lille bidrag til den overordnede kørselsmodstand, som coast-down modellen er en model for.

Eftersom FDA har været benyttet i forbindelse med store dele af dataanalysen, samt udviklingen af TPA, diskuteres anvendeligheden af denne. Det konkluderes, at FDA med fordel kan anvendes i forbindelse med coast-down modelleringen, samt at FDA har potentiale som analyseværktøj af eksempelvis rullemodstandsmålinger med trailer. Sidstnævnte har dog været svært at eftervise, da datagrundlaget var for småt. Til gengæld har FDA vist sig at være unødvendigt og overkomplicerende i forbindelse med udviklingen af den (avancerede) TPA.

Acknowledgements

The work presented here are the main fruits of my work as a Ph.D. student in the COOEE project at Roskilde University and it would not have been possible without a broad spectrum of people.

First of all I would like to thank my main supervisor, Jeppe Dyre, for many valuable observations and recommendations. Furthermore, Jeppe has shared his insights into the inner workings of the scientific community which have been extremely valuable. Besides Jeppe, I would also like to thank Jesper Larsen for our frequent and fruitful meetings as well as providing many good suggestions for the work in general and the thesis in particular. Both have been very open-minded and supportive of my vivid ideas.

I would also like to thank Johnny T. Ottesen for introducing me to the interesting topic of Functional Data Analysis several years ago.

Being a Ph.D. student at our department (IMFUFA) have been a pleasure. The general warm, welcoming, and social atmosphere among Ph.D. students and staff have been a vital source of motivation for which I am very grateful. In particular I would like to mention Kenneth, Johanne, Arno, Luna, Heine, Trond, Claire, Lorenzo, Jon, Trine, Elsje, Lasse, Sif, Ebbe, Jens and many more. Also a special thanks to my office mate Wence Xiao for good company in good as well as stressful times.

Besides IMFUFA I have had the opportunity to stay at the Danish Road Directorate and welcoming and kind attitude by all members of the department. Their enormous experience and knowledge about road engineering, road measurement and road maintenance have been crucial for this work. I can surely say that without them this thesis would not have been possible. Especially Niels Djuardin have been very patient with me and all my questions, but I would also like to mention Erik Nielsen and Jens Oddershede for good advice. Last but definitely not least, I would express my deep gratitude to Bjarne Schmidt at the Danish Road Directorate for his help in many aspects. His care and support for 'the new generation' have been unchallenged and I will aspire to this attitude myself when I one day become the experienced senior.

A special thanks goes to Thomas Steen Rasmussen for teaching me how to use FreeBSD, as well as several other wonderful IT- technologies and concepts that have served me well during these years. Much of the work I have done in asset management would not have been possible without his help.

Finally, I would like to thank my supportive family and especially my wife Mette. She has been, and continues to be, my life's Archimedean point when everything else falls apart. Without her affectionate support, patience, and care when things get rough, finishing this thesis would be the least of my concerns.

Lasse Grinderslev Andersen
April, 2015

List of commonly used notation and abbreviations

FDA	Functional Data Analysis
D^n	nth differential operator
y_i, t_i, s_i	Discrete data point measured at time t_i or distance s_i
$y(t), y(s)$	Functional data depending on time and distance, respectively
WLS	Weighted Least Squares
OLS	Ordinary Least Squares
PCA	Principal Component Analysis
fdPCA	Functional Principal Component Analysis
C_{RR}/C_R	Rolling resistance coefficient defined as $C_{RR} = F_{RR}/F_z$
K	Number of measurements between knots in the TPA measure
λ	Smoothing parameter in roughness penalized data functionalisation
e	Enveloping parameter representing tyre stiffness
d	Texture penetration depth
TPA	Texture Penetration Area
TPV	Texture Penetration Volume
MTD	Mean Texture Depth
MPD	Mean Profile Depth
IRI	International Roughness Index
RMS	Root Mean Square
Skew	Skewness
L_λ	Root Mean Square of third-octave band centred about λ

Contents

1 Introduction

This thesis is part of the research project "CO_2 emission reduction by exploitation of rolling resistance modelling of pavements" (COOEE) funded by The Danish Strategic Research Council. At the same time, the thesis is part of a Ph.D. school programme "Mathematical Modelling and its Mathematical Prerequisites" at Roskilde University. These two prerequisites, while having a lot of common ground, are also quite different in aim and goal. Roughly speaking, the COOEE project represents the engineering side and the Ph.D. school is the mathematical side of the thesis. How these distinct goals interplay and have formed the work contained in this thesis is the main topic of this chapter.

1.1 Thesis Aim & Scope

The primary and overall goal of the COOEE project is to model the relation between rolling resistance and pavement characteristics, most notably the pavement surface, which in turn makes it possible to derive the energy use and thus fuel consumption contribution of a given pavement. This enable National Road Administrators (NRAs) together with pavement entrepreneurs to optimize pavement construction with respect to rolling resistance and thus save CO_2 emissions by saving fuel. Other related objectives include molecular level investigations of bitumen and novel pavement development. Given the title of this thesis, it should be clear that its object of study lies at the core of the first and primary goal of the COOEE project, but to get a clearer idea of this we need to look at the general outline of the COOEE project. The present research is situated in Work Package (WP) 2 of the following WPs[1]:

WP1 Novel pavements: Development of pavements with low rolling resistance that simultaneously preserves durability

WP2 Models of rolling resistance: Modelling the relation between pavement, rolling resistance, and fuel consumption

WP3 Wear and ageing of pavement: Studying the process of chemical ageing to identify critical factors that can be targeted in trying to mitigate the ageing process.

WP4 Measurement of rolling resistance: Provide rolling resistance and pavement characteristics measurements for use in WP2.

WP5 Asset Management Systems: Incorporating the knowledge obtained in the COOEE project to build system components which enable NRAs to use this knowledge in actual road maintenance.

As this list indicates, there is a serialisation: WP4 $\rightarrow$ WP2 $\rightarrow$ WP5 where measurements of WP4 have been used in this work (WP2) and the results from rolling resistance modelling and investigations presented here will be the primary input for WP5. WP1 and WP3 are more

[1] See http://www.cooee-co2.dk/ for further description of the WPs and the project in general.

concerned with pavement development and thus not of much concern here[2]. What is important to note here, is that this work should be applicable to the asset management development in WP5 and this certainly restricts the possible methods and object of study in this thesis. For instance, a major requirement in the rolling resistance modelling efforts is that model input should be based on *production grade* data sources, i.e., the rolling resistance models should be usable with data routinely measured as part of ordinary road maintenance procedures. These sources are not as detailed as one could wish, but that is what we have at our disposal. Of course, it is possible to use more detailed measurements in the model development, as is indeed the case with the data presented in chapter 5 and 6, but the overall complexity and theoretical detail of the models are restricted by this. Moreover, it has forced the modelling approach to be mostly empirical in nature. Although this is on par with much of the existing literature on the subject, it excludes more theoretical approaches such as those employed in Finite Element Modelling (FEM) and the like. While some of these theoretical approaches are promising[66, 6, 7, 102] they are still remote from the practical reality of NRAs.

As mentioned above, this Ph.D. is also part of a Ph.D.-programme in applied mathematics that deals with mathematical modelling and its mathematical prerequisites. In this thesis it will come into play through the novel techniques of Functional Data Analysis (FDA) and parameter optimization. Especially FDA will be a topic in its own right, and a thorough introduction to the subject will be given in chapter 2 that also discusses the mathematical foundation of FDA, as as well as its connection to classical procedures that have a special formulation in FDA. These questions are not *directly* related to the COOEE project but are of pure (applied) mathematical interest that falls within the Ph.D. programme. Where rolling resistance modelling in the COOEE project and research topics in applied mathematics meet, is the application of FDA in the rolling resistance modelling efforts. Since FDA is quite new, its use in modelling efforts and data analysis are limited and non-existent in the rolling resistance modelling literature. This makes the application of FDA to rolling resistance modelling an interesting undertaking from the perspective of applied mathematics as well as road engineering.

Finally, since the rolling resistance modelling work here is so closely related to the work in WP5 about asset management, some overlaps have occurred. More specifically, a big part of the asset management development in WP5 has been undertaken by the author and the experiences gathered while working with data and models in relation to rolling resistance modelling in WP2 have inspired the asset management developments in WP5. Indeed, the work on rolling resistance modelling has raised some practical questions that can only be answered and dealt with in the context of asset management. Even though the work on asset management is quite remote from the purely mathematical goals, it fits perfectly as a natural extension to the rolling resistance and surface modelling part of the thesis. Therefore, some results and reflections related to asset management are also presented here, although to a far lesser extent than FDA and rolling resistance modelling. As noted above, the end goal of the modelling efforts has been the potential ability to use the work in asset management, and this has steered the modelling efforts away from more theoretical modelling approaches.

All in all, this gives three different topics that overlaps in this work: 1) FDA 2) rolling resistance and surface modelling, and 3) asset management. Each have their own set of questions inherent to the topic itself and irrelevant to the other topics, but in each topic there are also questions having common ground to the other topics of thesis, as illustrated in figure 1.1.

[2] Some of the results about aging in WP3 that may yield important information about pavement lifetime to use in the asset management system development (WP5).

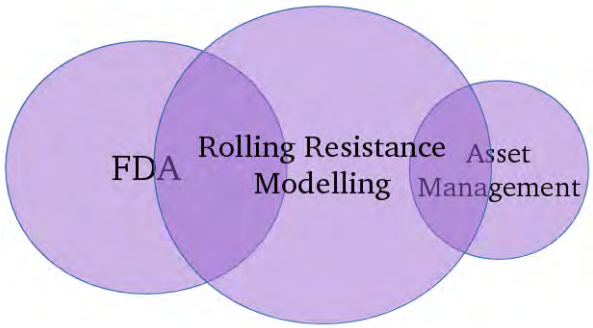

Figure 1.1 Illustration of subjects, their overlap, and relative scope in this thesis.

1.2 Thesis structure & reading guide

Because of the three different topics the thesis can be divided into three different parts that are almost self-contained. While the parts are almost self-contained there is an interdependence that gives a natural order of presentation: Rolling resistance modelling makes use of the vocabulary and theory from FDA so the chapters about rolling resistance modelling presupposes FDA. In turn, the asset management part presupposes the results, theory and vocabulary of rolling resistance modelling, so it is treated lastly. Thus, the order is FDA first, rolling resistance modelling second, and asset management last. Moreover, the interdisciplinary nature of this thesis makes the target audience more heterogeneous, i.e., the thesis should in principle be accessible to both researchers in applied mathematics and road engineering. This fact has been kept in mind while writing this thesis and therefore some of the discussions and expositions have been elaborated more than would be necessary had the work been targeting a narrow group of researchers. Therefore some passages might be too detailed for a mathematician while better fit for an road engineer and vice versa.

1.3 Reflections on the presented work

Writing an interdisciplinary thesis like this has been quite a challenge but also extremely rewarding. The collaboration with people from entirely different fields of interest and the necessary context switching it entails has been very instructive. A problem and its possible solutions can look quite different if viewed by an engineer working in road maintenance or a mathematician doing applied mathematics, and getting these different perspectives to meet is quite a challenge. Nevertheless, the author has a background in mathematics and the overall take on the subject of rolling resistance modelling has intentionally been from the point of view of a mathematician, not an engineer or physicist. This is probably reflected in some of the approaches as well as lingual subtleties, but hopefully it has provided interesting and refreshing views on the subject of rolling resistance modelling even though the author is not an experienced road engineer.

2 Functional Data Analysis

In this chapter we introduce Functional Data Analysis (FDA) and its mathematical foundations with an emphasis on topics needed for the investigations put forward in chapter 5 and 6. Therefore this chapter serves two purposes: 1) Introduction of FDA and the mindset underlying it, which is closely connected to its mathematical foundation. 2) Introduction of the mathematical tools that are going to be used in this thesis as well as other tools which could potentially be used in surface and rolling resistance modelling. In particular, some concepts from signal processing are presented in section 2.6. While this is not conceived as being core FDA knowledge, the mathematical foundation is quite similar so it is presented in connection with FDA and put into the overall functional paradigm. To quote the authors of the 'FDA-bible':

> ..it is not our intention to provide a cook-book for functional data analysis. In broad terms, we have a grander aim: to encourage readers to think about and understand functional data in a new way.[143, p. 18]

This chapter is written in the same spirit, and it is intended to be an integral part of the subsequent chapters.

2.1 Notation

Before we begin, lets state some notational conventions. In the following, bold capital letters such as $\boldsymbol{X}, \boldsymbol{Y}, \boldsymbol{\Phi}$ refer to matrices whereas normal bold letters $\boldsymbol{x}, \boldsymbol{y}, \boldsymbol{t}, \boldsymbol{\beta}$ refer to vectors. Using a ‘ behind vectors or matrices implies transposition. A sequence of discrete data $y_1, y_2, \ldots, y_n$ is related to an independent variable, which is usually time t or distance s, such that the y_i-values are said to be sampled at times $t_1, t_2, \ldots, t_n$ (or distances $s_1, s_2, \ldots, s_n$). This dependence is usually abbreviated with square brackets like $\boldsymbol{y}[\boldsymbol{t}]$. When discrete data are converted into functions, the standard function notation $y(t)$ is used, possibly with a tilde on top $\tilde{y}(t)$ to stipulate the fact that this is a function estimated from data. If we refer to a specific value, we use the notation $\tilde{y}(t_0)$ and if multiple values are referred to, we use $\tilde{y}(\boldsymbol{t})$. In many instances the reference to the independent variable, as well as whether it is discrete or functional, is implicit so we drop $\boldsymbol{t}, \boldsymbol{s}$ (or t, s) from the notation and use a plain $\boldsymbol{y}$ or $y_1, y_2, \ldots, y_n$ etc. For derivatives like

$$\frac{dy(t)}{dt} \quad , \quad \frac{dy^2(t)}{dt^2} \quad , \quad \frac{dy^n(t)}{dt^n}$$

we will use the simpler notation $Dy(t)$, $D^2y(t)$, and $D^ny(t)$. In addition, when using definite integrals the interval will usually be dropped since it will be given implicitly. Lastly, if a function is $\mathcal{C}^n$ it means that its nth derivative exist and is continuous.

2.2 Introduction

The main idea in functional data analysis is to perceive discrete data as observations of a *function* and to see the function as the primary object of study. A more mathematical formulation would be to say that traditionally, we generally view our data to be a finite subset of $\mathbb{R}^n$. For instance, each tuple (t_i, y_i) of a time series data set $[(t_1, y_1), \ldots, (t_n, y_n)] = y[\boldsymbol{t}]$ is an element of $\mathbb{R} \times \mathbb{R}$ (or more precisely, $(t_i, y_i) \in [t_1, t_n] \times \mathbb{R}$). In FDA we think instead of our data as belonging to a function space, and in this example it could be the Hilbert space of square integrable functions defined on the interval $[t_1, t_n]$, which we will denote $L^2[t_1, t_n]$. This implies that our data, essentially, are infinite dimensional and the finite set of measurements $y[\boldsymbol{t}]$ are merely samples from an uncountable amount of data points, i.e., for each $t \in [t_1, t_n]$ a corresponding value $y(t)$ exists. Thus, the discrete data set is viewed as *functional* data meaning that the data is inherently a function, hence the name of the subject. In addition, we often expect the underlying process, from which the data set has originated, to behave nicely, i.e., there are no abrupt changes in quantity (or rate of change of that quantity etc.). In other words, some degree of *smoothness* is assumed to hold for our functional data. With smoothness we refer to the degree of differentiability and what class $\mathcal{C}^n$ of functions that a given functional data belongs to, and smoothness becomes a property of the data which is used repeatedly in analysis and method. Incorporating derivatives in the data analysis is basically a study of the dynamics of the data[143, p.39]. As it turns out, the FDA approach is powerful in parameter estimation of differential equations[141].

Of course, the discrete data set is usually also assumed to be distorted by noise and therefore we do not expect the underlying function $y(t)$ to pass through all our observations $y[\boldsymbol{t}]$ of it. More generally, one should consider what features of the data set should be captured by an estimated function.

2.3 From Functional Data to Functions

The first step in FDA is to convert a set of data points $y[\boldsymbol{t}]$ into a function $\tilde{y}(t)$ such that all relevant features of the data set are captured by the function. We will call this process *funtionalization*. Since we only have a finite amount of data points, an upper bound to features that we are able to capture exists, i.e., we do not have any knowledge of events occurring between the points. As such, this is an inverse problem: Given a discrete set of (possibly noisy) occurrences, find the underlying function that gave rise to them. In principle, there is a continuum of possibilities since there is a continuum of functions that could be suspected of being the underlying phenomena behind the observations. This might a bit overwhelming, however, in practice we might expect some general/abstract properties to hold for the phenomena giving rise to the data, such as smoothness, periodicity, monotonicity, etc., which in turn affect and restrict the functionalisation process, thus the estimated function's behaviour between data points. Furthermore, we are only interested in a certain amount of accuracy. All in all, while functionalisation introduces an additional step in data processing and some additional considerations have to be dealt with in that account, it also introduces a lot of new possibilities and a few of these are introduced here. Note that although we might know of properties that holds of the observed phenomena and which we can be used in the functionalisation process, the point is to be descriptive: The intention is to capture significant features in the data that seems to be caused from the underlying phenomena and not the features that can be readily explained or captured by a theoretical model.

Another important aspect is the functionalisation *performance*, i.e. we should be able to

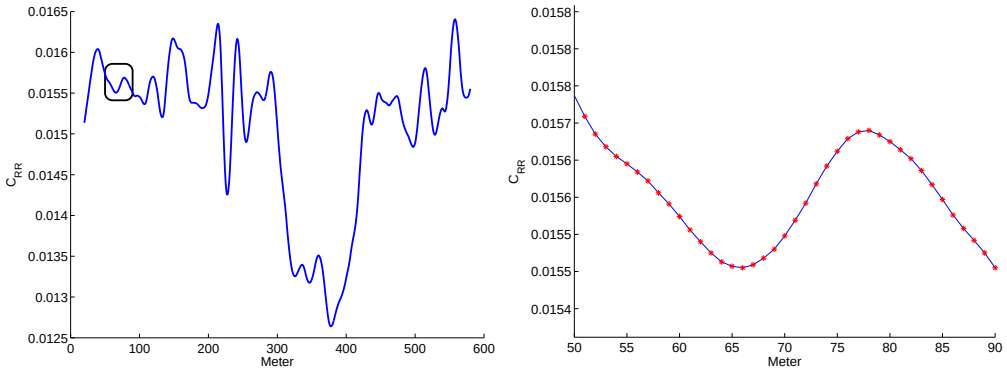

Figure 2.1 Example of rolling resistance measurements made by the TUG rolling resistance trailer at Værløse airbase treated in chapter 5. This shows the high resolution and act as an example of a data type where the resolution is much higher than the features present in the data. This i probably due to some filtering unkown to the author. For a discussion see chapter 5. Left: A single measurement run of one of the road sections. The rectangle indicates the part of the figure shown to the right. Right: A zoom-in of the figure to the left. The blue line is linear interpolation and the red markings are the actual measurement points.

convert the data set, extracting derivatives etc. relatively fast.

Having good performance while using a generic function that can capture a diverse set of features to a high precision, is accomplished by composing the data function $y(t)$ as a sum of simple functions $\phi_1(t), \phi_2(t), \ldots, \phi_n(t)$[143, p.43]. These simple functions are linearly independent, hence they are *basis* functions (more generally, vectors) and $y(t)$ is a linear combination of basis functions

$$y(t) = \sum_{k=1}^{n} c_k \phi(t) \tag{2.1}$$

where the c_k's are coefficients estimated from the data set. The amount of features present in the data that should be captured by $y(t)$ determines, informally, its dimension which then is related to the number of basis functions (and thus coefficients). The upper bound of features mentioned above is also reflected by a maximum number of basis functions that is sufficient for a satisfactory fit that captures all features in the data. What this maximum is exactly depends on what kind of basis functions that are being used. In many cases it is not necessary to use the maximum number of basis functions because small local features are noise and should not be present in an estimated function or the resolution of the data set is higher than the process it represents. These cases are illustrated in figure 2.2 and 2.1, respectively, using measurements used in later chapters.

The first step in data functionalisation is deciding which type of basis functions to use. Many different types exists, but only two will be treated here, namely B-spline and Fourier basis functions. Many more are covered elsewhere, for instance in [143][1]. These two basis function types are well known, and especially the latter is implicitly used in road engineering, where a common approach to the study of road surfaces is to represent road profiles in the frequency

[1] A lot of other examples can be found in functional analysis text books such as [178] although the material is approached in a much more mathematical way.

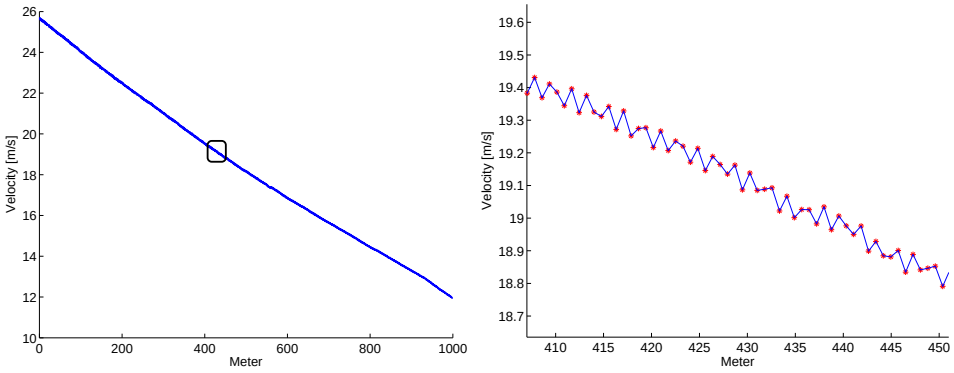

Figure 2.2 Example of coast-down measurements made by Swedish VTI in Sweden. The data set is treated in chapter 6. This show an even higher resolution than figure 2.1 and act as an example of data with both highly local features (measurement noise) and a global qualitative behaviour. These two phenomena are taking place at markedly different length-scales. Left: A single measurement run of one of the road sections. The rectangle indicates the part of the figure shown to the right. Right: A zoom-in of the figure to the left. The blue line is linear interpolation and the red markings are the actual measurement points.

domain. Using FDA terminology "represent road profiles in the frequency domain" translates to "representing the road profile *function* in the Fourier basis".

The concept of splines as a means for approximating functions traces back to Karl Weierstrass, who proved that any continuous real function defined on a real interval could be approximated to an arbitrary degree of precision by a polynomial. Since every polynomial can be expressed as linear combination of functions from $\{1, x, x^2, \dots, x^n, \dots\}$ it follows that this set forms a basis for the function space $C([a, b])$ of continuous functions defined on $[a, b]$. Indeed, this basis could also be used to represent our functional data, however, better polynomial-based solutions exists: Splines.

Splines are polynomials pieced together at specified points called *knots*, as illustrated in figure 2.3. B-splines are a special case of splines where any spline of order m can be expressed as linear combination of m-order B-splines[32, chapter IX]. In addition, B-splines have compact support and fast algorithms exists for evaluating basis functions, such as, e.g., de Boors algorithm[32, chapter X].

The B-spline system is defined in terms of a weakly increasing *knot sequence* $\tau = \{\tau_0, ..., \tau_k\}$, specifying where the basis function polynomials are glued together and the *order* m that refers to the number of parameters needed to define the polynomials or, equivalently, the degree of the polynomial. It is only required for the knot sequence to be weakly increasing, which can be utilised when discontinuities are required, since placing coincident knots at a point t_0 decrease the smoothness of the overall spline at t_0[2]. In the following it is assumed to be strictly increasing.

In general, an order m system with knot sequence τ containing $k + 1$ knots results in $m + k - 1$ basis functions $\phi_i(t)$. Thus, assuming we have a set of discrete data defined on

[2] A real world example where they need a discontinuous first derivative and thus used a knot sequence containing coincident knots is given in [138].

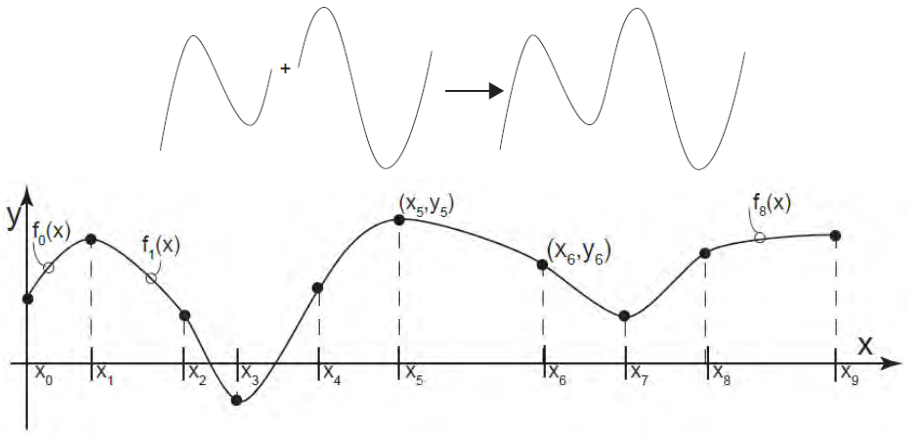

Figure 2.3 Splines are polynomials glued together in a smooth manner (top). For B-splines the degree of smoothness (i.e., differentiability) at these points, called knots, depend on the order of the polynomials used. The sequence of these points together with the order of the polynomials uniquely defines the spline.

$[t_1, t_n]$, our functional data $\tilde{y}(t) : [t_0, t_n] \to \mathbb{R}$ can then be viewed as

$$\tilde{y}(t) = \sum_{i=0}^{m+k-2} c_i \phi_i(t) = \boldsymbol{c'\phi}(t) \tag{2.2}$$

where the $\phi_i(t)$'s are $(m-1)$'th degree polynomials constructed by the following recurrence relation[32, p. 89-90]

$$\phi_j^1(t) = \begin{cases} 1, \text{ if } \tau_j < t < \tau_{j+1} \\ 0, \text{ otherwise} \end{cases} \tag{2.3}$$

for $m = 1$ and with $m > 1$ the polynomials are constructed as

$$\phi_j^m(t) = \omega_j^m(t)\phi_j^{m-1}(t) + [1 - \omega_{j+1}^m(t)]\phi_{j+1}^{m-1}(t) \tag{2.4}$$

with

$$\omega_j^m(t) = \frac{t - \tau_j}{\tau_{j+m+1} - \tau_j} \tag{2.5}$$

The resulting function $\tilde{y}(t)$ is $\mathcal{C}^{m-1}$ and, as mentioned above, the latter does not necessarily hold if τ is weakly increasing. In addition, the compactness is not formulated in equation 2.2 but can be described briefly as follows. Mostly, each $\phi_i(t)$ is only non-zero in the interval $[\tau_i, \tau_{i+m+1}]$, however, the last $m-1$ basis functions in either end covers less. More precisely, as the end-points are reached the basis functions decreases in range such that the last basis functions in either end only spans an interval spanned by two consecutive knots. This implies that all k intervals partitioned by $\boldsymbol{\tau}$ have m basis functions that are non-zero which also gives a total of $k + m - 1$ basis functions[3].

[3] This is actually more complicated as there are coincident knots in either end, however, it is not of practical importance here. For further details about the behavoir at the endpoints, see [143].

A crucial point when fitting a B-spline system to a discrete set of observations is defining a knot-sequence which reflects the process properly[143, p. 68]. A badly chosen knot-sequence could result in poor spline fits, which in turn reduce the quality of the subsequent model estimation[138], statistical analyses etc. However, when the number of observation points is low (whatever that may be) an obvious candidate for a knot-sequence is placing a knot at each data point. With large sets of measurement data this could be problematic since a large number of knots results in a large number of coefficients c_i, thus potentially increasing the computation time heavily when working with functional data. However, B-splines have compact support since each mth order B-spline $\phi_i(t)$ is non-zero only in the interval $[\tau_i, \tau_{i+m+1}]$. This makes it very efficient to compute a function value $\tilde{y}(t_0)$ since the amount of basis functions that requires evaluation only depends on the *order* of the $\phi_i(t)$'s and not the number of basis functions used on the entire data set. It also implies that many of the matrices used below will be sparse if B-splines are used as basis functions, e.g., the matrix of inner products $\langle f_i, f_j \rangle$ between B-splines basis functions will be a sparse matrix where the main diagonal and $m-1$ sub diagonals above/below the main diagonal are the only non-zero entries. An example of a matrix of inner products is shown in equation 2.21 with $f_i = D^2\phi_i$. In general, B-splines are a very flexible, robust and fast type of basis functions that is by far the most common basis function type available and will be directly used in the following chapters. For a detailed account on B-splines, see [32].

Another widely used type of basis functions is the Fourier basis which is well-known in a many areas such as signal processing, partial differential equation modelling etc. While we do not use this kind of basis functions directly, they are used implicitly in some of the investigations in later chapters that involves the frequency domain. Furthermore, the principles of Fourier analysis are also frequently used when investigating road surfaces influence on rolling resistance, skid resistance, and noise, so a brief introduction to Fourier series is given below.

Instead of polynomials as basis functions, trigonometric functions are used in Fourier analysis and instead of defining a basis in terms of order and knot sequence, a Fourier basis is defined by a range of frequencies. Fourier basis functions can be represented in many ways, and different representations are suited for different use cases. Given $L = t_n - t_0$ and a maximum frequency m, the data function $\tilde{y}(t) : [t_0, t_n] \to \mathbb{R}$ can be expressed in the following ways:

$$\tilde{y}(t) = = A_0/2 + \sum_{n=1}^{m} A_n \sin\Big(\frac{2n\pi t}{L} + f\Big) \tag{2.6}$$

$$= \sum_{n=-m}^{m} C_i e^{i\frac{2n\pi t}{L}} \tag{2.7}$$

$$= a_0/2 + \sum_{n=1}^{m} \left(a_n \sin\Big(\frac{2n\pi t}{L}\Big) + b_n \cos\Big(\frac{2n\pi t}{L}\Big)\right) \tag{2.8}$$

where

$$C_i = \begin{cases} \frac{A_n}{2} e^{i\phi_n} = \frac{1}{2}(a_n - ib_n) & \text{for } n > 0 \\ \frac{1}{2}A_0 & \text{for } n = 0 \\ c^*_{|n|} & \text{for } n < 0. \end{cases}$$

$$a_i = A_i \sin(f)$$

$$b_i = A_i \cos(f).$$

equation 2.6 emphasise the fact that each basis function represents a particular frequency, equation 2.7 is the representation used by the `FFT` algorithm and equation 2.8 is the presentation used in the FDA literature[143].

Just as polynomials constitutes a basis for the space $C[a, b]$ above so does the set of Fourier basis functions $\{e^{n2\pi it} | n \in \mathbb{Z}\}$ form an *orthogonal* basis of, e.g., the Hilbert space $L^2[0, 2\pi]$[4]. The orthogonality means low computation time since, e.g., the matrix of inner products of Fourier basis function pairs will be a diagonal matrix (inner product matrix shown in equation 2.21). A standard method in Fourier analysis is to study the spectrum of a data set (e.g., a road profile), which in FDA lingo becomes a study of the coefficients used in the linear combination of Fourier basis functions that represents the functional data. This is of course just hypothetical but illustrates the different mathematical perspectives. The work presented here is not using Fourier series as a basis function system since our data are not inherently periodic, which is one of the common reasons for using a Fourier basis[143, p.46]. However, Fourier series will be put to use in chapter 5 where they are used in the road surface analysis. Moreover, as Fourier analysis is used in the road engineering literature and in connection with road profile measurements, some of the challenges connected with this are treated later, in section 2.6, since this is not directly related to FDA.

Both Fourier and B-spline bases can be viewed as an infinite set of linearly independent functions in Hilbert spaces. While this serves as a theoretical foundation it is not very useful with our finite computers, so we pick a finite subset of basis functions which then spans a finite dimensional (function) subspace. Thus, the selected subspace depends on the types of basis functions used and the defining parameters pertaining to it. For B-splines it is the order and knot sequence that uniquely determines a subspace and for the Fourier basis it is the frequencies used. This gives us great flexibility in how we will represent our data and it stipulates that discrete observations are the result of an underlying phenomenon. After a proper subspace has been found, the next step is to find a proper representation of the data, i.e., finding a proper linear combination of basis functions. This amounts to finding the c_i's that results in the best fit.

Finally, it should be noted that several other bases exist to represent functional data, however, they will not be used in this work. Of potential interest in transportation engineering is the wavelet basis function system, which is a hybrid between the frequency approach of Fourier series and the spatial approach of splines[143, p.53].

2.4 Fitting Basis Functions

Once we have found a proper subspace to represent our data function, a proper fit to the data needs to be estimated. What makes up a 'proper fit' is not an easy question, and many answers exist. However, a specific answer that fits well within the paradigm of FDA is given here.

The classical way to estimate a parameter vector is by minimizing the sum of squared errors between model and data. In our case the model is a linear combination $\sum_{i=1}^{n} c_i\phi_i(t) = \boldsymbol{c'\phi}(t)$ of basis functions and both bases presented above can be put into this form. Thus, the objective function to be minimized is given by

$$L_{\text{OLS}}(\boldsymbol{c}) = \sum_{j}^{m}\big(y_j - \sum_{i=1}^{n}\phi_i(t_j)c_i\big)^2 = (\boldsymbol{y} - \boldsymbol{\Phi c})'(\boldsymbol{y} - \boldsymbol{\Phi c}). \tag{2.9}$$

[4] $L^2[0, 2\pi]$ is the space of all square-integrable functions defined on $[0, 2\pi]$ with inner product given by $\langle f(x), g(x)\rangle = \int f(x)g(x)dx$.

where

$$\boldsymbol{\Phi c} = \begin{pmatrix} \boldsymbol{\phi}(t_1) \\ \boldsymbol{\phi}(t_2) \\ \vdots \\ \boldsymbol{\phi}(t_m) \end{pmatrix} \begin{pmatrix} c_1 \\ c_2 \\ \vdots \\ c_n \end{pmatrix} = \begin{pmatrix} \phi_1(t_1) & \phi_2(t_1) & \dots & \phi_n(t_1) \\ \phi_1(t_2) & \phi_2(t_2) & \dots & \phi_n(t_2) \\ \vdots & \vdots & \ddots & \vdots \\ \phi_1(t_m) & \phi_2(t_m) & \dots & \phi_n(t_m) \end{pmatrix} \begin{pmatrix} c_1 \\ c_2 \\ \vdots \\ c_n \end{pmatrix}.$$

The resulting function estimate $\tilde{y}(t)$ is then

$$\tilde{y}(t) = \hat{\boldsymbol{c}}\boldsymbol{\phi}(t) \ , \ \hat{\boldsymbol{c}} = \min_{\boldsymbol{c}}[L_{\mathrm{OLS}}(\boldsymbol{c})]$$

This is standard linear regression and if we choose our subspace to be spanned by the first two monomials $\phi_1(t) = 1$, $\phi_2(t) = t$ we have simple linear regression with a straight line $y = ax + b$ as the model. $\hat{\boldsymbol{c}}$ can be found in a standard way by solving the linear system which is obtained by setting the derivative of $L_{\mathrm{OLS}}(\boldsymbol{c})$ equal to zero, i.e., solving

$$2\boldsymbol{\Phi}\boldsymbol{\Phi}'\boldsymbol{c} - 2\boldsymbol{\Phi}'\boldsymbol{y} = 0 \tag{2.10}$$

which, for the sake of completion, gives

$$\hat{\boldsymbol{c}} = (\boldsymbol{\Phi}\boldsymbol{\Phi}')^{-1}\boldsymbol{\Phi}'\boldsymbol{y}. \tag{2.11}$$

The usual statistical error model is $y_j = \tilde{y}(t_j) + \epsilon_j$ where the ϵ_j's are independent, normally distributed, homoscedastic, and with zero mean and variance σ^2. Furthermore, as the statistical model indicates, the independent variable is assumed to be practically error free. Many generalisations of this model exist, e.g., by relaxing homoscedasticity we get weighted least squares instead:

$$L_{\mathrm{WLS}}(\boldsymbol{c}) = \sum_{j}^{m} w_j \big(y_j - \sum_{i=1}^{n} \phi_i(t_j)c_i\big)^2 = (\boldsymbol{y} - \boldsymbol{\Phi c})'\boldsymbol{W}(\boldsymbol{y} - \boldsymbol{\Phi c}) \tag{2.12}$$

where $\boldsymbol{W}$ is the inverse of the covariance matrix, i.e. $w_j = 1/\sigma_j^2$. It follows from the independence that $\boldsymbol{W}$ is a diagonal matrix with the weights in the diagonal[5]. equation 2.12 coincides with equation 2.9 if $\boldsymbol{W} = \boldsymbol{I}$. Similarly to equation 2.11, $\hat{\boldsymbol{c}}$ can be expressed as

$$\hat{\boldsymbol{c}} = (\boldsymbol{\Phi}'\boldsymbol{W}\boldsymbol{\Phi})^{-1}\boldsymbol{\Phi}'\boldsymbol{W}\boldsymbol{y}. \tag{2.13}$$

Two different remarks about using this approach in FDA and the modelling efforts put forward here: 1) These classical methods rely on certain statistical assumptions which may or may not hold for a given data set. In the following chapters it is either hard to ascertain the statistical properties or an intuitive approach will suffice. An example is illustrated in figure 2.2 where the noisy fluctuations are clearly visible in the velocity measurements and visual inspection should be enough to determine noise and amount of smoothing from measurements without going into detailed statistical analyses. A quite different example is the high-frequency laser profiles investigated in both chapter 5 and 6 that have some potential sources of measurement errors. Although

[5] We can also relax the independence condition, in which case we have Generalized Least Squares(GLS) where the off-diagonal entries of $\boldsymbol{W}$ can be non-zero.

product information of common laser equipment indicates very low measurement errors[6], it is not a guarantee against measurement errors in actual road measurements. Furthermore, testing and calibration are made routinely by profiler operators, but it is usually performed on homogeneous surfaces with idealised profiles and are thus very far from production measurements. See section 3.3.3 for a discussion of these issues. However, given a large amount of road profile data it is assumed that the essential surface behaviour is approximated and calculations based on it should be relatively stable with respect to errors.

2) The w_j's in equation 2.12 can also be viewed as smoothing parameters since each w_j determines how important the residuals $(\tilde{y}(t_j) - y_j)^2$ are in the overall estimate. E.g., relatively low values of a set of consecutive w_j's implies that local features causing high residual values in that part of the data are suppressed by the low weights. In general, OLS/WLS methods are specific *linear smoothers* that (linearly) maps a set of observations $\boldsymbol{y}$ into a smoothed image $\boldsymbol{Sy}$. In case of OLS $\boldsymbol{S}$ can be derived from equation 2.11 by noting that $\tilde{\boldsymbol{y}} = \boldsymbol{\Phi}\tilde{\boldsymbol{c}}$, thus substitution gives

$$
\begin{aligned}
&\tilde{\boldsymbol{y}} = \boldsymbol{\Phi}\hat{\boldsymbol{c}} \;\Leftrightarrow \\
&\tilde{\boldsymbol{y}} = \boldsymbol{\Phi}(\boldsymbol{\Phi}'\boldsymbol{\Phi})^{-1}\boldsymbol{\Phi}'\boldsymbol{y} = \boldsymbol{S}\boldsymbol{y} \;\Leftrightarrow \\
&\boldsymbol{S} = \boldsymbol{\Phi}(\boldsymbol{\Phi}'\boldsymbol{\Phi})^{-1}\boldsymbol{\Phi}'.
\end{aligned}
$$

In the case of WLS $\boldsymbol{S}$ is similarly given by $\boldsymbol{\Phi}(\boldsymbol{\Phi}'\boldsymbol{W}\boldsymbol{\Phi})^{-1}\boldsymbol{\Phi}'\boldsymbol{W}$. If n is close to m, a perfect/near perfect fit to the data will result if OLS/WLS is applied, and additional smoothing must be made. Many other linear smoothers exists such as kernel smoothers which, can also be used together with basis function schemes[143, 76].

If statistical details are not a major concern or hard to obtain, WLS and kernel smoothers can be replaced by another class of linear smoothers where the smoothing is based on the data function itself, as opposed to OLS/WLS. Furthermore, it is a natural extension to the function defined in equation 2.12, and it relies on the observation that a function with many local features will exhibit higher absolute values of its derivatives compared to a function that does not have these features. A concrete example is the velocity data in figure 2.2 where many local (unwanted) features increases the absolute value of its derivatives. A function f that only captures the slow decrease will exhibit smaller absolute values of its derivatives compared to a function g that also captures the small fluctuations. Using vector space terminology, we say that the magnitude (or norm) of the derivatives of f are smaller than g's. In the Hilbert spaces mentioned above, and thus subspaces thereof, the norm of a function $h : [a, b] \to \mathbb{R}$ is given by $\int_a^b [f(x)]^2 dx$. An obvious candidate for this measure is the second derivative since it is used as a measure of *curvature* in differential geometry and it fits well with intuition[139, p. 24]. For instance, a straight line has curvature zero and the curvature of a circle is given by $1/\text{radius}$ so the curvature decreases as the size of the circle increases. Combining this with the classical approach in

[6] E.g., *worst* case vertical resolutions between 0.25 and 0.0015 mm for Selcom SLS5000 lasers, depending on exact model number.

equation 2.12 above, we get

$$\begin{aligned} L_{\text{PEN}}(\boldsymbol{c}) &= \sum_{j}^{m} w_j \big(y_j - \tilde{y}(t_j)\big)^2 + \lambda \int [D^2 y(t)]^2 dt \\ &= \sum_{j}^{m} w_j \big(y_j - \sum_{i=1}^{n} \phi_i(t_j) c_i\big)^2 + \lambda \int [\sum_{i=1}^{n} D^2 \phi_i(t) c_i]^2 dt \end{aligned} \tag{2.14}$$

as the objective function where the functional $\int [D^2 \tilde{y}(t)]^2 dt$ measures curvature (or variability) of the data function and λ determines the trade-off between fidelity of $\tilde{y}(t)$ to the discrete observations $\boldsymbol{y}$ and the variability of $\tilde{y}(t)$. The functional term is also called *roughness penalty*. Obviously, as $\lambda \to 0$ the estimated function $\tilde{y}(t) = \hat{\boldsymbol{c}}\boldsymbol{\phi}(t)$ approaches that which would be obtained with L_{WLS} and as $\lambda \to \infty$ we have that $\tilde{y}(t)$ approaches $\tilde{y}(t) = \tilde{a}t + \tilde{b}$. The latter comes from the fact that the *kernel*[7] of $\int [D^2 \tilde{y}(t)]^2 dt$ are the functions spanned by $\{1, t\}$, i.e., $\int [D^2 y(t)]^2 dt = 0$ for $y(t) at + b$ $(a, b \in \mathbb{R})$. L_{PEN} is the objective function that will be used whenever our functional data requires smoothing, however, other functionals than what is used in equation 2.14 can be used. Obviously, any derivative D^n can be used in equation 2.14, provided it exists, but more exotic functionals exists[143, 65], depending on the context of the data. For instance, using

$$F[y(t)] = \int D^2 y(t) + \omega D^3 y(t) dt$$

with

$$\text{Kern}(F) = a_0 + a_1 \sin(\omega t) + a_2 \cos(\omega t) \;\; a_0, a_1, a_2 \in \mathbb{R}$$

instead of $\int D^2 y(t)$ in equation 2.14 would imply that $\tilde{y}(t) \to a_0 + a_1 \sin(\omega t) + a_2 \cos(\omega t)$ as $\lambda \to \infty$ and this would fit very well with data where an underlying periodicity is expected. As mentioned above, this procedure fits very well with our needs and it gives an intuitive and holistic approach to the smoothing problem involved in functionalisation. Furthermore, this technique has been incorporated into many techniques developed in the framework of functional data analysis. Since the differential operator D^2 is used in the functionalization of our data, we will use it as the default roughness operator in the rest of this chapter.

Another important aspect of basis function fitting using equation 2.14 is computational efficiency which can be seen by observing that the roughness term can be rewritten as

$$\int [\sum_{i=1}^{n} D^2 \phi_i(t) c_i]^2 dt = \int [D^2 \boldsymbol{c}' \boldsymbol{\phi}(t)]^2 dt \tag{2.15}$$

$$= \int D^2 \boldsymbol{c}' \boldsymbol{\phi}(t) D^2 \boldsymbol{c}' \boldsymbol{\phi}(t) dt \tag{2.16}$$

$$= \int D^2 \boldsymbol{c}' \boldsymbol{\phi}(t) D^2 \boldsymbol{\phi}(t)' \boldsymbol{c} dt \tag{2.17}$$

$$= \boldsymbol{c}' [\int D^2 \boldsymbol{\phi}(t) D^2 \boldsymbol{\phi}(t)' dt] \boldsymbol{c} \tag{2.18}$$

$$= \boldsymbol{c}' \boldsymbol{R} \boldsymbol{c} \tag{2.19}$$

$$\tag{2.20}$$

[7] Not to be confused with the kernel smoothers briefly mentioned above.

where $\boldsymbol{R}$ is an $n \times n$ matrix. If we drop the independent variable t of $\phi_i(t)$ in our notation, $\boldsymbol{R}$ can be expressed as

$$\boldsymbol{R} = \begin{pmatrix} \int [D^2\phi_1]^2 dt & \int D^2\phi_1 D^2\phi_2 dt & \dots & \int D^2\phi_1 D^2\phi_n dt \\ \int D^2\phi_2 D^2\phi_1 dt & \int [D^2\phi_2]^2 dt & \dots & \int D^2\phi_2 D^2\phi_n dt \\ \vdots & \vdots & \ddots & \vdots \\ \int D^2\phi_n D^2\phi_1 dt & \int D^2\phi_n D^2\phi_2 dt & \dots & \int [D^2\phi_n]^2 dt \end{pmatrix} \tag{2.21}$$

When B-splines or Fourier series are used, the integrals can be computed analytically and thus very fast. If more exotic operators are used, numerical integration techniques must be deployed instead, such as Simpon's Rule. Another computational nicety with B-Splines and Fourier series is that many entries in $\boldsymbol{R}$ are zero. For Fourier series $\boldsymbol{R}$ is a diagonal matrix, and for B-splines it is a band matrix with bandwidth $m - 1$. All in all, this reduces the minimisation of equation 2.14 to fast linear algebra which can be expressed in compact matrix notation as

$$L_{\text{PEN}}(\boldsymbol{c}) = (\boldsymbol{y} - \boldsymbol{\Phi c})' \boldsymbol{W} (\boldsymbol{y} - \boldsymbol{\Phi c}) + \lambda \boldsymbol{c}' \boldsymbol{R} \boldsymbol{c}$$

which can be solved in a similar manner as equation 2.13 above, such that the estimate $\hat{\boldsymbol{c}}$ can be expressed in matrix form as

$$\hat{\boldsymbol{c}} = (\boldsymbol{\Phi}' \boldsymbol{W} \boldsymbol{\Phi} + \lambda \boldsymbol{R})^{-1} \boldsymbol{\Phi}' \boldsymbol{W} \boldsymbol{y}. \tag{2.22}$$

This approach is similar to regularisation techniques used in classical statistics such as ridge regression[113]. In our case we regularize our solution using the curvature which, in turn, is a global property of the function itself.

What have been presented above are some of the essential and basic techniques deployed in FDA and they form the basis for almost every approach to data analysis within this field. Since it is by far too comprehensible (and irrelevant) to give a thorough exposition of techniques available, we will try give a few examples that 1) exemplifies how the techniques above can be used as building blocks 2) hint at more advanced techniques that might be relevant in rolling resistance modelling, but which are out of scope of the present work.

2.5 PCA in FDA

Principal Component Analysis (PCA) is a well-known statistical technique frequently used in many different areas which can be readily adapted to FDA in a version that we will refer to as fdPCA.

Informally, the classical PCA method transforms a set of data vectors into a new set of vectors, called principal components, that identify the variation present in the original data. In addition, the principal components are ranked such that the first components captures as much variance of the data as possible, and the second component captures as much variance as possible under the constraint of being orthogonal to the first component and so on. More specifically, consider a set of data vectors $\boldsymbol{y}_i = (y_{i1}, \dots, y_{iP})'$ $i \in \{1, \dots, N\}$. Without loss of generality, we assume that each entry in the data vectors have zero mean across all vectors. PCA seeks to find vectors $\boldsymbol{\xi}_1, \dots, \boldsymbol{\xi}_N$ in the following manner

1. $\boldsymbol{\xi}_1$ is the vector that maximizes

$$N^{-1} \sum_{i=1}^{N} t_i^2 = N^{-1} \boldsymbol{t}' \boldsymbol{t} \quad \text{where} \quad t_i = \sum_{k=1}^{P} y_{ik} \cdot \xi_k = \boldsymbol{y}_i' \boldsymbol{\xi} = \langle \boldsymbol{y}_i, \boldsymbol{\xi} \rangle \tag{2.23}$$

with respect to $\boldsymbol{\xi}$ and under the condition that $\|\boldsymbol{\xi}\| = 1$. The latter ensures that $N^{-1}\boldsymbol{t}'\boldsymbol{t}$ cannot be arbitrarily large. Informally, given the constraint on the magnitude of $\boldsymbol{\xi}_1$, the only way to maximize equation 2.23 is by attributing high weight (value) in the entries ξ_k of $\boldsymbol{\xi}_1$ where the corresponding values of the y_{ik}'s are high across all $\boldsymbol{y}_i$'s. Given the zero-mean property, this coincides with high variance.

2. $\boldsymbol{\xi}_2$ is found in a similar way as $\boldsymbol{\xi}_1$ with the additional constraint that $\langle \boldsymbol{\xi}_1, \boldsymbol{\xi}_2 \rangle = 0$, i.e., $\boldsymbol{\xi}_1$ and $\boldsymbol{\xi}_2$ are orthogonal.

n $\boldsymbol{\xi}_n$ is found in a similar way as $\boldsymbol{\xi}_2$ except that $\boldsymbol{\xi}_n$ must be orthogonal to all the $n-1$ previous $\boldsymbol{\xi}_i$'s.

By letting $\boldsymbol{X}$ be the $N \times P$ matrix of stacked data vectors $\boldsymbol{y}_i'$ we have that $\boldsymbol{t} = \boldsymbol{X}\boldsymbol{\xi}$ which can be substituted into equation 2.23, and thus the maximisation can be expressed as

$$\max N^{-1}\boldsymbol{\xi}'\boldsymbol{X}'\boldsymbol{X}\boldsymbol{\xi} = \max \boldsymbol{\xi}'\boldsymbol{V}\boldsymbol{\xi} = \max\langle \boldsymbol{\xi}, \boldsymbol{V}\boldsymbol{\xi}\rangle \quad \text{with} \quad \|\boldsymbol{\xi}\| = 1 \tag{2.24}$$

where $\boldsymbol{V} = N^{-1}\boldsymbol{X}'\boldsymbol{X}$ is the $P \times P$ covariance (estimate) matrix. The fact that it is the covariance matrix is due to the zero-mean property of the data set. Since $\boldsymbol{V}$ is symmetric, it is diagonalisable and it can be shown that the solution to the eigenvalue problem

$$\boldsymbol{V}\boldsymbol{\xi} = \lambda\boldsymbol{\xi} \tag{2.25}$$

given as pairs $(\boldsymbol{\xi}_1, \lambda_1), (\boldsymbol{\xi}_2, \lambda_2), \ldots, (\boldsymbol{\xi}_P, \lambda_P)$ of eigenvalues and eigenvectors is also the solution to the PCA problem stated above. More specifically, the eigenvectors $\boldsymbol{\xi}_1, \ldots, \boldsymbol{\xi}_P$ are the principal components and their order is given by the order of the eigenvalues, i.e., $\lambda_1 > \lambda_2 > \ldots > \lambda_P$.

When we turn to fdPCA, the mathematical setting is not that of classical Euclidean vector spaces but infinite dimensional Hilbert spaces instead. Thus, our observations are now functions

$$\boldsymbol{y}(t) \ = \big(y_1(t), \ldots, y_N(t)\big) = \Big(\sum_{k=1}^{P} c_{1k}\phi_k(t), \ldots, \sum_{k=1}^{P} c_{Nk}\phi_k(t)\Big) \tag{2.26}$$

and the covariance matrix $\boldsymbol{V}$ is now a covariance function

$$v(t,s) = N^{-1}\sum_{i=1}^{N} y_i(t)y_i(s) = N^{-1}\boldsymbol{y}(t)'\boldsymbol{y}(s) \tag{2.27}$$

and just as the *symmetric* covariance matrix $\boldsymbol{V}$ can act on vectors $\boldsymbol{\xi}$, the covariance function can be used as a *self-adjoint* operator $\mathcal{V}[\xi(t)]$ acting on functions $\xi(t)$ by[8]

$$\mathcal{V}[\xi(s)] = \hat{\xi}(t) = \int v(t,s)\xi(s)ds. \tag{2.28}$$

With these generalizations, together with the fact that in function spaces an inner product can be defined as $\langle g(t), f(t)\rangle = \int g(t)f(t)dt$, we can express a functionalized version of equation 2.24 as

$$\max \Big\langle \xi(t) \ , \ \mathcal{V}[\xi(s)](t) \Big\rangle = \int \xi(t) \int v(t,s)\xi(s)dsdt \quad \text{with} \quad \|\xi(t)\| = 1 \tag{2.29}$$

[8] Compare this with the well-known Fourier operator: $\mathcal{F}[f(t)] = \hat{f}(s) = \int e^{-2\pi its}dt$

and just as in the Euclidean case, the fdPCA components are given as eigen*functions* of the functionalized eigenvalue problem

$$\int v(t,s)\xi(s)ds = \lambda\xi(t). \tag{2.30}$$

Thus our principal components are $(\xi(t)_1, \lambda_1), (\xi(t)_2, \lambda_2), \ldots$ with $\lambda_1 > \lambda_2 > \ldots$. Generally in infinite dimensional function spaces there are an infinite number of eigenfunctions which are too many for our practical purposes. However, as noted earlier, we are working in finite dimensional subspaces of these function spaces and so in practice there are only a finite set of eigenfunctions.

We began by considering the finite dimensional (Euclidean) case and then we generalized it to the infinite dimensional case. Now we will return to the finite arena by restricting the general infinite formulation to one of finite dimensional subspaces, when considering the computational details on how to calculate the functional principal components in practice. Since every functional observation is represented as a linear combination of the same basis functions spanning our subspace, we can express the vector of data functions as

$$\boldsymbol{y}(t) = \boldsymbol{C}\boldsymbol{\phi}(t) \tag{2.31}$$

where $\boldsymbol{\phi}(t)$ is the vector of length P containing the basis functions and $\boldsymbol{C}$ is the $N \times P$ matrix of parameters where row i contains the coefficients for $y_i(t)$. By noting that we can express $\boldsymbol{y}(t)'$ as $\boldsymbol{\phi}(t)'\boldsymbol{C}'$ we can express a finite subspace version of the covariance function in equation 2.27 as

$$v(s,t) = N^{-1}\boldsymbol{\phi}(s)'\boldsymbol{C}'\boldsymbol{C}\boldsymbol{\phi}(t). \tag{2.32}$$

Moreover, by assuming that an eigenfunction $\xi(t)$ is on the following form

$$\xi(t) = \sum_{k=1}^{P} b_k\phi_k(t) = \boldsymbol{\phi}(t)'\boldsymbol{b} \tag{2.33}$$

we can reformulate the self-adjoint operator in equation 2.28 in terms of the covariance function in equation 2.32 as

$$\mathcal{V}[\xi(s)] = \int v(t,s)\xi(s)ds. = \int N^{-1}\boldsymbol{\phi}(t)'\boldsymbol{C}'\boldsymbol{C}\boldsymbol{\phi}(s)\boldsymbol{\phi}(s)'\boldsymbol{b}ds \tag{2.34}$$

$$= \boldsymbol{\phi}(s)'N^{-1}\boldsymbol{C}'\boldsymbol{C}\boldsymbol{W}\boldsymbol{b} \tag{2.35}$$

where $\boldsymbol{W} = \int \boldsymbol{\phi}(s)\boldsymbol{\phi}(s)ds$ since it is the only part of the expression that is not constant under the integral. This derivation is similar to the derivation of $\boldsymbol{R}$ in equation 2.15. With a finite dimensional *but* functional version of the covariance operator we can easily substitute it into the eigenvalue problem stated in equation 2.30 and get

$$\boldsymbol{\phi}(s)'N^{-1}\boldsymbol{C}'\boldsymbol{C}\boldsymbol{W}\boldsymbol{b} = \lambda\boldsymbol{\phi}(s)'\boldsymbol{b} \tag{2.36}$$

Since equation 2.36 should hold for all s, by definition, we can drop $\boldsymbol{\phi}(s)$ and get the following eigenvalue problem

$$N^{-1}\boldsymbol{C}'\boldsymbol{C}\boldsymbol{W}\boldsymbol{b} = \lambda\boldsymbol{b} \tag{2.37}$$

with respect to the coefficient vector $\boldsymbol{b}$. However, the vectors $\boldsymbol{b}$ satisfying equation 2.37 is only of implicit interest since it is the functions $\xi_1(t), \ldots, \xi_P(t)$, that they provide coordinates for, that is of real interest. In other words, we are not interested in an orthonormal basis $\boldsymbol{b}_1, \ldots, \boldsymbol{b}_P$ (of $\mathbb{R}^P$) where each $\boldsymbol{b}_i$ satisfies equation 2.37, but an orthonormal basis $\xi_1(t), \ldots, \xi_P(t)$ (of a $L[a,b]^2$-subspace) where each $\xi_i(t)$ satisfies equation 2.36. Fortunately, the inner product used for the $\xi(t)$'s can be expressed as a inner product for the $\boldsymbol{b}$'s (using a similar derivation as in equation 2.15):

$$\begin{aligned}\langle \xi_1(t), \xi_2(t) \rangle &= \int \boldsymbol{b}_1' \boldsymbol{\phi}(t) \boldsymbol{b}_2' \boldsymbol{\phi}(t) dt \\ &= \boldsymbol{b}_1' [\int \boldsymbol{\phi}(t) \boldsymbol{\phi}(t)' dt] \boldsymbol{b}_2 \\ &= \boldsymbol{b}_1' \boldsymbol{W} \boldsymbol{b}_2 = \langle \boldsymbol{b}_1, \boldsymbol{b}_2 \rangle_{\boldsymbol{W}}\end{aligned}$$

so $\|\xi(t)\| = 1$ implies $\boldsymbol{b}\boldsymbol{W}\boldsymbol{b}' = 1$ and $\langle \xi_i(t), \xi_j(t) \rangle = 0$ implies $\boldsymbol{b}_i' \boldsymbol{W} \boldsymbol{b}_j = 0$. Thus, if we set $\boldsymbol{b} = \boldsymbol{W}^{-\frac{1}{2}} \boldsymbol{u}$ and substitute into equation 2.37 and rearranging we get a eigenvalue problem

$$N^{-1} \boldsymbol{W}^{\frac{1}{2}} \boldsymbol{C}' \boldsymbol{C} \boldsymbol{W}^{-\frac{1}{2}} \boldsymbol{u} = \lambda \boldsymbol{u} \tag{2.38}$$

where $\langle \boldsymbol{u}_1, \boldsymbol{u}_2 \rangle = \langle \boldsymbol{b}_1, \boldsymbol{b}_2 \rangle_{\boldsymbol{W}}$ and so the eigenvectors derived from 2.38 can be transformed into coordinates for the eigenfunctions $\xi(t)$ that we seek. This functionalized version of PCA is exemplified with our own data in section 5.2.1.

This derivation illustrates a general methodology used to adapt classical analysis techniques to functional data. The first step is analysing the linear algebra used in the classical technique and reformulate it using general concepts from functional analysis that also holds for infinite dimensional function spaces. Then reintroduce the linear algebra by using finite subspaces of the general infinite function space such that it can be computed in practice. Another direct approach is to convert the data functions back to discrete data by evaluating the functional data for a fine grid of values $t_1, \ldots, t_M$ ($M >> P$) and then perform the classical PCA on the resulting Euclidean vectors. However, this introduces computational overhead since the actual dimension of the problem is only P and it does not utilize any orthogonality or compact support properties of basis functions such as, e.g., the Fourier basis where $\boldsymbol{W} = \boldsymbol{I}$.

Note that fdPCA presented above can be extended in many different ways. For instance, it can be extended to deal with pairs $(y_i(t), z_i(t))$ (or n-tuples for that matter) of data functions or it can be extended to mixed data where, e.g., the data is composed of tuples $(y_i(t), \boldsymbol{z}_i)$ of data functions and vectors. Another extension concerns smoothing of eigenfunctions where the requirement $\|\xi(t)\| = 1$ is extended to take roughness of $\xi(t)$ into account, e.g., by using a penalty like $\lambda \|D^2 \xi(t)\|$ (used in equation 2.14) that utilises the smoothness of the functions. We will refrain from covering the nitty gritty details of these extensions as we did with fdPCA.

While fdPCA is the only classical technique examined here, many other techniques have been adapted to functional data. Most of these have also been extended to take advantage of smoothness properties of the data functions by. e.g., incorporating a roughness penalty. For instance, Cannonical Correlation Analysis (CCA)[9] as well as many different linear modelling approaches where combinations of parameters, independent, and dependent variables can be functional. Some of these techniques could prove valuable in rolling resistance modelling

[9] In the case of CCA, introducing a roughness penalty is not just a feature but a necessity for the functionalized version to work.

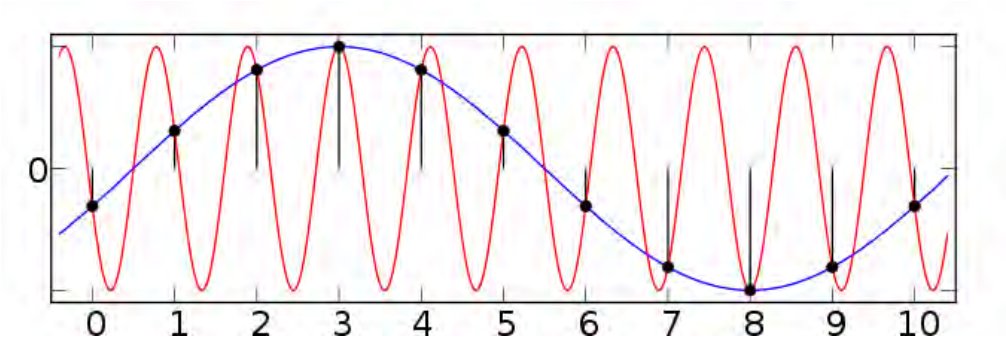

Figure 2.4 Illustration of aliasing. The black circles are discrete observations. The red and blue lines are two different sines that both are able to replicate the discrete set of observations.

approaches similar to this work, but with more comprehensive sets of data than what have been available here (and treated in chapter 5 and 6).

2.6 Fourier series revisited

Fourier analysis and Fourier series are popular tools in road engineering. Investigations are often undertaken by transforming road surface profiles into the frequency domain where wavelengths can be correlated to other quantities such as rolling resistance, skid resistance, noise, and so forth. In general, road engineers often characterise the road surface by partitioning spatial wavelengths into conceptual meaningful intervals (this classification is described in section 4.1 and an overview of it is given in figure 4.1). E.g., *macro-texture* is defined to be wavelengths from 0.5 to 50 mm. Moreover, the de facto standard for measuring road unevenness that is used in road maintenance today, the so-called *International Roughness Index* (IRI), relies, in practice, on the frequency domain for calculation (IRI is described historically in chapter 3 and the technical formulation is described in chapter 4). As mentioned in section 2.3 there are some challenges related to Fourier analysis when applied to road profiling, that will be discussed in detail now.

One of the phenomena discussed in road profiling literature is *aliasing* which occurs when a discrete set of observations are converted to the frequency domain (see chapter 3 for an overview of this issue). The root of the problem lies in the fact that a discrete set of observations cannot, in general, be uniquely replicated by a finite sum of sines, i.e. there are many possible (finite sums of) sines that will be able to replicate the observations. A simple example illustrating the matter is given in figure 2.4. If we imagine that the red sine in figure 2.4 represents a 2D road profile where its road length on the x-axis is plotted against vertical position on the y-axis and the black filled circles are measurements obtained of it. Then the blue sinusoid is the one given to us by a discrete Fourier transform that clearly is far from a fit to the actual profile. Thus, while the observations can be replicated, the frequency domain representation of the function is erroneous and so, e.g., any interpolation or spectrum derived from it will be wrong.

More precisely, assume a continuous function $y(t)$ can be expressed as a (finite) linear combination of Fourier basis functions from the orthonormal set $\{e^{n2\pi it} | \, n \in \mathbb{Z}\}$ and assume that the highest n needed is N. Then a sample rate B equal or higher than $2N$ is necessary to

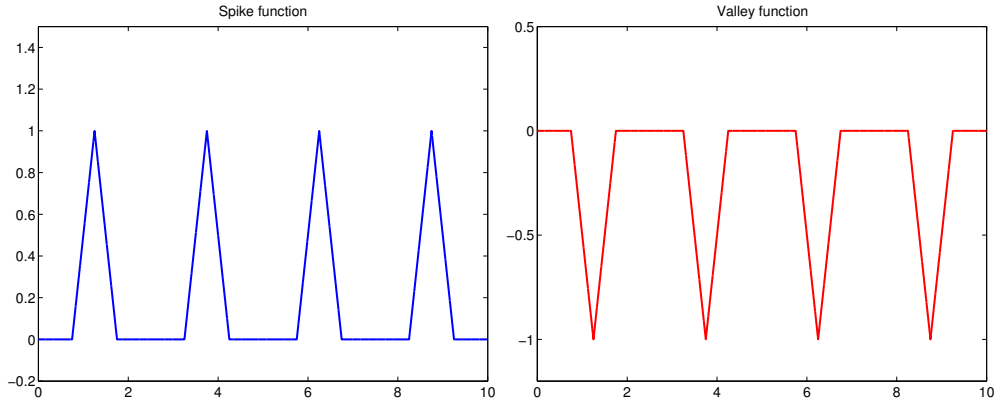

Figure 2.5 Two different functions representing idealised surfaces.

find the coefficients used in the linear combination. This is an FDA flavoured version of the so-called *Nyquist-Shannon sampling theorem*, and the sample rate $2N$ is called the Nyquist-rate[13, p.328]. Aliasing problems arise when the sample rate is *not* sufficient: If $y(t)$ is sampled with $2N$ and there exists frequencies $n > N$ which also contribute to $y(t)$, then they will contaminate lower frequencies as illustrated in figure 2.4. In the road profile studied later, we do not have any a priori knowledge of minimum frequencies so the problem of aliasing is not only a theoretical problem. This issue can be mitigated by applying analog filters that attenuate frequencies higher than the Nyquist rate before any discretization occurs. If there is only a discretized set of observations available and sampling frequency is much higher than the frequency range under investigation, observations can be aggregated into sub-averages before transformation to the frequency domain[87, p.14].

Another important aspect of Fourier analysis that will be relevant in our later investigations is correspondence between a function $y(t)$ and its frequency spectrum. The spectrum only plots information about amplitudes of each frequency component which is, in principle, only half the story, as can be seen from equation 2.6 where there is a *phase* parameter for each frequency component. Thus different $y(t)$'s can have equal spectra. To illustrate this, consider the two functions plotted in figure 2.5. While they do have the same period, they have qualitative different behaviours as one of them have spikes while the other have valleys. From our rolling resistance modelling point of view, these two functions are very different. Nevertheless, their spectra are identical with the most significant frequencies plotted to the left in figure 2.6. The reason the functions differ is because of their different phases and, as illustrated to the right in figure 2.6, for each frequency the valley and spike sinusoids are in antiphase. If these two functions represented two different road surfaces, we would not expect those surfaces to have equal properties with respect to skid resistance, rolling resistance etc. Therefore it is not enough to study the road profile spectra only, if the goal is to understand the relationship between road surface and, e.g., rolling resistance. This have also been mentioned in the road/transportation literature[112].

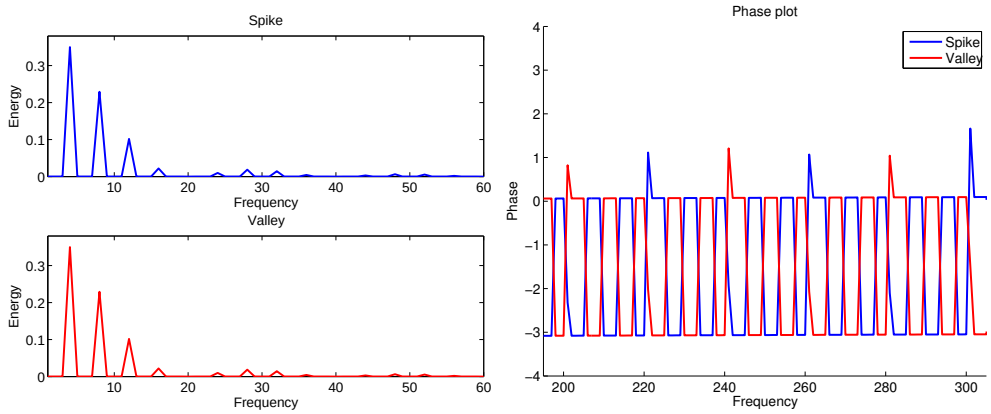

Figure 2.6 Spectra and phase plots of the two functions from figure 2.5.

3 Overview of Vehicle Rolling Resistance

In this chapter we present the general theory of rolling resistance of motor vehicles as well as measurement methods of rolling resistance and road surfaces. Much of the literature reviewed here and in chapter 4 have also been reviewed and published in [4], so there will be a slight overlap between the two expositions. However, the purpose and focus of these chapters deviates from [4] in a couple of respects: First of all, this is not intended as a neutral and descriptive exposition of rolling resistance research as is the case with [4]. Instead, the analysis put forward here will be of a critical nature, with the intention of creating research questions to be pursued in the following chapters. Secondly, the scope of [4] is broader compared to what is presented here, and [4] covers many more aspects of rolling resistance research than what is needed for our scientific endeavours in later chapters. E.g., detailed Finite Element Models as mentioned in chapter 1 are not considered here since their level of detail exceeds the practical goals of the present research.

The bulk literature reviewed here are of a peculiar nature, compared to the previous scientific fields that the author has been acquainted with. Much of the research and results that have been produced in the past decades have, to a large extent, been in the form of technical reports and therefore to a lesser extent as articles in scientific journals. An advantage of this is that these reports are usually publicly available, but unfortunately this also means they are scattered across various websites pertaining primarily to research projects and government bodies that produced them. A related observation is that the literature is generally quite fragmented with only a few common treads of research. Of course some publications stand out and are frequently cited in other works, but generally the links between different research projects and groups are more implicit than is the case elsewhere in the scientific and engineering communities.

3.1 Introduction to Rolling Resistance

In this section we are going to take a look at rolling resistance and what phenomena are causing rolling resistance, but first we will start by looking at all factors that resist vehicle movement. The exposition in this section is largely based on [154] and [49].

3.1.1 Driving Resistance

Rolling resistance is only one component among many that resist vehicle movement and thus consumes energy during driving. In [154] a list has been made that will inspire the list below. The main focus here is on energy loss and general phenomena that occur in different parts of the vehicle. Some of these are included rolling resistance components, which will be elaborated below. Of course, this is a simplification, but it will suffice for our purpose here. It is essentially an expanded version of the list in [63], which in turn is an expanded version of the list in [117].

a) **Tyre-related energy loss**: This is the main constituent of rolling resistance. This energy

loss comes from hysteresis effects of tyre deformation, shear of the tyre, and adhesion between surface and tyre.

b) **Suspension loss**: Energy loss in the shock absorbers, especially when driving on uneven roads.

c) **Aerodynamic drag**: Energy loss due to air drag. While aerodynamic drag holds for the whole car, a subset of it is specifically related to high-speed rotations of the wheels.

d) **Inertial resistance**: When accelerating, the entire vehicle resists change in speed which requires energy to overcome. This phenomena also occurs locally with angular acceleration of axles and wheels.

e) **Gravitational resistance**: When the road has a positive longitudinal gradient, energy is consumed to overcome earths gravitational pull. With a negative gradient potential energy is released instead.

f) **Transmission loss**: When the kinetic energy is transferred from the engine to the wheels, a transmission loss occurs. This loss is primarily due to friction, but aerodynamic drag of rotating axles might also play a minor role.

g) **Engine resistance**: Various components that gives rise to energy loss in the engine when transferring energy from the fuel to the drive-shaft. Examples are excess combustion heat and piston-related friction.

h) **(Loss from auxillary equipment)**: Additional energy consumed to power equipment not related to driving, such as air condition, radio etc. This is not really related to driving resistance.

There are a couple of alterations between this list and the one found in [154]. They will be mentioned here, as they illustrates some of the ambiguties that inevitably arise when categorizing driving resistance (and rolling resistance in particular). Firstly, 'side force resistance', i.e. resistance from driving in curves, is an independent item found in [154] which is implictly included under **a**) here. This is also mentioned as a possibility in [154]. Secondly, **a**) has been called rolling resistance in [154] but as subsequent discussions here and discussions in [154] suggests, this is not necessarily accurate. Indeed, several of the items in the list above could be viewed as contributors to rolling resistance. This will be the topic of the section below.

3.1.2 Rolling Resistance Constituents

Before going into detail with the constituents of rolling resistance we will give a definition first. Several definitions have been given in the literature and in connection with rolling resistance measurement standards such as SAE J1269, SAE J2454, and ISO 28580:2009. Historically, rolling resistance has been defined as a force[49], which traces back to initial work by Coulomb[163] in 1785, and is at the core of modern definitions exemplified by the standards above. However, in [163] Schuring argued, by analysing the work in [67], that rolling resistance should be defined in terms of energy loss (per unit distance traveled) instead of force, and thus renaming *rolling resistance* to *rolling loss*:

> *... rolling resistance is defined as work expended by the tyre per unit distance traveled.* [163, p.32]

While the definition of rolling resistance in terms of energy per unit distance or force is dimensionally equivalent, Schuring argued that defining rolling resistance in terms of energy per unit distance is a more general formulation that can account for a wider range of conditions compared

to the definition using force[163, p.32]. This definition might also be more suitable, since the main component in rolling resistance is energy dissipation due to hysteresis losses. Furthermore, given the aim of this research, as described in chapter 1, our interest is in determining energy consumption due to the tyre/road interaction and not the magnitude of the rolling resistance force. Regardless of Schurings discussions, rolling *resistance* is still a very common term used instead of rolling *loss*, but standards such as ISO 28580 defines rolling *resistance* in terms of *energy* consumed per unit distance[80, p.1]. We will use 'rolling resistance' and 'rolling loss' interchangeably in the following chapters. Unsurprisingly, rolling resistance of a tyre depends on the load F_z applied to the tyre. Studies have suggested that a linear relationship exists between rolling resistance F_{RR} and tyre load, so a dimensionless rolling resistance coefficient C_{RR} or C_R has been formulated[154, 80] as

$$C_R = F_{RR}/F_Z. \tag{3.1}$$

This is a widely used measure of rolling resistance and is used by, e.g., the rolling resistance trailer discussed below.

While Schurings general definition seems fit for our purposes, it does not specify any details as which phenomena give rise to the energy consumption. For our purpose here it seems suitable to partition different rolling resistance components into 3 broad categories: Components that takes place in the tyres (and vehicle) only, components that takes place in the pavement, and components that are a result of the interaction between pavement and tyre. Some of the components can be split into sub-components that are in different categories, and if that is the case they will be placed in all of them. First we have the wheel and tyre related components:

- Hysteresis loss due to tyre deformation. Even on a smooth and planar surface tyre deformations occur during rolling such as sidewalls and tread-block deformations. Besides tyre material composition and geometry, these phenomena depends on tyre pressure and the load applied to the tyre.
- Inertial resistance. When the vehicle changes speed, the tyres change rotation speed which causes inertial resistance.
- Aerodynamic drag of the rolling tyre. As the tyre moves through the air an aerodynamic drag is created. Note that this is not considered to be part of rolling resistance in ISO 28580 but is instead described as 'parasitic losses'.
- Transmission loss. Even though most of the transmission loss does not occur in the tyre, there is some energy loss due to bearing friction. This is also not considered to be part of rolling resistance in ISO 28580.

As mentioned above, some of the components do not count as rolling resistance by some drum measurement standards which suggests that the primary target of these is to measure the energy loss due to tyre deformation only. Even so, since the object of study in this thesis is rolling loss from tyre/road interaction and not the purely tyre-related losses, we will not go into a detailed discussion about it. The same goes for the tyre independent pavement rolling losses, which primarily consists of the following:

- Deflection of the pavement due to the load of the vehicle. While this of course depends on the load exerted by the tyre on the surface, it is mostly independent of the tyre.
- Deterioration and movement of chips and stones. Loose and loosened stones in the surface patch creates energy loss when moved between tyre and surface.

While these phenomena are relevant for, e.g., road administrators and pavement entrepreneurs the focus of the present work is on the tyre/road interaction as discussed in chapter 1. The portion of rolling resistance that is our primary object of investigations here are related to the tyre/road interaction which are summarized below:

a) Hysteresis loss by tyre deformation due to road longitudinal unevenness. This type of loss is happening at the larger end of the length-scales of rolling losses and is caused by irregualarities on the surface (like bumbs, holes, etc.) that causes the tyre to bounce, thus absorbing some of the corresponding shocks in, e.g., the tyre side-walls.

b) As above, but with tyre deformation due to transversal unevenness which can be caused by slanted road, rutting etc.

c) Hysteresis loss by tyre deformation due to road texture. Local tyre deformations occurring at the tyre/surface contact patch where tyre tread-blocks are deformed and penetrated by e.g., chips and stones in the pavement.

d) Deformation of tread-blocks also creates tangential motions that causes tread-blocks to 'slip out' of the contact patch when they leave it. This is also referred to as 'stick-slip'.

e) Molecular bonds between tyre and road surface in the contact patch also creates adhesive forces that needs to be overcome when tread blocks leaves the contact patch. This is also called the stick-snap phenomena.

As can be seen from the list above, many different phenomena account for the tyre/surface part of rolling loss which altogether are extremely complicated and detailed models capturing all of these phenomena would likewise be very complex. It should be noted that this categorisation is rough in the sense that distinctions between different length-scales have been made. For instance, item **a**) and **c**) are not completely separated, but represents two extremes in a continuous array of length-scales. If we imagine a road bump that is, e.g., 1 meter wide in the driving direction, we would say that the tyre deformation caused by driving over this bump would belong to the first item and a stone 1 cm in diameter would belong to the second first item. However, a rock 10 cm in diameter can cause side wall deformation as well as local tread block deformation and thus could be categorised into both. In practice, however, it is the road measurements available to us that determines which aspects of the road that we can model. How to measure these road properties as well as rolling resistance are the primary topics of the last sections in this chapter. In chapter 4 a new texture measure for rolling resistance assessment is proposed and it is especially item **c**) and **e**) that are relevant to consider there. While the phenomena in **d**) are also pertaining to the texture level, it does not seem to be directly dependent on the road surface geometry (although it should depend on speed).

3.2 Rolling Resistance Measurement Techniques

There are essentially two types of measurements that will be relevant for our investigations in later chapters: Rolling resistance and road surface measurements. We will begin by discussing rolling resistance measurement techniques.

Since the beginning of the twentieth century, several measurement techniques have been used to measure vehicle/tyre rolling resistance. Essentially four techniques are used, although the exact procedure can vary:

1. **Drum measurements**
2. **Trailer measurements**

3. **Coast-down measurements**
4. **Vehicle fuel consumption**

Note that they have been ranked according to idealization, i.e., the first one excludes most disturbing factors and the last item includes every driving and rolling resistance component mentioned earlier. Moreover, every step includes (more or less) the rolling and driving resistance components of the former step. What is excluded and what is included will be discussed for each method as it is described below.

3.2.1 Drum Measurements

This procedure goes back to (at least) 1922 with the work of [67]. The drum measurement technique is widely used in the tyre industry, and several standards have been made in order to harmonize the procedure[79, 80, 147]. In 2009 the EU label directive was put into effect, which requires tyre manufacturers to label their tyres with a rolling resistance efficiency indicator. The basis for these labels are drum measurements, and a report commissioned by the EU[1] set forth practices for these measurement procedures.

The basic idea is to have a tyre pushed onto a drum with an applied load and having the drum run by a motor attached to it. Rolling resistance will then retard the rotation of the drum and this retardation is measured in several ways. The ISO 28580 standard mentions tyre spindle force, drum input torque, drum deceleration, or drum motor power consumption[80]. In addition, parasitic losses have to be dealt with in the resulting measurements[80, p.9]. The standard also specifies measurement times, formulas for rolling resistance calculation, temperature correction, drum curvature correction etc.

The drum measurement are the most idealized method since almost all disturbances have been removed, including the road itself. The advantage of this is that we are closer to measure pure tyre rolling resistance, but it can be argued that important effects from the real setting are left out such as, e.g., pavement unevenness and texture. The latter can be accommodated by using a rough surface on the drum, but it is questionable whether or not this is a true representation of the texture variety of real roads. With our aim of understanding tyre/surface rolling resistance this makes the drum method unsuitable. Another unrealistic factor that has to be corrected for is the curvature of the drum[80, p.13][29]. The standard formula used for curvature correction has recently been questioned for correctness[47].

3.2.2 Measurement Trailer

This measurement technique is relatively new. The first trailer was developed and build in the eighties by the Belgian Research Road Center[154]. Measurement results with this trailer was presented in 1989[34] and showed a substantial influence on rolling resistance from the so-called 'megatexture' length-scale range (to be explained below). Since then, several other trailers for personal car tyres have been developed[2] by, e.g., Technical University of Gdansk (TUG) and Bundesanstalt für Strassenwesen (BASt), which have also developed a trailer for lorries together with Forschungsvereinigung Automobiltechnik (FAT)[154, p. 69]. The TUG trailer has recently been modernized by reducing aerodynamic drag[182] and reducing influence of,

[1] For more information about this, see the web resource http://ec.europa.eu/energy/en/topics/energy-efficient-products-and-labels/tyres (accessed 1st of February 2015).

[2] Hugo Lesdos from the Technical Campus of COLAS told the author in a personal communication (at the 'Green Road Infrastructure Workshop, November 2014) that COLAS is also working on a rolling resistance trailer.

e.g., inertia[183]. This trailer is widely used in rolling resistance measurement campaigns in Europe[15, 144, 145, 68, 144] (including the COOEE project) as well as America[41]. Unfortunately, the aforementioned trailers differ significantly in design and inter-trailer measurement comparisons have not been satisfactory[15, 145]. To rectify this, the ROSANNE project aiming at standardizing rolling resistance measurement trailers, among other things, has recently been launched[3].

The basic principle of the measurement trailer is to have a tyre mounted on the trailer with an applied load. When the trailer is towed by a vehicle with (preferably) constant speed, the rolling resistance of the mounted tyre exerts a retarding force which is then measured by the trailer. It can be measured in many different ways and in the case of the TUG trailer this is done by measuring the deflected angle of the measuring arm where the wheel is attached.

The measurement trailer is not as idealized as the drum measurements, since the measurement is performed on the actual roads. Thus, many tyre/surface interactions will be included in the measurements such as those arising from texture, cracks etc., as well as pure pavement losses like pavement deflection. Depending on the trailer construction, some suspension losses might also be present. The same goes for wheel bearing losses, which are also present in drum measurements, although specifications exists to correct for it[80]. Any correction terms for the trailer are not known to the author. In principle, the trailer measurement method seems ideal for our present purpose of assessing the energy consumption due to the tyre/surface interaction since the measurements includes relevant rolling resistance components and excludes irrelevant ones. On the other hand, this measurement technique, as hinted above, seems not entirely mature as inter-trailer comparison is not optimal[15]. Nevertheless, trailer measurements are a source of rolling resistance measurements in this thesis.

3.2.3 Coast-Down Measurements

According to [154, p.85] this kind of measurement traces back to the 1920s. Besides rolling resistance, the coast-down method has been used to assess vehicle aerodynamic drag[179, 176, 22, 43] which has been shown to correlate well with wind tunnel experiments [39, 21, 18, 169, 98]. The main idea of this measurement technique is to let a vehicle coast freely from an initial velocity and position, with clutch down in neutral gear. With engine and gear train disengaged, the velocity depends solely on gravity, rolling resistance, aerodynamic resistance, and a minor subset of the friction forces such as bearing friction. Most forces are retarding the speed of the vehicle with some exceptions such as those arising from tail wind and downhill coasting. By measuring the speed of the vehicle at (preferably) high resolution the resulting net force acting on the vehicle during the coast-down can be inferred. If, in addition, other quantities are measured such as road texture, gradient, wind speed/direction, barometric pressure etc., it is possible to determine the force contributions from, e.g., rolling resistance, side force resistance, and aerodynamic drag by fitting a model to the measurements. The model is based on Newtons second law of motion, but the exact formulation can vary in many respects depending on assumptions and the types of measurement available. As an example, the simple model used in[43]

$$a(t) = \frac{dv}{dt} = \frac{cv^2 + r}{m + m_{rot}} \tag{3.2}$$

[3] Since this project is far from finished there are no publications yet. For more information see the following webpage http://rosanne-project.eu/

where

$$c = \frac{1}{2}\rho A C_d \quad \text{and} \quad r = R + mg\theta. \tag{3.3}$$

m is the mass of the vehicle, m_{rot} is the inertial mass of rotating wheels, ρ is air density, A frontal area of the coasting vehicle, C_d the aerodynamic drag coefficient, R is rolling resistance, g is gravitational acceleration and θ is the longitudinal slope of the road. All quantities except R and C_d is measured in [43] so by approximating $a(t)$ from pairs of time and position measurements, the rolling resistance R and aerodynamic drag coefficient C_d can be estimated. From our point of view this model is rather coarse since, e.g., the rolling resistance is only represented as a constant. Recent coast-down experiements[63, 89] have expanded the model above as well as provide more measurements of other quantities such as transversal slope, road texture etc. These new models and data will be treated in chapter 6 and used in investigating our own attempts at assessing road surface induced rolling resistance.

Since the coast-down procedure involves the entire vehicle, it poses a significant step down from the idealized pedestal compared to the measurement trailer. This means that all vehicle transmission losses, except for losses occurring before the clutch and losses in connection with the gear train, are present during measurement. Suspension losses are also better captured than the trailer because the suspension losses experienced in the coast-down procedure stems from the vehicles actual suspension system. This is of course important if the effect of the roads unevenness is a specific subject of investigation. Furthermore, air resistance of the entire vehicle is captured by this method, hence the use of coast-down procedures to estimate aerodynamic drag coefficient. The closeness to actual driving is both the strength and weakness of this method: The closeness to actual driving makes it ideal for investigating phenomena that more idealized methods are unable to capture. On the other hand a good deal of modelling work (i.e. model formulation and parameter estimation) has to be made to be able to distinguish the different forces acting on the vehicle. A detailed model also requires a great deal of measurements which will be apparent in chapter 6 where a model much more detailed than the model in eq. 3.2 and 3.3 is used. In addition, these extra measurements and modelling efforts introduces additional layers where noise and other factors might distort the results. All in all this seems like an interesting measurement method to use in research and that is why it is included here.

3.2.4 Fuel Consumption Measurements

The last, in no way idealized, method is direct fuel consumption measurements where fuel consumption of the engine is measured directly. These kind of measurements have been brought into use in many different ways. For instance, high frequent measurements of fuel inflow to the engine have been used along with other data, such as measurements of the roads surface[151], to see if any correlation exists. Previously, fuel consumption measurements have also been used in investigating tyre energy loss[94, 162] and many different models of vehicle fuel consumption have been made[19] which recently have been used in general Vehicle Operating Cost models[58, 26]. Some of these are mechanistic and resembles the ones used in coast-down modelling. For an introduction to the development of these models, see [58, 26]. We will not go into detail about fuel consumption models here as they are too general for the present purposes of this thesis. Besides picking up the same driving resistance components as the coast-down method, fuel consumption also depends on the internal engine friction as well as energy consumption of auxiliary equipment. Since these sources of energy consumption are entirely irrelevant for the aims in this thesis, fuel consumption measurements have not been

considered. Nevertheless, they might be of interest if they are combined with other sources of data. Especially [151] showed some interesting use of fuel consumption measurements.

3.3 Surface and Pavement Measurement Techniques

The other source of key data to the present work is pavement measurements. In this section we are going to present some of the different measurement techniques that are relevant for surface induced rolling resistance. We are also examining the historical background as it explains some of the essential road engineering concepts and why they are used today. The focus will be on two kind of road properties that have been measured before the introduction of modern laser profilers and the subsequent development that it has resulted in. The first property is the so-called 'road unevenness', which, informally, refers to the 'bumpiness' of the road and other properties in the length scale of meters. The second property is 'road texture' and refers to mm scale irregularities that results from the mix of mineral aggregates in the pavement. Another way of expressing road texture is by using the term 'surface roughness'. Unfortunately, 'roughness' is a very ambiguous word in road engineering, since it is also used instead of 'unevenness' in American English for describing road unevenness mentioned above.

Another road property that is also frequently measured and studied, is the 'pavement deflection', i.e. the pavement deformation due to the load of a vehicle. This is not related to pavement surface as such, but relates to the layers below the pavement surface, and therefore it is out of scope of the present work. Furthermore, a study prior to the COOEE project estimated that at most a couple of percentages of total rolling resistance (measured with the TUG trailer) were due to pavement deflection on wearing surfaces from normal Danish state roads[161].

Much of the measurement equipment and techniques presented here produces a large amount of data. This is especially the case for modern laser-based equipment used today and thus also in this work. In order to use these data to assess rolling resistance, pavement condition, etc., they are reduced to *road metrics*. Road metrics are used to describe road properties, such as road unevenness, in an easy and quantifiable way, which can then be used for road research and maintenance purposes. Two of the most common road metrics are mentioned in this chapter but several more will be introduced in chapter 4 where a new road metric for rolling resistance assessment is proposed as well. The term 'road metric' will be used interchangeably with 'road measure' and 'road parameter' and 'road' will often be omitted if it is obvious from the context.

Finally, it should be noted that the distinction between road unevenness and texture is rather coarse and the description above is rather vague and intuitive at this point. A much more differentiated view of the surface is presented in chapter 4. However, the unevenness and texture terms suffices for this section as it reflects the practical way of measuring and are also common terminology used by engineers working in the field of road maintenance today[4].

3.3.1 Unevenness measurement

The initial interest in road unevenness traces back as early as 1920s when road engineers wanted to study the relationship between the roads unevenness and the suspension system[156, p.39] which in turn could be used to assess an important aspect of road condition and quality, namely the 'bumpiness'. Since a bumpy road is a great nuisance to its users[5] and can potentially compro-

[4] This is at least the terms used in the Danish Road Directorate.

[5] In the 1960's a correlation between pavement condition ratings (made by a panel of raters) and road unevenness was found in studies by American Association of State Highway and Transportation Officials (AASHTO)[54, p.1]

mise traffic safety, it is of central importance for maintenance purposes of road administrators to measure and quantify this quality of the road . To measure this, road engineers developed the so-called *road meters* or *response-type road roughness measuring system* (RTRRMS) which are vehicles equipped with a measurement device that records the deflection occuring in the suspension system during driving. That is, they did *not* measure the road itself, but the suspension systems *response* to the road. These devices were very popular among engineers[156, p.40] to determine, e.g., road quality, and many of these devices were developed and used in the following decades. Unfortunately, these devices that were the de-facto standard in determining unevenness were used without any standardization whatsoever. Since the measurements were affected by the suspension-system of the vehicle, the vehicle itself, and the measurement device, comparison between RTRRMS's was impossible. For this reason The World Bank initiated a project in 1982 to establish standard methods for correlation and calibration of various different unevenness measurement devices and published it in [158]. Based on the results of [158] and another study by the National Cooperative Highway Research Program (NCHRP) (published in [54]) a standardized measure of road unevenness was formulated. This is the so-called International Roughness Index (IRI) and it is based on a quarter-car model, i.e., a mathematical model of a single wheel and suspension system. IRI is our first example of a road metric/parameter. The mathematical model behind IRI is described in detail in chapter 4. Since it basically models the RTRRMS system it could be seen as a standard for calibration and measurement interpretation of RTRRMS's and this is probably one of the major reasons for IRIs success. The reason for mentioning IRI here, is that even though better and vastly different equipment have been developed since the RTRRM's, modern unevenness measurements are still converted to the IRI metric when used in research and road maintenance. This entanglement of IRI with road unevenness is so widespread that the two terms are used interchangeably by some engineers in the road maintenance community[168, p.25]. This entanglement also happens for road texture and MPD discussed in section 3.3.2.

Different kinds of methods and equipment exists today that attempts to measure the actual road unevenness and not the vehicle response to road unevenness. The most straight forward measuring approach is the so-called 'rod and level' method[156] which is in use today[88]. The idea is to keep a stationary reference stick fixed and then measure the elevation relative to this stick by placing a tripod, with a laser pointing at the reference stick, at a measured distance on the road from the reference stick. Example of usage shown to the right of Fig. 3.1. After measuring the vertical displacement from the reference stick, the tripod is moved a bit further away from the reference stick and a new measurement is made. This is a very slow and laborious process and unfortunately not very reliable[88, p.11]. Another approach is to use inclinometer-based devices such as The Dipstick to measure road unevenness. These devices work by having two supports separated by a fixed distance of 250-300 mm[156, 88] and the slope between the supports is used to calculate unevenness. Some of the inclinometers are on wheels and are hand-pushed by an operator but in the case of the Dipstick it is a cane with two supports mounted at the bottom. After each measurement the operator pivots the cane 180° such that the support that was in front (w.r.t. walking direction) at the last measurement is in the back on the next measurement and so forth. A pictogram of this device is shown to the left in Fig. 3.1.

While the above measurement techniques are used by the road maintenance community, the inertial profilers are by far the most popular and most of the profile data that we have at our disposal in this project originate from this kind of equipment. Nowadays inertial profilers are both used for unevenness and texture measurements, so some of the discussions that apply to both use cases are discussed in the end of this section. The inertial profiler, which was developed

Figure 3.1 Left: Pictogram of the dipstick (taken from [127]). Right: Surveyors measuring with a 'rod and level'. The picture is taken by Intergovernmental Committee on Surveying and Mapping (ICSM) and can be found at http://www.icsm.gov.au/mapping/surveying3.html. Licensed under Creative Commons Attribution 3.0 Australia (http://creativecommons.org/licenses/by/3.0/au/deed.en).

at General Motors Research Laboratories in the 1960s[156], consists of three components: An accelerometer that measures vertical acceleration of the vehicle, a non-contacting sensor (laser, infrared, optical or ultrasonic) measuring surface elevation, and a speed/distance measuring device usually mounted on a host vehicle such as a van. During measurement, the driving vehicle measures the vertical acceleration (cause by, e.g., bumps in the road) of the vehicle and uses this to correct a initial height reference set before driving. This continually revised reference height is subtracted from the elevation measurements performed by the non-contacting sensors thus yielding the final unevenness measurements. In general, laser, infra-red and optical height sensors gives precise and sufficient reproducible measurements of the road profile for use in IRI calculation, *if* profile measurements are properly processed afterwards[87, p.33]. Ultra sonic height sensors have been deemed insufficient[87, p.xiv] since they can be distorted by road texture and are unable to register cracks that would be well within the unevenness range. Optical sensors are sensitive to ambient light and can give erroneous measurements on, e.g., white pavement markings[87, p.11]. Today, lasers are the most widely used technology for height sensors and all of the equipment used in this work have been equipped with lasers for height sensoring. It is interesting to note that while laser, infrared, and optical sensors give reproducible results, there are significant differences in the results due to the different footprint sizes of the sensors, i.e., the diameter of the measuring beam they produce. For instance, in [87] they studied infrared sensors with a footprint of approximately 6 mm in diameter and lasers sensors with a footprint 1-2 mm in diameter and it was shown how the former was unable to capture cracks as precisely as the laser. More generally, the lasers capture much more detailed texture features than infrared sensors and whether this are desirable or not is an open question, that depend on the intended use of the measurements: Small cracks in the pavement does not affect ride quality, for instance, but it does tell road administrators something about the state of the road. It can be argued that local features such as cracks, can be removed by filtering if necessary, but it illustrates the need for clarification about what the measurements are used for.

3.3.2 Texture measurement

While unevenness measurements were initially used to assess road 'bumpiness' as perceived by road users, road texture has been used to assess another important aspect of road quality, namely their 'slipperiness' or 'skid resistance'. This is of course of vital importance in road safety as this is a key factor in breaking distance, etc. so ways of measuring and quantifying texture have been developed for many years. Road texture can be described informally as the 'roughness' of the pavement surface and is, roughly speaking, determined by the mineral aggregates in the pavement mix. The first widely used and investigated measurement method for pavement texture was the so-called 'sand-patch' method (also called volumetric technique[11]) which has been used in connection with skid-resistance research and assessment[110, 30] since at least 1960[100][6]. Although modern laser inertial profilers are gaining ground, the sand-patch method is still in use today and, e.g., sand-patch measurements as new as 2011 from Minnesota Department of Transportations MnROAD pavement test track is publicly available[7]. The popularity of the method is probably to low cost and simplicity, however extremely slow compared to modern measurement techniques used in network level monitoring. Test standards for the sand-patch method have been published by, e.g., the American Society for Testing and Materials (ASTM)[11] and standard EN 13036-1:2010 from the European Committee for Standardization (CEN). The procedure can be summarized as follows:

1. Find a suitable patch of the pavement without cracks or other irregularities and possibly sweep the patch for dirt with a brush.
2. Pour a pile of sand (or glass beads) of a known volume onto the patch.
3. Carefully spread out the sand with a puck or spreading disc such that a circular sand patch is formed.
4. When the level of sand is levelled with the top peaks of the surface, measure the diameter of the resulting circle. This could be repeated several times to get an average diameter
5. Calculate the Mean Texture Depth (MTD) as MTD $= \frac{4V}{\pi D^2}$ where V is volume of sand used and D is the measured diameter.

In the last step the measured quantities (V and D) are converted into MTD. MTD is another example of a road metric just as IRI, although it is easier derived from measurement results.

With the advent of laser inertial profilers, it became possible to make detailed (2D) surface profiles at operating speed but unfortunately the derivation of MTD made little sense with this new equipment. Given the large amount of research and data gathered over the years using the sand-patch method, a new road metric was sought that could correlate with MTD. The result of these efforts is the so-called Mean Profile Depth (MPD) which was standardized in 1996 and 1997 by ASTM and ISO, respectively[10, 75]. The details of the calculation is left for chapter 4, but the important thing here is the fact that MPD calculated by modern laser profilers have been shown to correlate with MTD and thus are compatible with the sand-patch test[45]. It is interesting to note a certain similarity with the development of the IRI metric presented above: The new road metric (MPD/IRI) is essentially a means to make newer measurement equipment backwards compatible, and thus relate them to older equipment[8]. While MTD and MPD were

[6] This is the year of the oldest reference found by the author. Older references might exist.

[7] Overview of MnROAD data collection can be found here: http://www.dot.state.mn.us/mnroad/instrumentation/surfacecharacteristics.html. Last accessed 08/20-2014.

[8] IRI also served another purpose, though, to give a golden standard to use in calibration of the old (RTRRMS) equipment.

primarily used in skid resistance investigations, they have recently also been used in rolling resistance research (discussed in chapter 4).

Today, inertial laser profilers are the preferred method to obtain texture measurements and MPD is the preferred road metric calculated from these measurements and used as an indicator of the surface texture. The principle of these inertial profilers are identical to the ones described in the section about unevenness and these measurement devices will be discussed in more detail below. These are the usual method of choice in network level measurements since they work at highway speeds, but several other texture measurement devices have been developed in recent years that are slower and more precise. These are usually used in research projects etc. Some of these devices measure texture in 3D, for instance the Texture Scanner, developed by Ames Engineering[9], is a stationary measurement device that scans a 100 mm times 75 mm patch of the surface at a vertical resolution of 0.015 mm. Another similar device is the Robotex measurement device developed by Transtec Group, which measures a 100 mm strip at walking speed. Measurements from the latter have been used in this project, and device specification is given in chapter 5. The ability to simultaneously scan the surface in both longitudinal and transversal directions seems very promising. The data they provide will probably prove valuable in future research into road noise, skid resistance and rolling resistance. The author has not heard about any laser 3D-scanning devices used at highway speeds in routine maintenance measurements. However, recent developments in road measuring technologies suggests that this might be possible in the near future[10].

3.3.3 Additional inertial profiler considerations

Inertial profilers are so widely used in road maintenance and research today and they are the primary source of road surface measurements in this project[11], so some additional considerations about these devices are given here.The discussions will generally hold for both texture and unevenness measurements and if any part holds specifically for one or the other it will be mentioned explicitly. We will also focus on factors that affect *laser* profilers in particular.

In [87] results of an elaborate empirical study concerning factors affecting accuracy of inertial profilers measuring unevenness is presented, and a handbook on recommended profiler operation guidelines was based on it[53]. The factors identified were based on decades of roughness profiling experience by members of, e.g., the American Road Profiler Users Group as well as previous studies on the subject[87, p.5] and while the road metrics used for comparison were IRI and Ride Number(RN)[12] the factors can easily be transferred to general profiling practices, surface texture measurement included. They are presented in a slightly modified form below followed by a brief discussion of each. An exhaustive discussion is out of scope here, but further details can be found in [87, 53]. Four distinct factors have been identified:

- **Surface Shape**: Geometrical properties such as isotropy, texture and cracking.
- **Environment**: Environment in which the measurements takes place, such as temperature, humidity etc.

[9] See http://www.amesengineering.com/TextureScanner.html. Last accessed 08-21-2014.
[10] A glimpse of these new developments have been shown at the TRIMM/ERPUG conference, 23rd-24th of October 2014.
[11] Since the 3D Robotex equipment also uses laser height sensors, some of the discussions here will also apply to this device.
[12] The Ride Number is index to describe ride quality. It was developed under the National Cooperative Highway Research Program[156, p.55].

- **Operation**: How the profiler is used, i.e. changes in speed, transversal position, awareness of road irregularities and so on.
- **Equipment design**: Design of the measurement equipment such as sample frequency, measurement resolution, initial data processing etc.

Surface and road shape

General properties of the surface can have a big effect on unevenness and texture profile measurements and their repeatability. One of the major factors are the transversal variation, i.e., different transversal positions of the height sensor yields different results. Transversal variation can be caused by many phenomena at many different length-scales: At the texture level, each small (mm-scale) mineral aggregate affect the profile such that two parallel longitudinal profiles, which are transversally close, exhibit significantly different profiles as different mineral aggregates lie in their paths. Even two profiles measuring across the same small stone can exhibit variation depending on where the two profiling paths crosses the stone. At larger length scales, there are various phenomena like rutting, polishing, crocodile cracking, potholes etc. that give rise to local variations. See Fig. 3.2 for examples of this. Some of these variations might be a primary concern for texture measurements, some for unevenness or some a concern for both. A special case is concrete pavements that can be textured by, e.g., diamond grinding which creates a systematically textured surface thus making it especially sensitive to transversal position (see Fig. 3.3 for an illustration of this). With asphalt based pavements, an additional factor is how the pavement mix is handled and laid out during road construction. Improper handling can cause, e.g., heterogeneous distribution of mineral aggregates in the pavement mix which might make profile measurements more sensitive to positioning. In [87] variation in unevenness measurements was studied through the road metric IRI, by letting the profiler operator keep the height sensor at the center line of the wheel tracks within a margin of $+/-30$ cm. The results showed[87, p.47] that on newly laid asphalt (less than 6 months) there was a variation in measured IRI of 0.13 and 0.05 on the two wheel tracks, respectively. On old worn asphalt with mild rutting the numbers were 0.65 and 0.37, respectively. By comparison, the overall IRI range of the experiment, which included pavements and in a variety of conditions was 0.56 to 4.40, so the variation is far from negligible. Transversal variation and general isotropy of surface texture will be investigated in chapter 5.

While transversal variation is to be considered when interpreting measurements, it is not necessarily caused by errors but rather reflect the fact that irregularities exists in the pavement. Even if we had two hypothetical 'true' profilers that measured the road with infinite detail, they would still produce different longitudinal profiles if they measured at different transversal positions. The following factors of the surface shape can cause outright erroneous measurements. Cracking is another contributor to inaccuracies in the measurements and if not handled properly, can cause erroneous or invalid readings that can bias the resulting road metric calculation. For instance, a crack with a width smaller than the sampling interval will, if detected, appear wider than it actually is. This phenomena is related to the problem of *aliasing*[85, p.73], the theoretical details of which have been discussed in section 2.6. It is not just a theoretical problem though, and aliasing-related problems have been observed and studied in connection with unevenness measurements and IRI calculation[87, p.119][85, p.2]. The latter is highly sensitive to distortion of the frequency domain. It is especially significant with laser profilers because of the narrow height sensor footprint[86, p.16] which makes it easier to detect local features and cracks that contributes to the higher frequencies. Thus, frequencies at, e.g., the texture level can affect

Figure 3.2 Pictures of pavement deterioration that introduces local features in the surface. The pictures have been taken from the Danish Road Directorates 'Vejregler'[174] (http://vejregler.lovportaler.dk).

Figure 3.3 Picture showing non-isotropic concrete pavement surface due to diamond grinding treatment. It was taken at the Minnesota MnROAD testing facility and can be found on the web at http://www.thetranstecgroup.com/fhwa-mndot-investigate-pavement-surfaces-effect-fuel-consumption/.

lower frequencies in the unevenness level. As mentioned in section 2.6 aliasing can be mitigated by applying a analog filter before digitisation or by measurement aggregation, however the implementation details of this are probably specific to the vendors of the profiling equipment and kept a business secret.

On a higher length scale, the road curvature can possibly affect profile measurements since it can distort the accelerometer measurements. Tests reported in [87, p. 77] showed that unevenness profile measurements where affected by curvature, although the affected wavelengths were rather large (8 - 40 m) and did not even affect calculations of IRI. Therefore it seems highly unlikely that curvature should affect profiling at the texture level. The error on unevenness measurements was also investigated for hills and grades and reported to be "extremely small" [87, p. 79].

Environment

While other height sensors might be sensitive to wind or ambient light, the laser sensor is incredibly robust. Nevertheless, there are a few environmental factors that can affect laser sensors. Temperature is mentioned in [87] as a potential cause for inaccuracies, especially with temperature gradients along the direction of measurement, although a previous study reportedly found the effect negligible[87, p.81]. The sensors are also very robust with respect to ambient temperature. Selcom, one of the main laser sensor manufacturers, specify their sensors to work in ambient temperatures ranging from 0 to 50° C and a temperature stability (error) of 0.01% of the total measurement range per $^{\circ}$ C[13] which should be sufficient for most locations and measurement objectives. The same goes for humidity which is specified to work in a relative humidity of 95% that is *not* condensing. It is of course important to avoid condensation on the equipment (especially on lenses, mirrors etc.) as this will distort the measurements. The same goes for surface moisture which is to be avoided entirely, especially when measuring in the texture range. Needless to say, profiling a road with snow or ice is not possible. Road contaminants like leaves, dirt etc. are also to be avoided, if possible. However, this can be hard to remove when measuring on, e.g., a highway and in that case if the operator observes contaminants in the vicinity of the height sensors, a marking should be made for removal in subsequent data processing. To illustrate the impact of road contaminants, a piece of tyre tread with a height and width of 2.5 cm can contribute 0.09 m/km to the measured IRI value of a 160 m section[87, p.83]. In the case of texture measurements the impact would be much higher, but extreme cases likes this should be easily detectable during data processing.

Another slightly different environmental factor that affects profiling is the general seasonal fluctuations in meteorological conditions such as precipitation, humidity, and temperature which affect the pavement, and pavement surface. In the case of asphalt pavements, subsurface layers can be sensitive to moisture which, when combined with freezing temperatures, can expand substantially and thus create bumps in the pavement which can subside when temperature rises again[87, p.59]. This is essentially a particular instance of the general phenomena called 'frost heave' [14] and is also the preliminary phase in pothole formation. While the seasonal meteorological variation plays a big part in this, it is not very systematic given the erratic behaviour of the weather. However, it is closely related to freezing temperatures[87, p.60]. In addition, large volumes of traffic and other factors can also play a role when looking at time scales of months or even years[15]. Note that these considerations concerns unevenness measurements only, and no known problems of this kind have affected texture which would probably also 'drown' in other disturbances such as wear and transversal positioning.

Operation

There are some important considerations to make when using a profiler which we will briefly touch upon below since it gives some background knowledge of the data used in the following chapters. However, a thorough treatment will not be relevant here. Some precautions have already been mentioned above: Checking height sensor equipment for condensation, keeping an eye on possible road contaminants or irregularities that would distort the measurements, and try to keep a steady transversal position. In many cases, the transversal position should be in

[13] Based on the specifications of the SLS7000 and SLS5000 16kHz laser series.
[14] See `http://en.wikipedia.org/wiki/Frost_heave` for a general description of frost heaving.
[15] Concrete pavements should also exhibit daily variations[87, p.55] but this is out of scope with the present investigations.

the wheel track since this is where most vehicles are driving. It is especially important in the case of texture measurements that are highly sensitive to smoothing of the surface. Another phenomenon that can introduce measurement errors is heavy vehicle deceleration/acceleration during operation which introduces wrong accelerometer readings, thus producing erroneous profiles.

Equipment design

In [87] a lot of investigations are devoted to studying profiling design. Some of this is relevant for texture profiling as well, but it should be kept in mind that a lot of technological developments have occurred in 15 years. For instance, the technology of height sensors has improved: It is mentioned in [87] that the sampling interval is as low as 10 mm[87, p. 6] and laser footprint is 1-4 mm in diameter with a vertical resolution of 0.06 mm[87, p. 32-33] for Selcom lasers. Nowadays Selcom lasers samples with a frequency of 16 to 64 kHz[16] and a laser footprint of 0.07 mm in diameter with a vertical resolution of 0.00015 mm (worst case 0.0015 mm)! This means we have much better data at our disposal, and detailed texture measurement can be made on a road network scale, and operating at highway speeds. The sampling interval given in [87] is not very precise since it is not mentioned what speed is used or if anti-aliasing measures have been performed before the measurements are stored. Nevertheless, since we know that highway speeds are around 100 km/h and that 64 kHz lasers are presently used in texture measurements, we have a sample interval of

$$\frac{100 \text{ km/h}}{64\text{kHz}} = \frac{1 \times 10^8 \text{ mm/h}}{64 \times 10^3 \text{ Hz}} = \frac{27.78 \times 10^3 \text{mm/sec}}{64 \times 10^3 \text{ sec}^{-1}} = 0.43 \text{ mm}.$$

Whether or not this sample interval includes anti-aliasing filtering is unknown and the filtering done on-the-fly by the profiling equipment is a business secret. This makes it hard to get information on the filtering algorithms, what algorithms are used, if they are applied to the analog or digital signals, etc. (see section 2.6 for a discussion of anti-aliasing). A further complication is the variability of equipment, algorithms etc. among different profiler manufacturers, which also explains why some variation between texture profilers have been observed[17]. Nevertheless, the sample interval derived above gives a rough estimate on the capabilities of present road profiling technology and is backed up by actual data: The road network level data used in appendix A includes texture measurements with an average sample spacing of 1 mm. While aliasing is still an obstacle to consider, it seems that technologies have improved on the data-acquisition side such that the aliasing problems encountered are primarily due to improper data processing.

While height sensor resolution has improved and error sources reduced, the longitudinal measurement devices were already rather stable 15 years ago: A study in [87] showed that five repeated longitudinal measurement runs by four different profilers of a 14.3 km road segment resulted in a variation of 0.04-0.07% of the total range between the maximum and minimum of the five runs. In addition, the inter-profiler variation was about 0.4%[87, p. 38]. The latter variations were suspected to be caused by calibration errors. All in all, this is a very small margin of error which could be due to small changes in effective rolling radius of the tyre since calibration[18]. Variations in effective rolling radius can be caused by changes in tyre pressure

[16] DRD has a road profiler with 78khz lasers, but this is an extraordinary high sampling rate.

[17] In a personal communication with Jens Oddershede from the Danish Road Directorate, he informed the author that measurements from a few profilers have indeed differed during comparison measurements on a known surface.

[18] The term 'effective rolling' refers to the fact that the tyre is loaded and rolling. The radius of a tyre differs between 1) loaded and stationary 2) Loaded and rolling (as in this case).

or temperature (which causes a change in tyre pressure as well). Although the longitudinal measurement error is small, it can accumulate over large distances and thus be a problem for network profiling. This is usually solved by comparing longitudinal measurements to chainage markings[19] on the roads.

The accelerometer can affect the resulting profile measurements if it is disturbed by, e.g., hills and curves on the road etc. as described above.

Another aspect that we are not going into here is the case where the signal from the measurement components are lost or disturbed. This can be hard to detect, but should be taken care of by the profiler operator. These signal disturbances can also introduce spikes in, e.g., texture profiles which can be detected and removed during data processing.

3.4 Concluding remarks

The intention of this chapter was to give a general introduction to the phenomena of rolling resistance with an emphasis on the rolling resistance components that are related to the road and surface geometry. Ideally, a continuum of different length scales are involved in the tyre/surface interaction, but in practice two concepts/properties have been used to identify two different length scales: Texture and unevenness of the road. The development of these two concepts are closely related to how they are measured and this development has also been covered. In addition, an overview of present measurement methods have also been given for both road surface properties and rolling resistance. It is interesting to note that the present popular road metrics IRI and MPD are so closely related to first generation road measurement methods, as have been described above. However, we have avoided the technical details of these metrics which will be covered in the next section. This chapter has set the scene by introducing general concepts and techniques together with a review of their developments. The next chapter will be focused on the present work in relation to rolling resistance and surface modelling.

[19] The term 'chainage' refers to a longitudinal length measure of the road used in road surveying and classification.

4 Development of new Texture Measure for Rolling Resistance Assessment

This chapter is a continuation of the previous chapter that concerned rolling resistance and measurement techniques in a general and historical perspective. Here we present some details of the popular road metrics as well as particularly interesting developments related to rolling resistance which leads to a proposal for a new texture metric for rolling resistance assessment. Some studies will be thoroughly discussed as they have directly influenced our own work in proposing a new texture measure. Other ideas and investigations are mentioned for completeness and because they were good candidates for further pursuit in this work.

Before going into specific studies and results, an introduction to the technical background behind the road metrics used today for measuring road unevenness, texture etc., is given. The history of the most important ones, namely International Roughness Index (IRI) and Mean Profile Depth (MPD), have already been covered in the previous chapter but the technical details will be described and discussed below.

4.1 Surface Classification and Current Road Metrics

As mentioned in section 2.6, Fourier analysis has been frequently used in road engineering (mostly in research about traffic noise) and the modern classification of road properties is expressed in the Fourier analysis terminology of wavelengths. The first reference relating surface wavelengths to noise, skid resistance, rolling resistance, etc., that the author could track down, is a technical report by PIARC in 1978[1, 42]. Furthermore, addition, the division of surface characteristics into 'unevenness' and 'texture' have also been expanded into more categories. An overview of wavelengths, texture classification, and influences was given in [42], which has been modified and updated in [152]. The latter has been reproduced in figure 4.1 with minor modifications. The old road surface characterisation with 'unevenness' and 'texture' which, historically, have been closely connected with measurement practices, are defined in figure 4.1 as 'unevenness' with spatial wavelengths in the range of 0.5 - 50 m and 'macrotexture' (i.e., 'texture') in the range of 0.5 to 50 mm. It is well established that macrotexture (usually represented by MPD) does affect rolling resistance, so the bar which indicates the frequencies relevant to rolling resistance in figure 4.1 has been lengthen closer to microtexture compared to the overview given in [152]. While the classification is rather coarse, it gives a good overall view of the different aspects of the road and the phenomena usually studied by road engineers.

Presently, laser-based 2D profiling equipment exists such that unevenness, megatexture, and macrotexture can be measured at traffic speed. In the Danish Road Directorate (DRD) this is accomplished by two different sets of profiling lasers, one set covers (approximately) megatexture to unevenness and the other set measures macrotexture. The microtexture range is too small for these kind of measurement, but a study of microtexture is possible by, e.g.,

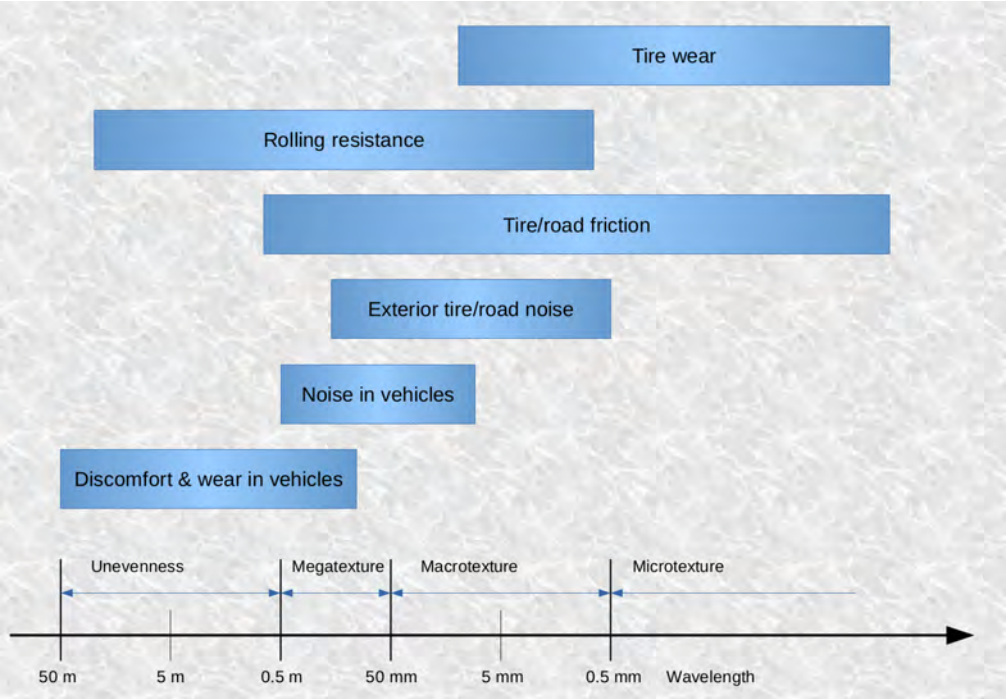

Figure 4.1 Illustration of the different road surface domains and some general indicators as to which wavelengths affect which aspect of road transportation.

extracting pavement samples and treating these in the laboratory[1]. However, since microtexture is not assumed to significantly affect rolling resistance, this is out of scope with the present work. It should be noted that with the recent developments in profiling equipment, routine measurements in 3D instead of 2D will be possible in the not so distant future[2].

As mentioned above, IRI and MPD are presently used in rolling resistance assessment, modelling, and they are used in the work described below. Thus, a description of them is given here.

IRI is defined in terms of quarter-car model, as mentioned in chapter 3. More specifically, it is defined as system of linear differential equations

$$m_s z_s''(t) = c_s z_u'(t) + k_s z_u(t) - c_s z_s'(t) - k_s z_s(t) \tag{4.1}$$

$$m_u z_u''(t) = c_s z_s'(t) + k_s z_s'(t) - c_s z_u'(t) - (k_s + k_u) z_u(t) + k_u h(t) \tag{4.2}$$

comprising of two masses m_s, m_u tied together by a spring k_s and a shock absorber c_s. m_s represents the quarter-car as a whole while m_u represents the wheel which in turn is related to the road profile $h(t)$ by another spring k_u representing the vibrations of the tyre.

[1] In DRD this is achieved by covering the samples with fluorescent epoxy which are then photographed through a microscope.

[2] An example of state-of-the-art in profiling equipment was demonstrated at the ERPUG 2014 meeting (23-24 Oct.) in Brussels.

A schematic drawing of the system is shown to the left in figure 4.2. Using this quarter-car model, the systems response R to the road profile $h(t)$ over a road segment of length L driving at speed v is defined to be

$$R = \frac{1}{L}\int_0^{L/v} |z_s(t) - z_u(t)|dt. \tag{4.3}$$

This should emulate the workings of the RTRRMS equipment mentioned in section 3.3.1. Reference parameters[54, p.78] defining the IRI quarter-car relative to car weight are

$$k_s/m_s = 62.31/\text{sec}^2 \quad k_u/m_s = 653\text{sec}^2 \quad m_u/m_s = 0.150 \quad c_s/m_s = 6.001/\text{sec}^2 \tag{4.4}$$

The response R defined in equation 4.3 is also the IRI value when parameter values in equation 4.4 are used. A description of the system in term of its frequency response function using the IRI parameters are given to the right in figure 4.2. This highlights the frequencies of the road profile that will be attenuated/enhanced by the system. Note how the response function varies significantly across different parameter sets. It also illustrates the problems with aliasing mentioned in 2.6 since high frequencies, if not properly filtered, might cause aliases at lower frequencies important to the IRI measure. IRI is widely used today (i.e., the de facto standard) as measure of road unevenness, and is usually derived from road profiles obtained from laser equipment. However, it is questionable whether the parameters in equation 4.4, which have been derived from a an American personal car in the seventies, are still representable for modern cars in use today. Moreover, IRI is used in ride comfort estimation, pavement condition number and as a road parameter in rolling resistance estimation[63, 15] and especially the latter use was not intended when the road metric was designed. Thus renewed investigations into road metrics, IRI in particular, aimed at the unevenness property of roads might be relevant, especially for rolling resistance. Nevertheless, the quarter-car model is a great simplification of reality, that has proven very useful in research and maintenance.

MPD is the other major road metric used in rolling resistance modelling, as well as skid resistance and noise assessment. As mentioned in chapter 3, MPD was created as a measure that could be calculated from 2D road profiles (usually measured by a laser) and correlated with volumetric methods like the sand patch test. Thus it is the macrotexture that this road metric tries to assess. How the idea for the algorithm came to be as it is, is unknown to the author, but the calculation procedure is specified and standardised in ISO 13473-1[75] and ASTM E1845[10]. The procedure described in ISO 13473-1 can be summarised as follows:

1. The profile data used in the calculations should be of proper quality. E.g., Longitudinal resolution should be at least 1 mm and vertical resolution must be at least 0.05 mm.
2. The profile data used in the calculations should be properly filtered such that wavelengths not in the range between 100 m and 2.5 mm are removed/attenuated. If step 4 is performed, the high pass part of the filtering can be omitted.
3. Partition the profile in 100 mm high-resolution segments.
4. Slope suppression: Normalise the profile by calculating the regression line based on the profile and subtract it from the original profile.
5. Divide the segment into 2 50 mm sub-segments and find the maximum value of both sub-segments.
6. Take the average of these two values which gives the Mean Segment Depth (MSD).

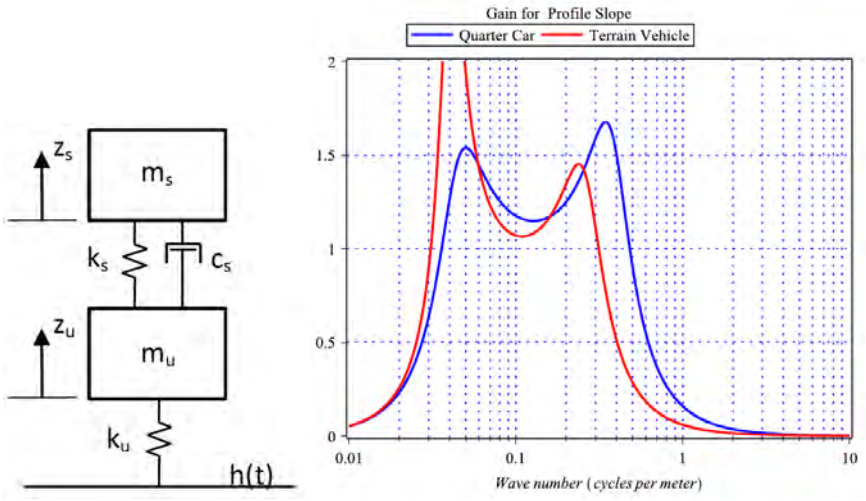

Figure 4.2 Left: Schematic drawing of the quarter car model. Right: Gain factor for quarter car system with 1) 'golden car' parameters used in IRI calculations[155] and 2) average parameters for terrain vehicles[101]. The plot is taken from [4].

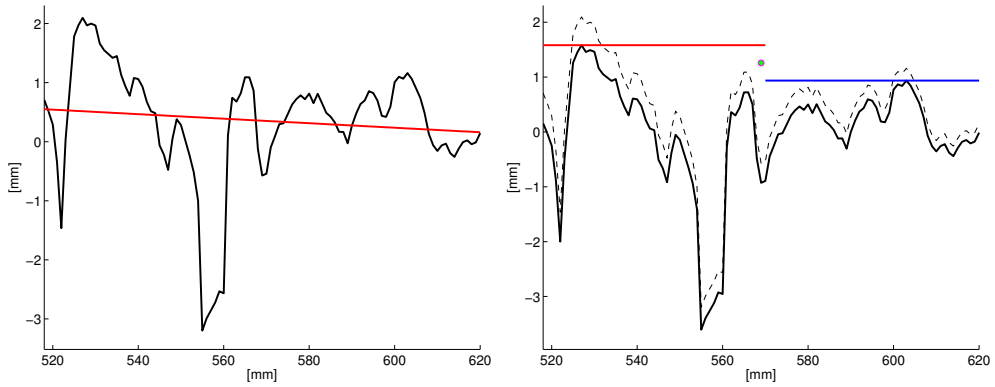

Figure 4.3 Illustration of MPD calculation algorithm using a piece of profile from coast-down measurements introduced in chapter 6. Left: Original profile and the regression line estimated from it. Right: Dotted line is original profile, solid black line is the profile after regression line has been subtracted, blue and red horizontal lines are the two halves maxima and the green dot is the resulting MPD value.

7. Take an average of at least 10 MSD values (i.e. for an entire meter of profile segment) which gives the MPD.

The essentials of the procedure are also illustrated in figure 4.3 using a real profile segment from the coast-down experiments from chapter 6. Note that MPD values correlates well with Mean Texture Depth (MTD), which is the number obtained by the sand patch method. In [75, p. 9] the

conversion is performed by using

$$\mathrm{ETD} = 0.2\mathrm{mm} + 0.8\,\mathrm{MPD}\,.$$

The author is not aware any theoretical or intuitive basis for this method, except that it should correlate with MTD. Nevertheless, this is the de facto standard road metric used to describe road texture and it is used in practically every study to be discussed below. It should be noted that as of writing this, the MPD calculation ISO standard is being revised. One of the general design goals of this revision is to make MPD calculations more uniform across different equipment of different quality. To achieve this goal high frequencies that less precise profiling equipment is unable to measure, should be attenuated[3]. Other proposals are the relaxation of the vertical and longitudinal resolution to 0.1 mm and 1.5 mm, respectively, and the Butterworth filter[24] is to be used for profile filtering. While this should improve comparability, it is hard to eliminate discrepancies entirely, given that profilers differ in equipment, algorithm implementation etc. as mentioned in section 3.3.3.

Other road metrics have been used concurrently with IRI and MPD in rolling resistance studies. For instance, ISO 13473-2 contains several different terms and parameters that can be used to handle and process profile data. In the following, $y(s)$ refers to a function representing vertical displacement at distance s[76, p.12]. Additionally, it is assumed that $y(s)$ have zero mean and low frequencies have been removed.

An example from ISO 13473-2 is Root Mean Square(RMS) deviation from the profile which has been used in some recent studies[153, 63] that measures the variability of a profile. It is defined as[76, p. 12]

$$\mathrm{RMS} = \sqrt{\frac{1}{L}\int_0^L y^2(s)ds}. \tag{4.5}$$

While the formulation in [76] is expressed in terms of a continuous function, the profile is made up of discrete measurements, so linear interpolation interpolation must be made beforehand. Another straightforward approach is to adapt equation 4.5 to handle a finite set of samples in which case equation 4.5 is transformed to

$$\mathrm{RMS}_{\text{discrete}} = \sqrt{\frac{1}{N}\sum_{i=1}^{N} y_i^2}. \tag{4.6}$$

Note that since the mean $\overline{y}$ of the samples is 0 by definition, equation 4.6 can be rewritten as

$$\mathrm{RMS}_{\text{discrete}} = \sqrt{\frac{1}{N}\sum_{i=1}^{N}(y_i - \overline{y})^2} \tag{4.7}$$

which is the formula for estimating sample variance (second moment) of a population. The RMS road metric can be adapted to specific wavelength ranges by applying proper filtering of the profile before calculating RMS[153, 63]. Thus, if the RMS of the megatexture is sought, wavelengths not in range of 50 mm - 0.5 m should be removed/attenuated. In [76, p.14] the 'texture profile level' is essentially based on this, where filtered RMS values are expressed as

[3] This was some of the content of the talk given by Ulf Sandberg at TRIMM/ERPUG conference, 23rd-24th of October 2014.

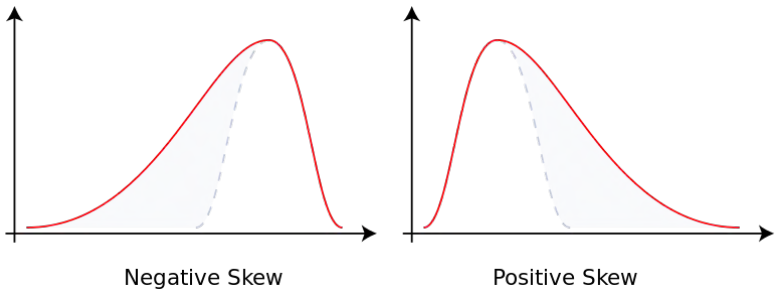

Figure 4.4 Illustration of the different modes of skewness.

ratios between RMS values for particular wavebands, usually expressed in third-octave bands, and the RMS value of the third-octave waveband centred about 10^{-6} m, i.e.

$$L_\lambda = 20 \log_{10}(a_\lambda / a_{ref}) \tag{4.8}$$

where L_λ is texture measure (in decibels) at the third-octave band centred about the wavelength λ, a_λ is the RMS value of the profile filtered with a third-octave band filter centred about λ, and a_{ref} is the RMS calculated from the the profile filtered by a third-octave band filter with centre wavelength of 10^{-6} m. Several variations of this approach exists, such as using octave band filters instead of third-octave bands. Another common approach, used in some of the studies discussed below, is to encompass several third-octave bands in a band filter, e.g., L_{Mi} refers to a band-bass filter where the passband is comprised of all third-octave bands in the microtexture range. Equivalently, L_{Ma} is defined with the macrotexture third-octave bands, L_{Me} used the megatexture third-octave bands, or even a custom passband can be used. A brief overview of the third-octave bands used in road characterization is given in table 4.1

While RMS describes variability, it does not distinguished between profiles consisting primarily of trenches and profiles consisting of spikes. In other words, it does not take the possible asymmetry or skewness in the distribution of vertical displacements into account. This, however, is what the Skew measures and it is expressed as[76, p.13]

$$\text{Skew} = \frac{1}{\text{RMS}^3}\Big(\frac{1}{L}\int_0^L y^3(s)ds\Big). \tag{4.9}$$

As illustrated in figure 4.4, a symmetric distribution (e.g., the normal distribution) has $\text{Skew} = 0$, a asymmetrical distribution with the density shifted to the left has $\text{Skew} < 0$, and $\text{Skew} > 0$ if the density is shifted to the right. Using analogous arguments as in the case of RMS, the Skew can be adapted to work with a discrete set of samples, and using the fact that $\overline{y} = 0$ it can be shown that it corresponds to an estimator of skewness (third moment) of a population distribution.

Another term, which is not a road metric directly, is the *envelope* of a profile[76, p.11]. When a tyre runs over a non-smooth road surface, the tyre is pushed down into surface by the weight of the vehicle and since the tyre is made up of visco-elastic material, the peaks/spikes of the surface is indented into the tyre. However, the tyre might not come in full contact with the road surface, since it usually has surface valleys/grooves, as illustrated in figure 4.5. The pseudo-profile that simulates this contact line between tyre/surface and tyre/air, in the case of valleys, is called the

Table 4.1 List of third-octave bands and the texture range they belong to. The table is an adapted version of table 1 in [76].

Centre Frequences [mm]	
Octave band	One-third-octave band
Microexture	
	0.4
0.5	0.5
Macroexture	
	0.63
	0.8
1.0	1.0
	1.25
	1.6
2.0	2.0
	2.5
	3.15
4.0	4.0
	5
	6.3
8.0	8.0
	10
	12.5
16.0	16.0
	20
	25
31.5	31.5
	40
	50
Megatexture	
63	63
	80
	100
125	125
	160
	200
250	250
	315
	400
500	500
Unevenness	
	630

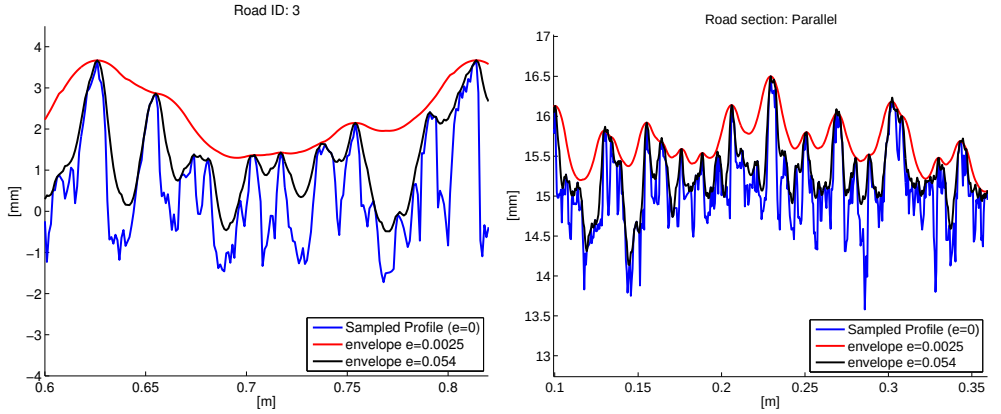

Figure 4.5 Illustration of the envelope procedure described in [115]. To the left is an example of enveloping of one of the VTI road sections used in chapter 6 and to the right is an example from a road section used in chapter 5.

profile envelope. Many different algorithms exists that are able to approximate this behaviour. Some of these are of a more empirical nature[115] while others are based on physical principles of visco-elastic bodies[93] and are thus much more theoretical in their formulation. However, while the latter kind of algorithms are much more theoretical they are still approximative, complex and not guaranteed to do a better envelope simulation[153, p.58] than the fast but empirical approach of [115]. Because of the complexity of the theoretical approaches, they are too remote from the practical goals of this work (as discussed in the introduction). Nevertheless, the ideas are very interesting and future work in this area is promising.

The method in [115] is basically to put an upper bound on the size of the second derivative of the profile $y(s)$, i.e.

$$|D^2 y(s)| \leq e \tag{4.10}$$

for some parameter e. If only (uniformly) samples values of $y(s)$ are available a finite differences method can be deployed to equation 4.10. Assuming the sample distance is Δs we can approximate $D^2 y(s)$ at sample point s_0 by

$$D^2 y(s_0) \approx \frac{Dy(s_0 - \frac{1}{2}\Delta s) - Dy(s_0 + \frac{1}{2}\Delta s)}{\Delta s}. \tag{4.11}$$

The two first order derivatives can be approximated by

$$Dy\Big(s_0 - \frac{1}{2}\Delta s\Big) \approx \frac{y(s_0) - y(s_0 - \Delta s)}{\Delta s} \text{ and } Dy\Big(s_0 + \frac{1}{2}\Delta s\Big) \approx \frac{y(s_0 + \Delta s) - y(s_0)}{\Delta s}. \tag{4.12}$$

Substituting equation 4.12 in equation 4.11 and rearranging yields

$$
\begin{aligned}
D^2y(s_0) \approx \frac{\frac{y(s_0)-y(s_0-\Delta s)}{\Delta s} - \frac{y(s_0+\Delta s)-y(s_0)}{\Delta s}}{\Delta s} \leq 2e \Leftrightarrow \\
\frac{y(s_0) - y(s_0-\Delta s) - (y(s_0+\Delta s) - y(s_0))}{\Delta s^2} \leq 2e \Leftrightarrow \\
\frac{2y(s_0) - [y(s_0-\Delta s) + y(s_0+\Delta s)]}{\Delta s^2} \leq 2e \Leftrightarrow \\
\frac{y(s_0) - \frac{1}{2}[y(s_0-\Delta s) + y(s_0+\Delta s)]}{\Delta s^2} \leq e
\end{aligned}
$$

where the last expression is the formula given in [115]. The parameter e from equation 4.10 can be interpreted as a parameter of the tyres stiffness. In [115] a value for e of $0.054[m^{-1}]$ was found to be optimal and is also the value used in the trailer comparison study [15]. The method from [115] was originally used in tyre/surface noise modelling, but recent studies in rolling resistance assessment have shown very interesting results when used in combination with classical road metrics such as MPD[15, 153]. This is the primary reason for using enveloping in later chapters.

4.2 Recent Work on Road Surface Influence and Rolling Resistance

In this section we will briefly discus some of the recent work on practical rolling resistance assessment that have inspired the work presented here. For instance, these studies also use 2D/3D texture laser profiles, trailer rolling resistance measurements and in general there is a similarity in methodology, which is empirical in spirit. Thus, the investigations presented in chapters 5 and 6 is seen as a continuation of the work presented here. In the latter chapter, however, the rolling resistance is not given directly as trailer measurements, but is extracted from coast-down measurements instead. The specifics of this, and the study it is based on, will be postponed until chapter 6.

Notice that the TUG rolling resistance trailer is frequently used for measurements in this kind of studies and besides our own data in chapter 5, it has also been used in the studies discussed here. All of TUGs rolling resistance measurements presented in this thesis use a small selection of tyre types. They are described in table 4.2 where it is also specified which measurement campaign uses which tyres.

4.2.1 MIRIAM project studies

The first study to be discussed here have been undertaken by the MIRIAM project which is a collaborative project between partners primarily from Europe but also USA. One of the MIRIAM projects major studies focused on rolling resistance trailer equipment. More specifically, they tested three different rolling resistance trailers with a collection of different tyres by doing comparable measurements on a French test track. In addition, the rolling resistance of the tyres was measured at two different drum testing facilities. Based on these measurements, several investigations were made and a subset of these that are interesting for our later investigations and discussions, will be examined here.

The three different trailers were supplied by TUG, the Belgian Road Research Centre (BRRC), and Bundesanstalt für Straßenwesen (BASt). These trailers varies significantly in design, which of course complicates comparison. However, they all measure in the center wheel

Table 4.2 Information about test tyres for all projects discussed in this thesis. MIRIAM-RRT refers to the study discussed in section 4.2.1, MnRoad refers to the study discussed in section 4.2.2, Dutch M+P refers to the study discussed in section 4.2.3, and COOEE refers to measurements obtained in this project which discussed in chapter 5.

Tyre	SRTT	AAV4	MCEN16	MCEN14
Manufacturer	Uniroyal	Avon	Michelin	Michelin
Size	P225/60R16	195R14C	225/60R16	195/70 R14
Index	97S	106/104N	98V	91T
Thread	TIGER PAW	SUPERVAN AV4	Energy Saver	Energy Saver
Measurement campaign	MIRIAM-RRT COOEE MnRoad Dutch M+P	MIRIAM-RRT COOEE MnRoad	MIRIAM-RRT COOEE MnRoad	MIRIAM-RRT

path. Some important design features are listed in table 4.3. Since the TUG trailer have also been used in the COOEE project it will be our primary focus. The test track used for measurements is

Table 4.3 Overview of trailer features. This table is reproduced from table 3.1 in [15].

Owner	BASt	BRRC	TUG
Test tyre size	14"-16"	14"	14"-16"
Wind shield	yes	no	yes
Measurement method	force	angle	angle
Number of test tyres	1	1	1
Number of supporting tyres	2	0 (test tyre supports)	2
Self-supporting construction	no	no	yes
Tyre load	4000 N	2000 N	4000 N
Tyre pressure	200 kPa	200 kPa	210 kPa
Tyre temperature measurement method	exterior	exterior/interior	exterior
Corrections made during measurement or afterwards	afterwards	afterwards	during measurement
Measurement wheel position	middle track	middle track	middle track

located in Nantes, France, and is owned by l'Institut Français des Sciences et Technologies des Transports, de l'Aménagement et des Réseaux[4] (IFSTTAR). It is composed of 12 test sections

[4] French institute of sciences and technology for transport, development and networks

between 50 and 250 meters in length, with different pavements and thus different surfaces. BRRC measured the test sections with laser profiling equipment at a resolution of 0.2 mm in the longitudinal direction and 1 μm in the vertical direction[15, p.72]. The surfaces spans a wide selection of textures with a range in MPD-values from 0.08 to 2.77. An overview of the test sections is given in table 4.4. As table 4.4 shows, there are some surface disturbances on

Table 4.4 Overview of road sections from the Nantes test track. This table is a simplified union of tables 4.2, 4.3, and 4.4 in [15].

Section	**Length** [m]	**Width** [m]	**MPD**	**Remarks**
M1	244	3.00	1.14	Grinded in middle, steel plate at 1550 km point.
F	250	3.00	1.00	-
L1	128	3.00	0.08	Epoxy Resin (smooth section).
L2	116	2.50	0.42	-
E1	252	3.45	0.59	Road markings in middle, crack.
E2	250	3.45	0.82	Disposed and existing road markings in middle.
M2	150	3.90	0.86	-
C	244	3.00	0.35	Transversally uneven, cracks, repaired cracks.
N	185	2.60	1.92	Interrupted at west end by concrete plates.
A	50	3.00	0.93	-
A'	220	3.00	2.77	-
CC	90	-	0.35	-

some of the road strips such as, e.g., road markings. In addition, the road sections vary in width, which make it hard for trailer operators to measure in the same path throughout the test track. All measurements in this campaign are divided into two categories with respect to speed, 50 km/h and 80 km/h. Moreover, before performing measurements the tyres were warmed up by driving approximately 80 km/h for 15 minutes. All measurements were performed from the 6th to the 10th of June, 2011, and no temperature corrections have been used in this study. An overview of the tyres can be seen in table 4.2 and specific hardness measurement results of each tyre is shown in table 4.5. As can be seen from table 4.5 the trailers have their own tyre of a given type and tyres of the same type varies in hardness. Finally, it should be noted that the trailer measurements and testing were performed by different teams, which is reflected in the results that sometimes differs slightly in content and presentation.

The three trailers were investigated for two kinds of variation, day-to-day and short term. Unfortunately, the TUG trailer was not investigated for day-to-day variation. Short term variation means variation between measurements performed immediately after one another. The short-term tests were performed by making several measurements for different combinations of tyre, test section, speed, and direction for each trailer. Of course, exhausting all possible combinations would be practically impossible[5], so only a small subset has been chosen and the subset varies with the trailer being tested. However, for each trailer, road section, tyre configuration all combinations of direction and speed were tested. The specific details and overall results of the short term measurements for each trailer are summarized below. For each configuration the standard deviation was calculated and expressed as a percentage of the mean rolling resistance value.

[5] There is a total of 576 combinations of trailer, tyre, test section, speed, and direction which should be measured *several* times.

Table 4.5 Information about hardness of test-tyres from [15, p.25]. Note that AAV4-CT refers to a specific AAV4 tyre with a poor tread alignment.

Tyre	**Hardness** [Sh]*
SRTT/TUG	65
SRTT/BASt	68
AAV4/TUG	62
AAV4-CT/TUG	64
AAV4/BASt	64
MCEN16/TUG	63
MCEN16/BASt	66
MCEN14/TUG	63
MCEN14/BRRC	66

BASt Measured the SRTT, AAV4 and MCEN16 tyres on L2 and M1. All combinations were measured 4-6 times except for L2 with ES16 at 50 km/h which was measured 2 and 3 times for east and west, respectively. Average standard deviation of all combinations is **2.6%**.

BRRC Measured the ES14 tyre on L2 and M1. Every combination were measured 10-11 times. Average standard deviation is **2.7%**.

TUG Measured all tyres on all test sections except section CC and N. Most combinations were measured 2 times, however 25 combinations were measured 4-8 times and a single combination was measured 17 times. Average standard deviation is **1.1%**.

The reproducibility of the TUG trailer is remarkable although the two other trailers also show quite stable results in the authors opinion. In [15] they refer to the results of the two other trailers as 'just acceptable'[15, p. 95], but considering the many factors that can potentially influence rolling resistance and the measurements thereof, it does not seem that bad. For instance, recall the many different effects mentioned in section 3.1 that causes rolling resistance, as well as transversal variation of pavements mentioned in section 3.2.

Another interesting aspect was the comparison between trailers, by measuring rolling resistance on several test sections with each trailer and comparing the result. BASt-TUG, BRRC-TUG, and BRRC-BASt comparisons have been made in [15] but we will only consider BASt-TUG here, since they are similar in construction, e.g., both have a wind shield protecting the measuring tyre from aerodynamic disturbances as well as 2 supporting tyres. In addition, the day-to-day results showed that the BRRC trailer was quite unstable and in the comparison test, and the BASt-TUG comparison showed significantly better results than BRRC-TUG and BRRC-BASt. Since each trailer had their own collection of tyres, measurements were made where the BASt and TUG trailers used their respective tyres as well as where both trailers used BASts tyres. Table 4.6 summarizes the results of the BASt-TUG comparison.

First of all, there are outliers with AAV4 at 80 km/h when the trailers use their own tyre and when they use BASts. This can be traced back to test sections M1 and L2 where BASt diverges substantially from TUGs measurements, but the exact reasons for this deviation is not known[15, p.58]. In the following we will omit these two cases in our consideration. By looking at the offsets (b-value) it can be seen that a substantial variation exists between the

Table 4.6 Results of trailer comparison between TUG and BASt trailers. Upper part of table is a summary of figure 8.5-8.12 and the lower part is a summary of figures 9.12-9.16 from [15].

Trailer comparisons: BASt and TUG use their respective tyres.

Tyre-[km/h]	Sections used	R^2	Reg. line (**TUG** $= a \cdot$ **BASt** $+ b$)
ES16-50	9	0.82	$y = 0.849x - 0.0017$
ES16-80	8	0.88	$y = 0.880x - 0.0035$
SRTT-50	9	0.79	$y = 0.629x + 0.0007$
SRTT-80	9	0.98	$y = 0.914x - 0.0015$
AAV4-50	9	0.91	$y = 0.807x + 0.0044$
AAV4-80	8	0.17	$y = 0.159x + 0.0129$

Trailer comparisons: BASt and TUG both uses the BASt tyres.

Tyre-[km/h]	Sections used	R^2	Reg. line (**BASt** $= a \cdot$ **TUG** $+ b$)
SRTT_BASt-50	9	0.84	$y = 1.380x - 0.0027$
SRTT_BASt-80	9	0.98	$y = 1.064x - 0.0001$
AAV4_BASt-50	9	0.88	$y = 1.047x - 0.0026$
AAV4_BASt-80	8	0.20	$y = 1.280x - 0.0052$

trailers, i.e., one of the trailers consistently measures higher or lower than the other. In rough numbers it is 10% - 30% of the overall mean rolling resistance coefficient and which trailer measures higher than the other changes for each measurement run. When the same (SRTT-Bast) tyre is measured by both trailers a significant difference in b-values is observed, 0.0027 vs. 0.0001. If we look at the slope of the regression line we see a difference between the two trailers that persist across comparisons: When the BASt trailer measures two C_{RR}-values that differs by a unit, the corresponding difference of the two values measured by TUG will be *less* than a unit. This trend holds for all comparisons in table 4.6 and could mean that the two different trailers indeed does diverge in what they measure. That being said, the goodness-of-fit is rather good ($R^2 > 0.8$) and in most cases despite the fact that these two trailers have been developed independently and uses different measurement principles etc. In addition, there is also variation among tyres and especially the two SRTT tyres used in the comparison above showed approximately 30% difference in rolling resistance when measured on a drum[15, p.51]. By comparison, the AAV4 tyres only showed $1\% - 2\%$ difference. Another aspect is that only 8-9 data points are used in the linear regressions in table 4.6. With the amount of disturbance and/or noise that seems to be present, this might be too small a data set. However, these results also illustrates that rolling resistance measurements by trailer does not give a bullet-proof result, and that errors and/or disturbances play a significant role. As noted in the previous chapter, the newly started ROSANNE project has a focus on rolling resistance trailer standardization which might improve the situation. Finally, the investigations in [15] only considered data in a test-section level manner, without investigating the measurements in finer detail. As illustrated in chapter 5 there might be more information to obtain by studying the data in more detail, i.e., by considering the data in 10-100 meter intervals. This would also be an obvious candidate for the FDA methodology as described in chapter 2.

Another type of investigation undertaken in [15] that is of interest here, is the road surface influence on rolling resistance. Based on the texture measurements by BRRC, several road

metrics were were correlated to rolling resistance measurements by linear regression. More specifically, macrotexture in the form of MPD and L_{Ma}, as well as megatexture quantified by L_{Me} were used. Additionally, these road metrics were calculated from both the 2D laser profiles directly, and after the profiles have been treated with the enveloping procedure expressed in equation 4.10. A value of 0.0025 mm^{-1} for the e parameter in equation 4.10 was used[15, p.20]. The results of the linear regression analysis for MPD is shown in table 4.7 and are based on test sections A, A', F, E1, E2, M1, M2, L1, and L2.

Table 4.7 Results of correlation analysis between MPD and rolling resistance (C_{RR}). Both normal MPD and MPD where the underlying profile have been enveloped is shown. Based on table 11.1-11.4 of [15].

	BASt				**TUG**			
Tyre-Speed	R^2	env. R^2	Slope	env. Slope	R^2	env. R^2	Slope	env. Slope
AAV4-50	0.79	0.91	0.0014	0.002	0.91	0.98	0.0014	0.0018
AAV4-80	0.27	0.29	0.0016	0.0032	0.92	0.97	0.0015	0.0019
SRTT-50	0.77	0.70	0.0024	0.0031	0.91	0.98	0.0020	0.0025
SRTT-80	0.82	0.93	0.0019	0.0027	0.92	0.97	0.0020	0.0025
MCEN16-50	0.87	0.82	0.0017	0.0021	0.88	0.92	0.0017	0.0021
MCEN16-80	0.40	0.60	0.001	0.0023	0.81	0.84	0.0018	0.0022
MCEN14-50	-	-	-	-	0.88	0.87	0.0016	0.0020
MCEN14-80	-	-	-	-	0.90	0.93	0.0015	0.0018
Mean	**0.65**	**0.71**	**0.0017**	**0.0026**	**0.89**	**0.93**	**0.0017**	**0.0021**

As can be seen from the results, TUG does provide the best correlation results for *all* common combinations of tyre and speed. It is also quite clear that enveloping significantly improves correlation quality for both trailers. This is a very interesting result as it is the first systematic application of enveloping in surface/rolling resistance influence investigations that the author know of, and the results seems promising. The enveloping method will be revisited in section 4.3 and used in our own data analysis in chapter 5 and 6. In general, the correlation results based on TUGs measurements are better in this study than in the following studies discussed in section 4.2.2 and 4.2.3.

Since the point of the enveloping procedure is to emulate indentation of the surface into the tyre, we would not expect any noticeable effect for higher wavelengths. However, correlations between L_{Me} (which is a measure pertaining to wavelengths between 63 mm and 500 mm) and rolling resistance, which is shown in table 4.8, shows that the enveloping procedure does in fact increase R^2 substantially, with an increases of R^2 between 0.21 and 0.28 for the TUG trailer. Given that the smallest wavelength contributing to L_{Me} is roughly half the length of the contact patch, it seems far from obvious that enveloping should increase correlation. This might indicate that enveloping has a more general effect on the 2D profiles which is not necessarily related to the aforementioned tyre/surface phenomena.

Table 4.8 Results of correlation analysis between L_{Me} and rolling resistance (C_{RR}). Both normal L_{Me} and L_{Me} where the underlying profiles have been enveloped is shown. Based on table 11.9-11.12 of [15].

	BASt		**TUG**	
Tyre-Speed	R^2	env. R^2	R^2	env. R^2
AAV4-50	0.53	0.80	0.61	0.92
AAV4-80	0.17	0.22	0.67	0.94
SRTT-50	0.59	0.77	0.62	0.91
SRTT-80	0.59	0.83	0.66	0.93
MCEN16-50	0.79	0.84	0.69	0.94
MCEN16-80	0.43	0.50	0.72	0.93
MCEN14-50	-	-	0.76	0.94
MCEN14-80	-	-	0.71	0.94
Mean	**0.52**	**0.66**	**0.68**	**0.93**

4.2.2 Measurements at MnROAD, USA

In 2011 3D texture measurements using the RoboTex line laser profiler and rolling resistance measurements using the TUG trailer were performed on the MnROAD test track in Minnesota, USA. Both measurement devices have been used in a small measurement campaign in the COOEE project at Værløse airbase and used in chapter 5. RoboTex measures the road with a line laser scanning at a width of 10 cm and a resolution of 1 mm, thus it stores 100 parallel 2D profiles spaced 1 mm apart (see chapter 5 for more equipment details). Rolling resistance measurements were performed with three tyre models that were also used in the COOEE measurements, but it is not known whether it was the exact same tyres. General tyre specifications are given in table 4.2 and specific hardness measurements are given in table 4.9. Rolling resistance measurements were performed at four different speeds, 50, 80, 110, and 130 km/h. The rolling resistance measurements discussed below are measured at 80 km/h using the SRTT tyre.

Table 4.9 Information about hardness obtained from [41, p.2].

Tyre	**Hardness** [Sh]*
SRTT	65
AAV4	62
MCEN16	63

The MnROAD test track is composed of two roads, Mainline and Low Volume Road (LVR), and each road is divided into cells containing different pavement types. The cells vary in size with the maximum and most frequent size being approx. 150 meters although some cells are smaller than 50 meters. A total of 58 cells are measured by both measurement devices and 34 of these are paved with asphalt. In addition to these measurements, tyre-pavement noise, friction, and unevenness measurements have been measured beforehand by Minnesota Department of Transportation (MnDOT)[168, p. 24]. The rolling resistance measurements are

described in detail in [41] while a more general and detailed analysis that also incorporates texture, unevenness, and friction, is given in [168].

A wide selection of road parameters and their influence on rolling resistance have been investigated in [168] by means of linear regression. The texture parameters includes RMS for specific octave bands, standard RMS, MPD measured in both longitudinal and transversal directions, as well as, skewness, and SMTD($= \mathrm{MPD} \,/\, \mathrm{RMS}$) in both directions. In [168], the specific waveband RMS measures are referred to as 'texture wavebands' and are denoted $L_{\text{waveband center}}$ (e.g., $L_{3.25\text{ mm}}$) while the rest is called 'texture variables'. Several other parameters are investigated although we will not go into details with these. Since the texture parameters are extracted from 3D texture measurements, several variations can be made, e.g., by calculating a particular measure in both transversal (tr) and longitudinal (lg) drection. Moreover, as there are 100 parallel longitudinal 2D profiles the 10%, 50%, and %90 precentiles can be chosen as well. This gives several different values for, e.g., MPD such as LgMPD, TrMPD, 10%MPD, 50%MPD, and 90%MPD and so on. All these variations across many different texture metrics yields a very high amount of parameters to use in linear regression. In [168] they report a total of 105 texture parameters which is too comprehensive to describe in detail, but it clearly illustrates the scope of their investigations. In addition to the texture measures they have 31 unevenness measures, including IRI, and 4 friction parameters.

Using all these data they were able to perform different kinds of regression analyses. Due to poor regression results the models were fitted separately for different groups of data.

- Asphalt
- Portland Cement Concrete with diamond grind finish (PCC grind)
- Portland Cement Concrete without diamond grind finish (PCC non-grind)

This grouping makes good sense since each group represents vastly different types of pavements, e.g., concrete pavements have direction-dependent surfaces as shown in figure 3.3 in chapter 3. Only the regression analyses concerned with asphalt pavements, are considered here. Furthermore, since our primary focus is texture parameters the following regression models used in [168] are the only ones discussed here (see [168, p.41] for the complete list of models they considered).

a) **MPD, IRI**: $C_{RR} = \beta_2\,\mathrm{MPD} \;+ \beta_1\,\mathrm{IRI} \;+ \beta_0 \;+\; \beta_q\mathrm{Road}$

b) **Texture, Unevenness**: $C_{RR} = \beta_2\mathrm{Texture} + \beta_1\mathrm{Unevenness} + \beta_0 \;+\; \beta_q\mathrm{Road}$

c) **Texture**: $C_{RR} = \beta_1\mathrm{Texture} + \beta_0 \;+\; \beta_q\mathrm{Road}$

d) **Texture, Texture**: $C_{RR} = \beta_2\mathrm{Texture}_2 \;+\; \beta_1\mathrm{Texture}_1 \;+\; \beta_0 \;+\; \beta_q\mathrm{Road}$

'Road' is a qualitative variable indicating whether the road is Mainline or LVR, that was added to the regression models since it showed to be significant in regression analyses. It is hypothesized that it might be due to, e.g., the difference in traffic volume[168, p.36]. This makes good sense since the trailer measured between wheel paths while texture profiling was performed in the right wheel path. Note that **c**) was performed for all possible parameters, including unevenness and friction, but it was only texture that showed meaningful proper fits with $R^2 > 0.4$. A brief overview of the results of **b**), **c**), and **d**) is shown in table 4.10. Notice that p-values have been calculated as well and used discard regression results having p-values below the threshold of 0.05, meaning there is over 5% chance that the null-hypothesis, stating that a given parameter $\beta = 0$.

a) is a special case of **b**) using the standard parameters (MPD50%) which of course makes it especially relevant here. The results of **a**) are poor with the asphalt pavement group having

Table 4.10 Overview of lineare regression results for the asphalt pavements in [168]. L_λ refers to third-octave band texture levels as described in section 4.1. $L_{\lambda_1-\lambda_2}$ refers to all third-octave bands from λ_1 to λ_2.

b) Texture, Unevenness			**c) Texture**		**d) Texture, Texture**		
Texture	Uneven.	R^2	Texture	R^2	Text.$_1$	Text.$_2$	R^2
$L_{3.15\text{mm}}$	$L_{5\text{m}}$	0.79	$L_{63\text{mm}}$	0.81	$L_{5\text{mm}}$	50%LgRdCf	0.77
$L_{3.15-8\text{mm}}$	$L_{5\text{m}}$	0.79	$L_{40\text{mm}}$	0.80	$L_{5\text{mm}}$	50%TrRpk	0.76
$L_{10\text{mm}}$	$L_{5\text{m}}$	0.79	$L_{3.15-50\text{mm}}$	0.80	$L_{5\text{mm}}$	50%LgRpk	0.76
$L_{12.5\text{mm}}$	$L_{5\text{m}}$	0.79	$L_{50\text{mm}}$	0.80	$L_{5\text{mm}}$	50%TrMaxPeak	0.76
$L_{8\text{mm}}$	$L_{5\text{m}}$	0.79	$L_{31.5\text{mm}}$	0.80	$L_{5\text{mm}}$	50%LgMaxPeak	0.76
$L_{4\text{mm}}$	$L_{5\text{m}}$	0.78	$L_{50-160\text{mm}}$	0.80	$L_{5\text{mm}}$	50%TrMaxHeight	0.76
$L_{6.3\text{mm}}$	$L_{5\text{m}}$	0.78	$L_{80\text{mm}}$	0.80	$L_{5\text{mm}}$	50%TrMPD	0.76
50% TrRpk	$L_{5\text{m}}$	0.77	$L_{25\text{mm}}$	0.79	$L_{5\text{mm}}$	50%LgMAxHeight	0.76
90% TrRpk	$L_{5\text{m}}$	0.77	$L_{20\text{mm}}$	0.79	$L_{5\text{mm}}$	50%LgMPD	0.76
50% LgMaxPeak	$L_{5\text{m}}$	0.77	$L_{3.15\text{mm}}$	0.79	$L_{5\text{mm}}$	50%LgRkTotal	0.76

$R^2 = 0.73$ while regressions using PCC grind, PCC non-grind, and all road sections had R^2-values between 0.29 and 0.45. Moreover, Asphalt, all road sections and PCC grind had $\beta_1 < 0$ which is counter-intuitive to the relation between road unevenness and rolling resistance.

In the general case of **b**) the top 10 in R^2 values lie in $[0.77 - 0.79]$. It would probably be too much to say that it is a good correlation, but it is a great improvement compared to **a**). As a side note, in the asphalt regression shown in table 4.10, the 7 best texture measures are texture levels L_λ for different third-octave bands going from 3.15 to 12 mm (all having $L_{5\text{m}}$ as the unevenness variable). This is peculiar because it is completely different measures, e.g., Tr/LgSkewness, in the top ten for PCC grind and non-grind[168, p. 52] (not shown here). Also, the unevenness components for PCC grind/non-grind are L_λ metrics for smaller octave bands (0.1-1.25 m) than asphalt. This divergence might be due to different surface characteristics of concrete pavements and asphalt, but given the overall low R^2 values it might also be due to deficiency of the road metrics.

With **c**) only RMS for specific wavelengths show up on the top ten (R^2-values from 0.77 to 0.81) with wavelengths between 3.15 and 80 mm. Although it is generally higher wavelengths compared to **b**) there are some overlap. It should be noted that in general most texture measures performed well here.

In the regression model **d**) Texture$_1$ ranges over texture band levels whereas Texture$_2$ ranges over median texture metrics (50%LgMPD, 50%TrSkew, etc.). The only Texture$_1$ waveband that is within a valid p-value is L_{5mm}, thus it is the only measure for Texture$_1$. This is rather strange since many texture band measures dominates the texture variable in **b**) and **c**). In fact, while many band level measures are represented in the models of **b**) and **c**), L_{5mm} is not one of them.

This summary of a 130 pager report is of course brief. However, the findings discussed here clearly illustrates a general trend that holds for the entire data analysis. Namely, that the relation between all the different texture variables and rolling resistance measurements is not very clear. It seems like many of the road measures investigated does quantify something that can be related to rolling resistance but the relation seems weak. This is shown, not only by low R^2 values, but also by the fact that different regression models rank the road metrics according to R^2 in substantial different ways. That MPD performed poorly is also interesting, and the

authors note that MPD might not be a optimal measure for rolling resistance[168, p.25]. One explanation might be that most texture measurements had been performed in the right wheel track, and the rolling resistance trailer measures between wheel-paths. However, the position of the TUG-trailer has not been discussed so this is an open question. All in all, this study did not identify any texture parameter as a potential candidate for rolling resistance assessment, and it illustrates the difficulties involved in these efforts.

It should be noted that the rolling resistance measurements performed here have been for smaller road sections that what is usually done in other studies. The road section lengths in, e.g., Swedish and Danish rolling resistance measurement campaigns (including the COOEE measurements) have been larger than what is measured here, which might be a reason for the bad correlations[41, p. 25]. All in all, this report stands out as a rather comprehensive study of a variety of road parameters, many of which are rather exotic and not used elsewhere.

4.2.3 Dutch Measurement Campaign

Another recent measurement campaign using the TUG trailer was carried out in April 2013 in the Netherlands[68]. In contrast to the MIRIAM and MnRoad studies, that was based on rolling resistance and texture measurements from a test track, this study is based on data obtained from actual roads of the Dutch road network. It is a fairly large data set with 68 main road sections consisting of both highway and provincial roads, where texture profiles and rolling resistance have been measured. Most of these road sections are above 500 meters with a total length of approximately 48 km. 25 of the 68 road sections have been measured 5 times whereas the rest have been measured once. Thus, a total of 168 measurement runs have been performed. In addition, the TUG trailer had measured approximately 150 kilometres spread across 38 additional road sections, but without any texture measurements. The texture laser was mounted directly on the TUG trailer, such that the laser and rolling resistance measurements are aligned, which is very important especially on real roads where the traffic load wears the pavement and causes transverse variation of the surface. All in all this is a very comprehensive measurement campaign using real roads.

One of the main goals in [68] is to study the relation between texture and rolling resistance, but some auxiliary investigations into, e.g., temperature and pressure dependence have also been undertaken. It was found that the influence on rolling resistance from tyre pressure changes were too small to be corrected for, given that the measurement procedure protocol adjusts tyre pressure if it is higher than 215 kPa and lower than 205 kPa. To investigate temperature influence on rolling resistance, two road sections were measured for rolling resistance 12 times, spanning several days. For each measurement run air, road, and tyre wall temperature were measured together with rolling resistance. A regression line was fitted for each combination of road and temperature type[68, p.20]. The tyre-wall temperature gave the best fit, so a formula was derived from tyre-wall temperature and used to correct all the rolling resistance measurements before subsequent analysis. Since the coefficients of the two regression lines derived from tyre wall temperatures differs it would have been interesting to see the result of a combined regression using both road sections together with a qualitative variable. Instead the authors use an average of the two. However, their investigations clearly illustrates the important role of temperature during rolling resistance measurements.

The texture/rolling resistance modelling in [68] is also based on linear regression, as in the previous studies discussed here. However, the amount of models and parameters is much smaller compared to the previous study discussed in section 4.2.2. The texture road metrics used are

MPD, RMS, SMTD($= MPD/RMS$), and Skewness together with the following linear models.

a) **Texture**: $C_{RR} = \beta_1 \text{Texture} + \beta_0$

b) **MPD, SMTD**: $C_{RR} = \beta_2\,\text{SMTD} + \beta_1\,\text{MPD} + \beta_0$

c) **RMS, Skewness**: $C_{RR} = \beta_2\,\text{RMS} + \beta_1\,\text{Skew} + \beta_0$

d) **Skew, RMS, MPD**: $C_{RR} = \beta_3\,\text{Skew} + \beta_2\,\text{RMS} + \beta_1\,\text{MPD} + \beta_0$

These models have been fitted to temperature corrected C_{RR} measurements on a road section basis, i.e., C_{RR} and texture parameter values have been aggregated into one average value for each road section. A summary of the modelling results is given in table 4.11. If we look at

Table 4.11 Overview of regression results from [68].

	Model	R^2	$\tilde{\beta}_3$	$\tilde{\beta}_2$	$\tilde{\beta}_2$	$\tilde{\beta}_0$
$C_{RR} =$	$\beta_1\,\text{MPD} + \beta_0$	0.65			0.96	7.92
$C_{RR} =$	$\beta_1\,\text{RMS} + \beta_0$	0.53			1.06	8.12
$C_{RR} =$	$\beta_1\,\text{Skew} + \beta_0$	0.10			0.65	10.0
$C_{RR} =$	$\beta_2\,\text{SMTD} + \beta_1\,\text{MPD} + \beta_0$	0.69		0.63	1.00	7.03
$C_{RR} =$	$\beta_2\,\text{RMS} + \beta_1\,\text{Skew} + \beta_0$	0.65		1.08	0.71	8.87
$C_{RR} =$	$\beta_3\,\text{Skew} + \beta_2\,\text{RMS} + \beta_1\,\text{MPD} + \beta_0$	0.68	0.17	0.55	1.36	8.13

the three single variable models, the model fits are very poor, especially with skewness as the explanatory variable ($R^2 = 0.10$) and MPD is the best ($R^2 = 0.65$) but still a very poor fit. The situation does not improve much by introducing more explanatory variables where the best fit is the model **b**) which is not that surprising since MPD is part of both explanatory variables. It should be noted that data obtained at a particular date they stood out compared to the rest and were corrected by adjusting the mean of that date to match the mean of the rest. Without this correction, the goodness-of-fit drops from $R^2 = 0.64$ to 0.52 and the slope changes from 0.95 to 1.14.

Given the huge dataset and high degree of averaging the results of the regression does not seem very satisfactory. Just as in the MnRoad study the correlations in the form of R^2 values do not seem very high. The overall results of these two studies are quite unfavourable compared to the results obtained in the MIRIAM project in section 4.2.1. Even though MPD also performed poorly in the last two studies, it still seems like the best choice compared to all the other road metrics explored here.

All in all, these three studies shows the difficulties involved in assessing surface induced rolling resistance by means of road profile measurements.

4.3 New Road Metric Proposal

Given the history, development and recent studies in rolling resistance modelling and road surface measurement characterisation, a new road metric for the macrotexture range is proposed. The reasons for doing so will be discussed below. As mentioned above, the present standard road metric for the unevenness range, IRI, might not be suitable for rolling resistance modelling. However, we have not made any attempts at defining a new metric for this road property since it would make the present work too comprehensive. In addition, the macrotexture is easier to

adjust with a new pavement mix, which is what the COOEE project intends to do. Nevertheless, road unevenness is a property that can be controlled to some extent by road administrators and research into the relation between rolling resistance and unevenness (not necessarily represented by IRI) would be a very interesting undertaking. An example of a recent large-scale study investigating the fuel consumption effect of road roughness is published in [3].

4.3.1 Background

The primary reason for the differences in rolling resistance caused by road macrotexture is that the rough surface causes local hysteresis losses when it indents into the tyre surface as well as energy loss due to adhesion or other chemical reactions. This also explains that all the different results presented in section 4.2 have one general conclusion in common: Rougher macrotexture implies higher rolling resistance. However, the different studies do not agree on the quantitative side, i.e., *how much* does rolling resistance increase with rougher macrotexture, let alone the question of how to quantify macrotexture roughness in terms of rolling resistance. As shown in section 4.2, different road metrics are able to correlate with rolling resistance, although to a limited degree of success. The question is what metric describes rolling resistance best in terms of macrotexture, and up until now it seems to be MPD.

MPD is derived from the sand patch test which was used in connection with skid resistance and while it has shown very useful in rolling resistance as well, there is not much in the specification that suggests this would be a good measure for rolling resistance. Implicitly there are some indicators which might explain its usability: 1) MPD measures the highest peak for each 5 cm and it seems reasonable to assume that higher peaks implies higher indentation and thus higher energy loss. 2) The slope suppression takes skewness into account since it 'pulls down' profiles with a negative skewness and thus reduces the height of the highest point in the profile. On the other hand 1) seems a bit arbitrary. Why should it only be the two highest peaks each 10 mm that counted? With 2) there is the risk of having deep cracks, or a road surface with many deep valleys, slope suppression pulls the profile down even though there are some high peaks which could indent deeply into the tyre and create substantial energy loss. The obvious solution is to use high pass filtering, however, this seems a bit implicit. What is sought is not to remove small frequencies per se, but to remove deep trenches in the surface profile. As a small aside, it is ironic that MPD is derived from the sand-patch test which actually *is* sensitive to cracks and valleys in the profile, assuming they are wide enough for grains of sand. All in all it can be argued that MPD might have some properties that makes it useful in rolling resistance assessment. However, as discussed above, these properties are *vaguely* related to the theory of macrotexture level rolling resistance and it would be desirable to have a measure that is more *explicit* in this relation.

Compare this situation to the IRI measure when used as a measure of ride comfort which was one of its first uses. IRI is based on a theoretical model of a vehicles response to road unevenness, and while the model greatly simplifies the complex reality, it is still based on basic principles about how a vehicle is reacting to the surface and how this reaction is reflected in the ride comfort. The MPD measure on the other hand is not as directly related to the phenomena for which it is used and seems closer to the RMS and Skew measures described above. RMS and Skew are statistical properties of the distribution of profile measurements, and while we can relate these statistical measures with a basic understanding of the relation between road texture and surface induced energy loss, the relation is based on *implicit* properties of the rolling resistance phenomena. For instance, we expect that, *in general*, a profile with a large negative

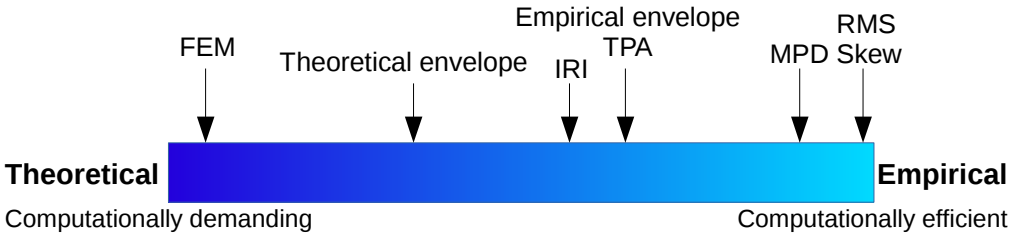

Figure 4.6 Illustration of different measures and modelling approaches and how theoretical and empirical they are perceived to be. The ranking is merely qualitative and should not be considered and exact quantification. Also note that ranking into computational efficiency should be taken with a grain of salt since IRI/TPA/MPD are all almost equally efficient to compute.

skewness will cause a higher energy loss than a profile with lesser negative skewness, mainly because the indentation is expected to be higher in the former case. However, we also know that this depends on the exact geometry of the profile as well as tyre, temperature etc. Since most profile geometries are very complex, the above rule of thumb is not guaranteed to hold and, e.g., the Dutch and MnRoad studies discussed above did not find very good correlations between skewness and rolling resistance[68, ch. 7].

Enveloping is a method that resembles IRI, in that it is founded on general knowledge concerning the phenomena that it is supposed to model. However, enveloping is not a road measure since it takes a profile and outputs a processed profile instead of a single value. Nevertheless, enveloping is based on the simple idea of mimicking the visco-elastic deformation of the tyre when it is pressed against a surface. Compare this to, e.g., the purely statistical RMS/Skewness measures. It is also interesting to note that the initial results with enveloping, in combination with MPD, have been very good and promising[15]. On the other hand, enveloping is still an empirical measure that lacks a solid theoretical foundation compared to other complex models such as the those presented in [93]. Unfortunately, the complexity of these models are also what makes them unusable here because they are impractical to compute for large data sets, which is needed in network level road maintenance and monitoring. As such, enveloping and IRI are optimal trade-off's between theory and practical needs and serves a template for the measure proposed below. To illustrate and clarify this discussion, figure 4.6 ranks the different measures and models that have been considered above, including the TPA measure described below. This also illustrates the main design goal behind TPA: Develop a measure that tries to be faithful to the theory behind macrotexture induced rolling resistance while still being practical enough for it to be used in road maintenance and asset management.

4.3.2 Description of the New Measure

The main source of macrotexture induced energy loss comes from local tyre deformations caused by the tyre being pushed down into the surface. Thus, the magnitude of the surface induced tyre indentation should be the quantity that we try to estimate or quantify. This is a much more explicit approach compared to MPD, RMS, and Skew since the indented volume should be directly related to the resulting energy loss. In the 2D-case this magnitude should be an area which can be extracted from profile data, although the details of this requires careful consideration. However, the main idea is to calculate the area of the peaks in the profile. What

is defined as a peak is an open question, but an obvious approach is to specify a depth d and then find the area of the profile larger than d, as shown in figure 4.7. Thus, d determines what is a peak, and finding a value for d will be a central question that is discussed below. Since this area can be found by integration, it is obvious to view the profile as a function $y(t)$ which can be transformed to a new function $\hat{y_d}(t)$ where $\int \hat{y_d}(t)dt$ will give the area of the peaks of $y(t)$ defined by d. Converting segments of profile data into functions is a interesting use case of FDA using a standard (cubic) B-spline subspace for the functional data. However, using simple linear interpolation is also worth exploring as it is very fast. How this is done in practice and the details of the function $y(t)$ will be discussed in section 4.3.3. For the rest of the thesis, this measure will be referred to as the "Texture Penetration Area"(TPA).

Because we are interested in the indentation area, it is obvious to combine this technique with the empirical enveloping procedure discussed above, since tyre indentation is exactly what profile enveloping is about. This is done by treating the profile with the enveloping procedure before applying the rest of the algorithm.

Another aspect of the calculation is the partitioning size and filtering where there is no reason not to follow the procedure described for MPD in ISO13473-1[75]. This means that the segment size of 100 mm is followed and segment normalisation using slope suppression (i.e., by subtracting the regression line) is also applied to the TPA measure. Low-pass filtering will not be explicitly used, but the smoothness technique from section 2.4 using a roughness penalty term with a roughness parameter λ will be deployed instead. Unfortunately, it is not known whether or not low-pass filtering is already performed on the data used in this work. In case of rolling resistance measurements by the TUG trailer, this definitely seems to be the case, although the applied algorithms could not be disclosed by TUG.

Given the description so far, there are several parameters whose values are not given to us a priori. The set of parameters involved depends on the implementation, but there are at least two and at most four different parameters:

Penetration depth d Represents how far the surface penetrates into the tyre. Important factors that influence this parameter is the visco-elastic properties of the tyre and geometry of the surface. How much this depends on the surface geometry/tyre is an open question that should be investigated, but in theory it should be stable over a road segment with the same pavement and tyre. Therefore, d should be estimated for each combination of tyre and road section, although it might be the case that a single value will suffice. It is also not clear whether the ambient and tyre temperatures will have an effect on this parameter. Given that data for every road section used in later chapters will be measured with a warmed up tyre, the tyre temperatures are fixed for each road section. There is also the question about how to determine and interpret d. A direct interpretation of d would be as the distance from the highest peak of the profile segment under consideration. However, that would make the resulting TPA algorithm extremely sensitive to outlier peaks in the profile. Instead d is a percentage of the upper profile curve such that $d = 10\%$ means that the highest 10% of the profile curve is used.

Envelope parameter e This parameter concerns the enveloping of the tyre with the road surface as described above. Since e can be viewed, intuitively, as a parameter describing tyre stiffness in the empirical algorithm of [115] it should, ideally, depend on tyre type. Thus, it would be preferable to consider it on a tyre/surface combination basis as well. However, in order to limit the investigations in chapter 5 and 6 we will only look at the parameter values used in the literature: $e = 0.0025$[15], $e = 0.054$[115] and of course $e = 0$ (i.e.,

no enveloping). This parameter together with d is the essential parameters used in TPA measure.

Roughness parameter λ (FDA-specific) As described in section 2.4 this parameter determines the amount of smoothing used when estimating a function from data and this should have an effect similar to low-pass filtering. This parameter is not present when $y(t)$ is piece-wise linear.

Knot Placement Parameter K (FDA-specific) Because of the large data sets it is interesting to investigate how many knots are needed in the B-spline basis. More precisely, how many data points between each knot: A knot at every data point ($K = 0$), every second data point ($K = 1$), every third ($K = 2$), and so on.

Of course, the devil is in the detail and the details are in the implementation, so we will consider a couple of the details in the next section.

4.3.3 TPA Calculation Details

Now that the parameters have been introduced and described, we can give a stepwise description of the algorithm. Assuming a texture profile $\boldsymbol{y}[\boldsymbol{s}] = (y_1(s_1), \ldots, y_N(s_N))'$ from which the TPA-measure is to be calculated for a fixed set of the parameters d_0, e_0, λ_0, K_0, we do as follows:

1 Apply the envelope operator $E_{e_0}(\cdot)$ (parametrised by e) to the profile data, i.e.

$$E_{\boldsymbol{e}_0} : \boldsymbol{y}[\boldsymbol{s}] \mapsto \widehat{\boldsymbol{y}}[\boldsymbol{s}] \tag{4.13}$$

We use the envelope algorithm proposed in [115] and used in [15], but other algorithms could be used as well. For the sake of completeness we define $E_{\boldsymbol{e}_0}$ to be the identity operator when $e = 0$.

2 Following ISO-13473[75] the initial step in the MPD calculation procedure, the profile is partitioned into 100 mm segments and for each of these sections, the regression line is subtracted. The next steps will be performed piecewise on each of these segments, as when calculating MPD.

3 In order to get a consistent measure in the last step, we require that $y_i(s_i) > 0$ for all i. Since slope suppression causes the measurements to be distributed around $y = 0$, we vertically translate the profile data by adding $|\min(\widehat{\boldsymbol{y}}[\boldsymbol{s}])|$ to $\widehat{\boldsymbol{y}}[\boldsymbol{s}]$.

4 Convert the discrete laser profile $\widehat{\boldsymbol{y}}[\boldsymbol{s}]$ into a functional form $\widehat{y}(s)$. Implicit in this conversion is of course the choice of basis functions. In principle any basis could be used, but given our discussion above, we have essentially two approaches here.

a) Define a cubic B-spline basis system using K_0 and fit the basis to each 100 mm segment using the smoothing value λ_0 supplied to obtain the $\mathcal{C}^2$-function $\widehat{y}(s)$.

b) Interpolate linearly between measurement points, thus giving a piecewise-linear $\mathcal{C}^0$-function $\widehat{y}(s)$. In this simple case each knot is trivially at every measurement point and there is no smoothing, thus K_0 and λ_0 is omitted using this approach.

5 In this step it is assumed that d_0^* has been derived as the height where d_0 percent of the profile function lies above. This conversion from percentage to height will be determined for each 100 mm profile segment. To calculate TPA, define a new function $\widehat{y}(d, s)$ by

$$\widehat{y}(d, s) = \begin{cases} 0 & \text{if } \widehat{y}(s) < d, \\ \widehat{y}(s) - d & \text{if } \widehat{y}(s) \geq d. \end{cases} \tag{4.14}$$

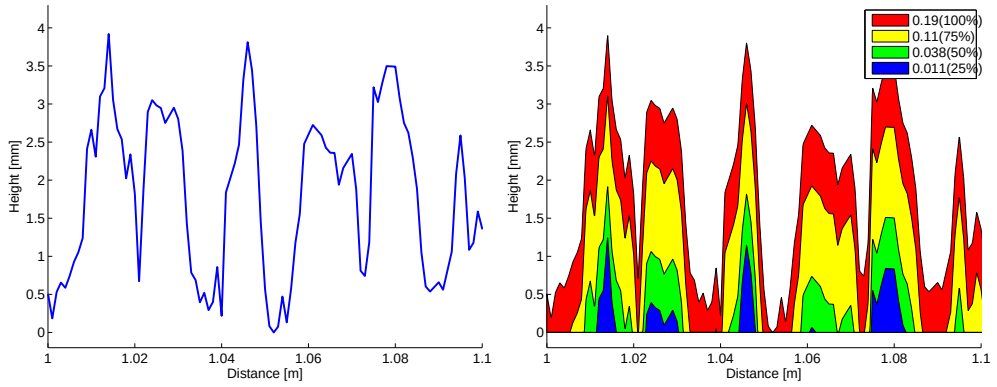

Figure 4.7 Illustration of the TPA measure. To the left is approx. 100 mm of texture profile $\widehat{y}(s)$ taken from road ID 3 of the VTI data investigated in chapter 6. $\widehat{y}(s)$ was obtained using linear interpolation using $e = 0$. The filled curves to the right are 4 different curves of $\widehat{y}(d, s)$ for four different values of d. The first number in the legend is the TPA value $[mm \cdot m]$ which is also illustrated by the coloured area of the curves. The TPA value of the red curve is the red area as well as all curves contained in it, and so on. The second number denotes the d values which each curve corresponds to. The curve with $d = 100\%$ seems rather unrealistic but is included for completeness.

Since we normalized the profile in step **3** we know that $\widehat{y}(d, s)$ will be non-negative for all s as long as $d_0^* \leq \max\big(\widehat{y}(s)\big)$. The TPA-value for each 100 mm segment is thus defined as

$$\mathrm{TPA}(d_0^*) = \int \widehat{y}(d_0^*, s)ds. \tag{4.15}$$

Explicitly denoting the d-value can be omitted if it is not necessary in the context.

6 Once again ISO-13473 is followed by taking the mean of 10 100 mm sections to get TPA values in approximately 1 meter intervals.

This procedure is formulated using mathematical terminology. When calculating step **5** in practice, the functional profile $\widehat{y}(s)$ is evaluated on each road section by choosing a suitable set of evaluation points $\boldsymbol{s^*} = (s_1, \ldots, s_{N'})'$ where $N << N'$ and then carrying out the calculations on the resulting function values. The integral is approximated using standard trapezoidal rule and the larger N' is, the higher the precision of TPA will be. Examples of $\widehat{y}(d, s)$ for $d \in \{25\%, 50\%, 75\%, 100\%\}$ are shown to the right in figure 4.7.

It follows from this formulation that $\mathrm{TPA}(d)$ as function of d is strictly increasing as d increases and that it does so smoothly. However, the way that TPA increases with d differs from each segment. The qualitative behaviour of TPA and its sensitivity to d is illustrated in figure 4.8.

4.3.4 Concluding Remarks on TPA Measure

All macrotexture road metrics discussed above have one thing in common, they are all extracted from a 2D profile of the road surface. This is of course a very rough approximation to the true 3D surface. Thus, an implicit assumption about isotropicity of the surface is underlying the

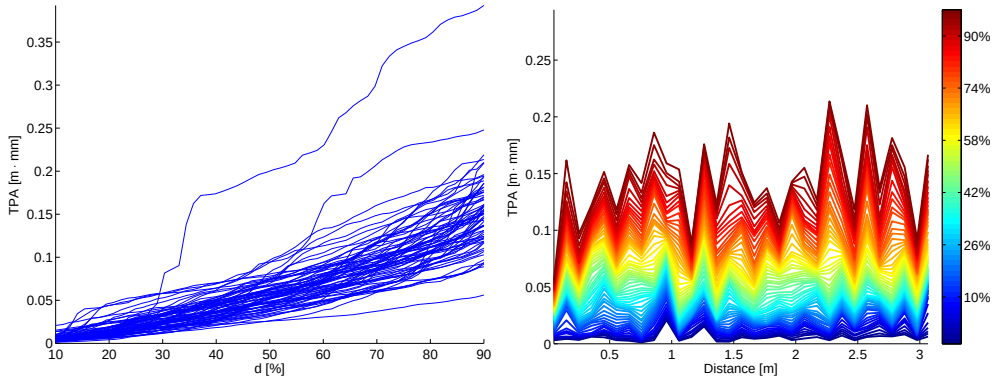

Figure 4.8 Illustration of the TPA values sensitivty to d. All segments are from road ID 3 of the VTI data investigated in chapter 6. To the left are TPA-values for several 100 mm segments shown as a function of d. To the right are several TPA curves, with varying d-values shown. Note the smooth transition as d increases as well as the variation among each segment.

hypothesis that it is possible to assess rolling resistance (or skid resistance) from a 2D profile. However, when dealing with asphalt pavements there are some circumstances that justifies this assumption. More specifically, the top layer of the pavement is basically composed of bitumen, filler[6] and mineral aggregates. It is specifically the latter which is responsible for the roads macrotexture. Since grain sizes of the mineral aggregates are tightly controlled, the resulting asphalt should be somewhat homogeneous. Furthermore, careful mixing of the asphalt also ensures a homogeneous material and if properly paved this should ensure an isotropic surface. Of course, since different batches of asphalt can be composed of filler, bitumen, and mineral aggregates from different sources their might be some variation between equal pavement types mixed at different times. This is not a problem as long as the isotropic assumption holds within each road segment being measured. However, there are some cautionary remarks that should be taken into account. First of all, when the pavement is laid out there can be some complications affecting isotropicity. For instance, if the pavement mix is not properly handled during pavement construction, the mineral aggregates in the asphalt mix can settle at the bottom of the asphalt container which result in non-homogeneous asphalt mix and thus a non-isotropic pavement surface. In addition, as the road is worn by traffic it becomes non-isotropic due to rutting and other traffic wear. This often creates transversal variation of the road as, e.g., the macrotexture of the surface is worn much more in the wheel paths compared to the rest of the road. In severe cases the wheel path surface is outright depressed compared to the rest of the road. This makes it extremely important to measure the road profile in the same wheel track where, e.g., rolling resistance is measured. Although isotropy seems a reasonable assumption, there is still high transversal variation in macrotexture profiles, as discussed in section 3.3.3. It will in turn result in high variation of TPA values (or MPD or any other macrotexture measure) which can be perceived as noise, complicating attempts at modelling the relation between macrotexture and rolling resistance. Thus, having a road metric that produces the least amount of variation across a homogeneous road section is a desirable property. In relation to this, it should be noted that the data used in chapter 5 have been obtained from a closed airbase that has not been used much,

[6] Filler is, roughly speaking, small mineral aggregates (<63μm) that stabilises the bitumen.

so the pavements were not noticeably worn and no rutting has been observed on the measured road sections. Since the profile data used in chapter 5 are 3D instead of the ordinary 2D, some investigations concerning isotropy have been undertaken to substantiate the hypothesis.

An interesting feature of the TPA measure is that, intuitively and formally, it can be adapted to be used on 3D surface profiles. In fact, this would be a much more natural setting compared to the 2D version. The latter, however, is still the standard way of measuring road surface texture, but as mentioned earlier this will probably change in the future. In the 3D version $y(s)$, $\hat{y}(s)$, and $\hat{y}(d, s)$ would be functions of two distance parameters, e.g., $y(s_1, s_2)$ so the TPA measure is reformulated as a double integral

$$\mathrm{TPV} = \iint \widehat{y}(d_0, s_1, s_2) ds_1 ds_2. \tag{4.16}$$

and renamed to TPV since the measured quantity is a volume instead of area. The envelope algorithm discussed above and used in the following chapters might also be modified to work in the three dimensional case although that is not immediately obvious. Note the relationship between TPV and the sand patch-test mentioned in chapter 3. Roughly speaking, the purposes of the sand patch test is, implicitly, to estimate the volume of the void in the surface texture, i.e., the volume of void between the surface and an upper bound given by the top peaks. TPV is a measures the volume of the *surface itself* between the same upper bound and some depth d. To clarify this relationship, assume a specified volume V has been spread out in a circle with area A and radius r according to the sand-patch test. Furthermore, assume that the sand used is ideal in the sense that it fills up every valley and crack in the surface. Set d' to be equal to the depth of the deepest crack/valley and calculate the TPV value of the circle obtained by the sand-patch using d' as the penetration depth (and no enveloping), i.e.,

$$\mathrm{TPV} = \iint_A y(d', s_1, s_2) ds_1 ds_2. \tag{4.17}$$

Then

$$\mathrm{TPV} + V = \pi r^2 d', \tag{4.18}$$

i.e., the TPV and the volume obtained in the sand-patch test give the entire volume of the cylinder and thus are complements to each other, relative to the surface patch A. Given this relationship between sand-patch and TPV, it is interesting that while MPD was created as a 2D substitute for the 3D sand-patch test, just as TPA is a 2D version of the 3D TPV measure, there is no connection between MPD and the sand-patch test except for a correlation. As we have seen above, TPA is direct 2D version of TPV. However, since 3D-profiling is on a very early stage far from network level monitoring practices we will not investigate these matters further in this work. Still, this potential generalization is a nice by-product of the TPA definition which deserves further study.

A final aspect that needs to be discussed is the estimation of d. By definition, and as can be seen from figure 4.8, each TPA value $\mathrm{TPA}(d)$ (derived from 100 mm of road profile) increases monotonically with d, starting with $\mathrm{TPA}(0\%) = 0$ and ending with $\mathrm{TPA}(100\%) = \mathrm{TPA}_{\max}$. Combining this with the observation that in principle d should vary across different pavements, this gives quite a lot of flexibility for any optimization routine in minimizing a given loss function. Thus, overfitting is a real concern that should be considered when investigating TPA in connection with real data. For instance, in chapter 5 a simple linear relationship between

rolling resistance measurements and TPA is investigated by using, essentially, two road sections. If the optimal correlation is found by having $\mathrm{TPA}(d_1)$ for one road section and $\mathrm{TPA}(d_2)$ for the other, where $d_1 << d_2$ which implies that, on average, $\mathrm{TPA}(d_1) << \mathrm{TPA}(d_2)$ then this is probably due to overfitting. On the other hand, letting d vary for different road section and studying the estimates that is produced can provide valuable information about the TPA-measure in general. In addition, there might be substantial differences between TPA values calculated within a given road section which might hinder overfitting.

Therefore, we will in general investigate two scenarios, one where d vary across road sections and one where d is kept fixed for all road sections. In the former case care will be taken to observe the estimated values of d.

4.4 New Road Metric Validation

The main purpose of the data analysis will be to test and examine the TPA texture metric as a rolling resistance indicator. The considerations put forward in the previous section have to be tested up against experimental data. As mentioned in chapter 3, several kinds of data exists for both pavement and rolling resistance. In addition, we have several sources of data available to choose from. Since the preparation of raw data is a cumbersome and time consuming process, only a selected number of data sets can be used in our investigations. Therefore careful considerations have to be made in order to use the proper data that best suits our needs at the lowest time-cost. At our disposal we have the following list (in chronological order):

1. Measurement campaign by the COOEE project in 2013 where approximately 125km of state road network of Zealand have been measured: RR data with TUG RR trailer as well as texture and unevenness measurements by the Danish Road Directorate.
2. Measurement campaign by the COOEE project in 2012 with 3D texture measurements by Transtec group and RR data by the TUG RR trailer. Measurements were performed on Værløse air base in June.
3. Dutch pavement and TUG RR trailer data from a measurement campaign in the Netherlands in 2012 by M+P Raadgevende ingenieurs BV for the Dutch Rijkswaterstaat.
4. Coast-down data from 2011 by VTI in Sweden on 8 different road strips. Includes many different pavement and vehicle measurements. Results on these measurements have been published in [89].
5. Measurement campaign by the MIRIAM project in 2009 at the IFSTTAR test track in Nantes, France. In this study, rolling resistance measurements from three different trailers, including the TUG trailer, where performed as well as texture and unevenness measurements. In addition RR drum measurements where made by TUG. Results on these measurements have been published in [15].
6. Coast-down data from 2009 by VTI in Sweden on 14 different road strips. Includes many different pavement and vehicle measurements. Results on these measurements have been published in [63] and [89].
7. Measurement campaign by the Danish Road Directorate in 2009 on approximately 8km of state roads on Zealand. RR trailer measurements by TUG and texture measurements by The Danish Road Directorate. Results of this have been published in [144].

Two test-sets that stand out from the rest are the ones from VTI, which are the only ones with no direct rolling resistance measurements. Instead, the rolling resistance has to be extracted

from a model fitted to various data sources, including texture and road gradient. Several factors have been taken into account when choosing the data: Preparation time, scope of measurements and type of measurements. All data sources have their pros and cons with respect to these factors. Although the preparation time is difficult to estimate, some key indicators to navigate by, are complexity and origin. Complex data involving many variables takes longer time to understand and parse, compared to a simple data set. By the same token, data of many road sections, directions etc. also increases complexity and thus time. By this indicator, item 7 is the easiest since involves only texture and trailer data for at a few road sections. 2 is also relatively easy although handling 3D data does require some additional effort. Origin refers to the owners of the data. If the data has been made in-house such as the COOEE and Road Directorate measurements, it is easier to prepare the data for analysis, compared to foreign data where knowledge about the data collection procedure is not as easily accessible. Once again, 7 and 2 rank high. Another aspect is the scope of data, i.e., size of the data set and spread in measured values such as MPD and rolling resistance. In this category many of the measurement campaigns rank high. 6 ranks high since the amount of measurements and spread i texture and unevenness values are high. The same goes for the 3 campaign and to some extent also 1, although the latter has discrepancies because texture is measured in the wheel tracks whereas rolling resistance is measured between wheel tracks. The scope of 5 w.r.t texture is also good, since the test track contains many different pavement types. Nonetheless, the length of the test sections are quite small which makes it difficult to get reliable trailer results. Of course, as the amount measurement of data increases the preparation time increases as well. Last but not least we have measurement types, i.e. what kind of measurements are available. Again 6 ranks high, since detailed data exists on texture, unevenness, cross fall, meteorological conditions etc. This also goes for 2 where there is detailed 3D measurements, but unfortunately the diversity is not optimal since only three road sections have been measured.

Based on the above considerations, data from 2 and 6 have been chosen. This gives different sources of data: Coast-down measurements and trailer data together with 3D texture profiles. It would have been desirable to have 3 as well, but it would have been too time-consuming and so this data set have unfortunately been omitted. Data from 1 have also been considered, but the difference in setting for RR and texture measurements mentioned above made these measurements less attractive.

5 Data from Værløse Airbase

The data used here has been made as part of WP4 in the COOEE-project and supervised by Niels Djuradin from the Danish Road Directorate. The measurements were made on Værløse military air base which was closed down (beginning in 2004), so the measurements could be performed without external disturbances. Three road sections were selected for the measurements: Curved, Main, and Parallel. A air photo of the location is shown in figure 5.1. Initial pilot measurements were performed on all three road sections to see if the spread in MPD/IRI resembles that of the entire state road network (which it did). See table 5.1 for an overview of these results. The main measurement campaign consisted of three kinds of measurements that were carried out on the test sections:

1. Measurements by the rolling resistance trailer developed at the Technical University of Gdansk (TUG) and performed by Prof. Jerzy A. Ejsmont from TUG. The trailer measured with 3 different tyres: SRTT, AAV4, and MCEN16. General information about these tyres is given in table 4.2 and specific details particular to these measurements are shown in table 5.3. Each tyre was measured three times on each of the three selected road sections. See table 5.2 for an overview of the results and additional information.
2. 3D laser profiles of the three road sections made by RoboTex, a measurement device developed by The Transtec Group Inc. These measurements were performed by Dr. Robert Otto Rasmussen and Richard C. Sohaney and consist of 100 parallel longitudinal lines on a 100 mm interval. Each road section was measured two times, in opposite direction, in approximately the same 100 mm track and the transversal, longitudinal and vertical resolution is **1.00**, **0.50** and **0.01** mm, respectively. See figure 5.2 for a 100 mm by 100 mm sample of these measurements.
3. 2D and '2.5D' measurements performed by the Danish Road Directorates noise research group to test their new equipment. These measurements have not been used in this study since the 3D laser profiles are of much higher resolution.

Unfortunately, the 'Curved' road section caused problems with the measurements. Both The Transtec Group and especially Prof. Ejsmont operating the TUG trailer said that their equipment was not well-suited for a curved road section, and therefore the data from this road has been used with caution, if at all.

While the primary goal is to validate the TPA measure we begin with two additional investigations that this data set is used for: Isotropy investigations and an illustration of how to use fdPCA with rolling resistance measurements.

5.1 Isotropy Investigations

In chapter 4 it was mentioned that the way asphalt mix is produced, it should be isotropic and this serves as an implicit assumption when using 2D texture profiles for assessing surface induced

Figure 5.1 Air photo of Værløse airbase.

Table 5.1 Information about texture measurements.

Road section		Main	Parallel	Curved
Length [m]		550	640	600
1st run	MPD left	1.81	0.87	1.23
	MPD right	1.47	0.79	1.20
	IRI left	0.97	1.71	1.65
	IRI Right	1.01	2.06	1.65
2nd run	MPD left	1.61	0.82	1.20
	MPD right	1.56	0.81	1.14
	IRI left	1.14	1.67	1.73
	IRI Right	1.11	1.99	1.62
Mean	MPD	1.61	0.82	1.19
	IRI	1.06	1.86	1.66

rolling resistance. A couple of investigations have been deployed here but they will only be limited in scope and merely substantiate the claim, not give a definitive answer.

5.1.1 Histogram comparison

An obvious examination is to look at the distribution of height values of the 3D-profiles, i.e., the height histograms. A necessary (but not sufficient) condition for isotropicity would be that different longitudinal 2D-profiles from the same road sections will have a similar height histogram. On the other hand, two longitudinal 2D-profiles from different road sections would generally have significantly dissimilar height histograms. Similarity is not well defined but fortunately we have a straightforward and intuitive way of determining dissimilarity. If the histograms differs in a statistically significant way from each other, i.e., if the difference persist across confidence intervals. Given the large amount of data, confidence intervals can easily be calculated from the 100 longitudinal lines and visually inspected. Since each line contains

Table 5.2 Overview of the rolling resistance measurement results and additional information.

Tyre	Section	Speed	C_{RR}	Temp. Air [C°]	Surface [C°]
SRTT		80	0.0111	12.0	16.0
AAV4	Main	80	0.0158	12.0	20.0
MCEN		80	0.0107	12.0	17.0
SRTT		80	0.0099	12.0	21.0
AAV4	Parallel	80	0.0153	12.0	24.5
MCEN		80	0.0107	12.0	20.5
SRTT		80	0.0094	12.0	19.0
AAV4	Curved	80	0.0151	12.0	22.5
MCEN		80	0.0099	12.0	21.0

Table 5.3 Overview of pilot measurement results.

Tyre	**Hardness** [Sh]*	**Max load** [kg]	**Max inflation** [kPa]
SRTT	65	730	240
AAV4	62	900	405
MCEN16	63	750	350

more than 10^6 measurements it should be more than enough for a detailed histogram, where the bin-size is given by the vertical resolution of 0.01 mm. Thus, for each road section a histogram with bin-size of 0.01 of the vertical values have been calculated, for each of the 100 lines. See an example of one of these in figure 5.3. Then the two maximum and the two minimum values of the 100 lines have been removed from each bin, such that the maximum and minimum values after this removal gives the 96% confidence interval, see figure 5.3.

As these confidence intervals show, there seem to be little deviation from the mean trend for a particular histogram and given the fact that most bins contain between 1000 and 5000 data points this suggests a rather stable behaviour. The confidence histograms from all three road sections are shown in figure 5.4 and it is quite clear from this plot that the three road sections have statistically significant differences in distributions of data points. This strengthens the hypothesis that some isotropicity in the longitudinal direction is present.

5.1.2 Spectral Analysis

The major drawback of the approach above is that the histograms are global for the entire road section in question. Thus, it is not possible to examine whether there are any differences in the longitudinal versus transversal direction. In this section this matter is addressed using Fourier analysis to compare quantities in the frequency domain between transversal and longitudinal 2D slices of the 3D profile.

Since the transversal width is 100 mm, the 3D road profiles will partitioned into 100 x 100 mm squares. Given that the sampling frequency in the longitudinal direction is twice as high as in the transversal direction, every second measurements in the longitudinal direction have been removed. For each square, the Fourier transform of the 100 transversal and longitudinal

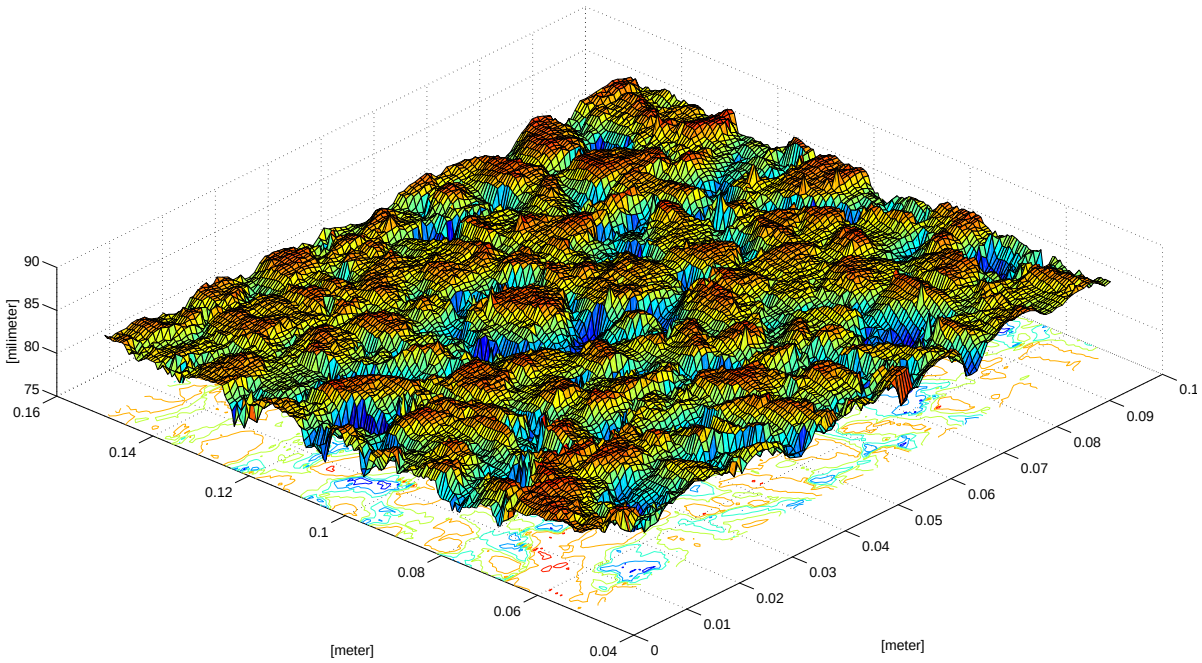

Figure 5.2 A sample plot of the 3D measurements made at Værløse air base. This sample is from the measurements made on the 'Main' road section.

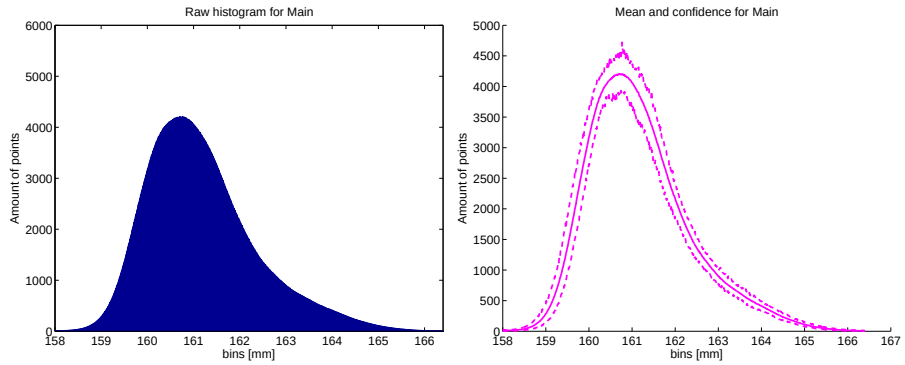

Figure 5.3 Left: Histogram (out of 100 for each section) from road section 'Main'. The bins have 0.01 mm in width and are not visible to the naked eye. Right: Mean and confidence for all the 100 histograms for road section 'Main'.

lines were calculated, and since the road sections are 550 to 640 meters in length, this gives 550.000-640.000 transversal/longitudinal transformed data sets to work with. In figure 5.5 spectral plots of three of these samples, in the longitudinal direction, are shown.

The approach of section 5.1.1 is also used here to calculate mean spectrum and corresponding 96% confidence intervals for both longitudinal and transversal data sets. Plots of the two non-

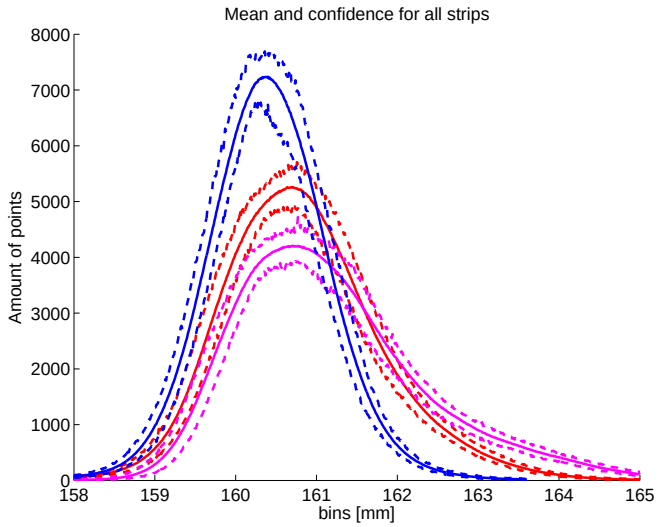

Figure 5.4 Mean and confidence limits calculated for all three road sections. The significant difference between them is apparent from this plot.

curved road sections are shown in figure 5.6 and 5.7, respectively. Unfortunately, each sample is based on a much lower set of points than the histograms of section 5.1.1, so the individual variation will play a much more significant role. This is also noticeable from figure 5.5 and figure 5.6. However, if we compare figure 5.6 and 5.7, it is clear that the spectra of the two road sections are significantly different while the transversal and longitudinal spectra for each road section are quite similar.

As discussed in chapter 3, merely looking at the amplitude for the frequencies in question does not give the entire picture. As illustrated in figure 2.5 and 2.6, radically different schematic profiles can have an approximately equal spectrum. Basically, since the Fourier transform is bijective, it follows that the differences in the frequency domain of the functions in figure 2.5 and 2.6 are solely due to phase differences. In other words, since their amplitudes are almost equal it must be the phases that makes them differ so much. Although the situation in figure 2.5 is rather schematic, it might be the case that a similar phenomenon occur for pavement profiles and these data in particular. By using the same procedure as above, a plot of mean + confidence intervals for the phases of the 'Main' road section is shown in figure 5.8. The figure suggests that there is a difference between the two directions: In the transversal direction the phases fluctuates with frequency as opposed to a more steady behaviour for the longitudinal direction, although they maintain approximately the same level. Note the large width of the confidence intervals, given that all the phases should be contained in $[-\pi, \pi]$. To get an overview of all data, the transversal and longitudinal phase plots for all road sections are shown in figure 5.9 and 5.10, respectively. From this it is clear that the phase distribution is almost equal for all frequencies, across all three road sections. It is especially noteworthy how close the mean and confidence interval of the three road sections follows each other in the transversal direction where the phase fluctuates the most. Therefore it seems safe to conclude that the phase distribution is equal for all three road

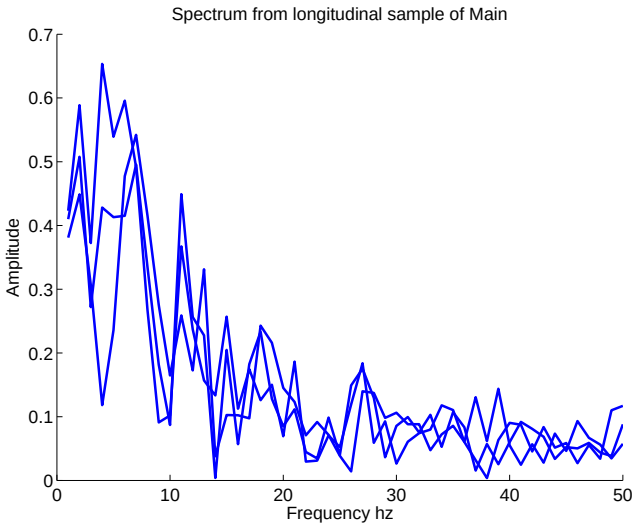

Figure 5.5 Three samples of spectrograms from the 'Main' road section. The samples have been obtained from 100x100 mm slices of the road section.

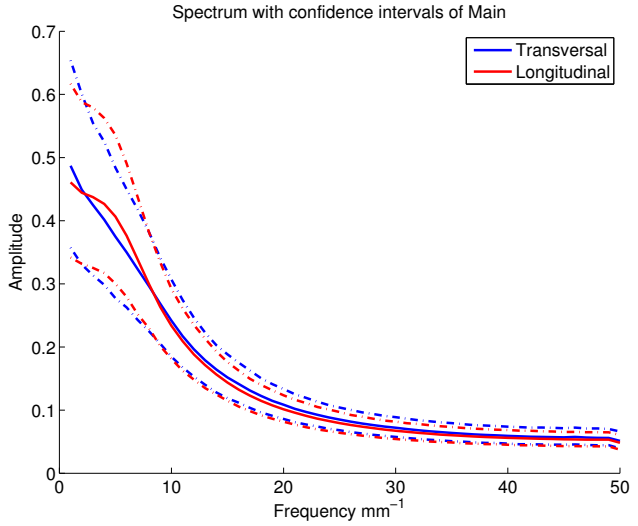

Figure 5.6 Mean and 96% confidence intervals for the two road sections

sections *and* that the distribution is different for the transversal and longitudinal directions. The latter observation is particularly interesting in light of the fact that the difference persist for all three road sections which suggests that the difference might be road section independent. The reason for this could be measurement accuracy. When Transtec Group provided the data, the

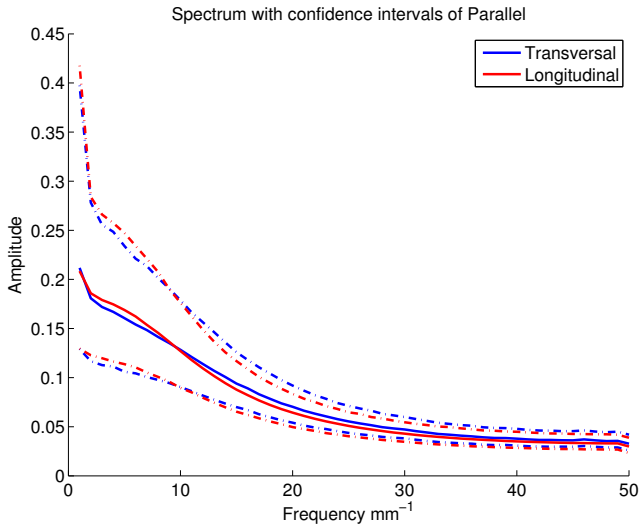

Figure 5.7

transversal measurement resolution was given implicitly, whereas the longitudinal resolution was provided with as an array of distance values. This array showed an *average* distance between measurements of 0.5 mm, but with small variation. More specifically it varied between 0.49800mm and0.53500mm. This variation could affect the Fourier transformation since the `FFT` routine requires uniform spacing between measurements. This explains the discrepancy in transversal and longitudinal phase distribution was identical for all road sections.

In conclusion, the isotropy investigations indicate that the leap from 3D to 2D seems reasonable, i.e., road sections have a uniform behaviour that does not depend on the exact position or direction. Furthermore, there were unambiguous differences between the road sections investigated. A couple of remarks should be tied to this conclusion. First of all, the dataset used above is scarce and using only three road sections, where one of them have not been measured under optimal conditions, might not be sufficient. Secondly, the plots showed differences between longitudinal and transversal direction. While the difference is suspected to come from the measurement equipment, it cannot be excluded that it is caused by direction-dependent differences in the surface. On the other hand note that the spread in MPD is very high, which indicates that the pavement might not differ that much in texture. Thus the results about the differences between road sections are even more interesting given that the road sections do not differ much in texture as measured with MPD.

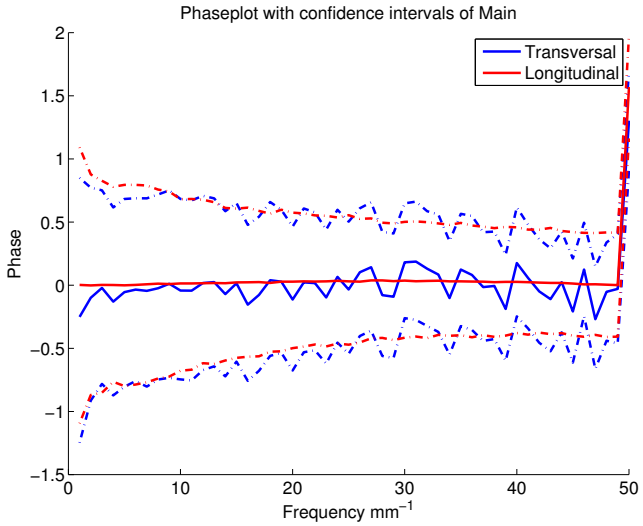

Figure 5.8 Example of mean and confidence intervals for the phases for the Main road section

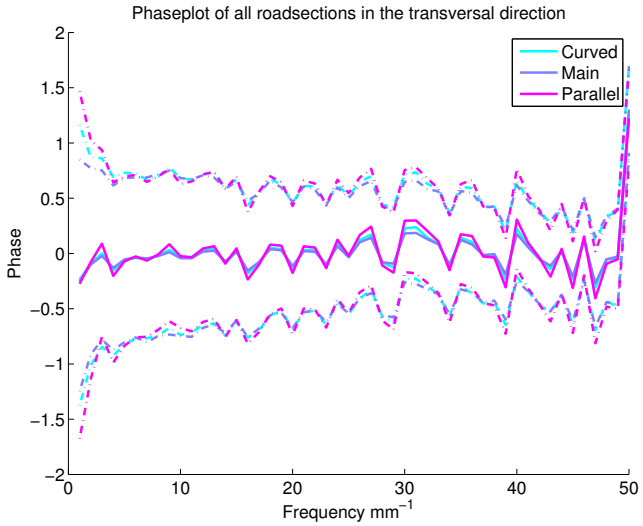

Figure 5.9 Phase plot of all three road sections in the transversal direction. Solid lines are mean phase plot and dashed lines denoted confidence intervals.

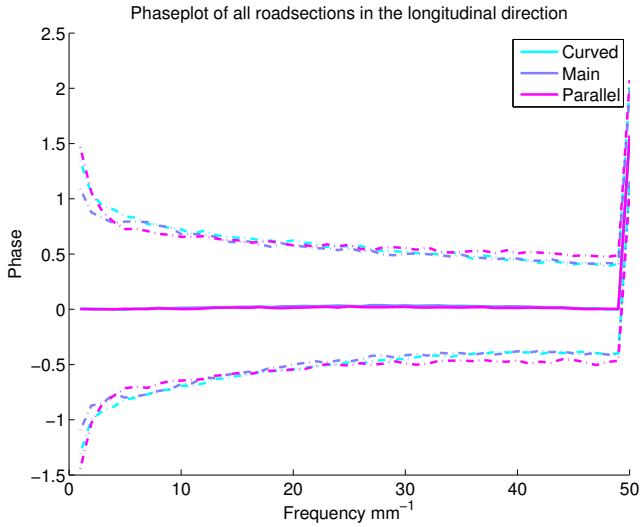

Figure 5.10 Phase plot of all three road sections in the longitudinal direction. Solid lines are mean phase plot and dashed lines denoted confidence intervals.

Figure 5.11 TUG trailer at the measurement site.

5.2 Trailer Data

As mentioned above, the rolling resistance trailer from TUG was used for these measurements. A picture of the trailer is shown in figure 5.11 which was taken from the measurement site at Værløse airbase. To get a rough overview of the data all three measurements of the SRTT-tyre have been plotted for all road sections in figure 5.12. There seems to be a rather good reproducibility of the trailer, so the three measurements for each road section are hard to distinguish from each other. Nevertheless, there are a few remarks to be made about figure 5.12. The measurements of the 'Curved' road section is by far the most fluctuating of the three, whichmight be caused by the high road curvature. This was mentioned in the beginning of this chapter as a potential problem since the trailer is not build to handle high road curvature. In contrast, the 'Main' and 'Parallel' road sections are much more stable and a mean difference in rolling resistance is clearly observable, although it is rather small. More precisely, the average of the two (taken over all three road sections) is 0.01113 for 'Main' and 0.00994 for 'Parallel'.

To get a clearer picture of the separate road sections, all measurements for all tyres from 'Main' and 'Parallel' have been plotted in figure 5.13 and 5.14, respectively. It is clear from the measurements that the AAV4 tyre has the highest rolling resistance, whereas MCEN and SRTT is ambiguous: On 'Parallel' the SRTT tyre has the lowest rolling resistance with the MCEN tyre having second lowest, while it is the other way around on the 'Main' road section. On the 'Curved' road section AAV4 also ranks highest and SRTT lowest, although close to MCEN. The reason for the interchange of MCEN and SRTT on 'Main' is unknown, but intuitively one would expect that the tyres were ranked equally for all three road sections.

The degree of measurement repeatability is also much clearer in figure 5.13 and 5.14. The average value of a single tyre is quite stable and there seem to be a good correlation in some of

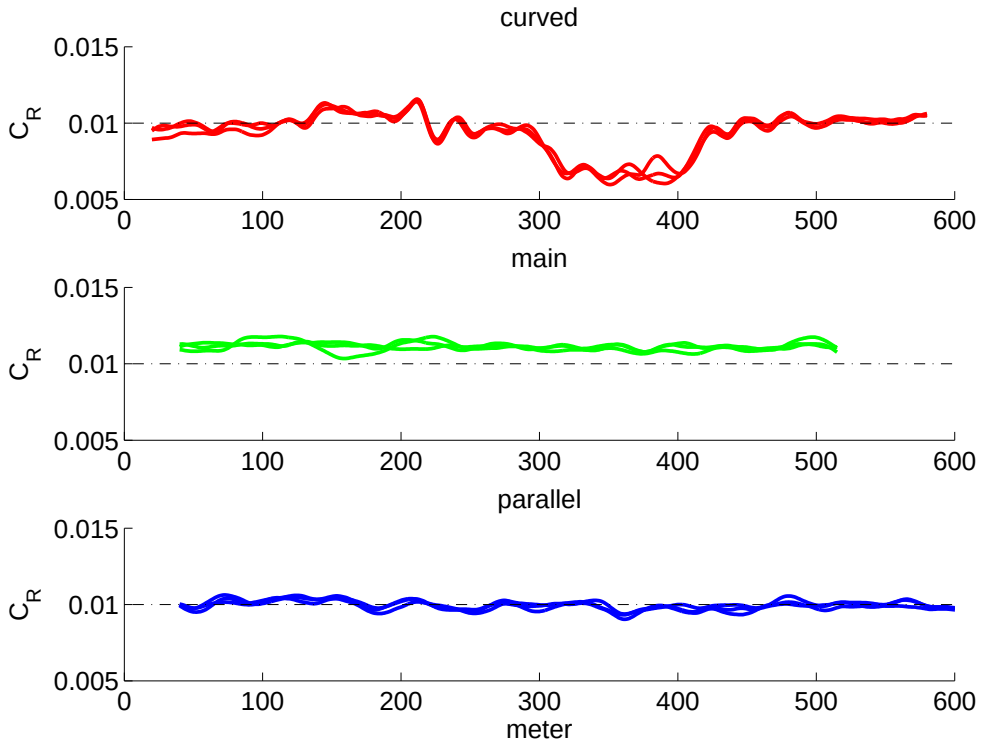

Figure 5.12 Overview of rolling resistance measurements for all three roads.

the fluctuations that occur during a measurement, especially for the same tyre. These fluctuations also holds to some extent across tyres as can be seen, e.g., between 180 m and 250 m in figure 5.14, as well as the valley at 360 m, the peak at 500 m or the valley at about 380 m in Fig 5.13. However, even within measurements using a single tyre there seems to be significant irregularities in all plots and the inter-tyre correlation seems much weaker in figure 5.13 than figure 5.14.

In general, the causes of variation in rolling resistance across a measurement run is not clearly understood. The variation occurs at approximately 20-100 m wavelengths and appears to be consistent in the sense that it varies smoothly across data points. In contrast, e.g., MPD values have a high data-point-to-data-point variation even though they are constituted as a mean of at least 10 MTD values. Therefore it seems implausible that the variation is due to macro texture. In addition, inertial resistance, aero dynamic drag, trailer tilting and road gradient should be dealt with in the design, according to TUG[182, 183] which should exclude, e.g., cross-sectional displacement, unevenness etc. Since the data has been delivered from TUG in a filtered form without any details disclosed, this is more or less a black box and therefore it is mere speculation whether, e.g., unevenness plays a role in the rolling resistance measurements (even though unevenness might explain the partial repeatability).

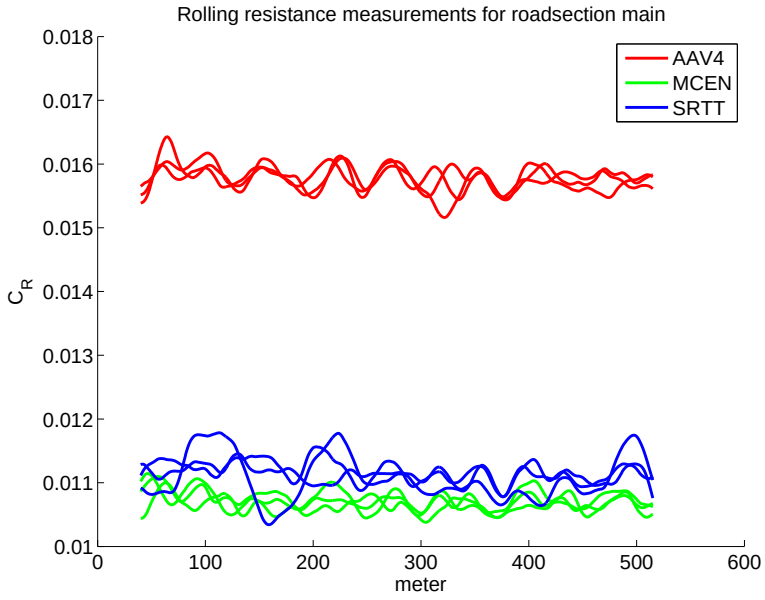

Figure 5.13 Rolling resistance measurements for all tyres on 'Main'.

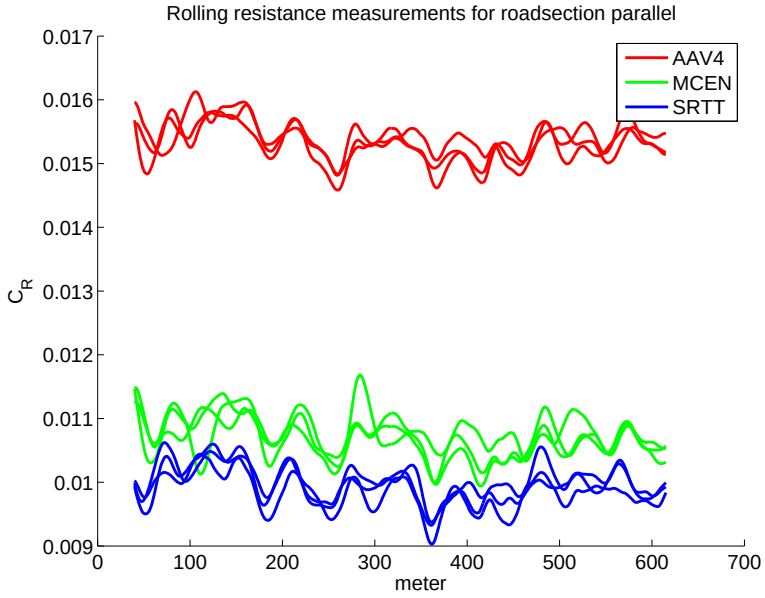

Figure 5.14 Rolling resistance measurements for all tyres on 'Parallel'.

5.2.1 Functional PCA example using Trailer Measurements

As mentioned in the previous section, the degree of reproducibility is ambiguous which will be investigated in more detail here. Another goal of this section is to illustrate the usage of fdPCA as discussed in section 2.5. Given the small amount of measurement runs for each combination of tyre and road section, the analysis will use data from all tyres on each road section. This gives 9-10 measurement runs per road section. However, it would be interesting to perform a similar analysis with more repeated measurements and road sections such as the data obtained in studies discussed in section 4.2.1 and 4.2.2. In addition, the focus will be on the 'Main' and 'Parallel' road sections. All in all, this analysis will merely serve as a concrete example using real measurements that hopefully illustrate the usefulness which would be more pregnant with a more comprehensive data set.

To get a better overview of the data than what can be provided by figure 5.13 and 5.14, new plots of the rolling resistance measurements, is shown in figure 5.16-5.15 where all measurements using a particular tyre have been normalized. This is done by subtracting the total mean across all runs and distances, i.e., we remove the mean rolling resistance measured for each tyre, thus highlighting the variability between individual measurement runs. The mean for all runs is also plotted in black to show the mean behaviour of all runs. From visual inspection of these plots, it seems that the 'Main' road section exhibit least reproducibility across measurements compared to 'Parallel' or even 'Curved' where some fluctuation would be expected due to road curvature. While there is variation across measurements of 'Parallel' it can be seen that much of it is mainly due to differences in amplitudes. If we compare this to the measurement runs of 'Main' in figure 5.17 we see a much more erratic behaviour with additional irregularities with respect to phases of common undulations and even significant fluctuations that seems to pertain to one or few measurement runs only. In this respect, the results from the 'Curved' road section seems to be more on par with 'Parallel' where large parts of the measured road section mainly have variation with respect to amplitude and not as much difference in phase. All in all, however, all road sections seem to exhibit quite substantial variation despite the fact that these data clearly have been filtered in some undisclosed way. Also, there seems to be no significant grouping in variation across tyre types, except for the 'curved' road section where blue curves represent measurements with the AAV4 tyre. This might be caused by the dip at 300 - 400 m.

To investigate the variation across each road section in more detail, consider figure 5.20-5.19 which are 'curved', 'parallel', and 'main', respectively. They show the mean function $\mu(t)$ for all road sections together with $\mu(t) \pm C\xi_n(t)$ $n \in \{1, 2\}$ where C is a constant that depends on $\mu(t)$ and a scaling factor chosen to give the visually best plot (see [143, p.155] for details). The figures illustrate the distribution of weight for the given principal component.

We start by the curved road section in figure 5.15 since it has the most obvious and clear interpretation. The first component accounts for about 67% of the variability while the second accounts for 11%. It is pretty clear from figure 5.20 that the first component accounts for the variation caused by tyre-related grouping in the data. The second component seems to be covering other variations such as the general high variation observed in the valley at 300 - 400 m where fluctuating weight seems to imply non-uniform oscillation across measurement runs. In addition, the last 100 m exhibits high variation as well. The variation in these two ranges is also observable by visual inspection of figure 5.15.

In figure 5.18 we see the two first components account for approximately 30% and 22% for the two first components, respectively, thus only showing 50% of the total variation in the data. Both components contributes a substantial amount of weight in the range of approx. 70 - 170 m.

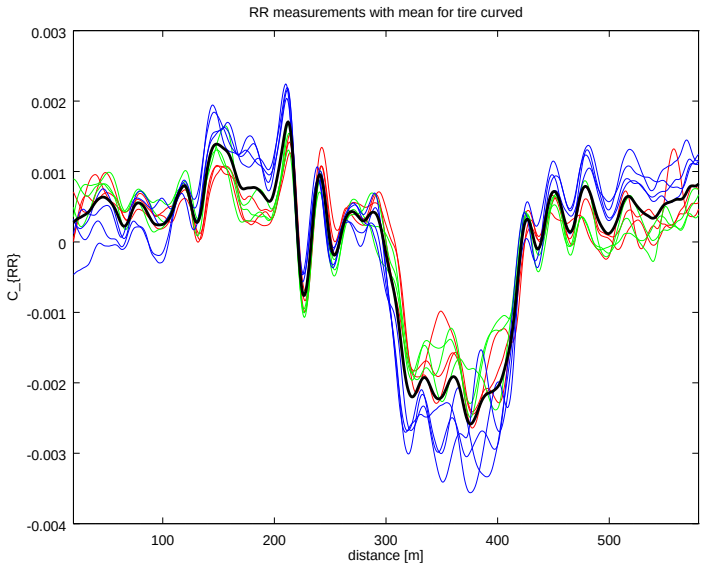

Figure 5.15 Normalized rolling resistance measurements from the 'curved' road section.

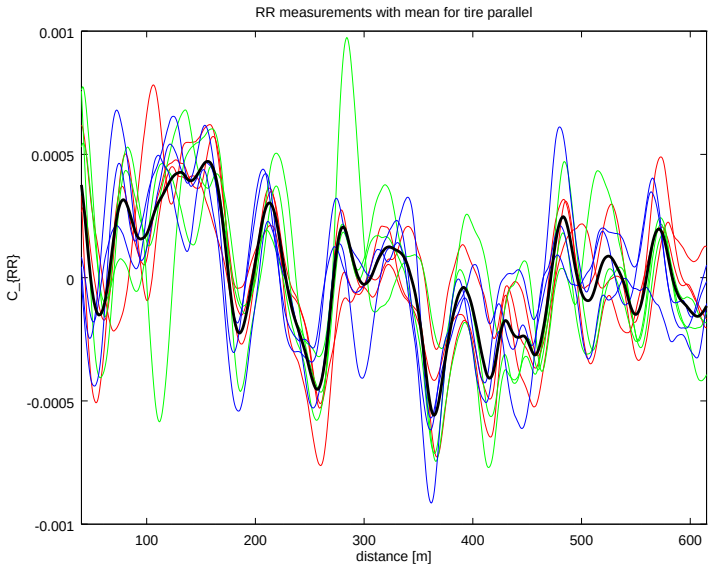

Figure 5.16 Normalized rolling resistance measurements from the 'parallel' road section.

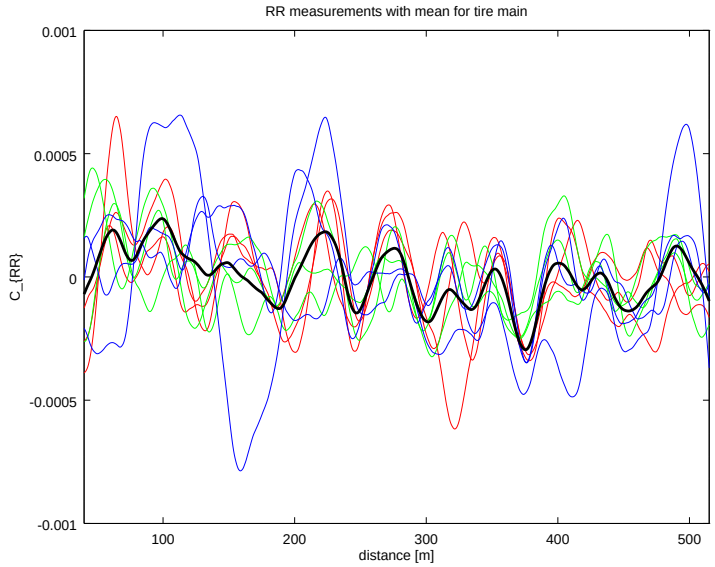

Figure 5.17 Normalized rolling resistance measurements from the 'main' road section.

Since the principal components are orthogonal, each of them covers different modes of variation. The 70 - 180 m variation seems to be different in nature whereas, e.g.,the twin peaks centered at 300 m seems to be related to differences in amplitude in both components. In the former case it seems to be very irregular variation whereas the latter seems to be mainly a question about the size of the amplitude. The first component of 'parallel' also attributes weight to the valley between peaks at 400 and 500 m and again in the oscillation occurring at approx. 500 - 550 m. Especially the latter seems to be caused by vertical shift. Finally, many of the peaks/valleys have a concentration of variation in both components which implies variation in amplitude.

figure 5.19 shows results for the 'main' road section where the first component covers about 49% of the variation while the second only covers 14%. The first component attributes a substantial amount of weight in the 100 - 200 m range and also some weight in what looks like a vertical shift of the oscillation starting at approx. 400 m. It is interesting to note that for the 100 - 200 m range the weight has the opposite sign of the outlier and by closer inspection it can be seen that the point (approx. 140 m) where the outlier and weight changes sign is also where the majority of measurements change sign in the opposite direction of the outlier and thus following the sign of the weight. A conclusion to be drawn from this is that the outlier is a major influence on the variation but the majority of measurements are the ones that have been prioritized when optimizing the sum of squared scores. In the second component there is most weight for the first peak after the 200 m mark with a phase shift component probably caused by the outlier, and again after the 300 m mark. As with the 'parallel' road section many peaks/valleys do have a concentration in variation.

One interesting conclusion to be drawn from all road sections is that the amplitudes seems, in general, to be subject to most variation. Whether this is a property of the phenomena being

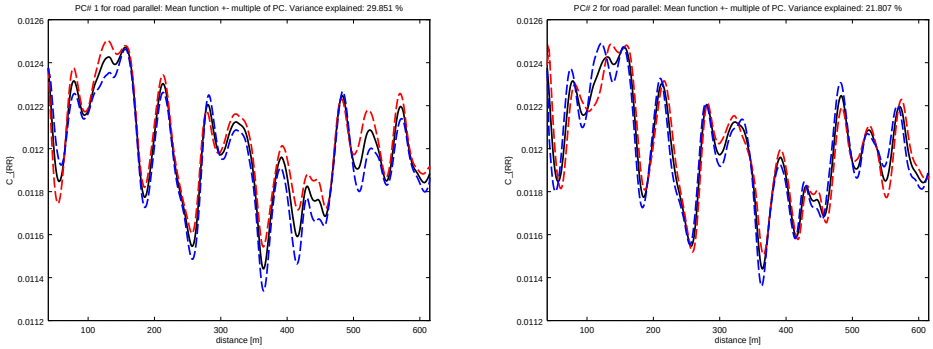

Figure 5.18 Plots showing mean function of 'parallel' measurements, together with the mean function where a multiple of the first (left) and second (right) principal components have been added (red) and subtracted from it.

measured or if phase shifts or other disturbances have been filtered is unknown. Nevertheless, some areas have been identified as having more erratic variation and in the case of 'curved' some areas are clearly identified as being more noisy. As such, this method seems fruitful in finding irregular parts of rolling resistance measurements thus aiding in locating parts of road sections where validity of the measurements are low. It has also been possible to identify the nature of the variation, i.e., if it is variation in amplitude, phase, vertical shift, a combination of these or something else entirely. This could be useful in analysing rolling resistance measurements in larger data sets. It would thus be interesting to make a similar analysis with rolling resistance measurements covering more road sections and with more repeated measurements, as in the studies discussed in section 4.2. This could potentially shed some light on the relationship between the low-frequency fluctuations observed in data, and the tyre and/or road.

Besides potential computational efficiency, the fdPCA approach used here might not differ substantially from what could have been performed with ordinary PCA. However, if we had unfiltered data at our disposal it would be obvious to include smoothness regularisation during functionalization or when calculating functional principal components. Regularisation could also be deployed if the measurement runs were longer and covering several pavements types as it could highlight potential variation on the road section level. Rolling resistance measurements performed in the Dutch study discussed in section 4.2.3 seem to be a good candidate for this kind of analysis.

5.3 Investigation of Texture Measures

In the previous sections we looked at the raw profile and trailer data in isolation. Now both types of measurements are used to compare TPA and MPD, i.e., we will calculate the MPD and TPA texture measures based on the raw profiles and investigate their relation to rolling resistance measurements. The typical way of assessing performance of a road metric is by assuming a linear relationship between texture measure and rolling resistance as it is done in the studies discussed in section 4.2. We will divide the investigation into two parts, the first part concerns the full TPA measure using fourth order B-splines, thus including parameters K and λ. Computing

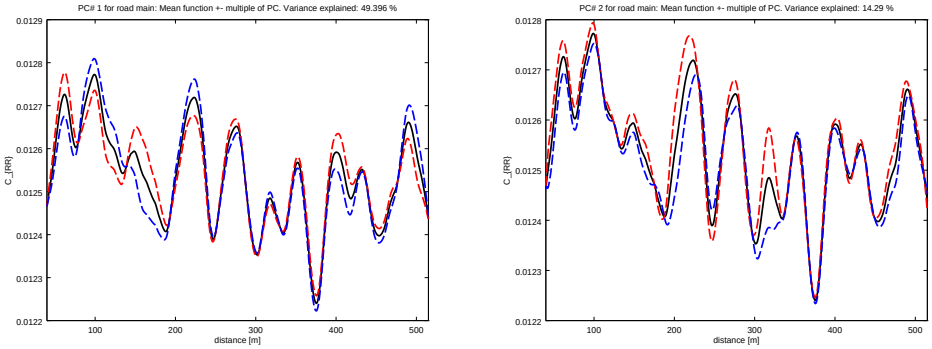

Figure 5.19 Plots showing mean function of 'main' measurements, together with the mean function where a multiple of the first (left) and second (right) principal components have been added (red) and subtracted from it.

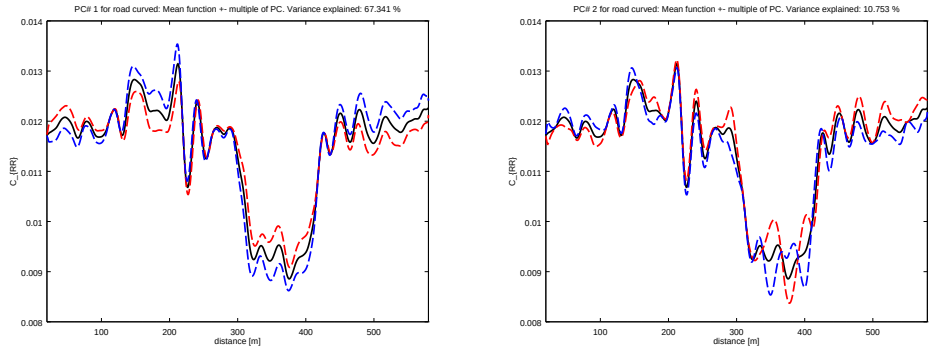

Figure 5.20 Plots showing mean function of 'curved' measurements, together with the mean function where a multiple of the first (left) and second (right) principal components have been added (red) and subtracted from it.

the full TPA measure is a rather laborious task and in this case, with 3D measurements, there are 100 2D-profiles per road section. Thus, to minimize computations the full TPA measure is only investigated for $e = 0$ which also enables a much more fine grained investigation of the remaining parameters. The second part concerns the simple version of TPA that relies on linear interpolation instead of fourth order B-splines. This is much faster to compute and does not depend on λ and K so all three values of e will be investigated.

Another consequence of the computational resources required is that we will not rely on numerical optimization methods to estimate the TPA parameters, which is the approach used in chapter 6. Instead, a suitable set of values from each parameter λ, K, d, e are selected for the full TPA (and d, e for the simple TPA) and every combination of these values are used to produce a TPA data set which can then be examined. As will be shown below, there is good reason to suspect that the simple TPA will suffice. The following sets of parameter values have

been chosen for the full TPA

$$\boldsymbol{\lambda} = \{10^{-13},\ 10^{-12},\ 10^{-11},\ 10^{-10},\ 10^{-9},\ 10^{-8}\} \tag{5.1}$$
$$\boldsymbol{K} = \{0,\ 1,\ 2,\ 3,\ 4\} \tag{5.2}$$
$$\boldsymbol{d} = \{10\%,\ 20\%,\ 30\%,\ 40\%,\ 50\%,\ 60\%,\ 70\%,\ 80\%,\ 90\%\} \tag{5.3}$$
$$\boldsymbol{e} = \{0\}. \tag{5.4}$$

The λ-values have been chosen by identifying extreme values by visual inspection, i.e., finding two opposing values where one gives a practically perfect fit to data and the other gives a highly (but reasonable) smooth fit to the data (an example of this is given in figure 6.6 of chapter 6). Then 4 different values (logarithmically scaled) between the extremes have been selected, which gives a total number of 6 different values, not too comprehensive to simulate. The K-values have been chosen as all values up until a maximum number of measurements between knots that have been assessed by visual inspection to give meaningful results. $\boldsymbol{d}$ is one of the primary parameters so every tenth percentile have been chosen except for 0 and 100% which is not physically consistent. Finally, as mentioned above, only $e = 0$ is used here. Thus, the set of different parameter configurations for the full TPA is

$$\boldsymbol{X} = \boldsymbol{d} \times \boldsymbol{e} \times \boldsymbol{\lambda} \times \boldsymbol{K}$$

and with the sizes of the sets described above, this gives

$$|\boldsymbol{X}| = |\boldsymbol{d}| \cdot |\boldsymbol{e}| \cdot |\boldsymbol{\lambda}| \cdot |K| = 9 \cdot 1 \cdot 6 \cdot 5 = 270$$

different TPA texture measure variations to calculate. For the simple TPA measure the parameter sets are

$$\boldsymbol{d} = \{10\%,\ 20\%,\ 30\%,\ 40\%,\ 50\%,\ 60\%,\ 70\%,\ 80\%,\ 90\%\} \tag{5.5}$$
$$\boldsymbol{e} = \{0,\ 0.054,\ 0.0025\} \tag{5.6}$$

and therefore only 27 different variations for each road section.

The following general approach has been used to determine the correlation between texture measures (MPD/TPA) and trailer rolling resistance measurements: The TPA/MPD measures were paired with the RR measurements and in case of, e.g., full TPA it was done for all parameter configurations $(\lambda_0, d_0, e_0, K_0) \in \boldsymbol{X}$. We will investigate a linear relationship, so simple linear regression was performed on these paired data, i.e., linear regression on $(x, y) = (\mathrm{TPA}, \mathrm{RR})$ and $(x, y) = (\mathrm{MPD}, \mathrm{RR})$. The coefficient of variation R^2 has been used as a goodness-of-fit and correlation measure as is customary in this field of research. As mentioned in section 4.3, d could potentially vary across road sections which is one of the primary questions to investigate below. The parameter configurations above only hold for the case were d is fixed/uniform on all road sections. When investigating varying/dynamic penetration depth d we will expand the parameter configuration tuple above to include a d-parameter for each road section. In case of the full TPA examined for all road sections, R^2-values will be generated for each parameter configuration $(d_P, d_C, d_M, e, \lambda, K)$ in the set of extended parameter configurations $\boldsymbol{X}'$ defined as

$$\boldsymbol{X}' = \boldsymbol{d}_P \times \boldsymbol{d}_C \times \boldsymbol{d}_M \times \boldsymbol{e} \times \boldsymbol{\lambda} \times \boldsymbol{K}$$

where $\boldsymbol{d}_P, \boldsymbol{d}_C$, and $\boldsymbol{d}_M$ are the sets of penetration depth values used for the Parallel, Curved, and Main road sections, respectively.

Finally, in the studies discussed in section 4.2 of chapter 4, calculated road metrics have been averages across all road sections. This seems quite coarse to the author and it is not known whether this is just a standard practice or if correlations quickly break down if less averaging is used. Therefore are different aggregation lengths from 10 to 100 meters considered here to examine how R^2-values behave under varying aggregation. Since most of the road sections considered in the aforementioned studies are more than 100 meters, our highest aggregation length is actually quite low. Investigations discussed below that is not concerned with aggregation uses 100 meters unless stated otherwise.

5.3.1 Results - full TPA

In this section we start looking at the case with no enveloping and we start by examining the case where the value of d is constant over all road sections.

As mentioned in the beginning, rolling resistance data from the road section 'Curved' might not be usable because of its curved geometry. Thus, the first thing to check is if the rolling resistance measurements from the 'Curved' road section is usable at all to this investigation, i.e., do the R^2 values drop significantly when using this road section in the regression described above. To verify this and compare overall correlation results, R^2 values for all road sections and when 'Curved' is excluded are plotted in figure 5.21 and 5.22, respectively. The former is for all road sections, whereas 'Curved' is excluded in the latter.

By direct comparison between the y-axes of figure 5.21 and 5.22 it is seen that correlation is non-existent if the 'Curved' road section is taken into account. The R^2 value drops from the best correlations above 0.9 in figure 5.22 to below 0.2 in figure 5.21! This was, unfortunately, expected and all subsequent analysis will omit the 'Curved' road section which limits the scope of the analysis.

If we take a closer look at the left plot in figure 5.22, some interesting observations can be made. There exists a substantial amount of variation between the different tyres. The SRTT tyre especially stands out with extremely poor correlation, in particular with MPD. While the rolling resistance between tyres is known to vary significantly, they should still correlate with MPD. The small data set could be the reason for the lack of correlation, but the drop is so consistent through all three plots (figure 5.21 and 5.22) that this does not seem to be the case. Another explanation might be measurement-problems for this specific tyre. If we look at figure 5.13 we see that the rolling resistance measurements for the SRTT tyre stand out as highly irregular compared to the others. The reason for this irregularity is unknown but the SRTT tyre has been unproblematic in other studies so it is likely because of some error related to the measurement of 'Main'.

If we compare the different texture measures, the results are mixed. In the left plot where d is constant across road sections, MPD and TPA seems to be rather close with respect to goodness of fit. With the AAV4 tyre the TPA measure has a slightly better R^2 value than MPD and with the MCEN tyre it is the other way around. It is noticeable that although TPA performs poorly on the SRTT tyre it is still significantly better than MPD. To get a clearer picture than merely looking at R^2 values, plots of raw data that give rise to the R^2 values are shown in figure 5.23 for the MCEN tyre and figure 5.24 for SRTT tyre. These two highlights best and worst cases of figure 5.22 where d is constant. When comparing figure 5.23 and figure 5.24 the difference in R^2 values are clearly seen in the amount of dispersion of data points. In the case of the SRTT

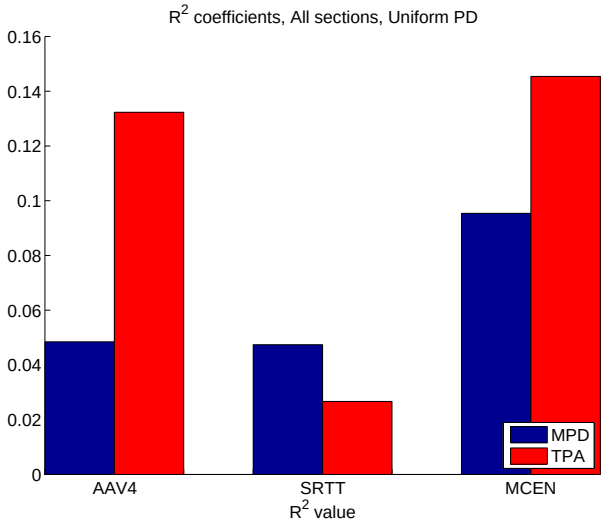

Figure 5.21 This plot shows the R^2 coefficients for the linear regressions based on all road sections. The plot shows MPD vs. TPA when the penetration depth d is held constant for all road sections.

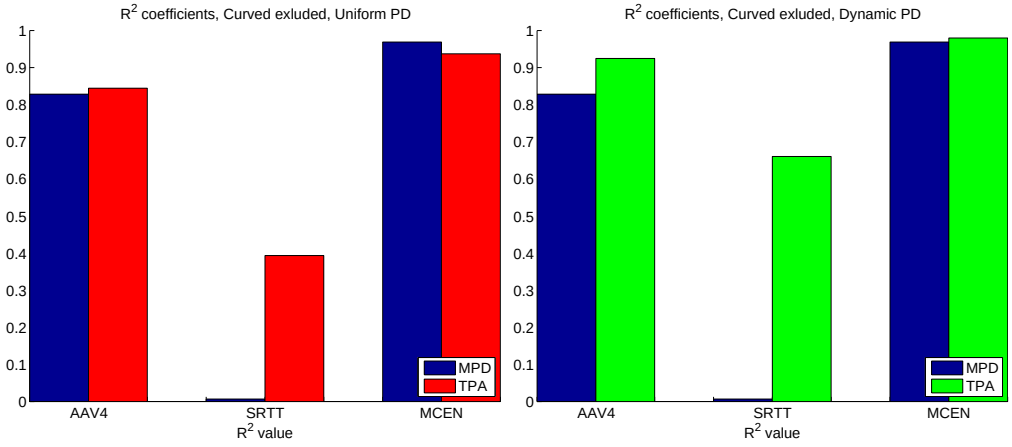

Figure 5.22 This plot shows the R^2 coefficients for the linear regressions based on 'Parallel' and 'Main'. The left plot shows MPD vs. TPA when penetration depth d is held constant for all road sections and to the left the optimal $d \in \boldsymbol{d}$ has been chosen for each road section. Note that the R^2-values for MPD are equal on both plots and have been included in both for completeness.

tyre with low R^2 in figure 5.24, the spread in rolling resistance values for a given texture metric is very high and the lack of correlation is apparent. The opposite conclusion could be said of figure 5.23 where data points from the two road sections are clearly separated in both the TPA and MPD plots. This behaviour is repeated with the AAV4 tyre which is not plotted here. One noticeable difference between MPD and TPA in figure 5.24 is how the texture metric values are

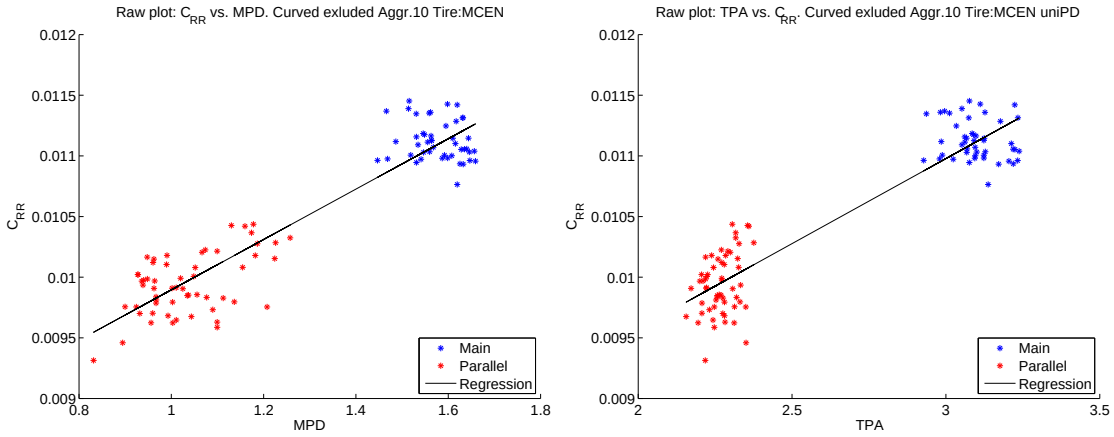

Figure 5.23 Both plots show the calculated texture measures vs. rolling resistance trailer measurements for the MCEN tyre. The measurements and texture measures have been aggregated into 10 meter segments . Equation for the regression line for the MPD-case to left is $y = 0.0021x + 0.0078$ and $y = 0.0014x + 0.0068$ for the TPA-case.

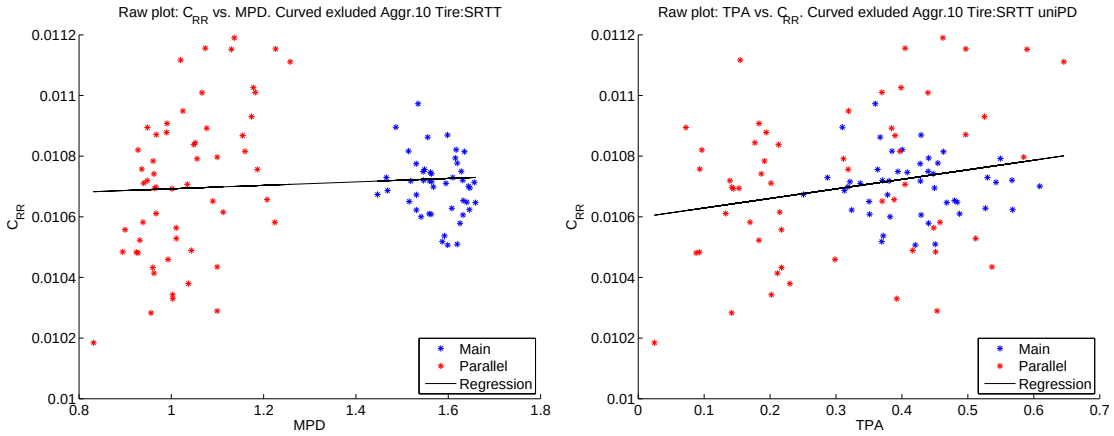

Figure 5.24 Both plots show the calculated texture measures vs. rolling resistance trailer measurements for the SRTT tyre. The measurements and texture measures have been aggregated into 10 meter segments. Equation for the regression line for the MPD-case to left is $y = 0.0001x + 0.0106$ and $y = 0.0003x + 0.0106$ for the TPA-case.

distributed on each road section. In the case of MPD, the spread in rolling resistance values is extremely high even though the MPD values of the two road sections are clearly separated. In the case of TPA the data points are much more mixed, but higher rolling resistance values do seem to correlate slightly with higher TPA-values on the Parallel road section. This might explain the better R^2 compared to MPD. All in all, the two texture measures seem to exhibit similar qualitative behaviour, but definitive conclusions are hard to make when only two road sections have been used. The TPA calculations used in the comparison above are primitive

compared to the full-fledged measure where d also varies across road sections which is depicted in the right plot of figure 5.22. In this plot the TPA-measure performs better than MPD on all tyres but the result should be taken with a grain of salt due to several factors: First of all it is to be expected a priori since the parameter space, when d is constant, is a subset of the parameter space where d can vary across road sections. The general aspects of this is discussed in section 4.3 of chapter 4 but in this particular investigation it is especially illustrative as there is only a finite set of d-values. The superset (where d vary across road sections) is defined as

$$A = \boldsymbol{d} \times \boldsymbol{d} = \{(d_1, d_2) \mid d_1, d_2 \in \boldsymbol{d}\} \tag{5.7}$$

corresponding to the set of possible penetration depth configurations tried out, before arriving at the results plotted to the right of figure 5.22. The situation with constant d across road sections can be described as

$$B = \{(d_1, d_2) \mid d_1, d_2 \in \boldsymbol{d} \text{ and } d_1 = d_2\} \subset A. \tag{5.8}$$

Thus, the configuration with the best result from B that can be found when d is constant, is also contained in A, i.e., since there are many more configurations in the former case, an improvement is to be expected. This, combined with the fact that the data set is particularly small makes the validity of the observed improvement in going from constant to dynamic d questionable. Therefore an in depth analysis is omitted here, but this question will be revisited in the next section when the simple TPA is investigated.

There is one notable difference between bar plots such as figure 5.22 and plots of raw data as figure 5.23, namely the amount of data aggregation used. In figure 5.22 the underlying data have been aggregated into 100 meters and for the raw data plot such as figure 5.23 the aggregation is 10 meters. The former resembles the practice of previous work, but it was found that a lower aggregation showed the true nature of the data better in figure 5.23. As expected, the correlation drops as data aggregation decreases. This is shown for all three tyres and uniform d in figure 5.25. It can be seen how quickly the correlation drops with aggregation[1]. Note the difference between rate of decrease between the MCEN and AAV4 tyre where the latter drops much faster than the former. Also, MPD gets a better correlation as aggregation decreases for the AAV4 tyre, although the overall difference is rather small. On the other hand, MPD drops quicker than TPA for the MCEN tyre. The SRTT tyre is plotted with the others for completeness. As with the results above, there is no clear conclusion to be drawn, except perhaps that high aggregation is needed to get proper results. This is probably not surprising, since the underlying phenomenon causing the energy loss that we are trying to measure, is subject to much noise.

We would also like to investigate the role of the global parameters λ and K and how they affect TPAs goodness of fit. Given the discussion about varying d versus keeping it constant across road sections, we will keep d constant here. We will also keep the data aggregation constant at 10 meter to include as much data as possible. Furthermore it would be desirable to keep the influence of d at a minimum, even though the value of R^2 is expected to vary substantially as a function of d. Therefore we normalise by subtracting the mean of R^2 for each tuple of R^2-values corresponding to varying λ (K, resp.) while keeping parameters d and K (λ, resp.) constant. In the case of λ we have $|\boldsymbol{d}| \times |K| = 45$ different R^2-tuples and $|\boldsymbol{d}| \times |\lambda| = 54$

[1] If we aggregated each road section into one texture measure value and one rolling resistance value, we would trivially have $R^2 = 1$

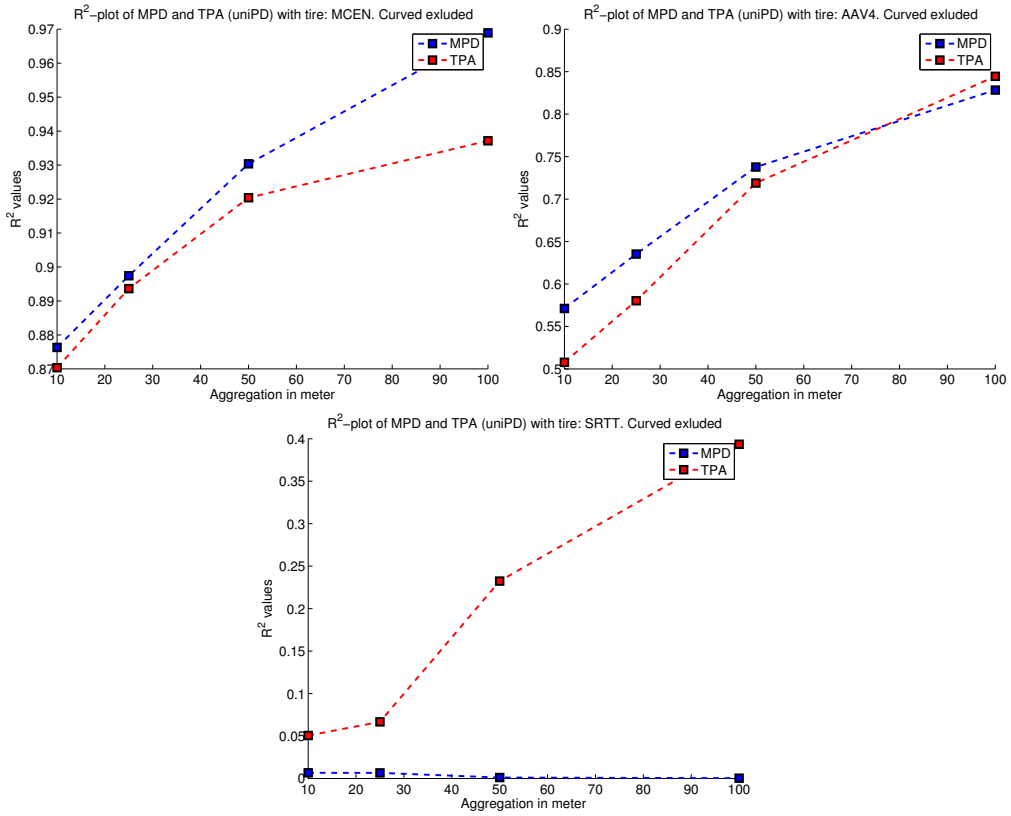

Figure 5.25 Plot of data aggregation vs. R^2 values. For each aggregation, the best possible value of R^2 is found out of different combinations of λ, K, and (uniform across road sections) d.

for K. After normalisation, a box plot[2] is made for each entry in the tuples corresponding to a specific value of λ or K. The results are plotted in figure 5.26 for λ and figure 5.27 for K. In figure 5.26 the result is unambiguous: The best distribution of normalised R^2-values occurs when $\lambda = 1 \times 10^{-13}$ and 1×10^{-12} which have almost equal distribution. But then it slowly and consistently drops until $\lambda = 1 \times 10^{-8}$ where it gets much worse. Although the underlying data set is small, the trend is clear: Low to no smoothing is optimal when converting discrete data into functions during TPA calculation. The results for K in figure 5.27 is not as unequivocal a result as in the case of λ. With 3 to 4 measurements between knots, the overall results seems to be a trend towards lower R^2 values with some positive outliers. 0-2 data points between knots gives significantly better correlation values than with 3-4 knots, but 0 knots between measurements seems like the optimal choice. Although the distribution of R^2 values is more dispersed for 0 knots than 1-2 knots, the spreading is skewed towards better R^2 values. All in all, it seems that

[2] A boxplot is a classical method for visualising data dispersion in a compact way. The graphical represententation is made as follows: The line in the box represents the median of the data. The bottom (top) of the box represents the first Q_1 (third Q_3) quartile of the data, respectively. The bottom (top) of the whiskers (vertical dotted lines) represents $Q_1 - 1.5 \cdot (Q_1 - Q_3)$ $(Q_3 + 1.5 \cdot (Q_1 - Q_3))$, respectively. The '+'-points represents outliers from the interval demarcated by the whiskers.

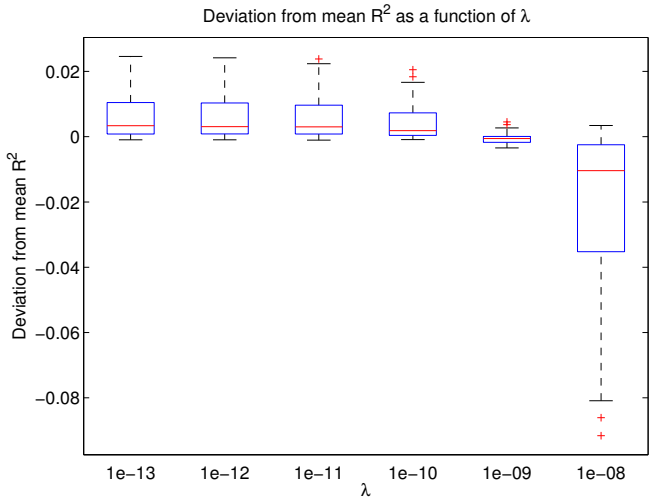

Figure 5.26 Box plot showing the effect of λ on values of R^2.

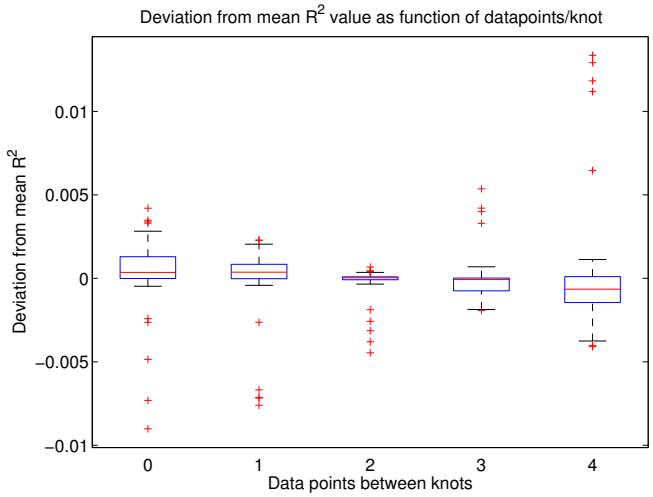

Figure 5.27 Box plot showing the effect of data points between knots (K) on values of R^2.

$K = 0$ is marginally better than $K = 1$ or $K = 2$.

5.3.2 Results - Simple TPA and Enveloping

Now the time has come for the results of the simple TPA investigations. As the discussion from the last section suggests, using fourth order B-splines might not be necessary. For an overall comparison of the two TPA measures, a bar-plot similar to figure 5.22 has been made for the simple TPA in figure 5.28. It shows that the simple TPA actually performs better for the MCEN and AAV4 tyres than the full version. For the MCEN tyre the simple TPA shows

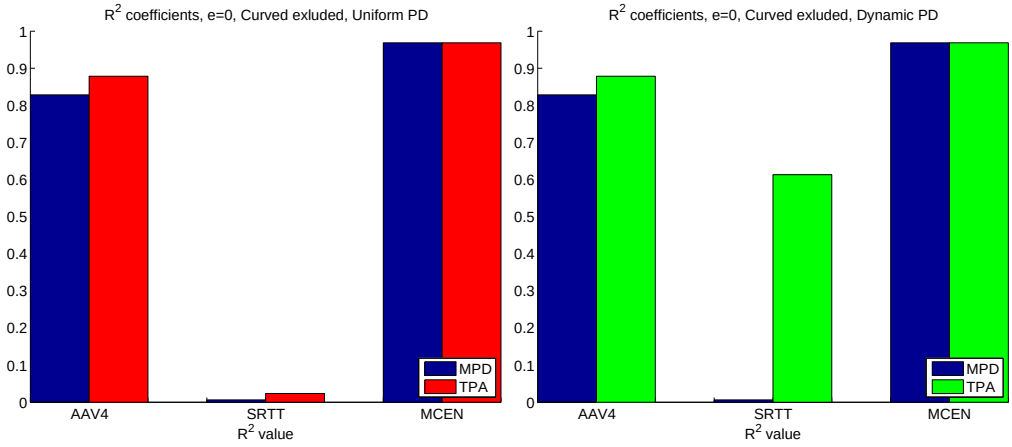

Figure 5.28 R^2 coefficients for the linear regressions based on 'Parallel' and 'Main' using $e = 0$. The left plot shows MPD vs. TPA when penetration depth d is held constant for all road sections and to the left the optimal d has been chosen for each road section. Note that the MPD values are equal on both plots and have been included in both for completeness.

an approximately equal correlation with MPD as opposed to figure 5.22 where MPD is slightly better. For the AAV4 tyre TPA has increased its lead from figure 5.22. The only drawback is the drop in correlation of the SRTT tyre, although it is still much better than MPD. However, the overall correlation for this particular tyre was very poor to begin with and so is not very interesting. Note that the situation does not improve for MCEN and AAV4 when d is dynamic, i.e., allowed to vary across road sections. This is in contrast to the full TPA where a significant improvement was observed in going from uniform to dynamic d. The exception is the SRTT tyre which improved substantially.

Besides the case with no enveloping shown in figure 5.28, similar results have been made with enveloping where $e = 0.0025$ and $e = 0.054$. To get a general overview of these results, for all values of e, see table 5.3.2 which shows R^2 values (rounded up to two significant digits). For the MCEN tyre all R^2-values are (almost) constant across envelope values and road metrics, showing very good correlations. The behaviour of the SRTT tyre follows the same pattern as shown in figure 5.28 for all values of e. For the AAV4 tyre the TPA measures performs better than MPD for all values of e and the R^2 values are equal for the uniform and dynamic cases. $e = 0.0025$ stands out by having the best correlations for both MPD and TPA, while R^2 values are almost equal for $e = 0$ and $e = 0.054$ for both measures, respectively. The result that enveloping improves correlations with $e = 0.0025$ substantiates the findings of the MIRIAM project discussed in section 4.2.1.

Since the differences between uniform and dynamic TPA are almost non-existent for the MCEN and AAV4 tyres, an examination of the underlying d-values is made here. The d-values underlying the results from table 5.3.2 have been listed in table 5.3.2, and it can be seen that the values of d for the two road sections are equal for most dynamic TPA calculations based on the MCEN and AAV4 tyres. This is rather surprising as it was expected that adjusting d could improve correlations, as discussed earlier. This result indicates that using a constant d-value for all road sections might be sufficient and even necessary for an optimal fit. It also explains the

Envelope	MPD	TPA Uniform	TPA Dynamic
MCEN			
0	0.97	0.97	0.97
0.0025	0.97	0.97	0.97
0.054	0.97	0.96	0.97
AVV4			
0	0.83	0.88	0.88
0.0025	0.88	0.92	0.92
0.054	0.84	0.89	0.89
SRTT			
0	0.01	0.02	0.61
0.0025	0.01	0.07	0.50
0.054	0.01	0.03	0.58

Table 5.4 Summarizing results of the simple TPA calculations: R^2-values for linear regressions between rolling resistance measurements and MPD/TPA for different tyres and values of e.

Envelope	Uniform	Dynamic
MCEN		
0	10	10, 10
0.0025	80	70, 60
0.054	50	50, 40
AAV4		
0	40	40, 40
0.0025	20	20, 20
0.054	10	10, 10
SRTT		
0	40	60, 80
0.0025	20	80, 90
0.054	10	40, 50

Table 5.5 Summarizing results of the simple TPA calculations: d-values used in the TPA calculations shown in a).

stability in results between uniform and dynamic TPA. However, the d-values vary across both tyres and enveloping. The former was anticipated since the tyres differ in visco-elastic properties (as discussed in section 4.3) and the latter is also unsurprising since enveloping transforms the profile substantially. In the case of the unstable results obtained with the SRTT tyre, where the relative improvement between uniform and dynamic TPA is large, the difference in d-values between them are large as well, which was expected.

Another interesting aspect of the simple TPA explored here is the aggregation. Figure 5.29 shows the influence of aggregation on correlation results. Only the MCEN and AAV4 tyres have been shown since the SRTT tyre showed poor overall results. Given the small difference between uniform and dynamic TPA, only uniform is showed in figure 5.29. For the AAV4 tyre correlations drops below 0.65 for all values of e with aggregation values of 25 meter (and less) which is indeed very poor correlations questioning the significance of the results. In most cases TPA retains the better performance compared to MPD, especially for the higher aggregation values, although the difference in correlations seems to drop. The latter is a general trend that holds for both tyres and values of e. With the MCEN tyre, correlations do not drop as rapidly, and even with an aggregation of 10 meters, R^2 keeps well above 0.8. Table 5.3.2 showed that MPD and TPA performed almost equally well for the MCEN tyre which is still the case for lower aggregations. However, it is interesting that TPA performs slightly better compared to MPD for $e = 0$ and $e = 0.0025$ for aggregation lengths of 25 and 50 meters. For $e = 0.054$ the performance of the two measures is almost equal. These results supports the presumption that TPA is an effective road parameter for rolling resistance. Moreover, reducing the aggregation sizes when investigating the relation between rolling resistance and surface texture seems possible. The robustness of road metrics across different aggregation values are also an aspect that should be taken into account. With a larger data set this could also provide a better picture of potential road metrics ability to be used in modelling rolling resistance.

From all these investigations we can summarise the following key points:

- Isotropy investigations indicated that the surface is isotropic.
- Investigations of the full and simple TPA showed that the simple version did suffice. With full TPA the examination of λ and K also showed that smoothing was not needed and relaxation in the amount of knots degraded correlation values.
- TPA as a road metric in rolling resistance assessment showed promising results, however, further studies are needed to see if the performance is indeed better than MPD.
- Investigations into enveloping substantiated the findings of [15] that enveloping improves correlations.

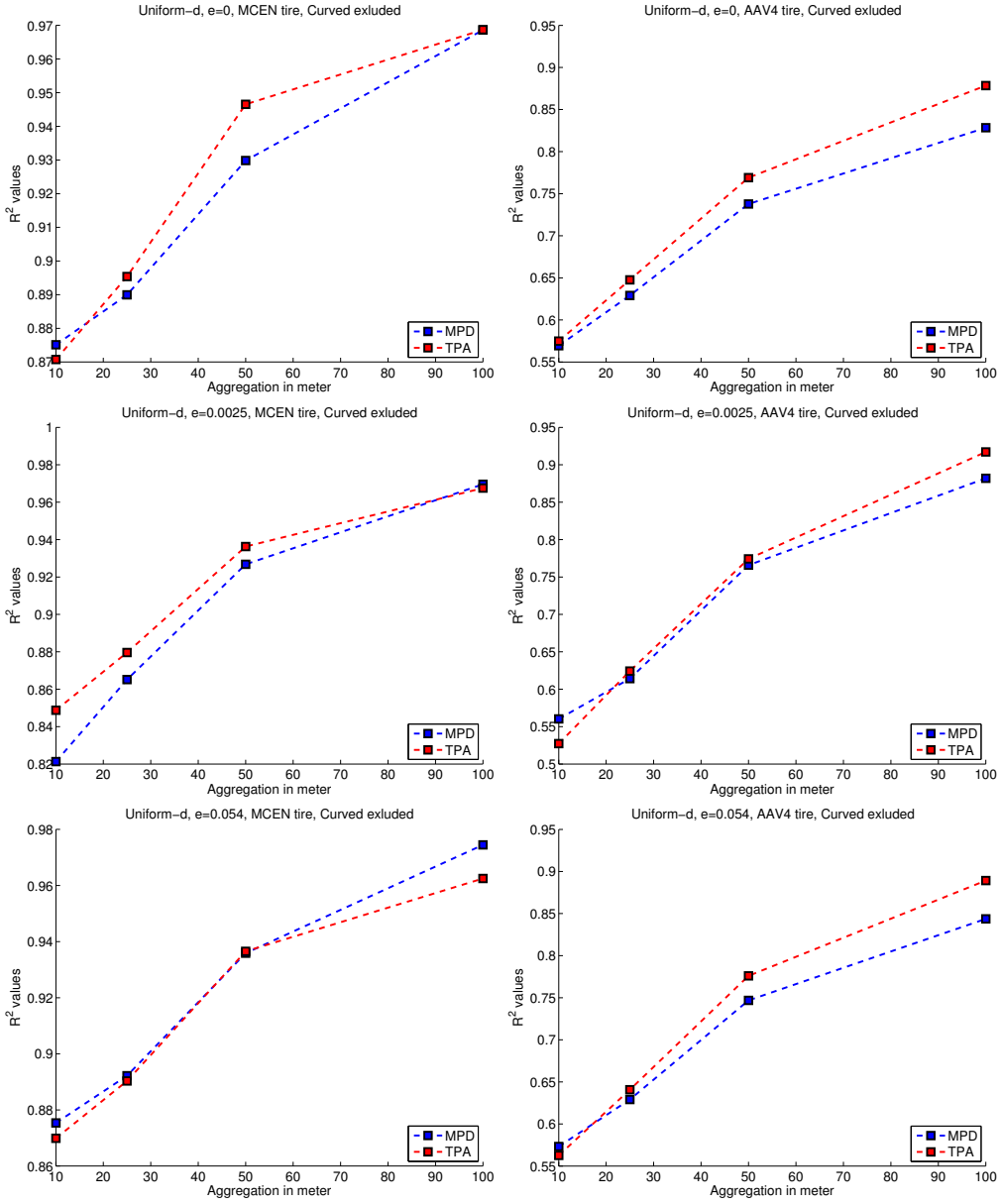

Figure 5.29 Plots of R^2-values as a function of aggregation length using Main and Parallel road sections. The first column show results for the MCEN tyre and the second column is AAV4. The first row is with no enveloping, the second is for $e = 0.0025$ and the last row is plots where $e = 0.054$.

6 Coast-Down data from the Swedish VTI

This chapter deals with a completely different kind of data compared to chapter 5. In this chapter we consider measurements made in connection with the coast-down measurement technique described in chapter 3.

The coast-down experiments have been performed by Swedish Statens väg- och transportforskningsinstitut (VTI) on Swedish roads as part of WP5 in the EU project "Energy Conservation in Road Pavement Design, Maintenance and Utilisation" (ECRPD) and presented in [63] in 2009. The measurements have also been used in a later study[89]. In [63] the data were primarily used to assess unevenness and macrotexture influence on rolling resistance. Unevenness and macrotexture were represented by IRI and MPD, but RMS for different wavelengths were also considered.

For this measurement campaign 14 different Swedish road sections were carefully selected. Since each road section have been measured in both directions this gives a total of 28 road sections. Besides being placed geographically convenient, the following criteria guided the road section selection[63, p. 29]

- The longitudinal gradient and road curvature must be low.
- The set of road strips must have high variation in Mean Profile Depth (MPD) and International Roughness Index (IRI) in order to get the optimal experimental setting.
- Differing speed limits ensuring that coast-downs could be performed with varying initial velocities.
- Proper length for performing coast-downs.

The road sections selected ranged between 400 and 1000 meters in length and a total of 421 coast-downs have been performed. An overview of the road sections is given in table 6.1.

In addition, coast-downs were only performed under suitable meteorological conditions, i.e., no rain, low wind, and steady temperature. Together with air pressure, these quantities were carefully measured and monitored during measurements as described in [63] section 6.8. Each road section were marked by reflective tape that could be detected by the photo sensor which was mounted on the rear bumper of the measurement vehicle. Velocity measurements were made by mounting a measurement device on the right rear wheel which, roughly speaking, emits a pulse approx. every 78th cm that is registered together with a time stamp from a high frequency (1 MHz) clock. From this, velocity can be calculated with high precision. An elaborate description is given in [63, p.26-27]. The measurement campaign performed coast-down measurements with three different vehicles, a personal car (Volvo 940), a van (Chevrolet CG21305 VAN), and a heavy lorry (Scania R143), although the personal car was the primary object of study. All measurement series were performed after a 30 minute warm up driving period[63, p. 99]. A small sub-study[63, p. 31] showed that tire temperature and pressure rose by 15°C and 0.2 bar, respectively, during warm up.

Table 6.1 Overview of road sections chosen for coast-downs in [63].

ID	Name	Direction	Coast-downs	Length	Speed limit [km/h]	Mean MPD	Mean IRI
1	Flygrakan	1	18	1000	90	1.10	0.83
2		2	18	1000	90	1.12	1.05
3	Stora Aska	1	21	300	70	2.54	2.04
4		2	19	300	70	2.49	1.79
5	Vikingstad	1	15	600	70	1.19	1.18
6		2	15	600	70	1.21	1.68
7	Fornåsa	1	14	1000	90	0.82	1.40
8		2	14	1000	90	0.76	1.08
9	Vaesterlösa	1	15	500	70	2.42	2.64
10		2	14	500	70	2.40	3.23
11	Vattenskidsklubben	1	15	900	90	1.00	3.30
12		2	14	900	90	0.93	3.55
13	MaspelösaA	1	14	500	70	1.07	2.18
14		2	13	500	70	0.90	2.15
15	MaspelösaB	1	14	400	70	0.74	2.57
16		2	14	400	70	0.59	2.84
17	MaspelösaC	1	14	580	70	0.86	2.82
18		2	14	580	70	0.86	2.48
19	Brokind	1	15	550	90	0.39	1.11
20		2	14	550	70	0.44	1.02
21	Hundklubben	1	15	570	70	1.76	2.23
22		2	16	570	70	1.72	2.40
23	Hycklinge	1	15	560	90	0.64	3.66
24		2	14	560	90	0.75	3.05
25	Kisa	1	14	620	70	0.59	1.77
26		2	14	620	90	0.58	1.50
27	Rimforsa	1	16	630	90	0.66	0.79
28		2	14	630	90	0.58	0.83

On each of the 28 strips various road quantities were measured with VTIs 'Laser RST' vehicle which measures several road surface properties with its 10 lasers mounted on a bumper-bar in front of the vehicle[9]. The following data have been supplied by VTI:

- Unevenness measurements in 10 cm longitudinal resolution (have not been used here)
- Texture measurements in 1 mm longitudinal resolution
- Road crossfall [%]
- Road curvature radius [1000/m]
- Longitudinal gradient [%]
- IRI [mm/m]
- MPD [mm]

Except for unevenness and texture measurements, the data have been supplied in a 1 meter resolution. The model used in [63] and adopted here is based on Newtons 2. law of motion and assumes that the total force acting on the coasting vehicle is composed of a sum of the following forces[63, p. 24]

$$F_{total} = F_{roll} + F_{air} + F_{side} + F_g. \tag{6.1}$$

where F_{total} is the total force acting on the vehicle, F_{roll} is the rolling resistance force, F_{air} is aerodynamic drag, F_{side} is the side force resistance from road curve/crossfall and F_g is gravitational pull. F_{roll} is the most interesting from our perspective and is given by

$$F_{roll} = m(\eta_0 + \eta_1 T + \eta_2 \,\mathrm{IRI} + \eta_3 \,\mathrm{IRI}(v-20) + \eta_4 \,\mathrm{MPD} + \eta_5 \,\mathrm{MPD}(v-20)) \tag{6.2}$$

where v is speed, T is temperature and $\eta_1, \ldots, \eta_5$ are parameters to be estimated during model fit. This term is purely empirical as there is no theoretical derivation of the relationship between MPD/IRI and rolling resistance. Furthermore, F_{roll} is defined in a fairly general way such that η_0 also accounts for transmission losses from, e.g., the gearbox [63, p.15], as well as surface independent tire losses. As we have discussed in, e.g., the Dutch study, rolling resistance is also dependent on temperature of the surroundings since it affects tire temperature/pressure equilibrium in the tire. Since this phenomena is considered to be independent of the surface itself, it is included as a term $\eta_1 T$ only dependent on air temperature T and not on MPD or IRI. Implicit in this formulation is the assumption that the tire temperature and pressure depends on the temperature of the surroundings. The temperature part of F_{roll} also covers temperature dependent components of transmission losses. Besides a linear relationship between MPD/IRI and rolling resistance, two additional terms are also included to account for speed dependence.

F_{air} is a simplified version of the drag equation

$$F_{air} = 0.5\rho(T,p)A_{yz}C_L[v - \cos(\alpha)w]^2 \quad \text{with } \rho(T,p) = K_\rho \frac{p}{T+T_0} \tag{6.3}$$

were A_{yz} is projected frontal area of the vehicle, C_L is the air dynamic drag coefficient, w is wind speed, α is the wind angle, and p is atmospheric pressure. $K_\rho = 0.3847\ ^\circ K s^2/m^2$ and $T_0 = 273.2^\circ K$ are conversion constants. Since w is low we can assume that $w^2 \approx 0$ and thus simplify equation 6.3 by expanding $[v - \cos(\alpha)w]^2$ and dropping the term containing w^2, i.e.,

$$F_{air} = 0.5\rho(T,p)A_{yz}C_L[v - \cos(\alpha)w]^2 \approx \eta_6\rho(T,p)v^2 + \eta_7\rho(T,p)\cos(\alpha)wv \tag{6.4}$$

where η_6 and η_7 are regression parameters. Substituting $0.5\rho(T,p)A_{yz}C_L$ with two regression coefficients η_6, η_7 seems reasonable since C_L and w are not very precise, i.e., the latter is measured only in the beginning of the coast-down and the former is hard to determine experimentally. This also supports the simplification by $w^2 \approx 0$ as well. More elaborate expressions of F_{air} can be formulated [63, 89], but since the term is being estimated by regression and since higher order terms of v and w are small, it has been omitted here.

Just as some of the parameters in F_{air} are estimated, we will also estimate the tire stiffness C_A occurring in the side force F_{side} term

$$F_{side} = -\frac{1}{C_A}F_y^2 = \eta_8 F_y^2 \tag{6.5}$$

where F_y is given by

$$F_y = m[\cos(\gamma)v^2/R - g\sin(\gamma)cos(\beta)] \tag{6.6}$$

with γ being crossfall angle, m vehicle mass, g gravitational constant, β longitudinal gradient and R radius of road curvature. Finally, F_g is straightforwardly formulated as

$$F_g = -mg\sin(\beta). \tag{6.7}$$

Now, the left hand side of equation 6.1 can be rewritten as follows

$$F_{total} = (m + m_{rot})\frac{dv}{dt} = (m + n_{wh}K_J J/r_{wh}^2)\frac{dv}{dt} \tag{6.8}$$

where m_{rot} is the inertial mass of a wheel (plus additional rotating transmission parts), n_{wh} is the number of wheels, r_{wh} is the radius of the wheels, J is the inertial moment per wheel, and K_J is a correction factor of J to include rotating transmission parts. Inserting equation 6.2, 6.4, 6.5, 6.7 and 6.8 into equation 6.1, and rearranging/simplifying yields

$$\begin{aligned}\frac{dv}{dt} &= \mu_0 + \mu_1 T + \mu_2\,\mathrm{IRI} + \mu_3\,\mathrm{IRI}(v-20) + \mu_4\,\mathrm{MPD} + \mu_5\,\mathrm{MPD}(v-20)\\ &\quad + \mu_6\frac{\rho(T,p)v^2}{m+m_{rot}} + \mu_7\frac{\rho(T,p)\cos(\alpha)wv}{m+m_{rot}} + \mu_8\frac{F_y^2}{m+m_{rot}} - \kappa g\sin(\beta)\end{aligned} \tag{6.9}$$

where $\kappa = m/(m + m_{rot})$ and $\mu_i = \kappa\eta_i$ for $i \in \{0, .., 5\}$ and $\mu_i = \eta_i$ for $i \in \{6, 7, 8\}$. $(\mu_0, ..., \mu_8)' = \boldsymbol{\mu}$ is the coefficient vector estimated by fitting the model to data obtained from the coast-downs. In this formulation it is as an ordinary differential equation with respect to $v(s)$. Since the road and velocity data have been supplied to us using distance as the independent variable, the final regression model must have distance as the independent variable as well. Therefore equation 6.9 is converted to

$$\begin{aligned}\frac{dv}{ds} &= \frac{1}{v}[\mu_0 + \mu_1 T + \mu_2\,\mathrm{IRI} + \mu_3\,\mathrm{IRI}(v-20) + \mu_4\,\mathrm{MPD} + \mu_5\,\mathrm{MPD}(v-20)\\ &\quad + \mu_6\frac{\rho(T,p)v^2}{m+m_{rot}} + \mu_7\frac{\rho(T,p)\cos(\alpha)wv}{m+m_{rot}} + \mu_8\frac{F_y^2}{m+m_{rot}} - \kappa g\sin(\beta)].\end{aligned} \tag{6.10}$$

which gives us the regression model that forms the basis for our investigations in this chapter.

Besides the velocity data which have been measured for each coast-down, there are also auxiliary road data which have been measured along the road sections. More precisely, we have macrotexture (MPD), unevenness (IRI), road curvature (R), road gradient (β), and road crossfall (γ). Since the coast-down model is an ODE it is functional by definition: A differential equation is an equation with functions and the solution is $\mathcal{C}^1$ at least. Thus, it seems obvious to functionalize the auxiliary road data using tools from FDA. More specifically, we will express the data in cubic B-spline bases making equation 6.10 look like

$$\begin{aligned}Dv(s) = &\frac{1}{v(s)}\Big(\mu_0 + \mu_1 T + \mu_2\,\mathrm{IRI}(s) + \mu_3\,\mathrm{IRI}(s)\big(v(s)-20\big)\\ &+ \mu_4\,\mathrm{MPD}(s) + \mu_5\,\mathrm{MPD}(s)\big(v(s)-20\big)\\ &+ \mu_6\frac{\rho(T,p)v^2(s)}{m+m_{rot}} + \mu_7\frac{\rho(T,p)\cos(\alpha)wv(s)}{m+m_{rot}}\\ &+ \mu_8\frac{F_y^2\big(v(s),\gamma(s),R(s),\beta(s)\big)}{m+m_{rot}} - \kappa g\sin\big(\beta(s)\big)\Big).\end{aligned} \tag{6.11}$$

which highlights data sources that are functionalized.

In [63] and [89] they estimate $\boldsymbol{\mu}$ by standard regression, i.e., if we denote the right-hand side of equation 6.10 by $G(\boldsymbol{\mu}; v, R, \beta, \gamma, \mathrm{MPD}, \mathrm{IRI})$, which highlights regression parameters and auxiliary data that vary with position s, the standard regression of equation 6.10 can be formulated as estimating $\boldsymbol{\mu}$ by minimizing

$$L_{reg}(\boldsymbol{\mu}) = \sum_i \Big(\frac{dv_i}{ds_i} - G\big(\boldsymbol{\mu}; v_i, R_i, \beta_i, \gamma_i, \mathrm{MPD}_i, \mathrm{IRI}_i\big) \Big)^2. \tag{6.12}$$

The functional version derived from equation 6.11 uses integration instead of summation, thus

$$L_{fdreg}(\boldsymbol{\mu}) = \int \Big(Dv(s) - G\big(\boldsymbol{\mu}; v(s), R(s), \beta(s), \gamma(s), \mathrm{MPD}(s), \mathrm{IRI}(s)\big) \Big)^2 ds \tag{6.13}$$

which can be reduced to a sum of squared residuals like equation 6.12 by using a quadrature scheme like the trapezoid or Simpson's rule for approximating integrals. Specifically, if we denote the discretisation by $s_1, \ldots, s_N$ then $L_{fdreg}(\boldsymbol{\mu})$ of equation 6.13 can be approximated as

$$L_{fdreg}(\boldsymbol{\mu}) \approx \sum_{i=1}^{N} w_i \Big(Dv(s_i) - G\big(\boldsymbol{\mu}; v(s_i), R(s_i), \beta(s_i), \gamma(s_i), \mathrm{MPD}(s_i), \mathrm{IRI}(s_i)\big) \Big)^2 \tag{6.14}$$

where w_i are weights. The precision of this approximation, and thus the dimensionality of the regression problem, can be varied as necessary. Also note that we have many coast-downs to use in the estimation, so in practice $L_{fdreg}(\boldsymbol{\mu})$ is composed of several integrals that are approximated like equation 6.14 and concatenated into one big least squares problem.

Using FDA in data processing enables a couple of convenient methodologies to be used:

- Smoothing by roughness regularisation discussed in chapter 2 is easily implemented. As can be seen in figure 2.2, velocity measurements have distinctive noise which is easily removed by the technique described in section 2.4.
- Approximation of $Dv(s)$ is straightforward and fast since it can be done analytically. Moreover, the result will be smooth as well, since we use cubic splines for $v(s)$ where the first derivatives of the functional data are $\mathcal{C}^1$. This method is more elegant compared to estimating $Dv(s)$ by finite differencing (used in, e.g., [63] and [89]) which is highly sensitive to noise.
- Since all auxiliary road data measured on each road section also have been functionalized, they can be integrated into the ODE model such that numerical solutions, requiring arbitrary evaluations of input functions, are possible. Numerical solutions are desirable for directly assessing model fit to data, as well as getting a direct overview of how the different components behaves during model simulation.
- The functional approach makes it easy to add noise sources to the data by expressing it directly in the linear combination of basis functions such that the qualitative behaviour of the data is preserved. An example using the gradient data $\beta(s)$ is discussed in section 6.1 below.

It is of course possible to use non-functional methodologies that would enable similar possibilities, but by using the basic apparatus of FDA we get it for free without any additional effort. Most of the data supplied by VTI are very well suited for functional data. For instance, in figure

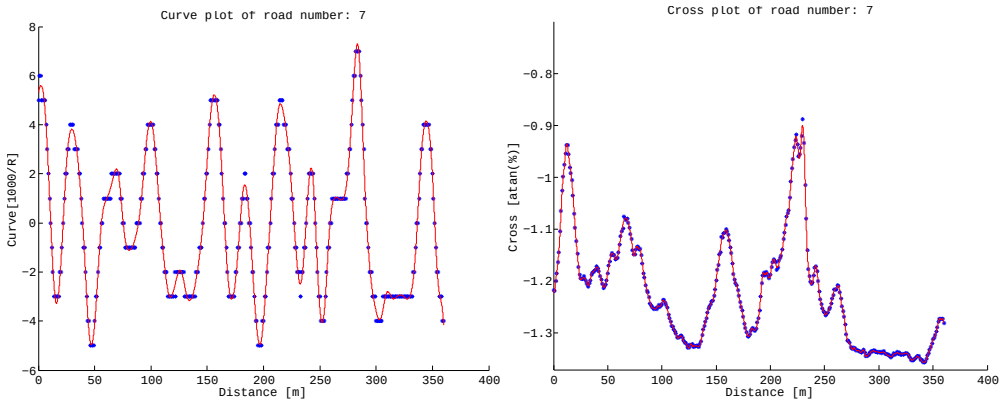

Figure 6.1 Example of road curve R data (left) and road crossfall γ (right).

6.1 road crossfall γ and road curvature R data are shown, together with their functionalized representations. As can be seen, the latter is given as discrete measurements, probably because of limitations of the measurement vehicle, although we know that the underlying road curve varies smoothly. The functionalized version does seem to be more faithful in this respect. In addition, some degree of smoothing has also been used to ease the the transition between discrete values.

Another more explicit example of smoothing concerns velocity measurements of the coast-down runs. As shown in figure 2.2 (chapter 2) the velocity measurements contains high-frequency noise which is easily removed by setting an appropriate value of the roughness penalty parameter λ during funtionalization, as shown in figure 6.2.

Being able to compute model simulations and comparing them to actual measurements offers a concrete way of determining model performance. Figure 6.3 shows a good and a bad fit to raw data and illustrates that some coast-downs are nicely replicated by model simulations, while others fit quite poorly. However, this only represents two extremes of a large data set and it does not show anything about the distribution of fits in between. To get a better overview of the entire data set, the best and worst fit (to the functional data) along with 16 intermediate coast-downs have been plotted in figure 6.4. It shows that many coast-downs are captured quite well by model simulations. The second-worst in figure 6.4 improves significantly compared to the worst, although not entirely satisfactorily. The two upper thirds of the simulations follow the measurements quite good. All in all, the model seems to capture a large part of the data set, but there is still room for improvement. This will be taken up in section 6.2.

Having all data on a functional form makes it easy to visualize model components, i.e., how the different resistance terms affect the vehicle during a coast-down run. Two examples of this are shown in figure 6.5. These plots clearly illustrates which components have the highest influence on vehicle speed. Unsurprisingly, the road gradient plays a major role while side force and temperature dependent rolling resistance contributions are very small. What is more interesting is the fact that IRI does not have any significant effect while MPD play a modest role in overall driving resistance. Also note that the the constant term also plays a substantial role which is probably because many different phenomena are subsumed under this parameter. All in all, this give a good overview of the different components in the model.

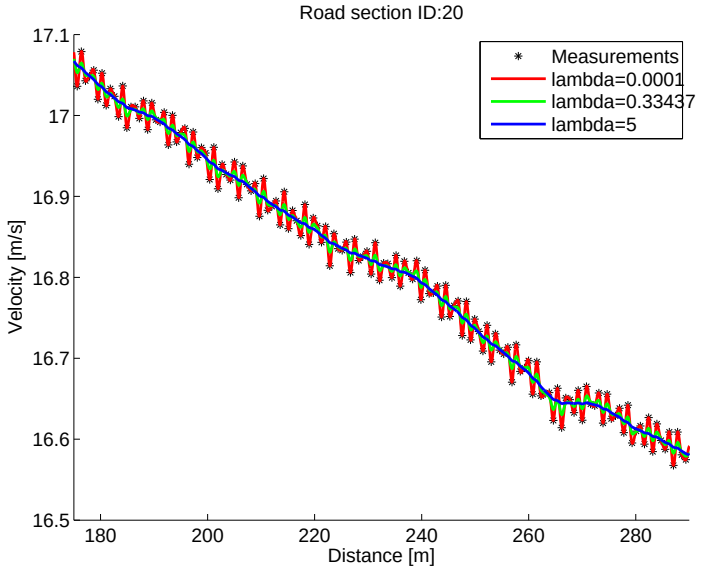

Figure 6.2 Coast-down velocity measurement sample showing effect of roughness penalized functionalization.

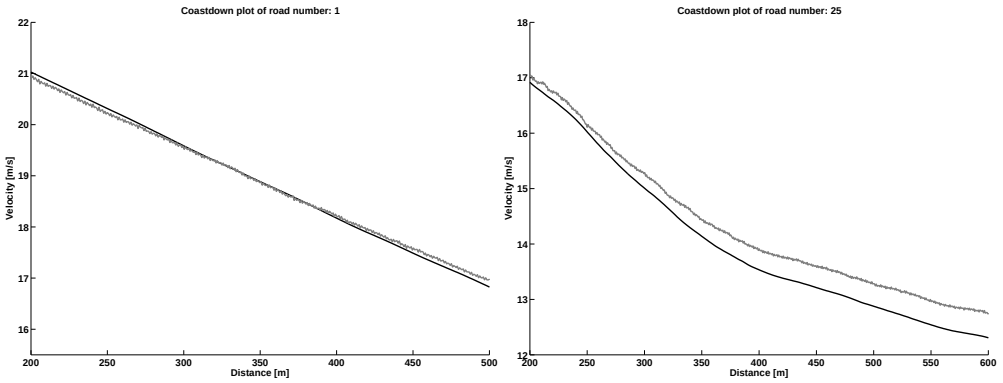

Figure 6.3 Two different coast-down plots illustrating the different degrees of fit to the data set. Black line is model simulation and grey line is raw velocity data. Reproduced from [5].

6.1 Sensitivity analysis

A preliminary investigation of the model in equation 6.10 have been undertaken and published in [5] and found in appendix B.2. In this section we only give a brief summary of the investigations and refer to appendix B.2 for further details.

First of all, the purpose of [5] was to demonstrate the usefulness of FDA in coast-down modelling, which entailed the convenient methodologies mentioned above. Moreover, several combinations of smoothing parameter pairs $(\lambda_{\mathrm{IRI}}, \lambda_{MPD})$ for $\mathrm{IRI}(s)$ and $\mathrm{MPD}(s)$ in equation 6.11 were tested to see which ones gave an optimal fit, using equation 6.13 as loss function. More

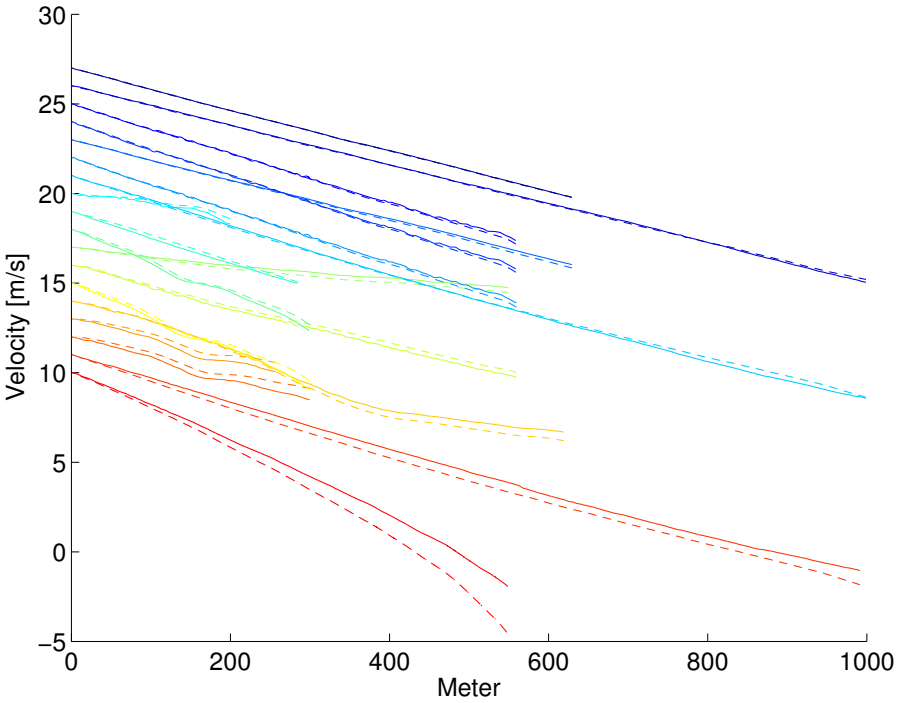

Figure 6.4 Coast-down runs ranked according to how well model simulations replicate measurements (normalized by length). Only coast-downs spanning more than 150 meters have been included in the ranking. Dashed lines represent (functional) measurement data and solid lines represent model simulation. Each measurement + simulation pair have been vertically shifted such that the rank is also reflected in vertical start position. The lowest (red) coast-down represents the worst fit, the highest (dark blue) represents the best fit and the intermediate coast-downs are of increasing goodness of fit and uniformly spaced between each other in the overall ranking.

specifically, the pairs $(\lambda_{\text{IRI}}, \lambda_{MPD})$ were defined as all elements of the Cartesian product $\boldsymbol{\lambda} \times \boldsymbol{\lambda}$ with $\boldsymbol{\lambda} = (\lambda_1, \ldots, \lambda_{19})$ being a vector of logarithmically equidistant points from 10^{-2} to 500. For each pair of smoothing parameters $(\lambda_{\text{IRI}}, \lambda_{MPD})$, MPD and IRI data were functionalized and an estimate $\tilde{\boldsymbol{\mu}}$ was found by minimizing equation 6.13. Using $\tilde{\boldsymbol{\mu}}$, a numerical solution $\tilde{v}(s)$ was computed by applying a Runge-Kutta scheme on equation 6.11 with $\tilde{\boldsymbol{\mu}}$. Finally, $\tilde{v}(s)$ was compared to the original discrete measurements as a goodness of fit. It was shown that $(\lambda_{\text{IRI}}, \lambda_{\text{MPD}}) = (0.0182, 4.0789)$ yielded the best model fitting result. As illustrated in Fig 6.6, this implied a substantial amount of smoothing in case of MPD. It is perhaps surprising that IRI did not show a similar result, but it might be because IRI contributes much less to the overall driving resistance compared to MPD and so the difference caused by smoothing is perhaps insignificant.

Another investigation in [5] concerned a sensitivity analyses performed on the model as an extension of the perturbation analysis in [63]. The amount of tests cases and aspects covered in [63] are incredibly comprehensive, but most tests were very simple involving only a few systematic changes of the data set in order to test the sensitivity of the parameter estimates. A few

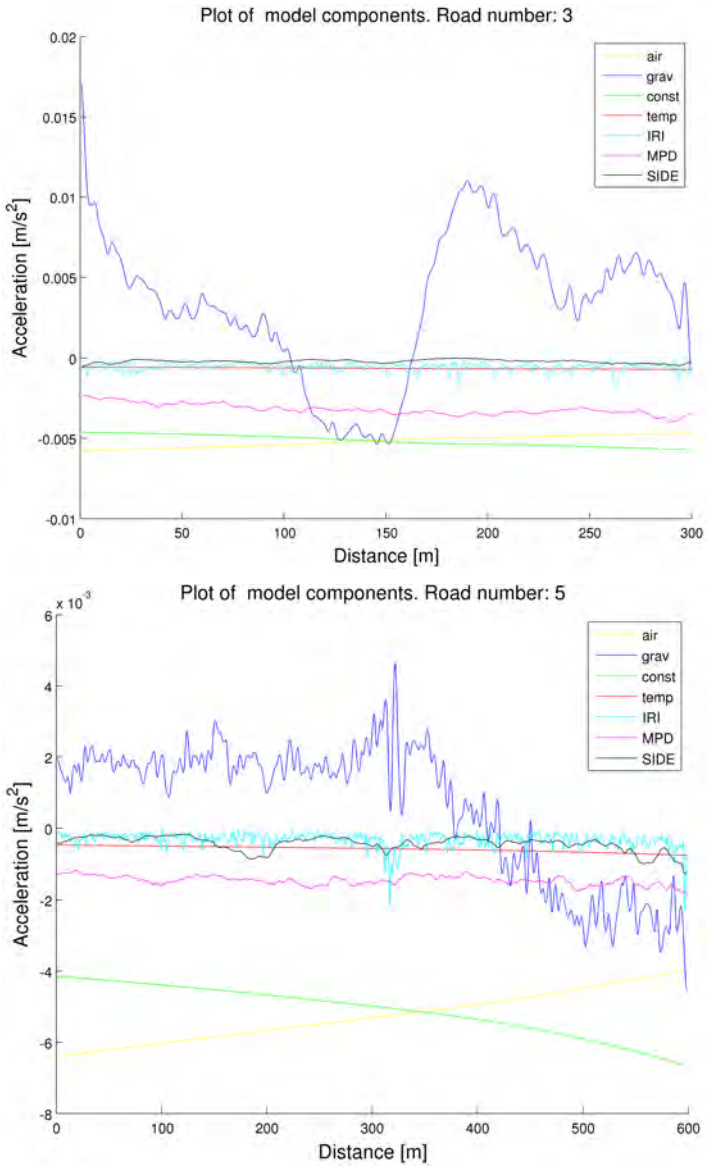

Figure 6.5 Plots showing how the contributions from the different components of the model evolve during coast-down experiements. 'air' refers to the air resistance terms, 'grav' is the gradient term, 'const' is the constant parameter that is part of F_{roll}, 'temp' is the temperature dependent part of F_{roll}, 'IRI' and 'MPD' are the contributions from unevenness and macrotexture, respectively, and 'side' refers to the sideforce resistance. Taken from [5].

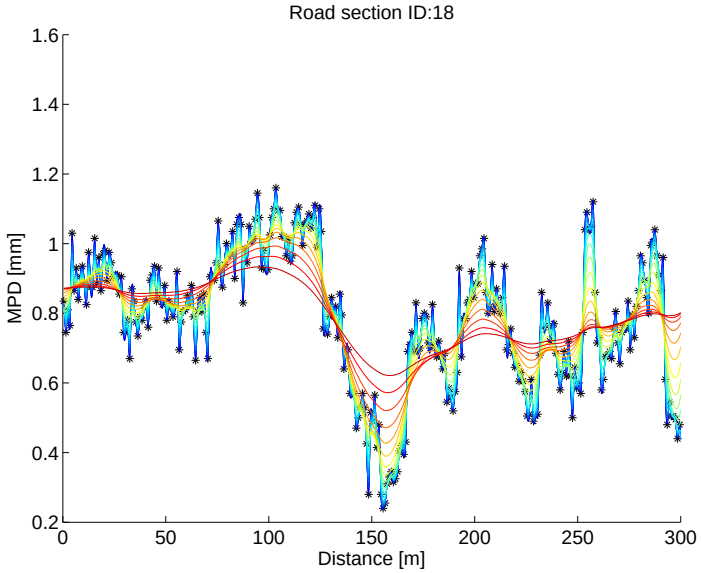

Figure 6.6 Illustration of all functionalizations (different λ-values) of the MPD data sets investigated in [5].

of these tests became too simplified for the authors taste and an example is given here to illustrate. Section 8.4.3.1.1 in [63] presents one of the test results on the influence of the meteorological conditions. The test scales wind speed w with a constant, thus modifying equation 6.9 to

$$\mu_7 \frac{\rho(T,p)\cos(\alpha)wv\varepsilon}{m+m_{rot}} \tag{6.15}$$

where ε is the perturbation error. This is done for different values 0.5, 1.0, 1.5, and 2.0 of ε and for each case the parameters are estimated and their values are compared. This general approach is used several times, i.e., a single (or one for each road section) constant random error is introduced to distort part of the data. The modified data set is then used to re-estimate model parameters $\boldsymbol{\mu}$ which are then compared to the original parameter fit and it is discussed how sensitive the model is to that particular part of the data. This seems like a small basis for assessing sensitivity, and in this particular example with w, the models response to the perturbation is readily explained. For all values of ε it is demonstrated that only the regression parameter for the wind dependent term μ_7 changes value. In addition, it can be seen that it scales with ε, i.e., $\mu_7 = -0.000303$ when $\varepsilon = 1$ and $\mu_7 = -0.000152$ when $\varepsilon = 2$ and so on[63, p. 60]. The reason for this is probably that the optimization algorithm can recreate the result of the original regression by scaling μ_7 and thus cancelling the random perturbation. I.e., if $\tilde{\mu}_7$ is the original estimate and the wind speed data is modified by ε set $\hat{\mu}_7 = \tilde{\mu}_7/\varepsilon$ and the perturbation is simply cancelled. A similar phenomena occurs with μ_0 and the gradient term when the gradient data is investigated in [63] and it illustrates the problem with too simplified perturbation analyses. In contrast, the gradient was selected in [5] and thoroughly tested using hundreds of samples for each test case instead of only one as above. Thus, results are produced in the form of confidence intervals. Each sample consisted of gradient (functional) data that had been perturbed using a

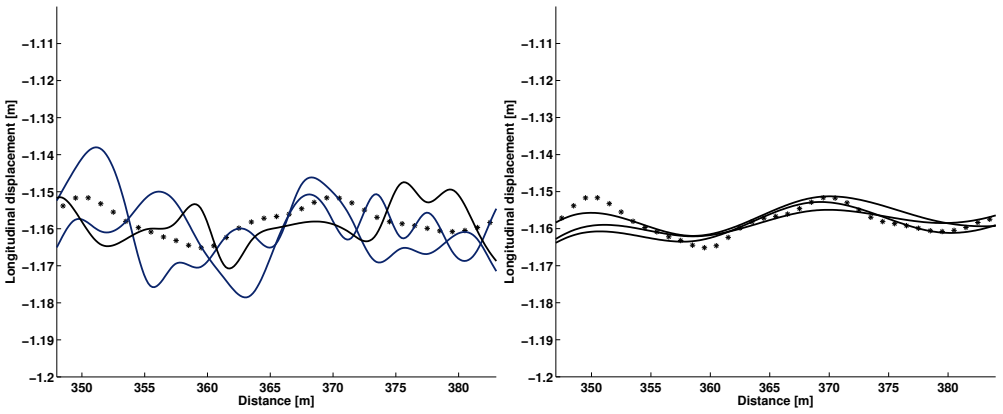

Figure 6.7 Different ways of incorporating random noise into the road elevation data. Solid lines are perturbed functional data and stars are measurements. Too many knots (left) will cause fluctuations in the functional data curve which does not reflect the behaviour of the underlying measurements. By using fewer knots (right) the noise introduced to the data causes fluctuations that reflects the qualitative behaviour of data. Taken from [5].

Gaussian noise source. As mentioned in the previous section, it was implemented directly on the functional data by adding noise to the coefficients of the basis function expansion. Since the features in the gradient data was much lower than the resolution of data points, a small number of knots sufficed to reproduce these features. When noise was added to the resulting functional data, the qualitative behaviour was preserved as illustrated in figure 6.7[1].

In addition to the gradient perturbation, two bootstrapping-techniques were used to investigate sensitivity of model parameters to data quantity. The results of these sensitivity tests are shown in [5, p.12-13] located in appendix B.2. We will only give the overall results here, while referring to the discussion of the article in appendix B.2 for further details. In general the model responds well to all tests, except for the parameters pertaining to the temperature dependent term and the two velocity dependent terms for IRI/MPD which fluctuates substantially. These parameters have one thing in common, namely that their contribution to the overall driving resistance is minute. This might explain the high variation as they need to adjusted a lot in order to achieve a significant effect on overall fitting results. In other words, the fact that they play a minor role in the model make them quite sensitive to change.

All in all, the sensitivity analysis showed that the model seemed quite stable with respect to model fit for MPD and IRI. In the next section we will try and incorporate the TPA-measure into the model.

6.2 Estimation of TPA parameters

The last section described how the coast-down model used in [63] and [89] is quite stable with respect to the perturbation of the data. Thus, this model seems fairly robust to measurement errors, although it does not fit all the coast-downs well. Therefore it would be interesting to try and modify the F_{roll} term by substituting the macro texture measure with the Texture Penetration

[1] A similar approach could have been to used more knots and a higher roughness penalty.

Area (TPA) described in chapter 4 and see if a noticeable improvement could be made. Recall from chapter 4 that the TPA measure depended on the penetration depth d, envelope parameter e, and possibly, if a cubic B-spline basis is used, a smoothing parameter λ and knot placement parameter K. Although it would be desirable to estimate λ and K, it will be clear from the considerations below that this will be far too computationally expensive. Fortunately, results from chapter 5 seemed to suggest that using a B-spline basis does not significantly increase correlations. Therefore it seems a reasonable modification to simplify the functionalization of the data by using linear interpolation instead and thus avoiding estimation of λ and K. As mentioned in chapter 4 this has the fortunate side-effect that the function fit can be performed directly by a simple subroutine in MATLAB/Octave which makes it really fast.

The model in equation 6.9 should be modified by substituting

$$F_{roll} = m(\eta_0 + \eta_1 T + \eta_2 \,\mathrm{IRI} + \eta_3 \,\mathrm{IRI}(v-20) + \eta_4 \,\mathrm{MPD} + \eta_5 \,\mathrm{MPD}(v-20)) \tag{6.16}$$

with

$$F^*_{roll} = m(\eta_0 + \eta_1 T + \eta_2 \,\mathrm{IRI} + \eta_3 \,\mathrm{IRI}(v-20) + \eta_4 \,\mathrm{TPA} + \eta_5 \,\mathrm{TPA}(v-20)) \tag{6.17}$$

and carrying out the loss function derivation similar to above we end out with

$$L^*_{fdreg}(\boldsymbol{\mu}) = \int \Big(Dv(s) - G^*\big(\boldsymbol{\mu}; v(s), R(s), \beta(s), \gamma(s), \mathrm{TPA}(s,d,e,\lambda), \mathrm{IRI}(s)\big)\Big)^2 ds. \tag{6.18}$$

similar to equation 6.13 where G^* is similar to G except that the expression for equation 6.16 has been replaced with equation 6.17. Obviously, this integral can be approximated to a form similar to equation 6.14. $\boldsymbol{\mu}$ needs to be re-estimated using equation 6.18 to see if that improves model fit and since TPA is parametrised by e, d, and λ these have to be considered as well.

The penetration depth d should depend on the particular road geometry and visco-elastic tire properties, and therefore it so should, ideally, be considered a vector $\boldsymbol{d}$ with values $(d_1, d_2, .., d_n)$ for each combination of tires and road types. Furthermore, d-values are supplied as percentages which are converted to heights during TPA calculation. Since these coast-down experiments were performed with the same tire on 14 different road sections, with a wide range of macro texture and unevenness values, $\boldsymbol{d}$ should be vector of length 14 with an element for each road section. However, raw profile data for one road section is missing, so there are only 13 different road sections (and 26 road strips) available with 320 coast-down runs. The enveloping should depend on tire and tire parameters such as pressure, temperature etc. and as mentioned in chapter 4 we will stick to the values used in the literature, i.e. $e \in \{0, 0.054, 0.0025\}$. Adding these to the parameters already discussed in section 6.1, gives a super-vector of parameters that needs to be estimated from the coast-down, i.e.,

$$\boldsymbol{\theta}_{all} = (\boldsymbol{\mu}, \boldsymbol{d}, e, \lambda_{out})'. \tag{6.19}$$

λ_{out} is the smoothing parameter used in transforming the TPA-measurements into a function that can be used as input function in the ODE coast-down model. The λ_{out} has been given a subscript to emphasize that it is used in converting road metric data to functions and not raw profile data to functions as a *means* for calculating a road metric. Also, the influence of λ_{out} has been investigated in [5] as mentioned in section 6.1 and since this investigation showed that high smoothing was preferable that is also being used here. Since MPD and TPA are roughly in the same range of values, using the same value for λ_{out} as that which was found in [5] seems

reasonable. Thus, λ_{out} will be fixed during estimation of $\boldsymbol{d}$ and so the core estimation will concern $\boldsymbol{d}$ only (which is also the largest part of $\boldsymbol{\theta}$). Although the general model regression parameters, $\boldsymbol{\mu}$, are important in analysing the coast-down model, they are of no direct interest in relation to the investigation of the proposed TPA measure and it is only used implicitly through model fitting. Therefore we will primarily focus on the reduced parameter vector

$$\boldsymbol{\theta} = (\boldsymbol{d}, e, \lambda_{out})' \tag{6.20}$$

in the following.

In section 6.1 (and chapter 5) a straightforward approach was used to find optimal sets of parameters by systematically computing a goodness-of-fit for a wide range of parameter combinations and comparing the result. This approach is not computationally feasible for the TPA-measure investigation (and appertaining parameters) here, as it involves far more parameters. More specifically, there are two primary reasons:

1) Computation time for one parameter guess: Calculating the numerical solution used for goodness-of-fit as described in section 6.1 was a computationally expensive task compared to the estimation of $\tilde{\boldsymbol{\mu}}$[2]. The reason for this was because it provided an intuitive goodness of fit directly related to the visual comparisons between model simulation and measurements. However, it required a cluster-computer to perform calculations within a practical time-span. Instead, the goodness of fit relying on numerical ODE solutions is substituted with the goodness of fit expressed in equation 6.13 (and adaptated to TPA in equation 6.18) which can be evaluated directly. Since equation 6.18 is also used in the regression, the new goodness of fit is computed along with the estimate $\boldsymbol{\mu}$ so we get it 'for free'. The downside of this approach, however, is that the model fit is assessed by squared residuals in the derivative domain which is not as intuitive.

2) Number of iterations: As described above, the size of $\boldsymbol{\theta}$ is much larger than, e.g., the pairs of smoothing parameters $(\lambda_{\mathrm{IRI}}, \lambda_{\mathrm{MPD}})$. Thus, checking combinations of parameter values based on a Cartesian product of vectors for each parameter in $\boldsymbol{\theta}$ would result in a huge number of parameter estimations. If, e.g., we would systematically check 4 different values for each element in $\boldsymbol{\theta}$ we would have to check $4^{18} \approx 6 * 10^{10}$ tuples to check all combinations! By comparison, $19 \times 19 = 361$ combinations were checked in [5]. In order to accommodate this problem, a fundamental change in the procedure presented in 6.1 has to be made. Since a systematic brute force check for an optimal model fit is practically impossible, an optimisation algorithm have to be deployed instead.

6.2.1 The objective function

Given the discussion in the previous section, as well as the outline of TPA in chapter 4, the objective function value is calculated by these steps for a fixed value $\boldsymbol{\theta}_0$ of $\boldsymbol{\theta}$:

1 From the raw texture profiles, calculate TPA values as prescribed in section 4.3.3 to obtain TPA values in a one meter resolution similar to the MPD data supplied by VTI.

2 Functionalize the discrete TPA values obtained in step **1** using λ_{out0} as the smoothing value. Denote the result by $\mathrm{TPA}(s)$.

3 Find the parameter estimate $\tilde{\boldsymbol{\mu}}$ of the coast-down model parameters by solving the least squares regression in equation 6.18, i.e., by minimizing $L^*_{fdreg}(\boldsymbol{\mu})$.

[2] A trick can be used to vectorize the problem: Numerically simulate several instances of equation 6.10 simultaneously for different values of $\tilde{\boldsymbol{\mu}}$, λ_{IRI} and λ_{MPD}. Nevertheless, the numerical ODE solution is still the most expensive part.

4 Calculate the goodness of fit by evaluating $L^*_{fdreg}(\tilde{\boldsymbol{\mu}})$ which is then the value of the objective function.

Roughly speaking, this gives a function $\mathcal{F}_N(\boldsymbol{\theta}) : \mathbb{R}_+^M \to \mathbb{R}_+^N$ where $M = |\boldsymbol{\theta}|$ and N depends on the concrete implementation. The largest value of N is the number of quadrature points used when approximating the integrals in $L^*_{fdreg}(\tilde{\boldsymbol{\mu}})$. Depending on the implementation, these quadrature points can reduced by summation: Coast-down wise, road section wise or summed up altogether. This comprehensive loss function does not have a closed form solution, so an iterative minimization or similar approach is needed one way or another. No matter what minimization algorithm is used, it will require several evaluations of $\mathcal{F}_N(\boldsymbol{\theta})$.

Computational considerations of the objective function

Given the massive amount of computation involved in an evaluation of $\mathcal{F}_N(\boldsymbol{\theta})$, careful analysis and consideration have been made to optimise the algorithm. First of all, since we only use three different values of e it is obvious to create three different scenarios with separate estimations of $\boldsymbol{d}$ for each case.

We will refer to the loss function as $\mathcal{F}_N(\boldsymbol{d})$ when $\boldsymbol{d}$ are the only parameters of interest. It should also be noted that in [5] an iterative procedure was used to estimate $\boldsymbol{\mu}$, however, as $L_{fdreg}(\boldsymbol{\mu})$ is linear in $\boldsymbol{\mu}$ the simple linear closed form solution is used below instead.

Another aspect, mentioned in chapter 4, is the observation that TPA values calculated in step **5** behaves nicely (is strictly monotone and smooth) as d increases, which can also be seen in figure 4.8. In addition, given the construction of d as a percentage, natural upper and lower bounds for meaningful values of d exists. This can be used to create an optimized version of $\mathcal{F}_N(\boldsymbol{d})$ by doing the following for each road section profile data. For each 100 mm segment $[s_i, s_{i+1}]$, we calculate

$$\mathrm{TPA}_i(d_k) = \int_{s_i}^{s_{i+1}} \widehat{y}(d_k, s)ds \;\text{ where }\; k \in \{1, \ldots, K\} \tag{6.21}$$

for a suitable grid of percentages $d_1, \ldots, d_K$. In the investigations used here $d_1 = 10\%$ and $d_K = 90\%$ since higher values are considered unrealistic. These discrete values can be functionalized using simple linear interpolation, such that a data function $\mathrm{TPA}_i(d)$ exists for each 100 mm segment i (a handful of these functions are shown to the left in Fig 4.8). Thus, for each $d_0 \in [d_1, d_K]$ we can efficiently produce all arrays of TPA-values by evaluating all data functions $\mathrm{TPA}_i(d_0)$ belonging to each road section as prescribed in step **1** above.

Furthermore, step **2** can also be optimized. Recall the matrix expression in equation 2.22 for calculating the coefficients vector which can be modified to

$$\hat{\boldsymbol{c}} = (\boldsymbol{\Phi}'\boldsymbol{\Phi} + \lambda \boldsymbol{R})^{-1}\boldsymbol{\Phi}'\boldsymbol{y} = \boldsymbol{S}_\lambda \boldsymbol{y} \tag{6.22}$$

($\boldsymbol{W} = \boldsymbol{I}$ since no weights are used here). This equation is used for functionalization of TPA-values in step **2** where $\boldsymbol{y} = \big(TPA_1(d_0), \ldots, TPA_1(d_0)\big)'$ and $\hat{\boldsymbol{c}}$ is the coefficient estimate for $\mathrm{TPA}(s)$. Since λ_{out0} is fixed during minimization of $\boldsymbol{d}$, $\boldsymbol{S}_\lambda$ is fixed and can be computed beforehand such that the basis function fitting in step **2** is only one matrix multiplication instead of the complex expression in equation 6.22 that involves matrix inversion which is computationally expensive.

Finally, another important aspect concerns the smoothness of $\mathcal{F}_N(\boldsymbol{d})$. Since each evaluation of $\mathcal{F}_N(\boldsymbol{d})$ requires many different steps including the solution of a couple of least squares fits,

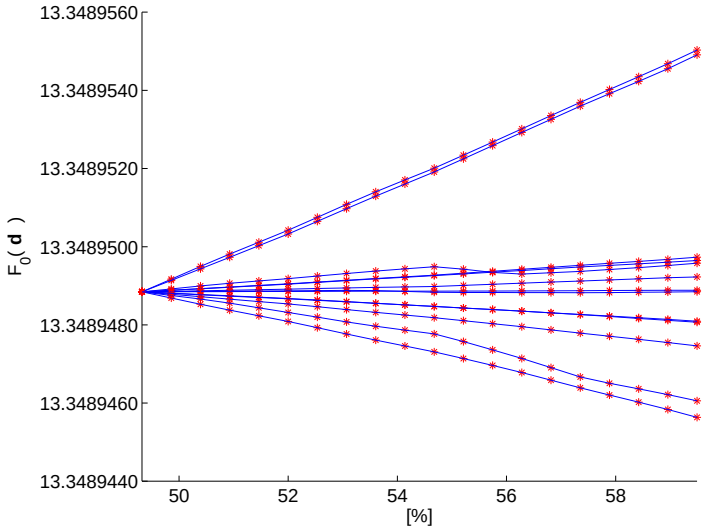

Figure 6.8 Plot of $\mathcal{F}_0(\boldsymbol{d})$ as function of $\boldsymbol{d}$ where each line represents the iterative incrementation of a single parameter d_i of the vector $\boldsymbol{d}$.

it is natural to ask whether this function, in practice, behaves smoothly. If it does, we can use iterative algorithms like Levenberg-Marquardt to estimate $\mathcal{F}_N(\boldsymbol{d})$. Figure 6.8 show the results of iteratively incrementing each μ_i of $\boldsymbol{\mu}$ and observing the corresponding value of $\mathcal{F}_0(\boldsymbol{d})$. It is quite clear that $\mathcal{F}_0(\boldsymbol{d})$ behaves nicely enough for derivative approximation to work. Note the small overall changes of $\mathcal{F}_0(\boldsymbol{d})$ when the d_i's are incremented. This will be investigated below.

6.2.2 Results

In chapter 5 we compared MPD and TPA by looking at correlations in linear fit but with these coast-down data, we evaluate $L_{fdreg}(\tilde{\boldsymbol{\mu}})$ or $L^*_{fdreg}(\tilde{\boldsymbol{\theta}})$ where $\tilde{\boldsymbol{\mu}}$ and $\tilde{\boldsymbol{\theta}}$ are estimates corresponding to the two different models, i.e., the model underlying $L_{fdreg}(\tilde{\boldsymbol{\mu}})$ using MPD as the macrotexture road metric and the model underlying $L^*_{fdreg}(\tilde{\boldsymbol{\theta}})$ that uses TPA instead. Three different model scenarios were investigated: 1) Standard model with MPD 2) TPA where 13 different penetration depths (one for each road section) have been estimated, and 3) TPA with only one penetration depth which is then applied to all road sections. The latter two scenarios involved iterative estimation of $\boldsymbol{d}$ and d, respectively, using Levenberg-Marquardt algorithm to minimize squared residuals obtained by approximating the integrals in $L^*_{fdreg}(\tilde{\boldsymbol{\theta}})$. This was done for three different values of e, as mentioned above, and the overall results are shown in table 6.2. The most conspicuous feature in table 6.2 is the small differences between the model fits which is measured in fractions of ten thousands. This will be discussed in detail below. For each value of e the goodness-of-fit improves from MPD to TPA with uniform d and then again from TPA uniform d to pure TPA. Given the small magnitude in the differences, the observed behaviour is probably due to minute improvements by estimation and not a indication of a better road measure. In other words, since TPA with uniform d has one parameter to adjust in order to improve model fit, it would be expected to be better than MPD which has no parameters and, similarly, with penetration depth d versus 13 penetration depths $\boldsymbol{d}$. The estimate of TPA

Table 6.2 Overall estimation results, compared to MPD, for three different degrees of enveloping. The upper half of the table presents the model fit directly as $\mathcal{F}(\boldsymbol{\mu})$ whereas the lower part presents it in a normalized fashion such that the results are easier to analyse. 'TPA uniform d' refers to the TPA measure where d is fixed for all road sections instead of varying across road sections as with the TPA-measure.

Envelope (e)	MPD	TPA uniform d	TPA
		$\mathcal{F}_0(\boldsymbol{\mu})$	
0	3.653628	3.653618	3.653606
0.0025	3.653652	3.653618	3.653614
0.0540	3.653663	3.653618	3.653610
		$(\mathcal{F}_0(\boldsymbol{\mu}) - 3.6536) \cdot 10^5$	
0	2.8	1.8	0.59
0.0025	5.2	1.8	1.4
0.0540	6.3	1.8	1

with uniform d is also constant for all three envelope values might be due simplicity of the optimization problem where one parameter translates all TPA values, across all road sections, up or down as d is increased and decreased. This could probably give a similar effect to what was described in section 6.1 in regard to the perturbation analysis performed in the ECRPD report.

As mentioned above, the differences in model fits are extremely small. This has been examined more concretely as it would be interesting to see, hands on, how much these differences actually affected model simulations. It was done by creating model simulations for every coast-down run using a Runge-Kutta solver using each of the three scenarios from table 6.2. All simulations have been made using no enveloping. The model simulation having greatest discrepancy between MPD and TPA simulation was identified and plotted in figure 6.9. It is clear that even for this coast-down their paths are almost identical. A small portion of the coast-down is shown to the right in Fig 6.9 and it is clear that TPA and MPD simulations do in fact differ, however, to a very small extent. Compared to the MPD models ability to replicate measurements, as shown in figure 6.4 TPA provides an insignificant improvement.

It is, however, interesting to investigate the extent of these small differences, i.e., is this a general trend or just an outcome of the optimization. For each value of e, 5200 uniformly chosen values of $\boldsymbol{d}$ have been created, where each entry $d_i \in \boldsymbol{d}$, have been sampled from the valid range of possible percentages permitted, i.e., $d_i \in [10\%, 90\%]$. For each sample the loss function $\mathcal{F}(\boldsymbol{d})$ has been evaluated to see the resulting goodness of fit. Combining these goodness of fit values for all e gives a total of 15600 different evaluations of $\mathcal{F}_0(\boldsymbol{d})$ and subtracting the lowest from the highest value of all these samples gives a difference of $2.0306 \cdot 10^{-5}$ which is roughly in the same range as the lowest and highest value in table 6.2. Thus, we can conclude that no matter what parameter configuration $\boldsymbol{d}$ is being used, the model gives roughly the same result. The most plausible explanation for this behaviour is that during the evaluation of $\mathcal{F}(\boldsymbol{d})$ the best fit $\tilde{\boldsymbol{\mu}}$, given $\boldsymbol{d}, e, \lambda_{out}$, to the coast-down model is found by linear least squares fit and apparently over-fitting occurs. Since, from a computational point of view, many different values of TPA can be obtained by adjusting d, this implies that the model is quite unaffected by changes in the macro-texture part of the F_{roll} term. As such, we could replace MPD/TPA with random noise and the model could adapt to it giving roughly the same fit.

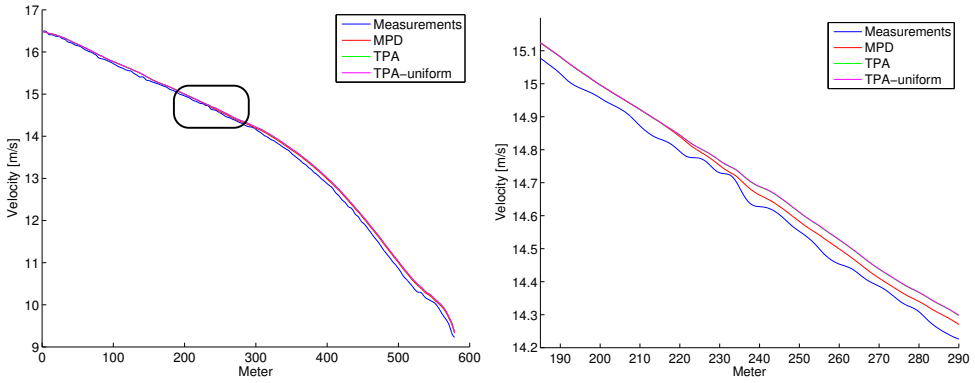

Figure 6.9 Measurements and model simulations of a coast-down run. To the left is the entire coast-down while a zoom-in is given to the right. The TPA simulation (green) is not visible as it almost coincides with TPA-uniform (magenta).

Finally, it is investigated how $\boldsymbol{d}$ behaves during optimization, i.e., how different components of $\boldsymbol{d}$ migrates during optimization. Again, randomly chosen initial values $\boldsymbol{d}_0$ have been sampled and the results $\tilde{\boldsymbol{d}}$ after optimization have been recorded as well. The differences between $\boldsymbol{d}_0$ and $\tilde{\boldsymbol{d}}$ have been illustrated in figure 6.10 for 96 samples and a few components d_i of $\boldsymbol{d}$. The two plots in figure 6.10 have been chosen to illustrate a common trend in estimates of $\boldsymbol{d}$. With very few exceptions the estimates converge to one of the endpoints, i.e., 10% or 90%. For some d_i it is the same endpoint for every iteration as with d_1 and d_2 to the left in figure 6.10, and sometimes the endpoint of convergence varies across samples, as seen with d_5 and d_7 to the right in figure 6.10. Thus, it seems that the destination of of these endpoints depends on the initial values of all components. Note that some of the estimated components of $\boldsymbol{d}$ that have not converged to the end points might be due to slow convergence of the optimization algorithm, i.e., the optimization algorithm stopped too early for proper convergence had been achieved. Nevertheless, this behaviour is a good indication that something is not quite right. The observation that the values of the TPA measure are driven to its extremes for each road sections suggests that the model tries to use the parameter $\boldsymbol{d}$ to compensate for something other than what it is intended for (macrotexture induced rolling resistance). This could mean that TPA as road metric for (macrotexture) rolling resistance is not satisfactory. However, since TPA performs almost identical to MPD, it is more likely that the lack of fit observed in figure 6.3 and 6.4 was due to, e.g., external disturbances that influenced measurements. As mentioned previously, the unevenness and macrotexture part of F_{roll} constitutes only a small part of the total driving resistance which makes this term especially sensitive to external disturbances and variations across all measurements.

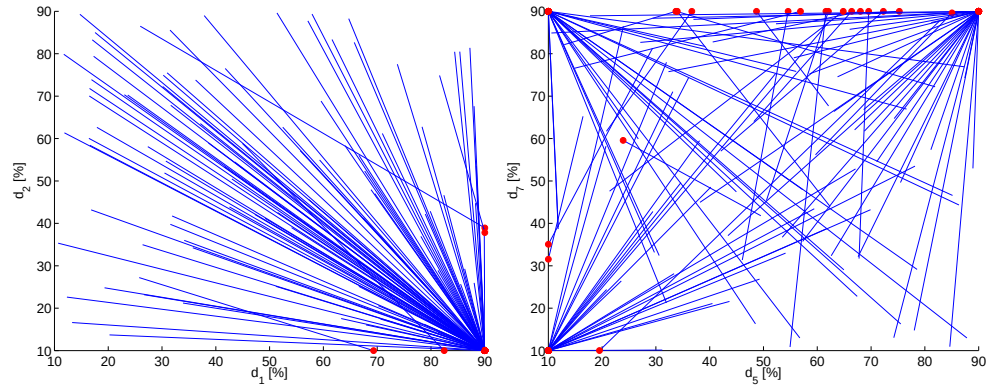

Figure 6.10 Movement of parameter values from a randomly chosen initial value to the result after optimization, for 96 samples of $\boldsymbol{d}$. Each entry d_i in $\boldsymbol{d}$ have been chosen from the uniform distribution between 10 and 90 %. The blue lines shows the distance travelled from initial value d_0 to estimated value $\tilde{d}$. The red filled circles are the endpoints, i.e., $\tilde{d}$.

7 Discussion

In this chapter we sum up and discuss the results of the of the present work. First and foremost we are going to discuss the new texture measure, TPA, proposed in section 4 as well as the results of using it to model rolling resistance in chapter 5 and 6. After that the role of FDA in rolling resistance modelling is evaluated and potential directions for further use of FDA are discussed as well. We conclude by some general remarks about the work as a whole, the general lessons learned, and directions of future work.

7.1 Discussion of Proposed Texture Measure

The TPA metric was developed for macrotexture induced rolling resistance assessment. The basic idea behind its development was to make a road metric based on the theory of what causes surface related rolling resistance on the macrotexture level. At the same time it should be suitable for practical purposes, i.e., for use with network level measurements in road maintenance and asset management, which substantially restricts the potential algorithmic complexity of the metric. The result was a road metric that is based on principles of what causes rolling resistance which is slightly different than the purely empirical texture measures used today. Present road metrics are largely based on Fourier analysis, statistical properties or algorithmic adaptations of previous practical methods, to the capabilities of modern measurement equipment. While TPA is definitely closer to the empirical measures than, e.g., complex FEM models, it shares one thing with the latter: It is based on principles of tyre/surface interaction and the energy loss pertaining to it, albeit in a very simple way.

This seems like a novel approach similar to the empirical enveloping algorithm of [115] which is used in chapter 5 and 6. However, enveloping is not a road metric since it does not reduce the profile data segments to a single index, but instead acts like a filter that transforms the profile. Nevertheless, the enveloping procedure is based on theoretical principles of tyre/surface interaction which is emulated in a simple way. In fact, TPA complements enveloping very well with respect to rolling resistance assessment: Enveloping emulates tyre indentation and TPA assesses the resulting area indented by the surface. In accordance with this, it was shown in chapter 5 that using TPA with enveloping ($e = 0.0025$) gave significantly better correlations than without enveloping. A similar improvement was seen with the classical MPD texture measure which underpin the previous studies in the MIRIAM project[15] and suggests that this enveloping should definitely be studied further.

To fully explore the idea of determining rolling resistance by assessing the road textures penetration into the tyre, two different variants of the TPA measure were proposed: The 'simple' version and the 'full' version. The full version was based on B-splines, fitted using a roughness penalty, and had a total of three parameters d, λ and K that should be estimated. The general idea of using such a complex formulation was to have some calibration parameters that could be tuned by estimation and subsequently analysed. This could potentially lead to some insights between

profile data and its relation to rolling resistance. For instance, had the full TPA significantly shown to perform better with substantial weight λ attributed to the roughness term, it would imply that local features of the profile where unimportant. However, the investigations of the full TPA in chapter 5 indicated that these parameters might be superfluous. In fact, the simple TPA, having only one parameter, d, performed slightly better.

Another related aspect concerned how d should be estimated. It was hypothesized that the penetration depth d could potentially vary across different road sections, i.e., across different surfaces. However, the simple TPA investigations of chapter 5 showed unambiguously that while d varied across tyres (which was also hypothesized) and enveloping, it did in fact *not* vary across road section for a given combination of tyre and envelope. Together with the discussion about the full TPA above, this cemented that the general approach in defining the TPA has been overly complex. The simple TPA using linear interpolation of the profile data and using a uniform value of d seems to suffice.

The results of correlating TPA/MPD with C_{RR} in chapter 5 showed that TPA, with or without enveloping, outperformed MPD for the majority of different combinations of tyre type, aggregation lengths, and enveloping. In some cases they performed almost equally well and only in a few cases did MPD perform better. All in all, these data shows that TPA could indeed be a serious candidate for a texture measure used in rolling resistance assessment. However, the data set consisted of only two road sections which is quite low so any results should be taken with a grain of salt. On the other hand, the length of the road sections is quite large compared to, e.g., the MIRIAM and MnRoad studies discussed above, so the results cannot be dismissed as mere coincidence. All in all, TPA shows very promising results with data created in COOEE project, but more investigations using a large number of road section needs to be made before any definite conclusions can be drawn.

Besides the rolling resistance measurements of chapter 5, coast-down data from VTI was used to investigate the performance of TPA in rolling resistance modelling. With this kind of data the rolling resistance is derived implicitly from velocity data by a mathematical model. Initially, this approach seems promising as the model showed robustness with respect to noise and TPA seemed to be performing just as well as MPD. However, during investigations into the estimation of d, the model produced strange results indicating that: 1) The model fits where almost equally good no matter the values of d, and 2) the values of d clearly indicated that the model was using d to compensate for something that probably had nothing to do with texture induced rolling resistance. While coast-down modelling might be fruitful when using an established measure, the investigations in chapter 6 suggests that it is not good for exploring new road measures. This is probably because surface induced rolling resistance components are only minor contributions to the overall driving resistance. Thus, distinguishing the rolling resistance term from noise and other disturbances is difficult enough in itself, let alone fine tuning and investigating new potential road metrics used to define it.

Irrespective of the problems encountered with the coast-down data in chapter 6, the general conclusion still stands: Simple TPA with a fixed d used together with the enveloping of [115] with $e = 0.0025$ looks very promising, but further investigations are needed. In relation to this, the question of how d depends on various factors like tyre and enveloping is still open and needs to be investigated further. Examining the 3D-version of TPA in the form of TPV is also a potentially interesting undertaking and its potential generalizability is an interesting feature of the TPA metric. It would be extremely advantageous to have a measure that is easily adaptable to, and could take advantage of, the next generation of measurement devices.

On a more general level, the overall approach of actually using basic knowledge of the

phenomena being assessed as an underlying basis for road metric development, seems like a fruitful approach in advancing in this field. Even though the road metrics are simple and based on profile measurements that are non-trivial to obtain and which is only a 2D-projection of a 3D world, the connection with theory seems important. This approach will hopefully also make it easier to use insights from highly theoretical FEM modelling in practical rolling resistance modelling and vice versa. Better measurement equipment would of course reinforce this synergy as well.

7.2 Discussion of FDA in Rolling Resistance Modelling

Another goal of this work was to try and evaluate the usability of FDA in this field of research. In connection with the coast-down data and modelling of chapter 6, FDA proved to be a natural setting for overcoming challenges associated with coast-down modelling. Challenges include implementation of data sources into the model and model stability testing using smooth noise. Furthermore, it made numerical solutions of the system straightforward, which was valuable in assessing model fit. The naturalness consisted in the fact that representing high-resolution data, originating from phenomena that is evolving smoothly, is very convenient. Moreover, the coast-down model was a differential equation which formally is an equation involving functions, so it is natural to use functions for data.

On the other hand, functionalization of texture profiles using a fourth order B-spline basis together with roughness penalty based fitting, as a means of calculating TPA, proved to be unnecessary. The reason is probably that the relation between TPA calculated from a 2D-profile and rolling resistance measurements is very noisy, so any improvements that could be achieved by a more advanced formulation of TPA would be insignificant. In other words, the full TPA was over-engineered and as discussed in section 7.1 above, even letting d vary across road sections might be irrelevant. Since we are only interested in determining an *average* energy loss on the meter length scale, of a phenomena that occurs on the mm length scale, the finer details of the profile are probably not relevant. The simple TPA which gave the best results, however, is based on linear interpolation and while this is also a kind of functionalization it is not smooth. Since smoothness is a fundamental aspect of FDA, the simple TPA is hardly relevant for methods of FDA.

Another example was the usage of fdPCA in chapter 5. While it did illustrate the potential, it was a quite simple application of the FDA technique. Using fdPCA or similar functionalized versions of classical techniques might be interesting with larger data sets of texture profiles and rolling resistance measurements, but the data presented in chapter 5 was just too small. With a larger data set it would be interesting to calculate MPD and TPA values, functionalize the result using a roughness penalty to avoid small fluctuations, and comparing the result with trailer measurements using a functionalized linear model. However, this seemed like an excess approach given the small data set. Moreover, standard linear regression is what was used in previous studies and by using the same technique it was easier to compare the results.

More generally, the author had hoped that more advanced FDA-techniques could have been deployed, but in many cases it seemed to be introducing unnecessary complexity. Besides the full TPA presented in the thesis, there was also a case with parameter estimation of the coast-down model. Initially it was believed that some non-linearities in the parameters would result from modelling efforts which would enable application of non-linear parameter estimation of the coast-down model parameters $\boldsymbol{\mu}$. Since non-linear parameter estimation of differential equations

is one of the areas in which FDA really shines, this would have been a perfect application example. However, as it turned out, non-linearity was not needed.

All in all, FDA did prove useful, especially in coast-down modelling, but the data sufficiency and the immediate challenges in connection with the new road metric formulation and subsequent investigation did not require the full potential of FDA.

7.3 General Remarks

The author began the present work with no prior knowledge of the field. This required elaborate preparatory studies but in the author's opinion this also gave a unique opportunity to approach the subject from a different perspective that what is customary. Some words on this below.

While the development of full TPA might be overcomplicating the matters, the general approach of founding a new road metric seemed like a non-standard approach. This also manifested itself when trying to acquire data from other measurement campaigns. Although there has been a great deal of goodwill in sharing measurements, which is greatly appreciated and acknowledged by the author as this is by no means a standard practice in other areas, getting hold of raw profile data have been quite difficult. This seems to be because standard road metrics is usually what people want so there is no need to exchange raw profile data. Unfortunately, getting raw profile data is essential in the kind of work put forward here, so making it easier to exchange data would, in the author's opinion, greatly benefit this area of research. In general it seems like there is a unused potential in the massive amount of data being produced in this area[1]. Another related observation is that dealing with road data is quite cumbersome from a programming perspective. Parsing and creating the right data structures for the data sets used in chapter 5 and 6, as well as implementing basic road metrics, have been laborious and time consuming. In addition, the initial efforts in using this kind of work in road network level asset management have also been undertaken by the author and it has further underlined the need for a solution to the difficulties of road data management. Similar work that the author has encountered deals with these difficulties by aggregating large amounts of measurements and using exemplary road sections. The former has also been used in measurement campaigns discussed in section 4.2 which was one of the reasons for exploring data aggregation in section 5.3. This might also explain the reluctance for dealing with raw profile measurements in many cases. What is required is the development of a software framework to deal with large amounts of road data which in turn requires careful considerations of architectural design and implementation details of a framework. While such considerations might be peripheral to the work described here, they are nonetheless very important and requires understanding of the data and its use in modelling. Therefore, they have been briefly described in appendix A together with sample results of the efforts in asset management.

[1] The author has also heard the term 'graveyard of data' referring to this circumstance.

Bibliography

[1] *Technical Committee Report on Surface Characteristics*. Permanent International Associations of Road Congresses (PIARC), 1978.

[2] W.M. Al-Momani and O.O. Badran. Experimental investigation of factors affecting vehicle fuel consumption. *International Journal of Mechanical and Materials Engineering*, 2(2):180–188, 2007.

[3] Dave Amos. *Pavement Smoothness and Fuel Efficieny*. Missouri Department of Transportation, 2006.

[4] Lasse G. Andersen, Jesper K. Larsen, S. Elsje Fraser, Bjarne Schmidt, and Jeppe C. Dyre. Rolling resistance measurement and model development. *J. Transp. Eng.*, 141(2), 2015.

[5] Lasss G. Andersen and Jesper K. Larsen. Introducing functional data analysis to coast down modeling for rolling resistance estimation. *SAE Int. J. Passeng. Cars - Mech. Syst.*, Accepted for publication, 2015.

[6] Patrik Andersson, Carsten Hoover, Juliea Winroth, and Wolfgang Kropp. Numerical modelling of tyre/road interaction. *Scientific Bulletin, Automotive Series*, 22:5–14, 2012.

[7] P.B.U. Andersson and W. Kropp. Time domain contact model for tyre/road interaction including nonlinear contact stiffness due to small-scale roughness. *Journal of Sound and Vibration*, 318(1-2):296–312, 2008.

[8] F. Anfosso-Lédée and M.-T. Do. Geometric descriptors of road surface texture in relation to tire-road noise. *Transportation Research Record*, (1806):160–167, 2002.

[9] Peter W. Arnberg, Michael W. Burke, Georg Magnusson, Roger Oberholtzer, Knut Råhs, and Leif Sjögren. *The Laser RST: Current Status*. Statens väg- och trafikinstitut, Lindköping, 1990.

[10] ASTM E1845 - 09. *Standard Practice for Calculating Pavement Macrotexture Mean Profile Depth*. American Society for Testing and Materials (ASTM), 2009.

[11] ASTM E965 - 96. *Standard Test Method for Measuring Pavement Macrotexture Depth Using a Volumetric Technique*. American Society for Testing and Materials (ASTM), 2006.

[12] J. Barrand and J. Bokar. Reducing tire rolling resistance to save fuel and lower emissions. *SAE International Journal of Passenger Cars - Electronic and Electrical Systems*, 1(1):9–17, 2009.

[13] S. Bendat Bendat and Allan G. Piersol. *Random Data - Analysis and Measurement Procedures*. John Wiley & Sons, Inc., fourth edition, 2010.

[14] Christopher R. Bennett. Calibrating road roughness meters in developing countries. *Transportation Research Record*, (1536):73–81, 1996.

[15] Anneleen Bergiers, Luc Goubert, Fabienne Anfosso-Lédée, Niels Dujardin, Jerzy A. Ejsmont, and Ulf Sandberg Marek Zöller. *Comparison of Rolling Resistance Measuring Equipment - Pilot Study*. Models for rolling resistance In Road Infrastructure Asset Management systems (MIRIAM), 2011.

[16] I.J.M Besselink, A.J.C Schemeitz, and H.B Pacejka. An improved magic formula/swift tyre model that can handle inflation pressure changes. *Vehicle System Dynamics*, 48:337–352, 2010.

[17] I.J.M. Besselink, A.J.C. Schmeitz, and H.B. Pacejka. An improved magic formula/swift tyre model that can handle inflation pressure changes. *Vehicle System Dynamics*, 48(SUPPL. 1):337–352, 2010.

[18] Christo J. Bester. Effect of pavement type and condition on the fuel consumption of vehicles. *Transportation Research Record*, (1000):28–32, 1984.

[19] D.C. Biggs and R. Akcelik. Interpretation of the parameters in the simple average travel speed model of fuel consumption. *Australian road research*, 15(1):46–49, 1985.

[20] Stijn Boere. Prediction of road texture influence on rolling resistance. Master's thesis, Eindhoven University of Technology, 2009.

[21] R. Buchheim, R. Unger, G. W. Car, A. Cogotti, A. Garrone, A. Garrone, and L. U. Nilsson. Comparison tests between major European automotive wind tunnels. *SAE Technical Paper*, 800140, 1980.

[22] F. Buckley, C. Marks, and W. Walston. Analysis of coast-down data to assess aerodynamic drag reduction on full-scale tractor-trailer trucks in windy environments. *SAE Technical Paper*, 760106, 1976.

[23] Frank T. Buckley. Abcd - an improved coast down test and analysis method. *SAE Technical Paper*, 950626, 1995.

[24] Stephen Butterworth. On the theory of filter amplifiers. *Experimental Wireless & the Wireless Engineer*, 1930.

[25] Y.P. Chang, M. El-Gindy, and D.A. Streit. Influence of tyre loading and inflation pressure on standing waves phenomenon using pam-shock. *Heavy Vehicle Systems*, 10(1-2):86–111, 2003.

[26] Karim Chatti and Imen Zaabar. *Estimating the Effects of Pavement Condition on Vehicle Operating Costs*. Number 108 in NCHRP Web Documents. Transportation Research Record, 2012.

[27] T.G. Clapp and A.C. Eberhardt. Computation and analysis of texture-induced contact information in tire-pavement interaction. *Transportation Research Record*, (1084):23–29, 1986.

[28] S. Clark and D. Schuring. Interlaboratory tests for tire rolling resistance. *SAE Technical Paper*, 780636, 1978.

[29] S.K. Clark. *Rolling Resistance Forces in Pneumatic Tires*. Report prepared for the U.S. Department of Transportation, Office of University Research, 1976.

[30] J.B. Corley-Lay. Friction and surface texture characterization of 14 pavement test sections in greenville, north carolina. *Transportation Research Record*, (1639):155–161, 1998.

[31] P.C. Curtayne, A.T. Visser, H.W. DuPlessis, and R. Harrison. Calibrating the relationship between operating costs of buses and road roughness on low-volume roads. *Transportation Research Record*, 2(1106):95–104, 1987.

[32] Carl de Boor. *A Practical Guide to Splines*. New York: Springer, 2001.

[33] Guy Descornet. Criterion for optimizing surface characteristics. *Transportation Research Record*, (1215):173–177, 1989.

[34] Guy Descornet. Road-surface influence on tire rolling resistance. In *Surface Characteristics of Roadways: International Research and Technologies STP 1031*. American Society for Testing and Materials, 1990.

[35] J. Deur, V. Ivanović, M. Troulis, C. Miano, D. Hrovat, and J. Asgari. Extensions of the LuGre tyre friction model related to variable slip speed along the contact patch length. *Vehicle System Dynamics*, 43(SUPPL.):508–524, 2005.

[36] M. Djordjevic, A. Jankovic, and B. Jeremic. Rolling resistance as the risk factor for fuel consumption. *International Journal of Vehicle Systems Modelling and Testing*, 4(3):185–200, 2009.

[37] G. Dubois, J. Cesbron, H.P. Yin, and F. Anfosso-Lédée. Macro-scale approach for rough frictionless multi-indentation on a viscoelastic half-space. *Wear*, 272(1):69–78, 2011.

[38] A.L. Dunn, G.D. Uhlenhake, D.A. Guenther, Gary .J. Heydinger, and J. Heydinger, Grant. Vehicle coast analysis: Typical suv characteristics. *SAE International Journal of Passenger Cars - Electronic and Electrical Systems*, 1(1):526–535, 2009.

[39] G. Eaker. Wind tunnel-to-road aerodynamic drag correlation. *SAE Technical Paper*, 880250, 1988.

[40] T.G. Ebbott, R.L. Hohman, Jeusette, and V. J.-P., Kerchman. Tire temperature and rolling resistance prediction with finite element analysis. *Tire Science and Technology*, 27(1):2–21, 1999.

[41] Jerzy A. Ejsmont and Grzegorz Ronowski. *Rolling Resistance Measurements at the MnROAD Facility*. Minnesota Department of Transportation, Research Services Section, 2012.

[42] Murat Ergün and Emine Agar. Optimisation of road surface friction from macro- and microtexture point of view. In *[130]*. Permanent International Associations of Road Congresses (PIARC), 2000.

[43] E.M. Evans and P.J. Zemroch. Measurement of the aerodynamic and rolling resistances of road tanker vehicles from coast-down tests. *Proceedings of the Institution of Mechanical Engineers, Part D: Transport Engineering*, 198(11):211–218, 1984.

[44] M. Faraji, V.J. Majd, B. Saghafi, and M. Sojoodi. An optimal pole-matching observer design for estimating tyre-road friction force. *Vehicle System Dynamics*, 48(10):1155–1166, 2010.

[45] Gerado W. Flintsch, Edgar de LÃ©on, Kevin K. McGhee, and Imad L. Al-Qadi. Pavement surface macrotexture measurement and application. *Transportation Research Record*, (1860):168–177, 2003.

[46] T.G. Frank and E.W. Abel. A technique for the accurate measurement of low values of rolling resistance. *Proceedings of the Institution of Mechanical Engineers, Part D: Journal of Automobile Engineering*, 202(D4, 1988):251–255, 1988.

[47] T. Freudenmann, H.-J. Unrau, and M. El-Haji. Experimental determination of the effect of the surface curvature on rolling resistance measurements 4. *Tire Science and Technology*, 37(4):254–278, 2009.

[48] R. Gall, P. Tkacik, and M. Andrews. On the incorporation of frictional effects in the tire/ground contact area. *Tire Science and Technology*, 21(1):2–22, 1993.

[49] Alan N. Gent and Joseph D. Walter. *The Pneumatic Tire*. U.S. Department of Transportation, National Highway Traffic Safety Administration, 2006.

[50] A.N. Gent. A test method for rolling resistance of rubber compounds. *Annual Technical Conference - ANTEC, Conference Proceedings*, 3:1610–1613, 2006.

[51] St. Germann and R. Isermann. Modelling and control of longitudinal vehicle motion. *Proceedings of the American Control Conference*, 1:1–5, 1994.

[52] M.H.R. Ghoreishy. A state of the art review of the finite element modelling of rolling tyres. *Iranian Polymer Journal (English Edition)*, 17(8):571–597, 2008.

[53] T.D. Gillespie, S. M. Karamihas, S. D. Kohn, and R. W. Perera. *Operational Guidelines for Longitudinal Pavement Profile Measurement*. National Cooperative Highway Research Program, 1999.

[54] T.D. Gillespie, M.W. Sayers, and L. Segel. *Calibration and Correlation of Repsons-Type Road Roughness Measuring Systems*. National Cooperative Highway Research Program, 1980.

[55] T.D. Gillespie, M.W. Sayers, and L. Segel. *Calibration of Response-Type Road Roughness Measuring Systems*. Number 228 in NCHRP Reports. Transportation Research Board, 1980.

[56] Alexandr Grecenko. Thrust and slip of a low-pressure tire on compressible ground by the compression-sliding approach. *Journal of Terramechanics*, 47:249–259, 2010.

[57] Ian D. Greenwood and C. R. Bennett. *Modelling Road User and Environmental Effects in HDM-4,*. The World Road Association (PIARC), 2001.

[58] Ian D. Greenwood and C. R. Bennett. *HDM-4 Fuel Consumption Modeling*. World Bank, 2003.

[59] M. Haider, M. Conter, and K.-P. Glaeser. *Discussion paper - "What are rolling resistance and other influencing parameters on energy consumption in road transport"*. Models for rolling resistance In Road Infrastructure Asset Management systems (MIRIAM), 2011.

[60] J.W. Hall, K.L. Smith, L. Titus-Glover, J.C. Wambold, T.J. Yager, and Z. Rado. *Guide for Pavement Friction*. Number 108 in NCHRP Web Documents. Transportation Research Record, 2009.

[61] K. Hamabe, K. Kitoh, H. Ogata, and T. Kobayashi. An estimation of aerodynamic drag coefficient of a passenger car by coast-down tests in windy environments. *JSAE Review*, (16):114–120, April 1985.

[62] Ulf Hammarström, Jenny Eriksson, Rune Karlsson, and Mohammad-Reza Yahya. *Rolling resistance model, fuel consumption model and the traffic energy saving potential of changed road surface conditions*. The Swedish Transport Administration and the MIRIAM project, 2012.

[63] Ulf Hammarström, Rune Karlsson, and Harry Sörensen. *Road surface effects on rolling resistance - coastdown measurements with uncertainty analysis in focus*. Energy Conservation in Road Pavement Design, Maintenance and Utilisation (ECRPD), 2009.

[64] C. Harnisch, B. Lach, R. Jakobs, M. Troulis, and O. Nehls. A new tyre-soil interaction model for vehicle simulation on deformable ground. *Vehicle System Dynamics*, 43(SUPPL.):384–394, 2005.

[65] Nancy E. Heckman and J. Ramsay. Penalized regression with model-based penalties. *The Canadian Journal of Statistics*, 28(2):241–258, 2000.

[66] Carsten Hoever. *The influence of modelling parameters on the simulation of car tyre rolling losses and rolling noise*. PhD thesis, Department of Civil and Environmental Engineering, Division of Applied Acoustics, Vibroacoustics Group, Chalmers University of Technology, 2014.

[67] W.L. Holt and P.L. Wormely. Power loloss in automobile tires. *Technologic Papers of the Bureau of Standards*, 16:451–461, 1922.

[68] J. Hooghwerff, E.W. van Gils, and H. F. Reinink. *Influence of Road Surface Type on Rolling Resistance*. M+P Raadgevende Ingenieurs BV and Rijkwaterstaat, 2013.

[69] J. Hooghwerff, E.W. van Gils, and H. F. Reinink. *Influence of road surface type on rolling resistance*. Rijkswaterstaat, Ministry of Infrastructure and the Enviroment, 2013.

[70] V. Hublau and A. Barillier. The equations of the rolling resistance of a tire rolling on a drum. *Tire Science and Technology*, 36(2):146–155, 2008.

[71] S.W. Hunt, A.M.C. Odhams, R.L. Roebuck, and D. Cebon. Parameter measurement for heavy-vehicle fuel consumption modelling. *Proceedings of the Institution of Mechanical Engineers, Part D: Journal of Automobile Engineering*, 225(5):567–589, 2011.

[72] F. N. Hveem. Devices for recording and evaluating pavement roughness. *Highway Research Board Bulletin*, 264:1–26, 1960.

[73] Mineichi Inagawa and Michiya Ohta. Contribution of vehicular parameters on fuel economy of trucks. *Proceedings - Society of Automotive Engineers*, pages 595–603, 1985.

[74] ISO 10844. *Acoustics – Specification of test tracks for measuring noise emitted by road vehicles and their tyres*. International Standards Organization (ISO), 1994.

[75] ISO 13473-1. *Characterization of pavement texture by use of surface profiles – Part 1: Determination of Mean Profile Depth*. International Standards Organization (ISO), 1997.

[76] ISO 13473-2. *Characterization of pavement texture by use of surface profiles – Part 2: Terminology and basic requirements related to pavement texture profile analysis*. International Standards Organization (ISO), 2002.

[77] ISO 13473-4. *Characterization of pavement texture by use of surface profiles – Part 4: Spectral analysis of surface profiles*. International Standards Organization (ISO), 2008.

[78] ISO 13473-5. *Characterization of pavement texture by use of surface profiles – Part 5: Determination of megatexture*. International Standards Organization (ISO), 2009.

[79] ISO 18164. *Passenger car, truck, bus and motorcycle tyres – Methods of measuring rolling resistance*. International Standards Organization (ISO), 2005.

[80] ISO 28580. *Passenger car, truck and bus tyres – Methods of measuring rolling resistance – Single point test and correlation of measurement results*. International Standards Organization (ISO), 2009.

[81] V. Ivanov, B. Shyrokau, K. Augsburg, and V. Algin. Fuzzy evaluation of tyre-surface interaction parameters. *Journal of Terramechanics*, 47(2):113–130, 2010.

[82] J. Ivens. Rolling resistance of some 13 inch tires and the correlation between rig and road. *SAE Technical Paper Series*, 870422, 1987.

[83] A. Kamoulakos and B.G. Kao. Transient dynamics of a tire rolling over small obstacles - a finite element approach with pam-shock. *Tire Science and Technology*, 26(2):84–108, 1998.

[84] Leslie Karafiath. Rolling resistance of off-road vehicles. *Journal of Construction Engineering and Management*, 114(3):458–471, 1988.

[85] S. M. Karamihas. *Critical Profiler Accuracy Requirements*. The University of Michigan, Transportation Research Institute, 2005.

[86] S. M. Karamihas and T. D. Gillespie. *AsseAssess of Profile Performance for Construction Quality Control: Phase I*. The University of Michigan, Transportation Research Institute, 2002.

[87] S. M. Karamihas, T.D. Gillespie, S. D. Kohn, and R. W. Perera. *Guidelines for Longitudinal Pavement Profile Measurement*. National Cooperative Highway Research Program, 1999.

[88] Seven M. Karamihas, Michelle A. Barnes, and Robert O. Rasmussen. *Pavement Surface Specification for Road Load Measurement*. The University of Michigan, Transportation Research Institute, 2014.

[89] Rune Karlsson, Ulf Hammarström, Harry Sörensen, and Olle Eriksson. *Road surface influence on rolling resistance - Coastdown measurements for a car and HGV - VTI notat 24A*. Swedish Road Administration (VTI), 2011.

[90] R.L. Keefe and A.S. Koralek. Precision measurement of tire rolling resistance. In *Rubber Division Symposia*, volume 1, pages 78–104. American Chemical Society, Rubber Division, Akron, Ohio, 1983.

[91] Thomas M. Kenny. Prediction of contained air temperature from SAE standard rolling resistance test data. *SAE Technical Paper Series*, 831796, 1983.

[92] E.C. Klaubert and H.A. Jongedyk. Highway effects on vehicle operation. *Civil Engineering for Practicing and Design Engineers*, 4(3):285–299, 1985.

[93] P. Klein and J.F. Hamet. *Road texture and rolling noise: An envelopment procedure for tire-road contact*. By Institut National de Recherche Sur Les Tranports Et Leur Securite (INRETS) for the SILVIA project, 2004.

[94] R.E. Knight. Correlation of truck tire rolling resistance as derived from fuel economy and laboratory tests. *SAE Technical Paper Series*, 1982.

[95] Richard E. Knight. Trends in rolling resistance and fuel economy for advanced design radial highway truck tires. In *Rubber Division Symposia*, volume 1, pages 383–398. American Chemical Society, Rubber Division, Akron, Ohio, 1983.

[96] A. G. Kokkalis, G. H. Tsohos, and O. K. Panagouli. Consideration of fractals potential in pavement skid resistance evaluation. *Journal of Transportation Engineering*, 128:591–595, 2002.

[97] S.-L. Koo, H.-S. Tan, and M. Tomizuka. Impact of tire compliance behavior to vehicle longitudinal dynamics and control. *Proceedings of the American Control Conference*, pages 5736–5741, 2007.

[98] H. Korst and R. White. Coastdown tests: Determining road loads versus drag component evaluation. *SAE Technical Paper*, 901767, 1990.

[99] P. Krehan. Measurement of rolling resistance in a road test. *Proceedings - Society of Automotive Engineers*, pages 295–299, 1990.

[100] Road Research Laboratory. *Road Note 27: Instructions for using the portable skid-resistance tester*. Road Research Laboratory, Crowthorne, Berkshire, 1960.

[101] S. Lajqi, S. Pehan, N. Lajqi, B. Baxhaku, and B. Ymeri. Influences of the suspension parameters on the vehicle suspension performance for a terrain vehicle. *Journal of Mechanics Engineering and Automation*, 2:550–554, 2012.

[102] K. Larsson and W. Kropp. A high-frequency three-dimensional tyre model based on two coupled elastic layers. *Journal of Sound and Vibration*, 254:889–908, 2002.

[103] A. Leinonen and M. Juhala. Development of measurement equipment for measuring tire rolling resistance on road. *Proceedings of 8th Biennial ASME Conference on Engineering Systems Design and Analysis, ESDA2006*, 2006, 2006.

[104] J. Lieh. A closed-form method to determine vehicle speed and its maximum value. *International Journal of Vehicle Systems Modelling and Testing*, 3(1-2):1–13, 2008.

[105] J. R. Luchini. Test surface curvature reduction factor for truck tire rolling resistance. *SAE Technical Paper*, 821264, 1982.

[106] John R. Luchini. Rolling resistance test methods. In *Rubber Division Symposia*, volume 1, pages 69–77. American Chemical Society, Rubber Division, Akron, Ohio, 1983.

[107] John R. Luchini and Lori A. Simonelli. Rolling resistance tests on smooth and textured-surface test wheels. In *Rubber Division Symposia*, volume 1, pages 140–150. American Chemical Society, Rubber Division, Akron, Ohio, 1983.

[108] J.R. Luchini, J.M. Peters, and R.H. Arthur. Tire rolling loss computation with the finite element method. *Tire Science and Technology*, 22(4):206–222, 1994.

[109] J.R. Luchini and J.A. Popio. Modeling transient rolling resistance of tires. *Tire Science and Technology*, 35(2):118–140, 2007.

[110] G.N. Lupton and T. Williams. Study of the skid resistance of different tire tread polymers on wet pavements with a range of surface textures. *ASTM Special Technical Publication*, 530:101–116, 1972.

[111] G.-L. Ma, H. Xu, and W.-Y. Cui. Computation of rolling resistance caused by rubber hysteresis of truck radial tire. *Journal of Zhejiang University: Science A*, 8(5):778–785, 2007.

[112] M. Männel and T. Beckenbauer. Characterisation of road surfaces by means of texture analysis. *VDI Berichte*, (2014):223–239, 2007.

[113] Donald W. Marquardt and Ronald D. Snee. Ridge regression in practice. *The American Statistician*, 29(1):3–20, 1975.

[114] W.V. Mars and J.R. Luchini. Analytical model for the transient rolling resistance behavior of tires. *Tire Science and Technology*, 27(3):161–175, 1999.

[115] A. von Meier, G. J. von Blokland, and G. Descornet. The influence of texture and sound absorption on the noise of porous road surfaces. *Proceedings of the PIARC Second International Symposium on Road Surface Characteristics*, pages 7–19, 1992.

[116] W. E. Meyer and J. Reichert, editors. *Surface Characteristics of Roadways: International Research and Technologies STP 1031*. ASTM, 1990.

[117] Michelin. *Michelin (2003): "The tyre - Rolling resistance and fuel savings". Book published by , 23 rue Breschet, FR-63000 Clermont-Ferrand, France (this is also available on CD).* SociÃ©tÃ© de Technologie Michelin, 23 rue Breschet, FR-63000 Clermont-Ferrand, France, 2003.

[118] A.J.P. Miege and A.A. Popov. The rolling resistance of truck tyres under a dynamic vertical load. *Vehicle System Dynamics*, 43(SUPPL.):135–144, 2005.

[119] K.V. Narasimha Rao, R. Krishna Kumar, and P.C. Bohara. A sensitivity analysis of design attributes and operating conditions on tyre operating temperatures and rolling resistance using finite element analysis. *Proceedings of the Institution of Mechanical Engineers, Part D: Journal of Automobile Engineering*, 220(5):501–517, 2006.

[120] Connie Nielsen and Trine de Fine Skibsted. *The energy-saving road - Improving socio-economic conditions by reducing rolling resistance*. NCC Green Road, 2010.

[121] J.W. O'Neal, Claude A. Brunot, A.D. Wanstedt, and T.C. Warholic. Interlaboratory rolling resistance testing - highway truck and bus tires. *SAE Technical Paper*, 821265, 1982.

[122] Hans Pacejka. *Tire and Vehicle Dynamics*. Elsevier, 2012.

[123] Hans B. Pacejka. *Tire and Vehicle Dynamics*. SAE International, 2006.

[124] O. K. Panagouli and A. G. Kokkalis. Skid resistance and fractal structure of pavement surface. *Chaos, Solitons and Fractals*, 9:493–505, 1998.

[125] H.C. Park, S.-K. Youn, T.S. Song, and N.-J. Kini. Analysis of temperature distribution in a rolling tire due to strain energy dissipation. *Tire Science and Technology*, 25(3):214–228, 1997.

[126] J.P. Pauwelussen and L. Laib. Exploration of the magic formula as a basis for the modelling of tyre-soil interaction. *Proceedings of the 7th European ISTVS Conference, Ferrara, Italy*, 1997.

[127] R.W. Perera and S. D. Kohn. *Quantification of Smoothness Index Differences Related To Long-Term Pavement Performance Equipment Type (Report FHWA-HRT-05-054)*. The Federal Highway Administration (FHWA), 2005.

[128] W. Petersen and J. McPhee. A volumetric contact model approach for off-road tire/soil dynamic simulation. *Proceedings of the ASME Design Engineering Technical Conference*, 4:73–80, 2010.

[129] V. Petrushov. Coast down method in time-distance variables. *SAE Technical Paper*, 970408, 1997.

[130] PIARC Technical Committee on Surface Characteristics. *Pavement Surface Characteristics - Fourth International Symposium 'SURF 2000', Nantes (France)*. Permanent International Associations of Road Congresses (PIARC), 2000.

[131] P.S. Pillai. Total tire energy loss comparison by the whole tire hysteresis and the rolling resistance methods. *Tire Science and Technology*, 23(4):256–265, 1995.

[132] P.S. Pillai and G.S. Fielding-Russell. Effect of aspect ratio on tire rolling resistance. *Rubber Chemistry and Technology*, 64(4):641–647, 1991.

[133] P.S. Pillai and G.S. Fielding-Russell. Tire rolling resistance from whole-tire hysteresis ratio. *Rubber Chemistry and Technology*, 65(2):444–452, 1992.

[134] Roger J. Pinnington. A particle-envelope surface model for road-tyre interaction. *International Journal of Solids and Structure*, 49:546–555, 2012.

[135] Roger J. Pinnington. Tyre-road contact using a particle-envelope surface model. *Journal of Sound and Vibration*, 332:7055–7075, 2013.

[136] J.A. Popio and J.R. Luchini. Fidelity of j1269 and j2452. *Tire Science and Technology*, 35(2):94–117, 2007.

[137] Simon Pouget, Cédric Sauzéat, Herve Di Benedetto, and Francois Olard. Viscous energy dissipation in asphalt pavement structures and implication for vehicle fuel consumption. *Journal of Materials in Civil Engineering*, 24:568–576, 2012.

[138] A.A. Poyton, M.S. Varziri, K.B. McAuley, P.J. McLellan, and J.O. Ramsay. Parameter estimation in continuous-time dynamic models using principal differential analysis. *Computers and Chemical Engineering*, 30:698–708, 2006.

[139] Andrew Pressley. *Elementary Differential Geometry*. Springer, 2006.

[140] X. Qiu. Full two-dimensional model for rolling resistance. ii: Viscoelastic cylinders on rigid ground. *Journal of Engineering Mechanics*, 135(1):20–30, 2009.

[141] J. O. Ramsay, G. Hooker, D. Campbell, and J. Cao. Parameter estimation for differential equations: A generalized smoothing approach. *Journal of the Royal Statistical Society*, 69:741 – 796, 2007.

[142] J.O. Ramsay and B. W. Silverman. *Applied Functional Data Analysis*. Springer, 2002.

[143] J.O. Ramsay and B.W. Silverman. *Functional Data Analysis*. Springer Series in Statistics, 2005.

[144] Jørgen Kragh. *Rolling Resistance - Copenhagen 2009 (Technical Note 77)*. Road Directorate, Danish Road Institute, 2010.

[145] M. S. Roovers, D. F. de Graaff, and R. K. F. van Moppes. *Round Robin Test Rolling Resistance / Energy Consumption*. Prepared for: Ministery of Traffic and Waterworks (DWW) by M+P consulting engineers, German Bundesanstalt für Straßenvesen (BASt) and Technical University of Gdansk (TUG), 2005.

[146] G. Roussillon. Contribution to accurate measurement of aerodynamic drag on a moving vehicle from coast-down tests and determination of actual rolling resistance. *Journal of Wind Engineering and Industrial Aerodynamics*, 9:33–48, 1981.

[147] SAE J1269. *Rolling Resistance Measurement Procedure for Passenger Car, Light Truck, and Highway Truck and Bus Tires*. Society of Automotive Engineers (SAE), 2006.

[148] SAE J2452. *Stepwise Coastdown Methodology for Measuring Tire Rolling Resistance*. Society of Automotive Engineers (SAE), 1999.

[149] P. Salerno. Considerations on fuel consumption and performance of a vehicle fitted with low rolling resistance tyres. *I Mech E Conference Publications (Institution of Mechanical Engineers)*, pages 31–40, 1983.

[150] Tony Sandberg. *Heavy Truck Modeling for Fuel Consumption Simulations and Measurements*. PhD thesis, Linköping University, 2001.

[151] Ulf Sandberg. Road macro- and megatexture influence on fuel consumption. In W. E. Meyer and J. Reichert, editors, *Surface Characteristics of Roadways: International Research and Technologies STP 1031*, pages 460–479. American Society for Testing and Materials, 1990.

[152] Ulf Sandberg and Jerzy A. Ejsmont. *Tyre/Road Noise Reference Book*. INFORMEX, Harg, SE-59040 Kisa, Sweden, 2002.

[153] Ulf Sandberg, Manfred Haider, , Luc Goubert, Anneleen Bergiers, Marek Zöller, Rune Karlsson, and Jerzy A. Ejsmont. *Road surface influence on tyre/road rolling resistance*. Models for rolling resistance In Road Infrastructure Asset Management systems (MIRIAM), 2011.

[154] Ulf Sandberg, Manfred Haider, Marco Conter, Luc Goubert, Anneleen Bergiers, Gernot Schwalbe Klaus-Peter Glaeser, Marek Zöller, Olivier Boujard, Ulf Hammarström, Rune Karlsson, Jerzy A. Ejsmont, T. Wang, and J.T. Harvey. *Rolling Resistance - Basic Information and State-of-the-Art on Measurement methods*. Models for rolling resistance In Road Infrastructure Asset Management systems (MIRIAM), 2011.

[155] M. W. Sayers and S. M. Karamihas. *Interpretation of Road Roughness Profile Data*. U.S. Federal Highway Administration, Contract DTFH 61-92-C00143, 1996.

[156] Michael W. Sayers and Steven M. Karamihas. *The Little Book of Profiling*. The Regent of the University of Michigan, 1998.

[157] M.W. Sayers. Two quarter-car models for defining road roughness: Iri and hri. *Transportation Research Record*, (1215):165–172, 1989.

[158] M.W. Sayers, T.D. Gillespie, and W.D.O Patterson. *Establishing Correlation and a Calibration Standard for Measurements*. World Bank Technical Paper Number 45, 1986.

[159] M.W. Sayers, T.D. Gillespie, and W.D.O Patterson. *Guidelines for Conducting and Calibrating Road Roughness Measurements*. World Bank Technical Paper Number 46, 1986.

[160] Bjarne Schmidt and Jeppe Dyre. CO_2 emission reduction by exploitation of rolling resistance modelling of pavements. *Procedia - Social and Behavioral Sciences*, 48:311–320, 2012.

[161] Bjarne Schmidt and Per Ullidtz. *Den energibesparende vej*. NNC Roads, 2010.

[162] D. Schuring and J. Refield. Effect of tire rolling loss on fuel consumption of trucks. *SAE Technical Paper*, 1982.

[163] D.J. Schuring. A new look at the definition of tire rolling loss. In *Tire Rolling Losses and Fuel Economy - an R&D Planning Workshop*, volume P-74, pages 31–37. SAE Conference Proceedings, 1977.

[164] D.J. Schuring. Effect of tire rolling loss on vehicle fuel consumption. *Tire Science and Technology*, 22(3):148–161, 1994.

[165] Z. Shida, M. Koishi, T. Kogure, and K. Kabe. Rolling resistance simulation of tires using static finite element analysis. *Tire Science and Technology*, 27(2):84–105, 1999.

[166] M.C. Smith and S.J. Swift. Power dissipation in automotive suspensions. *Vehicle System Dynamics*, 49(1-2):59–74, 2011.

[167] M. Sobhanie. Road load analysis. *Tire Science and Technology*, 31(1):19–38, 2003.

[168] Richard C. Sohaney and Robert O. Rasmussen. *Pavement Texture Evaluation and Relationships to Rolling Resistance at MnROAD*. Minnesota Department of Transportation, Research Services Section, 2013.

[169] A. Swift. Calculation of vehicle aerodynamic drag coefficients from velocity fitting of coastdown data. *Journal of Wind Engineering and Industrial Aerodynamics*, 37(2):167–185, 1991.

[170] C. Teodorescu. Influence factors on truck tyre rolling resistance. *UPB Scientific Bulletin, Series D: Mechanical Engineering*, 62(4):65–73, 2000.

[171] U.S. Department of Transportation. *Transportation's Role in Reducing U.S. Greenhouse Gas Emissions - Volume 1: Synthesis Report*, April 2010.

[172] V.V. Vantsevich and C. Stuart. Probabilistic interactions of vehicles with surroundings: Modeling for dynamic control. *ASME International Mechanical Engineering Congress and Exposition, Proceedings*, 9 PART C:1649–1658, 2008.

[173] M. Saeed Varziri, Kim B. McAuley, and P. James McLellan. Parameter estimation in continuous-time dynamic models in the pressence of unmeasured states and nonstationary disturbances. *Ind. Eng. Chem. Res.*, 47:380–393, 2008.

[174] Vejdirektoratet. *Vejvedligehold - Vedligeholdelse af Færdselsarealet*, 2009.

[175] A.T. Visser. *A Correlation Study of Roughness Measurments with an index Obtained from a Road Profile Measured with Rod and Level*. NITRR Technical Report RC/2/82, 1982.

[176] W. Walston, F. Buckley, and C. Marks. Test procedures for the evaluation of aerodynamic drag on full-scale vehicles in windy environments. *SAE Technical Paper*, 760106, 1976.

[177] T.C. Warholic. Rolling resistance performance of passenger car tires during warm-up (speed, load & inflation pressure effects). In *Rubber Division Symposia*, volume 1, pages 151–162. American Chemical Society, Rubber Division, Akron, Ohio, 1983.

[178] Joachim Weidmann. *Linear Operators in Hilbert Spaces*. Springer-Verlag, 1980.

[179] R. White and H. Korst. The determination of vehicle drag contributions from coast-down tests. *SAE Technical Paper*, 720099, 1972.

[180] R. Wille, F. Bö hm, and A. Duda. Calculation of the rolling contact between a tyre and deformable ground. *Vehicle System Dynamics*, 43(SUPPL.):483–492, 2005.

[181] F.R. Williams and T.J. Dudek. Load-deflection hysteresis and its relationship to tire rolling resistance. In *Rubber Division Symposia*, volume 1, pages 105–139. American Chemical Society, Rubber Division, Akron, Ohio, 1983.

[182] R. Wozniak, S. Taryma, and G. Ronowski. Modernization of the trailer for tyre/road rolling resistance measurements. *Key Engineering Materials*, 490:179–186, 2011.

[183] R. Wozniak, S. Taryma, and G. Ronowski. Relieving the measuring system of the trailer for tyre/road rolling resistance measurements from the inertia force. *Key Engineering Materials*, 490:265–272, 2011.

[184] G.Z. Wu and X.M. He. Effects of aspect ratio on the stresses and deformations of radial passenger tires. *Tire Science and Technology*, 20(2):74–82, 1992.

[185] L.H. Yam, D.H. Guan, J. Shang, and A.Q. Zhang. Study on tyre rolling resistance using experimental modal analysis. *International Journal of Vehicle Design*, 30(3):251–262, 2002.

[186] Mohan Yeggoni, Joe W. Button, and Dan G. Zollinger. Fractals of aggregates correlated with creep in asphalt concrete. *Journal of Transportation Engineering*, 122:22–28, 1996.

[187] R. N. Yong, P. Boonsinsuk, and E. A. Fattah. Tyre load capacity and energy loss with respect to varying soil support stiffness. *Journal of Terramechanics*, 17:131–147, 1980.

[188] Z.-X. Yu, H.-F. Tan, X.-W. Du, and L. Sun. A simple analysis method for contact deformation of rolling tire. *Vehicle System Dynamics*, 36(6):435–443, 2001.

A Appendix: Road Data Management

A.1 Introduction

The framework is written in Python and is build upon 'Numpy' which is the Python package for numerical and scientific computations. Python together with numpy package gives essentially the same capabilities as any other numerical tool like MatLab/Octave, R, SPSS etc. One important difference is the fact that Python is a powerful general purpose language which makes well suited for building a framework like this. A small example using a simplified way of calculating fuel consumption is shown here to illustrate the intent of the framework. The present version of the documentation is supplied in section A.2 and the code for the framework can be found at `https://github.com/lgandersen/RDMS`. Note that this repository will be continually updated.

In 2010 Niras made a socio-economic report[1] estimating the potential fuel savings from deploying so-called 'green pavements' to the road network. Green pavements are pavements with low rolling resistance due to lowered road texture and unevenness. Texture and unevenness are usually represented by the road metrics MPD and IRI. It was assumed that by introducing green pavements on the Danish state road network the MPD would be lowered to 0.55 and IRI to 0.9. For any road having larger MPD/IRI values, a fuel consumption reduction estimate could be derived. The parameters for the model are listed in the table A.1. Niras made the calculations on a road section basis, i.e., they made the calculation for an entire motorway, main road etc. This coarse approach have been improved by using the RDMS framework to import raw MPD/IRI values from the Danish Road Directorate[2] which have an approximate resolution of 1 0 m. Using these data gives us a much more detailed view of the state road network and some simple illustrations of this have been given below. In figure A.1 the differences between the distribution of MPD and IRI values on the state road network. Note how the IRI distribution is clearly *not* normally distributed. Also, the driven kilometres are based on Annual Daily Traffic of a low resolution. The author is aware of more precise data that should be available in the Danish Road Directorate and it would be interesting to see how a better resolution will affect the distribution of MPD/IRI for driven kilometres. More importantly, figure A.2 shows the effect of averaging several 10 m MPD/IRI values, and it clearly shows the different result that is obtained depending on the amount of data aggregation. Especially the calculated fuel consumption reduction by IRI is significant with a difference of about 40% and while IRI contributes the least, it still illustrates the importance of studying the road network in its entirety. While these calculations were simple, the data management was not, and it is hoped that this framework will facilitate the implementation of more advanced models of fuel consumption based on the wealth of data that is available at road administrators.

[1] C. Nielsen and T. de Fine Skibsted, *The energy-saving road - Improving socio-economic conditions by reducing rolling resistance*. NCC Green Road, 2010.

[2] These data are then again based on raw profiles with a 1 mm/1 dm resolution for MPD/IRI, respectively. However, these have not been supplied to the author yet.

Table A.1 Calculation parameters

Average spped	90km/h
Rolling resistance per unit MPD	30%
Rolling resistance per unit IRI	6%
Fuel consumption/Rolling resistance ratio	3%/10%
MPD scenario	0.55 [mm^{-1}]
IRI scenario	0.9 [mm/km]

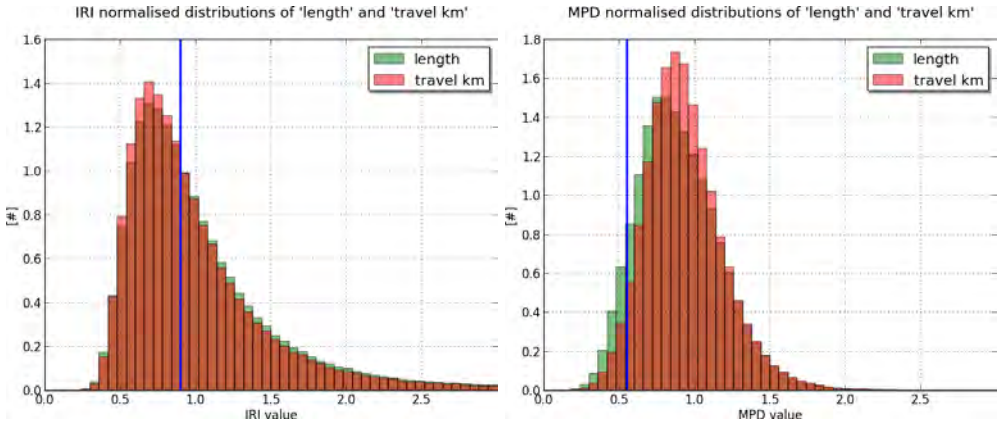

Figure A.1 Distribution of IRI (left) and MPD (right) according to road length (km) and driven km.

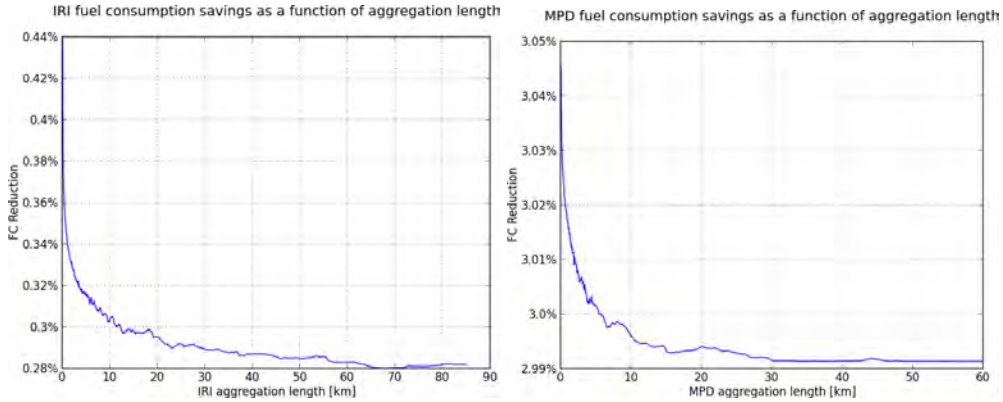

Figure A.2 Fuel consumption savings as a function of road network data aggregation.

Road Data Management System Documentation

Release 0.0.1

Lasse Grinderslev Andersen

April 28, 2015

CONTENTS

CHAPTER

ONE

INTRODUCTION

This software package is used to handle road data in both project-level and network-level applications by providing tools for handling, manipulating and surveying road-related data. Examples of road data:

- Road surface data such as rutting, texture, unevenness and road metrics derived from them such as Mean Profile Depth (MPD) and International Roughness Index (IRI).
- Traffic data such as Annual Daily Traffic (ADT), speed limits, and measured speed.
- Pavement related data such as pavement types and pavement age.

When working with road data (both in road maintenance and research) there are several essential challenges and routine tasks that users of road data have to deal with. Examples of challenges and tasks that this software package tries to facilitate:

- Handling data measured at different times. A road network is not static but evolves over time, and some roads disappear while new ones are created. Also, only parts of the road network might be measured. Dealing with these circumstances requires routines that:
  - Checks road data for consistency relative to a road network 'snapshot', i.e., a data set containing *chainage* [1] information for all roads in the network.
  - Merges road data measured at different times and therefore might contain incompatible parts which must be discared.

  Both types of routines should also produce detailed information about which data failed, why they failed as well as supplying the user with general statistics about how the chainage validation/data merge/etc. went.
- Calculating road metrics like MPD and IRI and filtering of raw profiles from bad readings, spikes, and unwanted wavelengths.
- Storing road data and calculated output in a large database that keeps track of processing flows. For instance, what raw profile data have been filtered to produce filtered laser profile data which in turn have been used in the calculation of a particular set of MPD data and so on.

[1] http://en.wikipedia.org/wiki/Road_surveying#Chainage_or_station

- Using road network level data in asset management. Tasks related to this is estimating pavement wear as function of pavement type, ADT, road metrics etc. and implementation of Markov Decision Models.

RDMS provides a python framework based on Numpy and a toolbox of routines to handle these tasks and challenges. In addition, a web-frontend is supplied, for road engineers to use when undertaking routine tasks such as importing/exporting, surveying and doing routine calculations on road data.

1.1 Data Structure in RDMS

The most fundamental part of RDMS is how roaddata is represented, stored, and accessed. Thus, we begin with a general outline of the data structure in RDMS.

1.1.1 Road Data Components

Almost all kinds of road data are comprised of a few common constituents which have been reflected in RDMS as well:

Road Identifier All road data and measurements have been obtained from a road/road section/road part etc. Moreover, each collection of roads, e.g., a road network or a test track, is equipped with a classification that uniquely identifies all parts of the roads. No matter how the classification is defined, it can always be described as a combination of *road identifiers*. As an example, consider a hypothetical road network where each road is determined by a *region* and a *road-id*. Each road within this classification is then identified by a (*region*, *road-id*) tuple. Thus:

```
('East', '12') # A road identifier
('East', '12A') # Another road identifier
('West', '64B') # Yet another road identifier
```

identifies different roads. In RDMS this is formalized through the `RoadIdentifier` classes which are similar to namedtuples. Usually they are determined and created implicitly whenever data is imported from, e.g., a csv-file. Each instance of a `RoadIdentifier` class uniquely determines a road segment/section/part/etc. in a road collection. Note that different types of roaddata can have different degrees of detail. For example ADT might be defined by (*Region*, *Road-id*) while MPD requires (*Region*, *Road-id*, *Direction*). This is also accomodated in RDMS such that it is possible to merge two different data sets like the example with ADT and MPD.

Road Data Another common aspect of road data is that they are usually composed of two parts

Chainage The (possibly degenerate) interval within a given road section where the data. At the moment chainage is usually given by four values: `km_start`, `m_start`, `km_end`, `m_end` but it could easily be modified to handle other units such as miles

and inches. Future support for GPS-coordinates could also be implemented if the need arise [2].

Data Actual data corresponding to a given chainage interval. This could be ADT, MPD, pavement type etc. and it can be single values or higher dimensional. The type of the data can be *str* or any type that numpy supports.

The data is usually composed of a chainage interval and one or more types of data and is contained by a `RoadData` object. `RoadData` is essentially a wrapper around a tuple of numpy arrays and is create during data import. Data can be accessed by an index or through attribute name. E.g.,:

```
roaddata.km_start
roaddata.m_end
roaddata.MPD
roaddata.ADT
roaddata[0]
```

It is also possible to extract the chainage or data, respectively. In addition, there is only some type-checking of the data behind the scenes that tries to preserve numpy array views. See `RoadData` for details. All the storage types described below uses `RoadData` with the only difference being size of the numpy arrays and whether they are views or not.

1.1.2 Road Data Storage and Access

Essentially the data is structured and accessed through three different layers:

Road Network The top layer in the data storage hierachy which contains road data from several road sections. In RDMS, a road network is primary road data storage and is represented by instances of the `RoadNetwork` class, which are usually created when importing data from, e.g., csv-files.

Internally, the data is stored as numpy arrays spanning all road sections with one array for each data component such as, e.g., 'MPD' or 'km_start'. Furthermore, information about which segments of the arrays corresponds to which road section is also stored such that road data can be accessed on a per road section basis. In general, Road network data can be accessed in three different ways:

1. *Directly*, by accessing the entire arrays and thus all road sections.
2. As *road sections*, by iterating through `RoadSection` type objects. See below for a description of road sections.
3. As *singletons*, by iterating through each single road data element. See below for a description of singletons.

[2] This is tailored to the DRD road network (atm.), and due to the format of some of these data (where the end mark might be given as the first meter of the next kilometer), the length of the consecutive interval is also required.

For details on how to access data from a road network in practice, see `RoadNetwork`.

Road Section As mentioned above, road network level data can be accessed on a per-road section basis. In practice this is usually done by iterating through all `RoadSection` objects contained in a `RoadNetwork`. Essentially, the `RoadSection` objects contain a `RoadIdentifier` defining the road section and a `RoadData` object holding the road data. Initially, the road data in the `RoadData` object are numpy views into the larger arrays of the `RoadNetwork`. However, if they are overwritten with arrays of a different shape, the underlying arrays of the road network will be resized automatically. See `RoadSection` for details.

The road data can be accessed in essentially two ways:

1. *Directly*, by accessing the (view) arrays of the road section.
2. As *singletons*, see below for a description of singletons.

For details on how to access data from a road section in practice, see `RoadSection`.

Singleton The smallest quantity of road data in RDMS. A singleton is a `RoadData` object with only one chainage interval and the data attached to it. Thus, all chainage components have only one value while the the rest of the data can have higher dimensions. Singletons are usually wrapped in a `Singletons` object which is a modified list type. The singletons are created as views into the larger `RoadSection` and/or `RoadNetwork`.

1.2 Chainage Management

Due to the fact that a road network evolves over time, the chainage is not necessarily homogeneous, i.e., a kilometer can be larger/smaller than 1000 meters and there might be holes within a chainage kilometer. This implies that when importing data with non-homogeneous chainage interval their length cannot be determined. To be able to determine lengths and verify that each road data singleton have a valid chainage specification, chainage information of the road network is needed.

As an example, assume we have a ADT measurement with the following chainage:

```
km_start=5, m_start=675, km_end=6, m_end=15
```

Then we do not know the length, since we do not know how many meters constitute the fifth kilometer nor if there are any holes. Now, assuming that the chainage information of the fith and sixth kilometer is given by the following `ChainageMark`'s:

```
ChainageMark(km=5, m_start=10, m_end=800)
ChainageMark(km=5, m_start=900, m_end=1050)
ChainageMark(km=6, m_start=0, m_end=1000)
```

we can determine the length. In this case it is:

```
(800 - 675) + (1050 - 900) + (15 - 0) = 290.
```

Doing this for all of our hypothesized ADT measurements we could we could throw away the chainage information. However, if we split up our ADT data in such a way that each singleton spanned only one `ChainageMark` we would preserve the chainage while being able to extract the length.

More precisely, if we split the data into three parts:

```
km_start=5, m_start=675, km_end=5, m_end=800
km_start=5, m_start=900, km_end=5, m_end=1050
km_start=6, m_start=0, km_end=6, m_end=15
```

we do not need any chainage information to determine the length of each singleton. The length can easily be obtained by subtracting `m_start` from `m_end`. Road data that have been brought to this form is referred to as *normalised* data. Note that data normalisation is *relative* to a specific chainage data set. The `RoadNetworkChainage` class handles chainage data on a road network level and its main use is to normalise the set of data contained in `RoadNetwork`. Since chainage data is also road data, it can be imported similarly to how `RoadNetwork` data is imported. See `RoadNetworkChainage` for a description of how this is done in practice.

CHAPTER

TWO

API REFERENCE

This is the entire list of modules, classes, functions and minor objects used in RDMS.

2.1 Data Containers

This module specifies the data containers used in RDMS as well as auxilliary classes and functions used in connection with them. See *Introduction* for a description of how the these containers are interrelated.

class rdms.containers.**Singletons**
list-like container of singleton RoadData with an additional attribute:

roadidentifier
RoadIdentifier object indentifying the road section that the singleton roaddata belongs to.

class rdms.containers.**RoadSection**
Object containing data and metadata for a single road section. It is usually not constructed directly but is obtained, e.g., looping over a RoadNetwork object.

Attributes

roadidentifier
RoadIdentifier object indentifying this road section in the road network.

metadata
RoadMetaData object that stores meta information about the road data.

roaddata
RoadData object that contains data for this road section.

Methods

edit()
Create a context with a copy of the road section data as a list of singleton roaddata. As

the context code block is exited the singleton roaddata list is converted to arrays and reinserted into the road section:

```
with roadsection.edit() as roaddata_singletons:
    # Do some manipulation of the singleton_list within this block:
    roaddata_singletons.pop()
print 'Now the contents of singleton_list is reinserted into networkdata'
```

class rdms.containers.**RoadNetwork**

Iterable of RoadSection objects and primary container of road data. It is usually created by calling a class-methods such as from_csv().

Attributes

roaddata

RoadData object contain all data for the road network. Each chainage and data fields contains a numpy array spanning all roadsections.

metadata

RoadMetaData object that stores meta information about the road data.

roadsection_keys

list of RoadIdentifier objects pertaining to the road sections in the road network.

Methods

classmethod from_csv(*fname*, *columns*, *delimiter=','*, *nline2skip=0*, *reverse=None*, *check_interval_consistency=True*)

Read a csv file and return a RoadNetwork object.

Parameters

- **fname** (*str*) – File name and path to the csv-file.
- **columns** (list of Column objects) – Which columns csv-file should be used and how to process them. The order of the columns in the list determine the order of datatuples in the RoadIdentifier and RoadData classes.
- **delimiter** (*str*) – Delimiter used in the CSV-file.
- **nline2skip** (*int*) – Number of first lines to skip (e.g., to avoid importing headers).
- **reverse** (*function*) – Function to determine direction of the chainage interval. The function is passed a RoadIdentifier object and should return *True* if data should be reversed and *False* otherwise. If *None* no reverser is used.
- **check_interval_consistency** (*bool*) – Whether or not to check for negative or zero data interval lengths

classmethod load (*fname*)
Shortcut for unpickling the object.

save (*fname*)
Shortcut for pickling the object.

class rdms.containers.**RoadNetworkChainage**
Special container for network level chainage data to be used in chainage validation and modification. Its primarily used for the chainage processing functions described in *Chainage Validation and Normalisation*.

Methods

add_km (*roadidentifier*, *km*, *m_start*, *m_end*)
Adds a chainage mark to the road section identified by *roadidentifier*.

classmethod from_csv (*fname*, *columns*, *delimiter=', '*, *nline2skip=0*)
Read a csv file and return a RoadNetworkCSVReader object.

Similar to the RoadNetwork.from_csv() method where the only differences are that the columns *list must* contain the following names:

- km Chainage kilometer.
- m_start Start meter of the interval.
- m_end End meter.
- length Length which is used in case the end meter is 0 (referring to the next kilometer).

The *kind* attribute of the column objects will not be used.

classmethod load (*fname*)
Shortcut for unpickling the object.

roadsection_length (*roadidentifier*)
Returns the length (*int*) of the road section defined by *roadidentifier*.

save (*fname*)
Shortcut for pickling the object.

2.1.1 Container Related Classes and Functions

class rdms.containers.**RoadData**
Basic data structure for storing road data in RDMS and used by RoadNetwork, RoadSection, and Singletons. This class is customized at creation and usually not created manually but by data importing methods such as RoadNetwork.from_csv(). It can be created manually, however, by using

`create_roaddata_cls()`. Upon creation, the names of the data components is supplied by the user and a `RoadData` class is returned. To illustrate, consider the following `RoadData` class creation:

```
>>> RoadData = create_roaddata_cls(['km_start', 'km_end'], ['data'], ['int
```

This *RoadData* class is extremely simple but illustrates how RoadData classes generally behaves. See `create_roaddata_cls()` for further details on how to create *RoadData* classes yourself. We are now able to create some instances:

```
>>> km_start, km_end, data = (np.arange(1, 4), np.arange(1, 4), np.zeros((
>>> roaddata1 = RoadData(km_start=km_start, km_end=km_end, data=data)
>>> roaddata1
RoadData(km_start=array([1, 2, 3]), km_end=array([2, 3, 4]), data=array([
>>> roaddata2 = RoadData(km_start=1.0, km_end=2, data=0.0)
>>> roaddata2
RoadData(km_start=array([1]), km_end=array([2]), data=array([ 0.]))
>>> roaddata3 = RoadData(*[1, 2, 0.0])
>>> roaddata3
RoadData(km_start=array([1]), km_end=array([2]), data=array([ 0.]))
```

Notice how the input data for *roaddata2* are converted to numpy arrays of the dtype supplied when we created the *RoadData* class. Internally, RoadData always stores the data as numpy arrays of the dtype supplied when the class was created. Another important feature of *RoadData* instances is that they try to preserve the original numpy arrays, if possible:

```
>>> roaddata1.data = np.arange(1336, 1339)
>>> roaddata1
RoadData(km_start=array([1, 2, 3]), km_end=array([1, 2, 3]), data=array([
>>> data
array([1336, 1337, 1338])
```

The RoadData instances always tries to write *into* the arrays already stored. This behaviour is especially benficial when the arrays stored are actually views into larger arrays, which is the case with, e.g., `RoadSection` objects created from a `RoadNetwork`.

<data_component_name>
: Upon creation, an attribute is created for each data name component by which this particular piece of data can be accessed.

fields
: Tuple of data component names. The ordering of the names is the same as the ordering of the data.

Methods

get_chainage

Returns a tuple of the chainage.

get_data
Returns a tuple of the data.

rdms.containers.**create_roaddata_cls**(*chainage_names*, *data_names*, *dtypes*, *rename=False*)
Create a RoaoData class where *chainage_names* and *data_names* are lists containing the names for the data attributes. The underlying data tuple is ordered like `chainage_names + data_names`. *dtypes* is a list of dtypes for the data of length `len(chainage_names) + len(data_names)` ordered like `chainage_names + data_names`. *rename* have the same meaning as *collections.namedtuple*.

class rdms.containers.**RoadIdentifier**
Contains and represents all road identification components used to identify a given road section. This class is a namedtuple and is usually created by RDMS when importing road data. See documentation on `collections.namedtuple()` for further details.

rdms.containers.**create_roadidentifier_cls**(*roadidentifier_names*)
Creates a namedtuple called RoadIdentifier with attribute names given by *roadidentifier_names*.

class rdms.containers.**RoadMetaData**
Meta data of roadnetwork data.

Contains meta-information about the roaddata, i.e., the classes used in constructing road sections and data.

RoadIdentifier
See RoadIdentifier

RoadData
See RoadData

class rdms.containers.**ChainageMark**
Namedtuple used by RoadNetworkChainage for chainage data.

2.2 Chainage Validation and Normalisation

This section specifies all functions that modify and validates chainage related issues. In this section it is implicityly assumed that all RoadData have well-defined chainage, i.e., contains the following data names: km_start, m_start, km_end, and m_end.

For a general description of chainage management, see *Introduction*.

rdms.dataprocessing.**singletons_normalize_chainage**(*singletons*, *networkchainage*)

Normalises all singleton RoadData in *singletons* as described in *Introduction* (relative to *networkchainage*). It is done by calling the following ordered list of functions:

1. singletons_validate_chainage()
2. singletons_splitup_many_km_chainage()
3. singletons_splitup_1km_chainage()

rdms.dataprocessing.**singletons_validate_chainage**(*singletons*, *networkchainage*)

Removes all singleton RoadData in *singletons* that are not consistent with *networkchainage*. A singleton is consistent if its the chainage end-points fall within a ChainageMark from *networkchainage*.

To exemplify, consider the following ChainageMark's

```
ChainageMark(km=1, m_start=10, m_end=100)
ChainageMark(km=2, m_start=10, m_end=100)
ChainageMark(km=4, m_start=10, m_end=100)
```

which validates a selection of RoadData as follows:

```
RoadData(km_start=1, m_start=10, km_end=1, m_end=100, ...) # Valid
RoadData(km_start=1, m_start=50, km_end=2, m_end=50, ...) # Valid
RoadData(km_start=1, m_start=50, km_end=4, m_end=50, ...) # Valid
RoadData(km_start=1, m_start=150, km_end=2, m_end=50, ...) # Invalid
RoadData(km_start=1, m_start=150, km_end=3, m_end=10, ...) # Invalid
```

rdms.dataprocessing.**singletons_splitup_many_km_chainage**(*singletons*, *networkchainage*)

Splits up every singleton RoadData in *singletons* into one or more new singletons containing the same data but with a chainage interval within one kilometer. A new singleton is created for each kilometer contained in the chainage interval of the original singleton. All singleton road data in *singletons* whose chainage interval is contained within one kilometer are unchanged. Only the largest/smallest ChainageMark's (in *networkchainage*) for each kilometer is checked, respectively. Any intermediate kilometers in a singletons chainage mark missing in *networkchainage* is ignored.

Note: It is assumed that the *singletons* have a valid chainage relative to *networkchainage*. This can be achieved with singletons_validate_chainage().

To exemplify, the following ChainageMark's

```
ChainageMark(km=1, m_start=10, m_end=100)
ChainageMark(km=2, m_start=100, m_end=200)
```

```
ChainageMark(km=2, m_start=210, m_end=300)
ChainageMark(km=4, m_start=20, m_end=100)
```

will cause the following singleton:

```
RoadData(km_start=1, m_start=50, km_end=4, m_end=50, ...)
```

to be splitted up into:

```
RoadData(km_start=1, m_start=10, km_end=4, m_end=100, ...)
RoadData(km_start=2, m_start=100, km_end=2, m_end=300, ...)
RoadData(km_start=4, m_start=20, km_end=4, m_end=100, ...)
```

rdms.dataprocessing.**singletons_splitup_1km_chainage**(*singletons*, *networkchainage*)

Any singleton RoadData in *singletons* contained within one kilometer is splitted up in one or more new singletons such that each new singleton corresponds to exactly one ChainageMark in *networkchainage*. The remaining singletons in *singletons* is ignored.

Note: It is assumed that the *singletons* have a valid chainage relative to *networkchainage*. This can be achieved with singletons_validate_chainage().

To exemplify, the following ChainageMark's

```
ChainageMark(km=2, m_start=100, m_end=200)
ChainageMark(km=2, m_start=210, m_end=300)
ChainageMark(km=2, m_start=300, m_end=400)
```

will cause the following singleton:

```
RoadData(km_start=2, m_start=150, km_end=2, m_end=350, ...)
```

to be splitted up into:

```
RoadData(km_start=2, m_start=150, km_end=2, m_end=200, ...)
RoadData(km_start=2, m_start=210, km_end=2, m_end=300, ...)
RoadData(km_start=2, m_start=300, km_end=2, m_end=350, ...)
```

rdms.dataprocessing.**roadsection_normalize_chainage**(*roadsection*, *networkchainage*)

Wrapper around singletons_normalize_chainage() that takes a RoadSection object as input instead of a list of *singletons*.

rdms.dataprocessing.**roadsection_chainage_validate**(*roadsection*, *networkchainage*)

Wrapper around singletons_validate_chainage() that takes a RoadSection object as input instead of a list of *singletons*.

rdms.dataprocessing.**roadsection_splitup_many_km_chainage**(*roadsection*, *networkchainage*)

Wrapper around `singletons_splitup_many_km_chainage()` that takes a `RoadSection` object as input instead of a list of *singletons*.

rdms.dataprocessing.**roadsection_splitup_1km_chainage**(*roadsection*, *networkchainage*)

Wrapper around `singletons_splitup_1km_chainage()` that takes a `RoadSection` object as input instead of a list of *singletons*.

rdms.dataprocessing.**network_normalize_chainage**(*roadnetwork*, *networkchainage*)

Wrapper around `singletons_normalize_chainage()` that takes a `RoadNetwork` object as input instead of a list of *singletons*.

rdms.dataprocessing.**network_chainage_validate**(*roadnetwork*, *networkchainage*)

Wrapper around `singletons_validate_chainage()` that takes a `RoadNetwork` object as input instead of a list of *singletons*.

rdms.dataprocessing.**network_splitup_many_km_chainage**(*roadnetwork*, *networkchainage*)

Wrapper around `singletons_splitup_many_km_chainage()` that takes a `RoadNetwork` object as input instead of a list of *singletons*.

rdms.dataprocessing.**network_splitup_1km_chainage**(*roadnetwork*, *networkchainage*)

Wrapper around `singletons_splitup_1km_chainage()` that takes a `RoadNetwork` object as input instead of a list of *singletons*.

2.3 Miscellaneous

class rdms.misc.**Column**

Configuration information for a single column in a csv-file.

Parameters

- **kind** (*str*) – Which kind of data this column contains: 'roadidentifier', 'chainage' or 'data'.
- **name** (*str*) – Name of the data contained in this column. This will be the attribute name in the `RoadData` instances.
- **idx** (*int or list*) – 0-indexed index or list of indices referring to the columns containing the data.

- **parser** (*str*) – Function that parses the content of the column when importing data. Besides a user-supplied function several parsers exists and can be used by using appropriate strings:
  - "*float*" treat data as floating point number
  - "*int*" treat data is integer
  - "*string*" treat data as string
  - "*vd_km*" and "*vd_m*" refers to special DRD parsing that extracts the kilometer or meter from the special DRD chainage mark.
  - "*static*" enables a field value to be hardcoded into the data. If this is set, the csv-importer assumes that the *idx* parameter is not a row index, but the value to be hardcoded into data.
- **dtype** – The dtype to use when storing data in numpy arrays. Must be given as a string.

2.4 Exceptions

List of special exceptions used by RDMS

exception `rdms.exceptions.`**`ChainageValidationError`**
Raised when a chainage inconsistency have been detected. This usually occurs during chainage validation and normalisation.

exception `rdms.exceptions.`**`DataParsingError`**
Raised when data failed to parse into the proper type. For instance, if a column value in a CSV-file was 'example' but that particular column have been configured as a *float* then a:class:.*DataParsingError* will be raised.

CHAPTER

THREE

INDICES AND TABLES

- *genindex*
- *modindex*
- *search*

PYTHON MODULE INDEX

r

B Appendix: Articles

Rolling Resistance Measurement and Model Development

Lasse G. Andersen[1]; Jesper K. Larsen[2]; Elsje S. Fraser[3]; Bjarne Schmidt[4]; and Jeppe C. Dyre[5]

Abstract: There is an increased focus worldwide on understanding and modeling rolling resistance because reducing the rolling resistance by just a few percent will lead to substantial energy savings. This paper reviews the state of the art of rolling resistance research, focusing on measuring techniques, surface and texture modeling, contact models, tire models, and macro-modeling of rolling resistance. **DOI: 10.1061/(ASCE)TE.1943-5436.0000673.**

Introduction

The total annual emission of CO_2 in the United States exceeds 7 billion t of which the transport sector's share is 29% (U.S. Department of Transportation 2010). Consequently, a reduction of rolling resistance will lead to substantial energy savings and CO_2 emission reductions. Although the European Union has been able to reduce total greenhouse gas emissions by approximately 5% between 1990 and 2006, CO_2 emissions from road transport in the same period increased by 26% and now constitute 12% of total CO_2 emissions in the European Union (Schmidt and Dyre 2012), so rolling resistance reductions are also important here.

Fuel consumption, and hence CO_2 emission in road transport, depends on a number of factors that relate to the vehicles, the quality of the road, and their interaction. Low rolling resistance tires have been available from the tire industry since 1993, and every second tire sold today is a low rolling resistance tire.

Rolling resistance related to the road surface is responsible for about 20% of the CO_2 emitted by a passenger car driving at 100 km/h (Haider et al. 2011). This paper focuses on the role of the road surface on rolling resistance.

In order to overcome the resistance, vehicles consume fuel. The resistance can be categorized as follows (Sandberg et al. 2011b):

- Rolling resistance.
- Air resistance.
- Inertial resistance.
- Gradient resistance.
- Side force resistance.
- Transmission loss.
- Losses from the use of auxiliary equipment.
- Engine friction.

The rolling resistance is defined as the energy loss per distance traveled by the vehicle due to nonelastic deformations of the tires and losses in the wheel suspension system. Energy dissipation in asphalt pavement structures also contributes to the rolling resistance, but studies [e.g., Pouget et al. (2012)] show this to be of minor importance. Because energy (measured in Joules) divided by distance (measured in meters) has the unit of force (measured in Newtons), the rolling resistance coefficient, defined as the energy loss per tire per distance travelled divided by the normal force on the tire, is dimensionless.

The emphasis in this paper is on the literature from the 1980s to the present day. First, the different ways of measuring rolling resistance are reviewed. Then the literature on surface roughness and texture modeling is considered. The interaction between road surface and tire is considered in the next two sections, and finally there is a section on macro-modeling of rolling resistance. Due to the wide diversity of areas connected with rolling resistance measuring and modeling, this paper will not go into specifics nor engage in in-depth critiques of the presented material; the aim is primarily to provide an overview of the references in the area and uncover common threads in the research field.

Rolling Resistance Measuring Techniques

Measurements of rolling resistance date back several centuries and originated with the military's interest in reducing the horsepower for the traction of canons (Luchini 1983). Great scientists such as Coulomb and Reynolds contributed to the field. Only in the last 50 years, however, has a systematic treatment been attempted with the aim of establishing standards for the measurement of rolling resistance. Recently, Sandberg et al. (2011b) classified the rolling resistance measuring techniques into:

- Drum tests of tires;
- Trailer methods;
- Coast-down methods; and
- Fuel consumption methods.

The drum test is ideal for testing of tires in the laboratory. Trailer methods add the variation of the road surface to the testing and also monitor some of the transmission loss [see the discussion in Section 3 of the Models for rolling resistance In Road Infrastructure Asset Management systems (MIRIAM) project report Sandberg et al. (2011b)]. Coastdown methods include still further properties

[1]Ph.D. Student, Indsatsområdet for Studiet af Matematik og Fysik samt deres Funktioner i Undervisning, Forskning og Anvendelser, Dept. of Sciences, Roskilde Univ., Postboks 260, DK-4000 Roskilde, Denmark.

[2]External Consultant, Indsatsområdet for Studiet af Matematik og Fysik samt deres Funktioner i Undervisning, Forskning og Anvendelser, Dept. of Sciences, Roskilde Univ., Postboks 260, DK-4000 Roskilde, Denmark (corresponding author). E-mail: jesperla@ruc.dk

[3]Scientific Assistant, Indsatsområdet for Studiet af Matematik og Fysik samt deres Funktioner i Undervisning, Forskning og Anvendelser, Dept. of Sciences, Roskilde Univ., Postboks 260, DK-4000 Roskilde, Denmark.

[4]Senior Consultant, Danish Road Directorate, Guldalderen 12, DK-2640 Hedehusene, Denmark.

[5]Professor, Indsatsområdet for Studiet af Matematik og Fysik samt deres Funktioner i Undervisning, Forskning og Anvendelser, Dept. of Sciences, Roskilde Univ., Postboks 260, DK-4000 Roskilde, Denmark.

Note. This manuscript was submitted on January 11, 2013; approved on October 14, 2013; published online on August 26, 2014. Discussion period open until January 26, 2015; separate discussions must be submitted for individual papers. This paper is part of the ***Journal of Transportation Engineering***, © ASCE, ISSN 0733-947X/04014075(10)/$25.00.

of the car, while fuel consumption methods measure all the energy losses experienced by the car.

Drum Tests of Tires

Rolling resistance of tires can be measured by the drum test, which, as the name suggests, is performed by holding the test tire up against a drum and applying a load to the tire. By rotating the drum and measuring the resistance the tire exerts on the rotation of the drum, the rolling resistance force of the tire can be deduced. The advantage of this setup is the exclusion of various factors that influence the rolling resistance of a tire. Before 1975 the experiment protocol varied with different studies, e.g., different loads on the test tire, different inflation pressure and drum setup. This was standardized in 1975 when the Society of Automotive Engineers (SAE) formed a committee to standardize the drum testing procedure (Luchini 1983). Today several standards have been published by the International Organization for Standardization (ISO) and SAE [SAE J2452 (SAE 1999), SAE J1269 (SAE 2006), ISO 28580 (ISO 2009), ISO 18164 (ISO 2005)] and a physical and mathematical justification for ISO 18164 has been proposed by Hublau and Barillier (2008). For an overview of the different standards the reader is referred to Gent and Walter (2006, Chapter 12) and Sandberg et al. (2011b). Several aspects of the drum testing procedure have been investigated, such as interlaboratory correlation (Clark and Schuring 1978; O'Neal et al. 1982) and curvature correction (Clark 1976; Luchini 1982) when converting drum results to a flat surface, although the latter was recently disputed by Freudenmann et al. (2009).

Besides direct rolling resistance measurement, drum testing has been used for several other related purposes such as surface texture testing (Luchini and Simonelli 1983), warm-up effects (Warholic 1983), wheel cornering effects (Keefe and Koralek 1983), prediction of cavity air temperature (Kenny 1983), and prediction of transient rolling resistance (Luchini and Popio 2007; Mars and Luchini 1999).

Trailer Methods

The trailer method uses a trailer with one or more test wheels being towed by a vehicle while the test wheels' resistance to rolling is measured by force transducers. The trailer method has been in development since the 1980s up until today and has been documented in Sandberg et al. (2011b). In the 1980s the Belgian Road Research Centre (BRRC) designed a trailer to assess rolling resistance, and in 1990 data produced with the trailer were published and correlated with road profile spectra (Descornet 1990). The trailer was improved in 2009 (Sandberg et al. 2011b). Since then, the Technical University of Gdansk (TUG), the Federal Highway Research Institutte of Germany (BASt), and Helsinki University of Technology (HUT) have developed trailers, the latter with limited success, though, according to Leinonen and Juhala (2006). The TUG trailer depicted in Fig. 1(a) has been described in the literature (Wozniak et al. 2011a, b). BRRC, BASt, and TUG trailers are used today in various projects dealing with rolling resistance and road asset management, see, e.g., the results from the European-American MIRIAM project (Sandberg et al. 2011a), the Danish NordFoU project (Kragh 2010), as well as two Dutch studies (Roovers et al. 2005) and (Boere 2009).

In Sandberg et al. (2011a), the trailer measurements are a key component in creating a linear model for the rolling resistance's dependence on the road surface. The BRRC, BASt, and TUG trailers were used. The NordFoU project compared macrotexture in the form of mean profile depth (MPD) values with TUG trailer measurements with mixed results. The first Dutch study (Roovers et al. 2005) mentioned previously used the BASt and TUG trailers to determine differences in rolling resistance for different pavement types, but no low rolling resistance pavement was indentified within statistical significance. In Boere (2009) a good correlation between tire model predictions of rolling resistance and TUG trailer measurements was found. The tire-interaction model in Boere (2009) has two main components: One component accounts for rolling resistance of a smooth road, i.e., the hysterectic losses due to the flattening of the tire in the tire/surface contact zone. The second component relates to surface-texture-induced tire deformations and is based on Andersson and Kropp (2008), which uses a linear spring system and a nonlinear stiffness function to account for the tire-texture interaction.

A subproject of MIRIAM made an extensive comparative study between the BRRC, BASt, and TUG trailers on a test track in Nantes, France, and showed overall good correlations with both macrotexture and megatexture (Bergiers et al. 2011). Short-term repeatability was found to be acceptable with approximately 3% variation for the BRRC and BASt trailer and approximately 1% for the TUG trailer (Bergiers et al. 2011). Unfortunately,

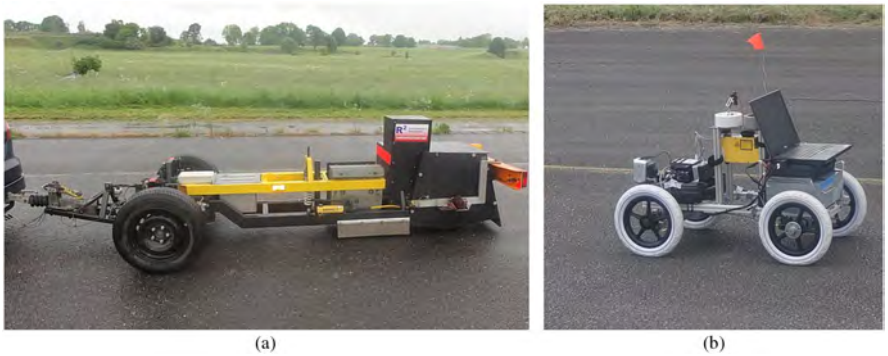

(a) (b)

Fig. 1. (a) Rolling resistance trailer developed by the University of Gdansk, Poland (for further details on the device pictured, please refer to Wozniak et al. 2011a); (b) RoboTex laser profilometer for obtaining a three-dimensional surface profile (for further details on the device pictured, please refer to Rasmussen and Sohany 2011) (images courtesy of The Danish Road Directorate)

day-to-day variations were significant. As Bergiers et al. (2011) suggests, this should be subject to further study. More generally, this also shows that further research and perhaps trailer standardization are needed. Nevertheless, the trailer measurement approach seems fruitful: On one hand, many disturbing factors such as transmission losses and air resistance have been reduced or eliminated in contrast with coast-down experiments (see "Coast-Down Methods"), and on the other hand the trailers are still measuring rolling resistance on actual roads in contrast to the laboratory drum tests.

The above-mentioned trailers focus on the personal car, but recently BASt and Forschungsvereinningung Automobiltechnik (FAT) have developed a rolling resistance trailer using trucks and truck tires (Sandberg et al. 2011b, p. 66).

Coast-Down Methods

The coast-down method pinpoints all significant contributions to driving resistance, not merely the rolling resistance. The principle in coast-down measurement is to accelerate a vehicle to a certain speed and then let it roll freely in neutral gear or clutch down (Sandberg et al. 2011b). As the car "coasts down," velocity and time are measured as a minimum (Evans and Zemroch 1984), but other quantities like wind speed and road texture may be measured as well (Hammarström et al. 2009). The velocity is usually measured at a high frequency for accurate results. This method does not yield any direct results on rolling resistance, but must be fitted to a mathematical model by, e.g., estimating parameters with least-squares regression. The formulation and complexity of the model may vary depending on the experimental setting, sources of data, and so on. The development of models is treated in "Rolling Resistance Macromodeling."

Fuel Consumption Methods

Measurement of fuel consumption is the most general way of assessing rolling resistance because it includes all possible factors that influence the rolling resistance assessment. The tire rolling resistance obviously affects the fuel consumption (Schuring 1994; Hammarström et al. 2012), but because many factors influence the energy loss experienced by a car, it is difficult to pinpoint the rolling resistance loss in the fuel consumption method (Barrand and Bokar 2009). Modern fuel consumption models are complex and include many components such as, e.g., submodels of engine, powertrain, wheels, driver and brake control, road and meteorological conditions as detailed in, e.g., Sandberg (2001). The fuel consumption measurement method will not be discussed further in this paper; the reader is referred to Greenwood and Bennett (2001) for an introduction to fuel consumption measurement and modeling.

Surface Roughness and Texture Modeling

The basic challenge in roughness modeling is to extract useful information from road data. This depends on what kind of road data are available and what kind of information is sought. In the case of rolling resistance modeling, there are different kinds of information extractable on various length scales, as well as different measurement techniques. Fig. 2 shows effects related to vehicle and surroundings during driving, such as noise, rolling resistance, and tire wear, plotted against texture wavelength.

Two road measures, the International Roughness Index (IRI) and the MPD, are widely used in rolling resistance estimation today (Hammarström et al. 2009; Karlsson et al. 2011; Sandberg et al. 2011a, b; Kragh 2010); both have been derived from early measurement practices. They aim at modeling two of the texture types shown in Fig. 2, i.e., roughness and unevenness (IRI) and macrotexture (MPD). These two measures are briefly summarized now.

MPD has been derived from the sandpatch test, which was an early measure of macrotexture in the research of, e.g., skid resistance (Lupton and Williams 1972; Corley-Lay 1998). The test consists of spreading out a known amount of sand (or small glass spheres) on a road surface with a puck, in a large circle, and measuring the diameter [ASTM E965-96 (ASTM 2006), ISO 10844 (ISO 1994)]. The ratio between area covered and amount of sand used gives the mean texture depth (MTD) measure of macrotexture

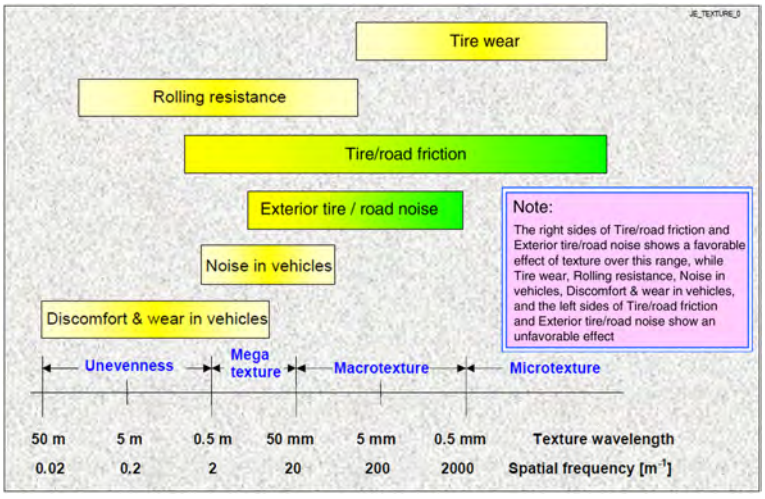

Fig. 2. Illustration of texture wavelengths, anticipated effects, and the classification into, e.g., megatexture, macrotexture; rolling resistance is affected by unevenness or roughness, megatexture, and macrotexture [reproduced with permission from Sandberg and Ejsmont (2002)]

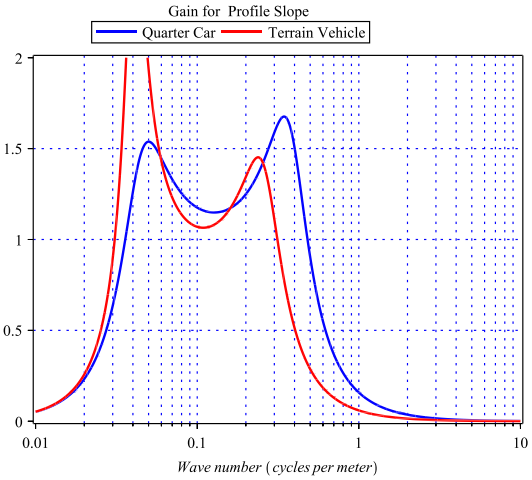

Fig. 3. IRI gain obtained from a quarter-car model with the golden car parameters (Sayers and Karamihas 1996) and the average parameters for terrain vehicle (Lajqi et al. 2012); the gain is highly sensitive to the parameters

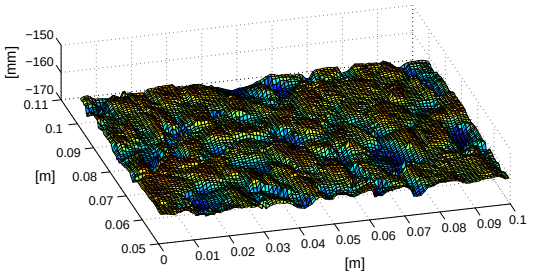

Fig. 4. Detailed surface elevation of the Værløse, Denmark, airfield pavement as obtained by the RoboTex laser profilometer shown in Fig. 1(b)

as described in Annex A of ISO 10844 (ISO 1994). The sandpatch test is simple and robust, although prone to error because the test has to be carried out manually. With the advent of laser profilometers, MPD is used to describe macrotexture in a similar way, i.e., to obtain a number that correlates well with the sand patch test (Flintsch et al. 2003) and for which a simple transformation exists for conversion of MPD to MTD [ASTM E1845-09 (ASTM 2009), ISO 13473-1 (ISO 1997)]. In ISO 13473-1 (ISO 1997) the MPD is calculated as follows:

1. Take at least 10 100-mm laser profile segments of the road section where the MPD is to be found;
2. For each segment, substract the regression line such that the average vertical displacement is zero;
3. Find the maximum vertical displacement values of the first and second half of each segment and take the average of these; and
4. Take the average across all segments of the values found previously that yield the MPD value of the road section.

Both ISO and ASTM have developed several standards to account for macrotexture, and these texture measures are used today in road safety, maintenance, and research (Hall et al. 2009). In some cases the root-mean square of the road profile has been used instead of MPD (Boere 2009), although this is not common.

Measurement of road roughness has been developed since the 1920s according to Sayers and Karamihas (1998, p. 39), and road roughness has been measured by the so-called response-type road roughness measuring systems (RTRRMSs). The general construction of RTRRMSs consists of a wheel mounted to a spring that records and accumulates any bumps in the longitudinal road profile (measured in, e.g., meters). By dividing this quantity with the distance travelled (in, e.g., kilometers), a measure of road roughness (m/km) is obtained. Other roughness measurement techniques have been developed, e.g., the rod and level profiler and the inertial profiler (Sayers and Karamihas 1998, 1996; Visser 1982; Bester 1984; Hveem 1960), but the RTRRMS devices form the basis of the IRI measure. They were developed as a common standard for calibration (Gillespie et al. 1980; Sayers et al. 1986; Bennett 1996) of RTRRMSs and are based on a quarter-car model simulating the RTRRMS measuring device. The IRI measure stems from a mathematical model that represents a (quarter) vehicle's damping response to the road's longitudinal profile. An equivalent way of describing this is in terms of a frequency response function of the road profile frequency spectrum, as shown in Fig. 3. Modifications to the IRI measure have been proposed in, e.g., Sayers (1989), where the quarter-car model is expanded to a half-car model.

Instead of just modeling and measuring a fraction of the frequency domain like macrotexture or road unevenness and roughness, the entire profile spectrum can be used. This simple but powerful approach to road texture and roughness modeling transforms the longitudinal road profile into the frequency domain. This has been especially useful with the introduction of laser profiles because they measure with high frequency and precision, c.f. the profile shown in Fig. 4. A standardization of the profile spectrum can be found in ISO 13473-4 (ISO 2008). The disadvantage is that it does not yield a single number, but, e.g., correlation analyses working in the frequency domain seems ideal as shown in Sandberg (1990). The spectral analysis approach has also been used to highlight the influence of megatexture on rolling resistance (and noise), which has usually been attributed to macrotexture (Descornet 1989, 1990).

Different texture types are defined in terms of wavelengths (Fig. 2). This approach may hardly deserve the term modeling, but by reducing a laser profile to a spectrum, an idealization is made and information is lost. More specifically, the surface profile spectrum omits phase information, and by doing this, surface properties relevant to rolling resistance modeling are lost. In Männel and Beckenbauer (2007), a discussion of these matters is undertaken with examples of different schematic profiles that should result in different tire-surface interaction dynamics, but which yields similar power spectra. Another example of different profiles with characteristics invisible in surface spectra are given in Pinnington (2012).

Recently, various other approaches have been investigated as alternatives to the classical measures mentioned previously. In Anfosso-Lédée and Do (2002), certain geometric descriptors and their properties have been developed and extracted from laser profiles. More specifically, peaks, valleys, and the angles of these are calculated from the profiles and correlated with the tire-road noise (Anfosso-Lédée and Do 2002). Even though a correlation was observed, it was concluded that further research is needed (Anfosso-Lédée and Do 2002, p. 167), and the methods' usefulness has been disputed (Sandberg and Ejsmont 2002). Another approach is the use of fractals in surface modeling (Panagouli and Kokkalis 1998; Kokkalis et al. 2002) and design (Yeggoni et al. 1996).

By estimating the fractal dimension of a surface laser profile, a surface measure relating to macrotexture and microtexture is obtained. This has been shown to correlate well with the skid resistance number (SN) (Panagouli and Kokkalis 1998; Kokkalis et al. 2002), and in addition the fractal dimension drops with SN, as expected, when the pavement wears (Kokkalis et al. 2002). Fractals are also being used in Pinnington (2012) in which a surface model is constructed and comprises three different layers corresponding to different length scales. Yet another approach is to use classical measures like MPD, obtained from road laser profiles, in conjunction with an envelope algorithm that mimics the viscoelastic properties of the tire. A purely empirical formula developed in Meier et al. (1992) has increased the correlation between MPD and trailer measurements of rolling resistance in studies from the MIRIAM project (Sandberg et al. 2011a). Similar enveloping methods have been reported and developed in Klein and Hamet (2004), based on the viscoelastic properties of the tire instead of a purely empirical algorithm. In addition, Klein and Hamet (2004) discuss how the enveloping procedure affects the surface profile spectra.

Contact Models

In the 1980s efforts to understand and quantify texture effects on the tire-pavement interaction were limited. There were many difficulties in theoretically and experimentally determining the many individual contact areas and contact pressures produced by irregularly shaped asperities indenting the tire tread. In Yong et al. (1980), an analytical model is developed using experimental data for individual tire types to predict the contact area. A numerical method is demonstrated in Yong et al. (1980) to approximate the collective contact stress for individual contact areas using a computational algorithm requiring only the two-dimensional (2D) road profile geometry and tire inflation pressure as input.

Gall et al. (1993) introduced a finite-element model for the tire in the contact area, focusing on the correct representation of the contact area including the edge effects of the tire-soil contact, a friction law including normal stress, and correct modeling techniques such as the use of symmetry.

By the beginning of this century, considerable advances had been made in numerical computing resources, giving the opportunity to investigate the contact area in more detail. It became possible to include the nonlinear behavior of the contact zone that was previously overlooked or simplified. In Andersson and Kropp (2008) the contact geometry is discretized into smaller length scales using multiple pairs of matching points with nonlinear springs between each pair of contact elements. The stiffness functions of these springs are determined from a method for assessing the stiffness of the nonlinear springs based on detailed scans of the surface geometry, elastic data of the tread, and a flat circular punch-indenting method for normal (out-of-plane) contact model of an elastic layer. The Newton-Raphson iterative scheme is used to solve the nonlinear contact equations. Green's functions calculate analytically the dynamic response of the tire by convolving the contact forces.

Ivanov et al. (2010) identify and address parameters that characterize the interaction of a tire-soil interaction using fuzzy set theory. The contact of the tire with both hard and soft soil is discussed with specific focus on how to handle the parameters of tire-soil friction and rolling resistance. The advantage of these methods lies in their ability to take into account fluctuating external conditions that are not directly related to a vehicle.

Dubois et al. (2011) deal with the numerical study of a frictionless viscoelastic tire-road contact area. This is done by means of a macroscale approach in which only the contact forces are calculated for a rough multi-indentation surface of a viscoelastic half-space based on an imposed load at road surface asperities peaks. This approach takes into account both the viscoelastic behavior of the tire and the roughness of the road surface. The viscoelastic solution is reduced to an elastic solution, significantly reducing the calculation time, and a simplified description of the viscoelastic material behavior by a rheological model is used.

The Lund-Grenoble (LuGre) model, describing three-dimensional tire friction dynamics simplified by assuming constant slip along the contact patch, is elaborated in Deur et al. (2005). This model includes the effects of lateral deformation of the tire tread, which leads to varying slip speeds along the contact patch. This is done using a stepwise approximation of the slip speed. In Faraji et al. (2010), this simplification is not used and a quarter-car model and an average lumped LuGre model are used instead.

The current trend in modeling the contact zone between tire and pavement is to include all the major aspects, i.e. noise, rolling resistance, and skid resistance, cf. Andersson et al. (2012).

Tire Models

The relation of tire rolling resistance to the viscoelastic and dynamic hysteresis properties of typical tire materials is complex. The combination of operational variables such as pressure, load, speed, and deflection, and the tire design variables complicate the characterization of the stress-strain hysteresis contribution of each tire component and the interaction between them, and hence the determination of the rolling resistance of the tire on a given surface. In the 1980s, Williams and Dudek (1983) compared the sinusoidal radial load-deflection cycling of a rolling tire with a non-rolling tire. From these comparisons, relations were made between the footprint load-deflection hysteresis and the rolling resistance drag force, and the contribution of tread and sidewall deformation to the hysteresis was determined.

An alternative to viscoelastic models is given in Luchini et al. (1994), detailing a finite-element strain-based model using directional incremental hysteresis to predict rolling resistance. The tire material model is here developed for the rubber components only, while the cords are included for structural aspects of the model. Shida et al. (1999) presents a static finite-element model for fiber-reinforced rubber capable of handling anisotropic loss factors. The algorithm proposed by Shida et al. (1999) estimates the energy dissipation from the hysterectic loss in a tire, using the variations of the approximated stresses and strains. These stresses and strains are calculated using a Fourier series with a viscoelastic phase lag in the frequency domain.

Due to hysteresis losses, heat energy is generated, which leads to higher tire pressure and thus lower rolling resistance and vehicle fuel consumption. The complex relationship between the various design attributes and operating conditions makes it difficult to develop analytical models. Various attempts have been made to model the total behavior through a semicoupled representation. Three models, the dissipation, deformation, and thermal models, have been considered. In the late 1990s, Park et al. (1997) used these three major analysis models and viscoelastic theory to calculate the heating of a rolling tire. Results were compared with physical measurements and comparisons made between quadratic and linear finite elements. Due to the delicate nature of the prediction of energy loss in a tire, specifically the numerical analysis of the

strain dependent carbon black-filled rubber, special attention is paid to the material representation in Ebbott et al. (1999). In this paper the dissipation and deformation models are based on the strain-amplitude dependence of carbon black-filled rubber, and the thermal model does not require the use of correlation coefficients for accurate results. The algorithm developed takes both strain and temperature dependence into account. Tire temperatures are obtained by solving steady-state linear heat transfer equations using the finite-element technique. This algorithm was used and expanded in the following decade in Narasimha Rao et al. (2006). A three-stage finite-element model consisting of a deformation model, a dissipation model, and a thermal model is used to determine characteristics for tires with smooth and circumferential groove tread patterns. In Narasimha Rao et al. (2006) variations in several aspects affecting rolling resistance is made and the results discussed. These include the tire rolling speed, tread profile, inflation pressure, a varying normal load, and ambient temperature. Comparisons are made between a flat road surface and a circular drum. Various hyperelastic and viscoelastic properties of the tread material are considered. The results are summarized in a table showing that the effective rolling radius is insensitive to parameter variations, whereas the rolling resistance (and hence the total energy loss per revolution) is insensitive to rolling speed, convection loss, and friction, but increases significantly with increasing normal load, tread profile, and tread material loss modulus and decreases significantly with increasing ambient temperature, convection loss, tread mechanical stiffness, and tread thickness.

A widely used empirical tire model is expressed in the so-called Magic Formula, the development of which started in Delft, Netherlands, in the mid-1980s (Pacejka 2012). By way of example the authors give the relation between the side force F_y and the slip angle α, i.e., the angle between the lateral and forward velocities of the wheel center

$$F_y = D\sin(C\arctan\{B\alpha - E[B\alpha - \arctan(B\alpha)]\}) \qquad (1)$$

Here B, C, D, and E are parameters that are determined by fitting the relation to data. The Magic Formula produces characteristics that closely match measured curves for the side force and longitudinal force as a function of their respective slip qualities. A typical graph of the magic formula is shown in Fig. 5. For a full treatment of the Magic Formula, the reader is referred to Pacejka (2012). The Magic Formula has been extended to cope with large camber angles and tire inflation pressure by Besselink et al. (2010). The ability to deal with pressure changes eliminates the need to have separate parameter sets for different tire pressures, leading to a reduction in the total number of measurements required. In addition, the description of the rolling resistance and overturning moment is improved. Changes in the modeling of the tire dynamics allow a smooth and consistent switch from simple first-order relaxation behavior to rigid ring dynamics. The effect of inflation pressure on the loaded radius and the tire enveloping properties is discussed by Besselink et al. (2010) and some results are given to demonstrate the abilities of the model.

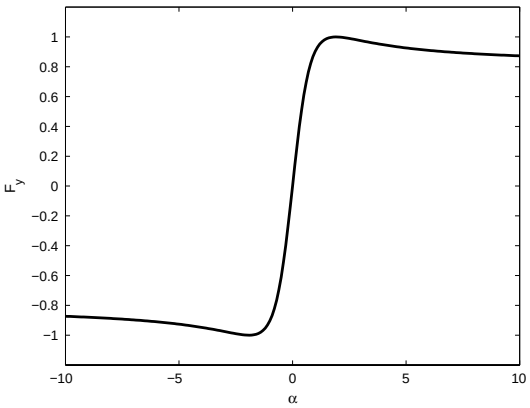

Fig. 5. Illustration of the Magic Formula (Pacejka 2012) showing the nondimensionalized side force F_y ($D = 1$) as a function of the slip angle α ($B = 1$), with parameters $C = 1.4$ and $E = -0.2$

The development of tire models is constantly improving and expanding. A methodology using probabilistic characteristics of a vehicle and road to model the interaction between them, including rolling resistance, is presented in Vantsevich and Stuart (2008). The authors represent the interaction of the vehicle with the road by means of a quarter-car model, the characteristics of which are varied randomly for the interaction with the vehicle surroundings. A full two-dimensional semianalytical model for viscoelastic cylinders rolling on a rigid surface is developed in Qiu (2009). Problems arising from high-speed contact for layered viscoelastic rollers rolling on a rigid surface and standing-wave phenomena are addressed here.

The previously mentioned papers all use a finite-element model for simulation of various aspects of the rolling pneumatic tire. A general review of the literature on finite-element modeling of rolling tires is given by Ghoreishy (2008). This review gives a survey on finite-element modeling of rolling tires, application of rolling tire models, and finite-element codes. The challenge is to obtain realistic material models, model the tread blocks, further develop the finite-element models to include multiphysics, include transient behavior, and finally include the modeling of nonrigid surfaces. Finite-element modeling of the rolling tire is complex, and although more comprehensive and true to physical first principles, for many applications they are not yet fast enough for realistic vehicle simulations. Here empirical models are still needed.

Rolling Resistance Macromodeling

Apart from the detailed tire and contact models of rolling resistance, more empirical macromodels exist and have been in development since 1935 according to Petrushov (1997). These models focus on coast-down experiment data (see experiment description in "Rolling Resistance Measuring Techniques"). Initially, the primary goal of these models was to assess vehicle aerodynamic drag (White and Korst 1972; Walston et al. 1976; Buckley et al. 1976), which correlates well with wind-tunnel experiments (Eaker 1988; Buchheim et al. 1980; Bester 1984; Swift 1991; Korst and White 1990). In recent years, coast-down models have been used for rolling resistance assessment as well (Roussillon 1981; Hammarström et al. 2009; Karlsson et al. 2011). The general formulation of coast-down models is based on Newton's second law (Hammarström et al. 2009, p. 24), i.e.

$$F_{\text{total}} = m\frac{dv(t)}{dt} = F_{\text{roll}} + F_{\text{air}} + F_g + F_{\text{misc}} \qquad (2)$$

where the total force F_{total} acting on the coasting vehicle is given by the rolling resistance contribution F_{roll}, aerodynamic drag F_{air}, the gravity's component in the direction of motion F_g, and F_{misc} representing various other forces like side force or transmissionlosses,

although the latter can be included in F_{roll} (Hammarström et al. 2009; Karlsson et al. 2011). The mathematical formulations of the coast-down model equations, the experimental setup, and quantities measured vary greatly from study to study in the literature. A few of the different approaches are summarized below.

The complexity of the mathematical models varies from relatively simple equations governing vehicle motion with only velocity and gradient data and a simple empirical quadratic reistance model (Evans and Zemroch 1984) like

$$\frac{dv(t)}{dt} = a_0 + a_1 v(t) + a_2 v(t)^2 \tag{3}$$

to much more complex nonlinear models (Hammarström et al. 2009; Karlsson et al. 2011). The complex models depend on a large amount of additional data being measured, such as gradient, road crossfall, macrotexture, roughness, and meteorological conditions, which greatly enhances the resulting rolling resistance estimates. The advantages of choosing simple models lies in the possibillity of obtaining an analytical solution to the differential equation model as in, e.g., Ivens (1987), thus greatly reducing the computational demands. In Petrushov (1997), the analytical solution is used to convert the velocity-time function to distance-time instead, thus reducing error sources. Another approach is to simplify the experimental setting by, e.g., having a flat test section such that the road gradient can be neglected (Hamabe et al. 1985; Djordjevic et al. 2009) or using data from an anemometer mounted on the vehicle (Buckley 1995). As mentioned previously, coast-down models have been used for several purposes, and apart from rolling resistance and aerodynamic drag assessment, the methodology has been used to estimate fuel consumption (Hunt et al. 2011), transmission losses (Dunn et al. 2009), and maximum vehicle speed (Lieh 2008).

Although macromodels of rolling resistance are primarily based on coast-down models, other approaches have also been developed like, e.g., viscoelastic models used in connection with laboratory rolling resistance experiments to predict rolling resistance of tires. These experiments have shown that tire rolling resistance energy loss is correlated with hysteresis loss in the tire (Pillai 1995; Pillai and Fielding-Russell 1991). Thermomechanical models have also been developed and used to predict transient rolling resistance (Mars and Luchini 1999), and thermomechanical principles were essential in developing a new macromodel of rolling resistance that showed the importance of tire temperature on rolling resistance (Sandberg 2001).

Concluding Remarks

This paper briefly reviewed the state of the art of rolling resistance modeling. Regarding the optimal quantitative characterization of a road surface for predicting the rolling resistance, more work is needed. On the one hand, MPD, although a purely empirical adaptation of the sand patch test derived MTD to laser profiles, is widely used throughout the rolling resistance literature. MPD's popularity is probably due to the historical background and the simplicity of the algorithm. This combined with correlations with diverse rolling resistance measurements makes it a practical choice when a texture measure needs to be extracted from laser profile data. On the other hand, in recent studies such as, e.g., Sandberg et al. (2011a), MPD was combined with a physically intuitive envelope procedure that improved correlations substantially. Taking fundamental physical considerations into account when using laser profiles or other modern measurement techniques for surface characterization thus seems promising. A similar trend can be seen in the development of macromodels, from the simple and purely empirical approach of coast-down modeling in Evans and Zemroch (1984) to elaborate models based on physical principles in Karlsson et al. (2011).

Because of advances in numerical computing resources, it is now possible to model the tire pavement contact zone in much more detail than previously. This development will continue and likely be combined with more detailed tire models. Tire modeling depends on the overall purpose of modeling. Magic Formula type of modeling is used for fast response in real-time vehicle modeling, whereas the tendency in modeling the interaction between tire and pavement surface is to use some kind of finite-element modeling.

In a recent study (Nielsen and de Fine Skibsted 2010), it has been estimated that potential savings in fuel consumption (and hence CO_2 emissions) from optimizing the pavement with respect to rolling resistance represent a value to society as large as the entire cost of maintaining the pavement. Because the optimization in an asset management system requiring reliable models of rolling resistance, further research in rolling resistance modeling is warranted by their benefits to society.

Acknowledgments

We acknowledge support by the Cooee project (Schmidt and Dyre 2012) sponsored by the Danish Council for Strategic Research via Grant #11-108727.

References

Andersson, P., Hoover, C., Winroth, J., and Kropp, W. (2012). "Numerical modelling of tyre/road interaction." *Sci. Bull. Automot. Ser.*, 22, 5–14.

Andersson, P., and Kropp, W. (2008). "Time domain contact model for tyre/road interaction including nonlinear contact stiffness due to small-scale roughness." *J. Sound Vib.*, 318(1–2), 296–312.

Anfosso-Lédée, F., and Do, M.-T. (2002). "Geometric descriptors of road surface texture in relation to tire-road noise." *Transportation Research Record 1806*, Transportation Research Board, Washington, DC, 160–167.

ASTM. (2006). "Standard test method for measuring pavement macrotexture depth using a volumetric technique." *E965–96*, West Conshohocken, PA.

ASTM. (2009). "Standard practice for calculating pavement macrotexture mean profile depth." *E1845–09*, West Conshohocken, PA.

Barrand, J., and Bokar, J. (2009). "Reducing tire rolling resistance to save fuel and lower emissions." *SAE Int. J. Passenger Cars Electron. Electr. Syst.*, 1(1), 9–17.

Bennett, C. R. (1996). "Calibrating road roughness meters in developing countries." *Transportation Research Record 1536*, Transportation Research Board, Washington, DC, 73–81.

Bergiers, A., Goubert, L., Anfosso-Lédée, F., Dujardin, N., Ejsmont, J. A., and Zöller, U. S. M. (2011). *Comparison of rolling resistance measuring equipment—Pilot study*, Models for Rolling Resistance in Road Infrastructure Asset Management Systems (MIRIAM), ⟨http://miriam-co2.net/Publications/MIRIAM_Pilot_RRT_report_111231_final.pdf⟩ (Jul. 11, 2014).

Besselink, I., Schemeitz, A., and Pacejka, H. (2010). "An improved magic formula/swift tyre model that can handle inflation pressure changes." *Veh. Syst. Dyn.*, 48(Suppl. 1), 337–352.

Bester, C. J. (1984). "Effect of pavement type and condition on the fuel consumption of vehicles." *Transportation Research Record 1000*, Transportation Research Board, Washington, DC, 28–32.

Boere, S. (2009). "Prediction of road texture influence on rolling resistance." M.S. thesis, Eindhoven Univ. of Technology, Eindhoven, Netherlands.

Buchheim, R., et al. (1980). "Comparison tests between major European automotive wind tunnels." *SAE Technical Paper, 800140*, SAE International, Warrendale, PA.

Buckley, F., Marks, C., and Walston, W. (1976). "Analysis of coast-down data to assess aerodynamic drag reduction on full-scale tractor-trailer trucks in windy environments." *SAE Technical Paper, 760106*, SAE International, Warrendale, PA.

Buckley, F. T. (1995). "Abcd—An improved coast down test and analysis method." *SAE Technical Paper, 950626*, SAE International, Warrendale, PA.

Clark, S. (1976). "Rolling resistance forces in pneumatic tires." *Rep. prepared for the U.S. Dept. of Transportation, Office of Univ. Research* ⟨http://books.google.dk/books?id=esLRGwAACAAJ⟩ (Jul. 11, 2014).

Clark, S., and Schuring, D. (1978). "Interlaboratory tests for tire rolling resistance." *SAE Technical Paper, 780636*, SAE International, Warrendale, PA.

Corley-Lay, J. (1998). "Friction and surface texture characterization of 14 pavement test sections in Greenville, North Carolina." *Transportation Research Record 1639*, Transportation Research Board, Washington, DC, 155–161.

Descornet, G. (1989). "Criterion for optimizing surface characteristics." *Transportation Research Record*, Transportation Research Board, Washington, DC, 173–177.

Descornet, G. (1990). "Road-surface influence on tire rolling resistance." *Surface characteristics of roadways: International research and technologies STP 1031*, American Society for Testing and Materials, Philadelphia.

Deur, J., Ivanovi, V., Troulis, M., Miano, C., Hrovat, D., and Asgari, J. (2005). "Extensions of the LuGre tyre friction model related to variable slip speed along the contact patch length." *Veh. Syst. Dyn.*, 43(Suppl. 1), 508–524.

Djordjevic, M., Jankovic, A., and Jeremic, B. (2009). "Rolling resistance as the risk factor for fuel consumption." *Int. J. Veh. Syst. Model. Test.*, 4(3), 185–200.

Dubois, G., Cesbron, J., Yin, H., and Anfosso-Lédée, F. (2011). "Macro-scale approach for rough frictionless multi-indentation on a viscoelastic half-space." *Wear*, 272(1), 69–78.

Dunn, A., Uhlenhake, G., Guenther, D., Heydinger, G. J., and Heydinger, G. J. (2009). "Vehicle coast analysis: Typical SUV characteristics." *SAE Int. J. Passenger Cars Electron. Electr. Syst.*, 1(1), 526–535.

Eaker, G. (1988). "Wind tunnel-to-road aerodynamic drag correlation." *SAE Technical Paper, 880250*, SAE International, Warrendale, PA.

Ebbott, T., Hohman, R., Jeusette, J.-P., and Kerchman, V. (1999). "Tire temperature and rolling resistance prediction with finite element analysis." *Tire Sci. Technol.*, 27(1), 2–21.

Evans, E., and Zemroch, P. (1984). "Measurement of the aerodynamic and rolling resistances of road tanker vehicles from coast-down tests." *Proc. Inst. Mech. Eng. Part D Transp. Eng.*, 198(3), 211–218.

Faraji, M., Majd, V., Saghafi, B., and Sojoodi, M. (2010). "An optimal pole-matching observer design for estimating tyre-road friction force." *Veh. Syst. Dyn.*, 48(10), 1155–1166.

Flintsch, G. W., de Lon, E., McGhee, K. K., and Al-Qadi, I. L. (2003). "Pavement surface macrotexture measurement and application." *Transportation Research Record 1860*, Transportation Research Board, Washington, DC, 168–177.

Freudenmann, T., Unrau, H.-J., and El-Haji, M. (2009). "Experimental determination of the effect of the surface curvature on rolling resistance measurements 4." *Tire Sci. Technol.*, 37(4), 254–278.

Gall, R., Tkacik, P., and Andrews, M. (1993). "On the incorporation of frictional effects in the tire/ground contact area." *Tire Sci. Technol.*, 21(1), 2–22.

Gent, A. N., and Walter, J. D. (2006). *The pneumatic tire*, U.S. Dept. of Transportation, National Highway Traffic Safety Administration, Washington, DC.

Ghoreishy, M. (2008). "A state of the art review of the finite element modelling of rolling tyres." *Iran. Polym. J.*, 17(8), 571–597.

Gillespie, T., Sayers, M., and Segel, L. (1980). "Calibration of response-type road roughness measuring systems." *Number 228 in NCHRP Rep.*, Transportation Research Board, Washington, DC.

Greenwood, I. D., and Bennett, C. R. (2001). *Modelling road user and environmental effects in HDM-4*, Association mondiale de la Route/ World Road Association (AIPCR/PIARC), La Defense, France.

Haider, M., Conter, M., and Glaeser, K.-P. (2011). *Discussion paper what are rolling resistance and other influencing parameters on energy consumption in road transport*, Models for Rolling Resistance in Road Infrastructure Asset Management Systems (MIRIAM), AIT, Austria.

Hall, J., Smith, K., Titus-Glover, L., Wambold, J., Yager, T., and Rado, Z. (2009). "Guide for pavement friction." *Number 108 in NCHRP Web Documents*, Transportation Research Record, Washington, DC.

Hamabe, K., Kitoh, K., Ogata, H., and Kobayashi, T. (1985). "An estimation of aerodynamic drag coefficient of a passenger car by coast-down tests in windy environments." *JSAE Rev.*, 16, 114–120.

Hammarström, U., Eriksson, J., Karlsson, R., and Yahya, M.-R. (2012). *Rolling resistance model, fuel consumption model and the traffic energy saving potential of changed road surface conditions*. The Swedish Transport Administration and the MIRIAM Project, Linköping, Sweden.

Hammarström, U., Karlsson, R., and Sörensen, H. (2009). *Road surface effects on rolling resistance—Coastdown measurements with uncertainty analysis in focus*, Energy Conservation in Road Pavement Design, Maintenance and Utilisation (ECRPD), Linköping, Sweden.

Hublau, V., and Barillier, A. (2008). "The equations of the rolling resistance of a tire rolling on a drum." *Tire Sci. Technol.*, 36(2), 146–155.

Hunt, S., Odhams, A., Roebuck, R., and Cebon, D. (2011). "Parameter measurement for heavy-vehicle fuel consumption modelling." *Proc. Inst. Mech. Eng. Part D J. Autom. Eng.*, 225(5), 567–589.

Hveem, F. N. (1960). "Devices for recording and evaluating pavement roughness." *Highway Res. Board Bull.*, 264, 1–26.

International Organization for Standardization (ISO). (1994). "Acoustics—Specification of test tracks for measuring noise emitted by road vehicles and their tyres." *ISO 10844*, Switzerland.

International Organization for Standardization (ISO). (1997). "Characterization of pavement texture by use of surface profiles—Part 1: Determination of mean profile depth." *ISO 13473-1*, Switzerland.

International Organization for Standardization (ISO). (2005). "Passenger car, truck, bus and motorcycle tyres—Methods of measuring rolling resistance." *ISO 18164*, Switzerland.

International Organization for Standardization (ISO). (2008). "Characterization of pavement texture by use of surface profiles—Part 4: Spectral analysis of surface profiles." *ISO 13473-4*, Switzerland.

International Organization for Standardization (ISO). (2009). "Passenger car, truck and bus tyres—Methods of measuring rolling resistance—Single point test and correlation of measurement results." *ISO 28580*, Switzerland.

Ivanov, V., Shyrokau, B., Augsburg, K., and Algin, V. (2010). "Fuzzy evaluation of tyre-surface interaction parameters." *J. Terramech.*, 47(2), 113–130.

Ivens, J. (1987). "Rolling resistance of some 13 inch tires and the correlation between rig and road." *SAE Technical Paper Series, 870422*, SAE International, Warrendale, PA.

Karlsson, R., Hammarström, U., Sörensen, H., and Eriksson, O. (2011). *Road surface influence on rolling resistance—Coastdown measurements for a car and HGV—VTI notat 24A*, Swedish Road Administration (VTI), Linköping, Sweden.

Keefe, R., and Koralek, A. (1983). "Precision measurement of tire rolling resistance." *Rubber division symposia*, Vol. 1, American Chemical Society, Rubber Div., Akron, OH, 78–104.

Kenny, T. M. (1983). "Prediction of contained air temperature from SAE standard rolling resistance test data." *SAE Technical Paper Series, 831796*, SAE International, Warrendale, PA.

Klein, P., and Hamet, J. (2004). *Road texture and rolling noise: An envelopment procedure for tire-road contact*, Institut National de Recherche Sur Les Tranports Et Leur Securite (INRETS) for the SILVIA project, France.

Kokkalis, A. G., Tsohos, G. H., and Panagouli, O. K. (2002). "Consideration of fractals potential in pavement skid resistance evaluation." *J. Transp. Eng.*, 10.1061/(ASCE)0733-947X(2002)128:6(591), 591–595.

Korst, H., and White, R. (1990). "Coastdown tests: Determining road loads versus drag component evaluation." *SAE Technical Paper, 901767*, SAE International, Warrendale, PA.

Kragh, J. (2010). *Rolling resistance—Copenhagen 2009 (technical note 77)*, Road Directorate, Danish Road Institute, Hedehusene, Denmark.

Lajqi, S., Pehan, S., Lajqi, N., Baxhaku, B., and Ymeri, B. (2012). "Influences of the suspension parameters on the vehicle suspension performance for a terrain vehicle." *J. Mech. Eng. Autom.*, 2, 550–554.

Leinonen, A., and Juhala, M. (2006). "Development of measurement equipment for measuring tire rolling resistance on road." *Proc., 8th Biennial ASME Conf. on Engineering Systems Design and Analysis, ESDA2006*, American Society of Mechanical Engineers, New York.

Lieh, J. (2008). "A closed-form method to determine vehicle speed and its maximum value." *Int. J. Veh. Syst. Model. Test.*, 3(1–2), 1–13.

Luchini, J., Peters, J., and Arthur, R. (1994). "Tire rolling loss computation with the finite element method." *Tire Sci. Technol.*, 22(4), 206–222.

Luchini, J., and Popio, J. (2007). "Modeling transient rolling resistance of tires." *Tire Sci. Technol.*, 35(2), 118–140.

Luchini, J. R. (1982). "Test surface curvature reduction factor for truck tire rolling resistance." *SAE Technical Paper, 821264*, SAE International, Warrendale, PA.

Luchini, J. R. (1983). "Rolling resistance test methods." *Rubber division symposia*, Vol. 1, American Chemical Society, Rubber Div., Akron, OH, 69–77.

Luchini, J. R., and Simonelli, L. A. (1983). "Rolling resistance tests on smooth and textured-surface test wheels." *Rubber division symposia*, Vol. 1, American Chemical Society, Rubber Division, Akron, OH, 140–150.

Lupton, G., and Williams, T. (1972). "Study of the skid resistance of different tire tread polymers on wet pavements with a range of surface textures." *ASTM special technical publication*, SAE International, Warrendale, PA, 101–116.

Männel, M., and Beckenbauer, T. (2007). "Characterisation of road surfaces by means of texture analysis." *VDI Ber.*, 2014, 223–239.

Mars, W., and Luchini, J. (1999). "Analytical model for the transient rolling resistance behavior of tires." *Tire Sci. Technol.*, 27(3), 161–175.

Meier, A. v., Blokland, G. J. v., and Descornet, G. (1992). "The influence of texture and sound absorption on the noise of porous road surfaces." *Proc., PIARC 2nd Int. Symp. on Road Surface Characteristics*, Association mondiale de la Route/World Road Association (AIPCR/PIARC), La Defense, France, 7–19.

Narasimha Rao, K., Krishna Kumar, R., and Bohara, P. (2006). "A sensitivity analysis of design attributes and operating conditions on tyre operating temperatures and rolling resistance using finite element analysis." *Proc. Inst. Mech. Eng. Part D J. Autom. Eng.*, 220(5), 501–517.

Nielsen, C., and de Fine Skibsted, T. (2010). *The energy-saving road—Improving socio-economic conditions by reducing rolling resistance*, NCC Green Road, Allerød, Denmark.

O'Neal, J., Brunot, C. A., Wanstedt, A., and Warholic, T. (1982). "Interlaboratory rolling resistance testing—Highway truck and bus tires." *SAE Technical Paper, 821265*, SAE International, Warrendale, PA.

Pacejka, H. (2012). *Tire and vehicle dynamics*, Elsevier, Amsterdam, Netherlands.

Panagouli, O. K., and Kokkalis, A. G. (1998). "Skid resistance and fractal structure of pavement surface." *Chaos, Solitons Fractals*, 9(3), 493–505.

Park, H., Youn, S.-K., Song, T., and Kini, N.-J. (1997). "Analysis of temperature distribution in a rolling tire due to strain energy dissipation." *Tire Sci. Technol.*, 25(3), 214–228.

Petrushov, V. (1997). "Coast down method in time-distance variables." *SAE Technical Paper, 970408*, SAE International, Warrendale, PA.

Pillai, P. (1995). "Total tire energy loss comparison by the whole tire hysteresis and the rolling resistance methods." *Tire Sci. Technol.*, 23(4), 256–265.

Pillai, P., and Fielding-Russell, G. (1991). "Effect of aspect ratio on tire rolling resistance." *Rubber Chem. Technol.*, 64(4), 641–647.

Pinnington, R. J. (2012). "A particle-envelope surface model for road-tyre interaction." *Int. J. Solids Struct.*, 49(3-4), 546–555.

Pouget, S., Sauzéat, C., Benedetto, H. D., and Olard, F. (2012). "Viscous energy dissipation in asphalt pavement structures and implication for vehicle fuel consumption." *J. Mater. Civ. Eng.*, 10.1061/(ASCE)MT.1943-5533.0000414, 568–576.

Qiu, X. (2009). "Full two-dimensional model for rolling resistance. ii: Viscoelastic cylinders on rigid ground." *J. Eng. Mech.*, 10.1061/(ASCE)0733-9399(2009)135:1(20), 20–30.

Rasmussen, R. O., and Sohaney, R. C. (2011). "Geometric and functional characterization of pavement Texture." *Int. Symp. on Pavement Performance: Trends, Advances, and Challenges*, Tampa, FL.

Roovers, M. S., Graaff, D. F. d., and Moppes, R. K. F. v. (2005). "Round robin test rolling resistance/energy consumption." *Prepared for Ministery of Traffic and Waterworks (DWW) by M+P consulting engineers, German Bundesanstalt für Straßenvesen (BASt) and Technical Univ. of Gdansk (TUG)*, Delft, Netherlands.

Roussillon, G. (1981). "Contribution to accurate measurement of aerodynamic drag on a moving vehicle from coast-down tests and determination of actual rolling resistance." *J. Wind Eng. Ind. Aerodyn.*, 9(1-2), 33–48.

Sandberg, T. (2001). "Heavy truck modeling for fuel consumption simulations and measurements." Ph.D. thesis, Linköping Univ., Linköping, Sweden.

Sandberg, U. (1990). "Road macro- and megatexture influence on fuel consumption." *Surface characteristics of roadways: International research and technologies STP 1031*, W. E. Meyer and J. Reichert, eds., ASTM, West Conshohocken, PA, 460–479.

Sandberg, U., et al. (2011a). "Road surface influence on tyre/road rolling resistance." Models for Rolling Resistance in Road Infrastructure Asset Management Systems (MIRIAM), ⟨http://miriam-co2.net/Publications/MIRIAM_SP1_Road-Surf-Infl_Report%20111231.pdf⟩.

Sandberg, U., et al. (2011b). "Rolling resistance—Basic information and state-of-the-art on measurement methods." Models for Rolling Resistance in Road Infrastructure Asset Management Systems (MIRIAM), ⟨http://miriam-co2.net/Publications/MIRIAM_SoA_Report_Final_110601.pdf⟩.

Sandberg, U., and Ejsmont, J. A. (2002). *Tyre/road noise reference book*, INFORMEX, Kisa, Sweden.

Sayers, M. (1989). "Two quarter-car models for defining road roughness: IRI and HRI." *Transportation Research Record 1215*, Transportation Research Board, Washington, DC, 165–172.

Sayers, M., Gillespie, T., and Patterson, W. (1986). "Guidelines for conducting and calibrating road roughness measurements." *World Bank Technical Paper Number 46*, International Bank for Reconstruction and Development, Washington DC.

Sayers, M. W., and Karamihas, S. M. (1996). *Interpretation of road roughness profile data*, U.S. Federal Highway Administration, Contract DTFH 61-92-C00143, Washington, DC.

Sayers, M. W., and Karamihas, S. M. (1998). *The little book of profiling*, Univ. of Michigan, Ann Arbor, MI.

Schmidt, B., and Dyre, J. (2012). "CO_2 emission reduction by exploitation of rolling resistance modelling of pavements." *Procedia Social Behav. Sci.*, 48, 311–320.

Schuring, D. (1994). "Effect of tire rolling loss on vehicle fuel consumption." *Tire Sci. Technol.*, 22(3), 148–161.

Shida, Z., Koishi, M., Kogure, T., and Kabe, K. (1999). "Rolling resistance simulation of tires using static finite element analysis." *Tire Sci. Technol.*, 27(2), 84–105.

Society of Automotive Engineers (SAE). (1999). "Stepwise coastdown methodology for measuring tire rolling resistance." *SAE J2452*, Warrendale, PA.

Society of Automotive Engineers (SAE). (2006). "Rolling resistance measurement procedure for passenger car, light truck, and highway truck and bus tires." *SAE J1269*, Warrendale, PA.

Swift, A. (1991). "Calculation of vehicle aerodynamic drag coefficients from velocity fitting of coastdown data." *J. Wind Eng. Ind. Aerodyn.*, 37(2), 167–185.

U.S. Dept. of Transportation. (2010). *Transportation's role in reducing U.S. greenhouse gas emissions—Volume 1: Synthesis report*, Washington, DC.

Vantsevich, V., and Stuart, C. (2008). "Probabilistic interactions of vehicles with surroundings: Modeling for dynamic control." *ASME Int. Mech. Eng. Congr. Exp. Proc.*, 9 PART C, 1649–1658.

Visser, A. (1982). "A correlation study of roughness measurements with an index obtained from a road profile measured with rod and level." *NITRR Technical Rep. RC/2/82*, Council for Scientific and Industrial Research (CSIR), Pretoria, South Africa.

Walston, W., Buckley, F., and Marks, C. (1976). "Test procedures for the evaluation of aerodynamic drag on full-scale vehicles in windy environments." *SAE Technical Paper, 760106*, SAE International, Warrendale, PA.

Warholic, T. (1983). "Rolling resistance performance of passenger car tires during warm-up (speed, load & inflation pressure effects)." *Rubber division symposia*, Vol. 1, American Chemical Society, Rubber Div., Akron, OH, 151–162.

White, R., and Korst, H. (1972). "The determination of vehicle drag contributions from coast-down tests." *SAE Technical Paper, 720099*, SAE International, Warrendale, PA.

Williams, F., and Dudek, T. (1983). "Load-deflection hysteresis and its relationship to tire rolling resistance." *Rubber division symposia*, Vol. 1, American Chemical Society, Rubber Div., Akron, OH, 105–139.

Wozniak, R., Taryma, S., and Ronowski, G. (2011a). "Modernization of the trailer for tyre/road rolling resistance measurements." *Key Eng. Mater.*, 490, 179–186.

Wozniak, R., Taryma, S., and Ronowski, G. (2011b). "Relieving the measuring system of the trailer for tyre/road rolling resistance measurements from the inertia force." *Key Eng. Mater.*, 490, 265–272.

Yeggoni, M., Button, J. W., and Zollinger, D. G. (1996). "Fractals of aggregates correlated with creep in asphalt concrete." *J. Transp. Eng.*, 10.1061/(ASCE)0733-947X(1996)122:1(22), 22–28.

Yong, R. N., Boonsinsuk, P., and Fattah, E. A. (1980). "Tyre load capacity and energy loss with respect to varying soil support stiffness." *J. Terramech.*, 17(3), 131–147.

No number

Introducing Functional Data Analysis to Coast down Modeling for Rolling Resistance Estimation

Lasse Grinderslev Andersen, Jesper Kampmann Larsen
Department of Sciences, Roskilde University, Postboks 260, DK-4000, Roskilde, Denmark

Abstract

Coast-down modeling has been widely used to assess vehicle aerodynamic drag and rolling resistance by fitting a vehicle resistance model to speed measurements and thereby get an estimate on model parameters. Here a coast-down model is used for assessing how road surface characteristics influence rolling resistance. Parameter estimation as well as an extensive perturbation analysis of the parameter fit with respect to data noise has been performed. Functional Data Analysis (FDA) is introduced and discussed. It is concluded that FDA is a powerful tool for 1) approximating derivatives, 2) assessing the degree of smoothing of the data 3) handling noise sources in the perturbation analysis and 4) enabled numerical solutions of the coast-down ODE model. Investigations showed that MPD was the most important parameter compared to IRI although MPD data required smoothing for optimal model fit. Furthermore, it is concluded that the model responds nicely to the statistical tests in the perturbation analysis. However, certain parameters associated with surface related rolling resistance were unstable in the sensitivity tests.

INTRODUCTION

Environmental concerns related to energy consumption has increased rapidly in the last decades. Since transportation by car accounts for about 20% of the worlds energy consumption [21], reducing energy consumption in this area is highly desirable. One way of lowering energy consumption in car transportation is to decrease rolling resistance, primarily by developing low rolling resistance tires and pavements. Thus a deeper understanding of the relationship between rolling resistance and the tire/pavement interaction is an important step in reducing energy consumption (as well as noise) and thereby reducing CO_2 emissions.

Four standard methods exist for measuring or estimating rolling resistance [19]: Drum (laboratory) measurements , measurements by trailer [4, 18, 23, 24], coast-down procedures [6, 11, 20, 2, 12, 7, 8, 9] and fuel consumption measurements [17, 1]. These methods can be ranked by how idealized the test setup is: The drum only measures the tire, the trailer method includes road properties and some transmission losses, coast-down includes even more features such as whole-car transmission losses, various road properties etc. Finally, the fuel consumption measurement procedure is the most natural setting compared to real-world car transportation. As the measuring methods come closer and closer to actual driving, the number of error sources increases as more and more factors influence the measurements and have to be taken into account. Thus, these four methods represents different trade-offs between disturbing factors and affinity with actual driving on real roads. Each of these methods have their advantages and shortcomings so they are suited for different purposes. In this paper the coast-down method is used since it includes transmission losses that can be considered as part of rolling resistance, and which is not included in trailer measurements. The downside of the coast-down is the many potential disturbing factors that can influence measurements such as, wind, traffic, and ir-

regularities in transmission losses etc.

Large data sets with a comprehensive amount of supplement data, obtained by the Swedish National Road and Transport Research Institute (VTI) [7], is analyzed. The widely used coast-down procedure can be performed to various degrees of detail both with respect to data and regression model. In this coast-down experiment different measurements accounting for road properties and meteorological conditions have been collected in connection with speed data. A suitable model that utilizes these data has been formulated.

The mathematical and statistical framework of 'Functional Data Analysis'(FDA) is proposed as a resourceful tool in handling these large data sets and the primary goal of this paper is to show that FDA is a useful choice in handling these amounts of high resolution data. In addition, Monte Carlo and bootstrapping methods are applied in a sensitivity analysis of the coast-down parameter estimation results.

COAST-DOWN DATA AND MODEL

The coast-down measurements used here have been performed by VTI and the procedure will be briefly described here. For a detailed account of the coast-down measurement procedure, see [7]. A suitable set of road strips were selected which was subject to certain requirements. Among these are

- The longitudinal gradient and road curvature must be low.
- The set of road strips must have high variation in Mean Profile Depth (MPD) and International Roughness Index (IRI) in order to get the optimal experimental setting.
- Different speed limits such that the coast-downs could be performed with varying initial velocities.

Furthermore, meteorological variations had been kept at a minimum, e.g., no rain, low wind and steady temperature. Fourteen different road strips have been selected and by including direction this yields 28 different road strips. The average length of the strips ranged between 400 and 1000 meters. Beginning and end of the coast-down sections were marked by reflective tape which could be detected by a photo sensor mounted on the rear bumper of the car. On each of the 28 strips various quantities were measured with a 1 meter resolution before the actual coast-down procedures were performed. The measured quantities of interest here are

- Roughness: IRI [#]
- Road texture: MPD [mm]
- Longitudinal gradient [%]
- Road crossfall [%]
- Road curvature radius [m]

Other measured quantities of interest are wind speed, air temperature and air pressure which are measured at the beginning of the coast-down. An overview of measured quantities and extreme values are shown in table 1. The test car used is a Volvo 940 that had been warmed up at least 30 minutes before every coast-down series to ensure equilibrium tire temperature and pressure. The speed measurements were obtained by a wheel pulse instrument that measured position and time at approximately every 77 cm. In order to have a data set of varying speed, coast-down measurements were carried out in sequences of varying speed. Depending on the speed limit for at a particular road strip, the measurements were carried out in sequences of 70-65-60-65-70 km/h or 90-80-70-80-90 km/h. The initial velocities are target values, since a specific initial speed is difficult to achieve. To avoid additional error sources, the driver was able to press an abort button to indicate that the measurements henceforth were invalid in subsequent analysis. E.g., if oncoming traffic occurred during a coast-down procedure, the abort button was activated and the measurements discarded. An average of 15 coast-downs were performed for each road strip and direction yielding approximately 420 coast-downs.

The measurements were used to estimate the coefficients of a coast down model [7], which can be written as a sum of forces acting on the vehicle during coast-down

$$F = F_{roll} + F_{air} + F_{side} + F_g. \tag{1}$$

where F is the total force acting on the vehicle, F_{roll} is the rolling resistance force, F_{air} is aerodynamic drag, F_{side} is the side force resistance and F_g is gravitational pull. It is assumed that the forces acting on the vehicle is additive. Note that F_{roll} used here is empirical and tentative. The former is given by [7, p. 24]

$$\begin{aligned} F_{roll} =& m(\eta_0 + \eta_1 T + \eta_2 \,\mathrm{IRI} + \eta_3 \,\mathrm{IRI}(v-20) \\ &+ \eta_4 \,\mathrm{MPD} + \eta_5 \,\mathrm{MPD}(v-20)) \end{aligned} \tag{2}$$

with v being speed, T temperature and the η_i's ($i = 1..5$) are rolling resistance regression coefficients to be estimated. F_{roll} is defined in a fairly general way such that η_0 also accounts for transmission losses from, e.g., the gearbox [7, p.15], in addition to surface independent tire losses. Since the latter is

known to be dependent on air temperature through the pressure-temperature relation of the tire at equilibrium, an additional surface independent and temperature dependent term $\eta_1 T$ is added. The surface texture and roughness dependent part of the rolling resistance are assumed to be linearly dependent on speed, as shown in the latter four terms. F_{air} is a simplified version of the drag equation

$$F_{air} = 0.5\rho(T,p)A_{yz}C_L[v - \cos(\alpha)w]^2 \quad (3)$$

were A_{yz} is projected frontal area of the vehicle, C_L the air dynamic drag coefficient, w wind speed, α is the wind angle, and $\rho(T,p)$ is the air density function given by

$$\rho(T,p) = K_\rho \frac{p}{T + T_0} \quad (4)$$

with p being atmospheric pressure, $K_\rho = 0.3847$ $^\circ K s^2/m^2$ and $T_0 = 273.2^\circ K$ are conversion constants. Since w is low, eq. 3 can be simplified by expanding the quadratic term and only retaining the linear term (assuming $w^2 \approx 0$) such that

$$\begin{aligned} F_{air} &= 0.5\rho(T,p)A_{yz}C_L[v - \cos(\alpha)w]^2 \\ &\approx \eta_6\rho(T,p)v^2 + \eta_7\rho(T,p)\cos(\alpha)wv \end{aligned} \quad (5)$$

where η_6 and η_7 are regression parameters. Simplifying the expression by substituting $0.5\rho(T,p)A_{yz}C_L$ with two regression coefficients η_i seems reasonable since C_L and w are not very precise (i.e. the latter is measured only in the beginning of the coast-down and the former is hard to determine experimentally) , thus viewing them as unknowns. The fact that eq. 5 is reduced by $w^2 = 0$ supports this decision as well. More elaborate expressions of F_{air} can be formulated [7, 9], but since the term is being calibrated by regression, it has been omitted here. By the same argument, tire stiffness C_A in

$$F_{side} = -\frac{F_y^2}{C_A} = \eta_8 F_y^2 \quad (6)$$

is replaced by a regression parameter η_8. F_y is given by

$$F_y = m[\cos(\gamma)v^2/R - g\sin(\gamma)cos(\beta)] \quad (7)$$

with γ being crossfall angle, m vehicle mass, g gravitational constant, β longitudinal gradient and R radius of road curvature. F_g is straightforwardly formulated as

$$F_g = -mg\sin(\beta). \quad (8)$$

Finally, the inertial force is

$$F = (m + m_{rot})\frac{dv}{dt} = (m + n_{wh}K_J J/r_{wh}^2)\frac{dv}{dt} \quad (9)$$

where m_{rot} is the inertial mass of a wheel plus additional rotating transmission parts, n_{wh} is the number of wheels, r_{wh} the radius of of the wheels, J the inertial moment per wheel and K_J a correction factor of J to include rotating transmission parts. See table 2 for an overview of the parameters presented here. Inserting eq. 2, 5, 6, 8 and 9 into eq. 1, and rearranging, yields

$$\begin{aligned} \frac{dv}{dt} &= \mu_0 + \mu_1 T + \mu_2\,\mathrm{IRI} + \mu_3\,\mathrm{IRI}(v-20) \\ &\quad + \mu_4\,\mathrm{MPD} + \mu_5\,\mathrm{MPD}(v-20)) + \mu_6\frac{\rho(T,p)v^2}{m+m_{rot}} \\ &\quad + \mu_7\frac{\rho(T,p)\cos(\alpha)wv}{m+m_{rot}} + \mu_8\frac{F_y^2}{m+m_{rot}} - \kappa g\sin(\beta) \end{aligned} \quad (10)$$

where $\kappa = m/(m+m_{rot})$ and $\mu_i = \kappa\eta_i$ for $i \in \{0,..,5\}$ and $\mu_i = \eta_i$ for $i \in \{6,7,8\}$. $\boldsymbol{\mu} = [\mu_0,...,\mu_8]'$ are the regression coefficients to be estimated from the coast-down data above. See table 2 for at complete list of parameters. Since the road data is measured per meter the final regression model must have distance as the independent variable. Therefore eq. 10 is converted to

$$\begin{aligned} \frac{dv}{ds} &= \frac{1}{v}[\mu_0 + \mu_1 T + \mu_2\,\mathrm{IRI} + \mu_3\,\mathrm{IRI}(v-20) \\ &\quad + \mu_4\,\mathrm{MPD} + \mu_5\,\mathrm{MPD}(v-20)) + \mu_6\frac{\rho(T,p)v^2}{m+m_{rot}} \\ &\quad + \mu_7\frac{\rho(T,p)\cos(\alpha)wv}{m+m_{rot}} + \mu_8\frac{F_y^2}{m+m_{rot}} - \kappa g\sin(\beta)] \end{aligned} \quad (11)$$

making an assessment of rolling resistance and its various components achievable. Normally the acceleration data have to be calculated by finite differencing of the speed measurements, which usually yields noisy fluctuating results. For this reason, speed measurements have been sought to be avoided entirely[12]. Below the derivative of the speed data is extracted from the speed data in functional form. Furthermore, the supplement data will be converted to functions as well, such that it is possible to study the model by solving eq. 11 numerically by, e.g., a Runge-Kutta algorithm.

FUNCTIONAL DATA ANALYSIS

This is a very brief introduction to functional data analysis tailored to the present needs. For a general and thorough exposition to the computational, mathematical and statistical aspects, see [15] and [16]. The basic idea in FDA is to convert discrete data into functions for further study, e.g., statistical investigations. Data in functional form can be treated by different methods that utilizes properties pertaining solely to functions, such as smoothness. Usually a functional data function is a linear combination of several basis functions. This can be a truncated Fourier series

expansion, sum of wavelets or a sum of B-spline polynomials, the latter being used here. We have

$$\tilde{y}(t) = \sum_{i=0}^{m} c_i \phi_i(t) = \boldsymbol{c}'\boldsymbol{\phi}.$$

where $\boldsymbol{\phi} = [\phi_1(t), ..., \phi_m(t)]'$ is the vector of B-spline basis polynomials and $\boldsymbol{c} = [c_1, ..., c_m]'$ is the vector of coefficients ($'$ denotes the transpose operation). Since B-splines are closed with respect to linear combinations $\tilde{y}(t)$ is a B-spline as well. The degree of smoothness of $\tilde{y}(t)$ depends on the degree of the $\phi_i(t)$'s such that N degree polynomials $\phi_i(t)$ yields a $\mathcal{C}^{N-1}$ function $\tilde{y}(t)$. For a detailed account of B-splines, see [3]. Normally $N = 3$ which is also the case here, so the functional data used below have continuous second order derivatives.

Fitting the B-spline basis system is done by an extension of the ordinary least squares (OLS) algorithm that includes a *smoothness penalty*. Assuming a set of data points $\boldsymbol{y} = [y_1, .., y_n]$ measured at times $\boldsymbol{t} = [t_1, ..., t_n]'$ we have

$$\begin{aligned} L(\mathbf{c}) &= \sum_{i=1}^{n} [\tilde{y}(t_i) - y_i]^2 + \lambda \int [D^2\tilde{y}(t)]^2 dt \\ &= (\mathbf{y} - \mathbf{\Phi c})'(\mathbf{y} - \mathbf{\Phi c}) + \lambda \mathbf{c}'\mathbf{R}\mathbf{c} \end{aligned} \tag{12}$$

where the first term is classical OLS and the second term is the aforementioned smoothness penalty. $\boldsymbol{\Phi}$ is the $n \times m$ matrix of basis function evaluated at times $\boldsymbol{t}$ and $\boldsymbol{R}$ is the $m \times m$ matrix of inner products where the (i, j) entry is given by $\int D^2\phi_i(s) D^2\phi_j(s) ds$. The specific choice of differential operator $D^2 f(t) = \frac{d^2 f}{dt^2}$ is based on the assumption that a smooth curve means a curve with low curvature [16, p.84]. Since the integral equals zero if $\tilde{y}(t) = at + b$ the fit based on eq. 12 will converge to a straight line as $\lambda \to \infty$. Thus, the smoothness parameter λ represents a balance between fitting the data and obtaining a smooth curve with zero curvature. Estimating λ for some of the data is one of the objectives here. For fixed λ a unique $\hat{\boldsymbol{c}}$ exists which minimizes eq. 12. Since no numerical optimization is involved, finding $\hat{\boldsymbol{c}}$ is quick and computationally simple.

When the speed and additional data have been brought in a functional form it is straightforward to estimate the regression parameters $\boldsymbol{\mu}$ by minimizing

$$L(\boldsymbol{\mu}) = \int \{\frac{d\tilde{v}(s)}{ds} - F[\tilde{v}(s), \tilde{R}(s), \tilde{\beta}(s), \tilde{\gamma}(s), \tilde{\mathrm{MPD}}(s), \tilde{\mathrm{IRI}}(s)]\}^2 ds \tag{13}$$

where F is the right hand side of eq. 11 and $\tilde{v}(s)$, $\tilde{R}(s)$, $\tilde{\beta}(s)$, $\tilde{\gamma}(s)$, $\tilde{\mathrm{MPD}}(s)$, $\tilde{\mathrm{IRI}}(s)$ are the additional data in functional form. In the optimization process the integral must be approximated by a quadrature rule which is Simpsons in this case. Using a quadrature rule reduces the optimization problem to a squared residual one, for which several specific algorithms exist, e.g., the Gauss-Newton optimization routine. More advanced FDA-based parameter estimation techniques exist, taking e.g. $\boldsymbol{c}$ into the optimization process [14, 22]. However, this case is linear in the parameters so a simple method have been used.

Several advantages exist in the simple methodology sketched above. Firstly all the functional approach assumes, is that the measurements represent samples from a continuous process which is certainly true here. Secondly estimating $\boldsymbol{\mu}$ requires the derivative of the speed which is easily obtained by analytically calculating the first derivative which is smooth and without fluctuations caused by numerical methods such as finite differencing. Thirdly, having the data set in functional form makes it possible to numerically solve the non-autonomous differential equation model given by eq. 11 by, e.g., a Runge-Kutta scheme. Last but not least, the adjustment of λ makes it possible to adjust the smoothness of the functional data according to an expected noise intensity. The high frequency fluctuations in the speed measurements are clearly noise, but measurements of MPD and IRI also show high fluctuations (see fig.1) and estimating λ in these two cases points to how much the fluctuations can be attributed to noise and what is actual variations in the measured phenomenon.

The fluctuations in the MPD and IRI measurements have been tested up against the model in the following way: A 19×19 grid of points is made, where each point in the grid represents λ-values $(\lambda_{\mathrm{IRI}}, \lambda_{\mathrm{MPD}})$ used in functional fit of IRI and MPD. The λ value in each component have been chosen as a set of logarithmically equidistant points in a interval where the end points represents the lower and upper bound on the degree of smoothing. Lower and upper values are 10^{-2} and 500 for both IRI and MPD. The maximum and minimum values have been chosen by visual inspection of the functional data plots. See Fig. 2 for an illustration of the relationship between λ and functional data smoothness. Each point $(\lambda_{\mathrm{IRI}}, \lambda_{\mathrm{MPD}})$ has been used in converting the IRI and MPD data into functional form. An estimation of the regression parameters $\boldsymbol{\mu}$ have subsequently been performed according to the method presented above. A numerical solution $v(t)$ to eq. 11 based on the regression parameter estimate $\tilde{\boldsymbol{\mu}}$ (and the functional data giving rise to $\tilde{\boldsymbol{\mu}}$) was compared to the speed data by calculating the sum of least squares between them. In short: Estimate $\boldsymbol{\mu}$ for different values of λ_{IRI} and λ_{MPD} and calculate the fit

to the functional data in the OLS sense. The results can be visualized with a 3d-plot where the xy-plane is spanned by $\log(\lambda_{\mathrm{MPD}})$ and $\log(\lambda_{\mathrm{IRI}})$, and the z-axis represents the summed OLS values.

The results have been plotted in figure 3 and shows generally that a small value of λ_{IRI} and large a value of λ_{MPD} yield the best OLS fit with λ_{IRI} being the most sensitive parameter. The overall minimum is, as the 3d-plot suggests, when $(\lambda_{\mathrm{IRI}}, \lambda_{\mathrm{MPD}}) = (0.0182, 4.0789)$ which is used in the following stability analysis.

STABILITY ANALYSIS

In [7] and [9] an extensive selection of factors that could potentially affect estimation results were investigated. Two interesting results have formed the basis for further investigation: Errors in the longitudinal gradient data and reduced data set size seem to have a substantial impact on the estimation results. It is of course of vital importance to asses the magnitude of these error sources and to this end we devise some techniques based on Monte Carlo and bootstrapping methodologies [5, chap. 14].

The effect of the gradient have been tested by introducing error sources into the data, which can be sampled many times yielding a large amount of pseudo-data. Each of these sets of pseudo data can be used in the parameter estimation procedure introduced above and statistical information can be extracted from the results. Two kinds of error sources have been used: 1) Assume that the measurement error is systematic, i.e. the deviation from the true profile accumulates linearly as the test section is being measured. 2) Assuming random error perturbations while measuring the gradient. In the systematic case the amount of deviation per meter of the data set is given by a normally distributed variable and in the random case the specific data points is perturbed by a normally distributed error. Since normal stochastic variables are preserved under linear transformations, the variance σ^2 of the perturbed data points can be transformed into variances of perturbed coefficients of the basis function expansion instead. Given that the knots are properly spaced, this preserves the qualitative behavior of the gradient data instead of fluctuating the data in a unrealistic way, see fig. 4 for an illustration of this.

To asses the variance on model estimation results, a classical bootstrapping technique have been deployed. More specifically, by using uniform sampling with replacement of our original data set, a bootstrapped data set is obtained having an equal number of measurements as the original. In order to keep the road strip diversity of the original data, the bootstrap sampling is partitioned, corresponding to each road and direction giving a total of 28 partitions. Bootstrap samples is then performed separately on each partition and the union of these sub-samples constitutes the bootstrapped data set which is used to estimate model parameters. Iterating the this procedure a large number of times will give a general picture of the stability of the estimation results, i.e., if the number of measurement runs on each road strip is sufficient for stable parameter estimates. The classical bootstrap technique is used as base case to be used when comparing the results of the other techniques used here as it represents a sensitivity measure of the entire system, i.e., both data and model.

Given the large amount of measurement runs for each road section, it is also of interest to investigate how much a *reduced* data set will affect the estimation results. To this end the classical bootstrap technique described above will be slightly modified. The partitioning scheme is used again, however, uniform sampling *without* replacement is used to randomly pick a subset of each partition that will be *omitted* in the parameter estimation. Once again, this procedure is repeated a large number of times and statistical information extracted. Three different scenarios where 3, 5, and 7 measurement runs are removed from each of the 28 partitions, have been investigated here. Note that these two methods are not directly comparable except that the classical bootstrap is standard and thus can be seen as a reference study.

RESULTS

Since all road data is on a functional form, they serve as input functions to the ODE model in eq. 11. Numerical solutions have been made and all 421 coast-downs were compared to the speed data by visual inspection. The model fits data very well in many cases as shown in Fig. 5. The quality of the fit is specific to a specific road, i.e., if one model fit is good/bad in one coast-down on a specific road, it will be good/bad for all other coast-downs made on that road. Also, for some roads, the numerical solution deviates from the measurements, see Fig. 5.

When the data have been put on a functional form it is also possible to get an overview of how the different terms in eq. 11 affect vehicle resistance. A plot of the different components during a two coast-downs is shown in Fig. 6. It is confirmed from Fig. 6 that the gradient plays a substantial role in vehicle resistance, as well as air resistance for high velocities. Furthermore, MPD has a significant effect as opposed to IRI

that shows almost the same effect as side force resistance. While low side force resistance was expected, the IRI effect is surprisingly low even though it is a widely used parameter in road surface characterization and considered an important parameter in the relationship between surface and rolling resistance[18] as well as skid resistance.

In table 3, 4 and 5 the results of the bootstrap/Monte Carlo stability analysis are shown. The first two columns indicates parameter estimates obtained from the original data and the remaining columns shows of the stability methods in the form of *normalized* confidence intervals containing 90% of the parameter estimates. To ease readability the intervals have been normalized as follows: The absolute value of the endpoints have been used since all parameter and confidence limits are negative. The result have been divided with the absolute value of the parameter estimate from the first column and the result is shown in the tables. Thus, the actual confidence interval is obtained by multiplying the normalized values with the estimate value from the first column (and reversing the interval since the sign have been changed). The normalized numbers can also be interpreted as a percentage reduction/increase, e.g., $[0.96, 1.04]$ indicates a confidence interval where the lower limit is a 4% reduction of the estimated value and the upper limit is a 4% increase. The number of samples indicate how many pseudo-data sets and subsequent parameter estimates have been used for the 90% intervals and it should be chosen high enough for the results to converge and stabilize.

A general trend that holds for all results is that confidence intervals of μ_1, μ_3, and μ_5 are much larger than the rest. E.g. for the classical bootstrap method in table 3 they have confidence intervals of 40% to 50% decrease/increase of their parameter estimates indicating high fluctuations in their estimates. This is quite unsettling, however, a possible explanation might be that their contribution is small compared to the total driving resistance. Therefore these parameters will be highly sensitive to disturbances while having minimal influence on the overall fit to measurements. Moreover, all three parameters, representing temperature and velocity dependent surface contributions, are part of the empirical rolling resistance F_{roll} term of the model and thus is rather tentative. This is also substantiated by the observation that while μ_7 and μ_8 also have a minimal influence on overall model fit, their confidence intervals are more akin to the remaining parameters. For the rest of this section μ_1, μ_3, and μ_5 will be considered as outliers and omitted from the statistical considerations below.

Table 3 shows results for the bootstrapping method described above. By considering the classical bootstrap results it can be seen that the average confidence limits for the stable parameters is a 7.8% decrease and a 8.8% increase, respectively. Given the comprehensive measurement campaign with many disturbing factors as well as the difficulty in modeling surface rolling resistance this seems rather robust. The rest of the columns shows results of the bootstrap reduction where n in $n \times 28$ denotes the amount of randomly chosen road segments per road strip that have been removed prior to parameter estimation. The results show that reducing the amount of coastdowns per road strip by $3 - 5$ does not significantly affect overall estimation results compared to classical bootstrap. When $n = 7$, average spread in parameter estimates starts to resemble classical bootstrapping with average confidence limits given by a 8.2% decrease/increase in estimated parameter. This is a very interesting result, but it should be noted that the classical bootstrap is not directly comparable with the reduction bootstrap method as no duplicates are present in reduction bootstrapped samples.

The systematic perturbation of the road elevation is shown in table 4. $\sigma^2 = n$ denotes the size of the variance used in the normal distribution from which the amount of deviation have been sampled. Since the road elevations have been measured in both directions for each road section, a value sampled for one direction will have same value but with opposite sign in the other direction. The spread in estimation results increases rapidly, which is not too surprising since the systematic deviation will attain rather high values in the end of the road section. E.g. a deviation of 1 mm/m from the true profile yields almost one meter in the end of the longest road segments! Since the gradient contributes substantially to overall driving resistance it is not that surprising that even for error source with $\sigma^2 = 1$ [mm/m] gives rise to higher fluctuations in parameter estimates compared to the classical bootstrap technique. The average confidence interval for the stable parameters is 11.5 smaller and 12% larger for $\sigma^2 = 1$ and 22.4% smaller and 38.4% larger for $\sigma^2 = 2$.

The random perturbation results in table 5 has the same meaning for σ^2 as above except the unit is now cm instead of mm/m. The spread in the estimates is quite low for $\sigma^2 = 1$ and 2 while resembling that of classical bootstrap for $\sigma^2 = 5$ and 10 cm. For $\sigma^2 = 2$ the confidence interval is 3.4% smaller and 4.2% larger while it is 7.7% smaller and 9% larger for $\sigma^2 = 5$ and 14.2% smaller and 17.7% larger for $\sigma^2 = 10$. Note that the noise intensity used in the systematic and random perturbation are high compared to measurement accuracy of modern road profiling equipment. Thus, the estimation results seem

quite stable with respect to measurement noise in the road elevation data, even though the road gradient is a major component in vehicle resistance. However, as mentioned above, some of the parameters behaved rather unstable.

CONCLUSION

Regarding FDA, both implementation and subsequent analysis of the data and model relied heavily on the apparatus of FDA:

1. Derivative estimation of velocity measurements to obtain acceleration.
2. Data-smoothing was used for the measured quantities such as velocity, IRI, and MPD.
3. Numerical solution of the cost-down model using a Runge-Kutta scheme was also possible since the data was put on a functional form and thus could be viewed as smooth input functions to the ODE model. Solving the system numerically enabled a direct comparison of model simulation and actual data, as shown in Fig. 5. In addition, these simulations were used to make component plots showing the evolution of the different components during entire measurement runs, as shown in Fig. 6.
4. Data on a functional form enabled implementation of noise sources that were in accordance with the qualitative behavior of the data.
5. Parameter estimation of differential equations is straightforward in FDA as the optimization process does not require repeated numerical simulations.

This shows that the FDA methodology is fruitful in this area of research, as well as other areas with detailed data sets available. In particular, several insights and results about coast-down modeling were obtained:

1. IRI only gave a small contribution to the overall driving resistance.
2. MPD on the other hand gave a substantial contribution and it was shown that a high degree of smoothing gave the best model fit.
3. Numerical simulations showed that generally the coast-down model was able to reproduce the data. However, for a few selected road strips, model simulations diverged greatly from measurements which prompts for further model developments.
4. The perturbation analysis showed that the model responded nicely to the sensitivity tests and slight reduction in the number of measurement runs for each road strip does not significantly increases estimate uncertainties. However, three parameters of the rolling resistance term in the model showed very high fluctuations which require further investigations.

A general conclusion to be drawn for this, is that the model does have some shortcomings and the results points to the empirical F_{roll} term, and the road measures it is based on, as possible cause. It is questionable whether the fluctuations in both IRI and MPD values reflects a change in the surface contribution to rolling resistance, or if the MPD/IRI measures also captures features that play a minor role in vehicle rolling resistance. It could be accommodated by averaging (although the MPD measure is already constructed by averaging) or by considering new road measures as alternatives to MPD and IRI [10, 13]. More generally, modifying the expression of F_{roll} might improve model fit. These questions require further study. In addition, the relationship between road surface texture contribution to RR and vehicle speed need a more careful investigation as the literature on the subject is ambiguous.

ACKNOWLEDGEMENT

The provision by Rune Karlsson and Ulf Hammarström - Swedish National Road and Transport Research Institute - of the coast down data used in this paper is gratefully acknowledged.

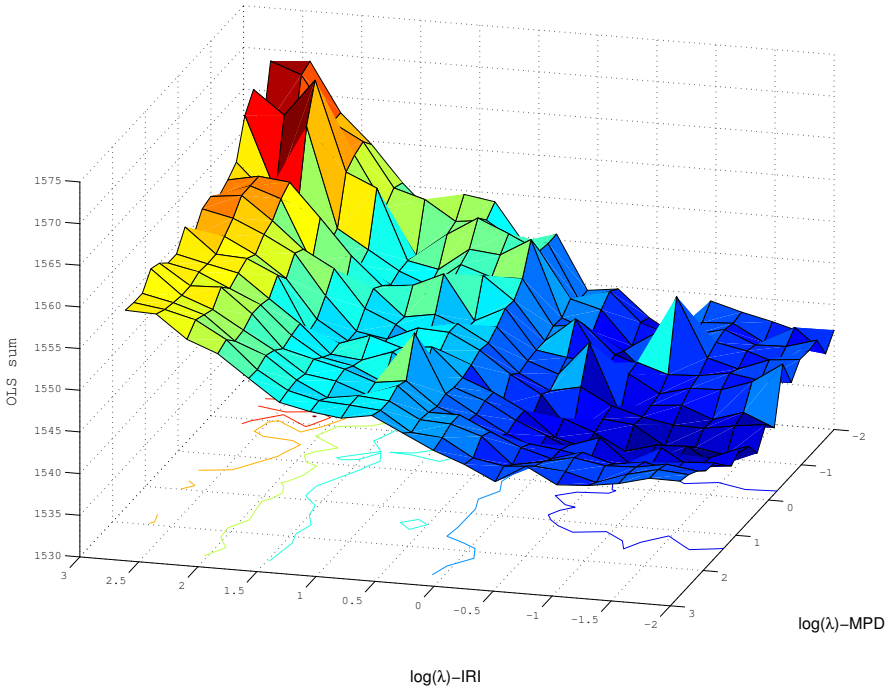

Figure 3: Plot of the sum of ordinary least squares for different λ-values used in functional data conversion.

Table 1: Overview of road sections

Road ID	Length [m]	Speed Limit [km/h]	# of runs	Avg. IRI [mm/m]	Avg. MPD [mm]
1	1000	90	19	0.83	1.10
2	1000	90	19	1.05	1.12
3	300	70	21	2.04	2.54
4	300	70	19	1.79	2.49
5	600	70	13	1.18	1.19
6	600	70	15	1.68	1.21
7	1000	90	14	1.40	0.82
8	1000	90	14	1.08	0.76
9	500	70	15	2.64	2.42
10	500	70	14	3.23	2.40
11	900	90	15	3.30	1.00
12	900	90	14	3.55	0.93
13	500	70	14	2.18	1.07
14	500	70	14	2.15	0.90
15	400	70	14	2.57	0.74
16	400	70	14	2.84	0.59
17	580	70	14	2.82	0.86
18	580	70	14	2.48	0.86
19	550	90	15	1.11	0.39
20	550	90	14	1.02	0.44
21	570	70	14	2.23	1.76
22	570	70	15	2.40	1.72
23	560	90	15	3.66	0.64
24	560	90	14	3.05	0.75
25	620	70	14	1.77	0.59
26	620	70	14	1.50	0.58
27	630	90	16	0.79	0.66
28	630	90	14	0.83	0.58

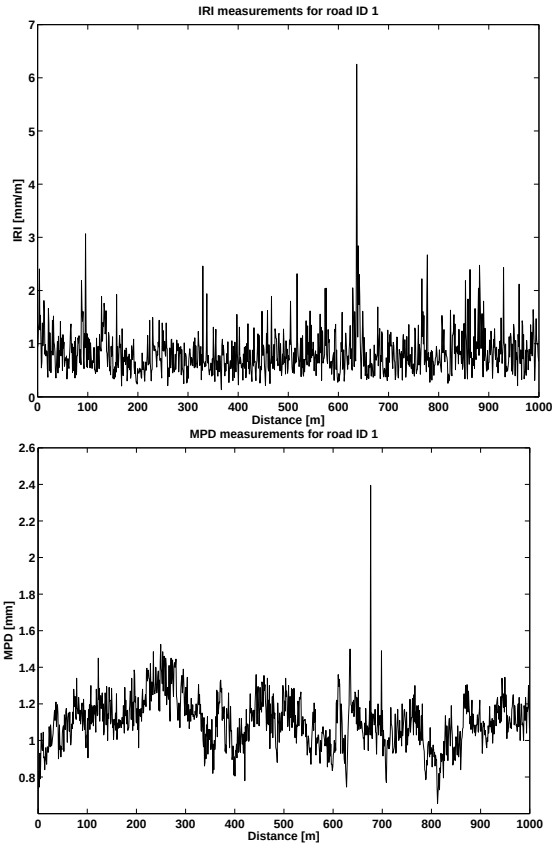

Figure 1: Example of MPD and IRI measurements.

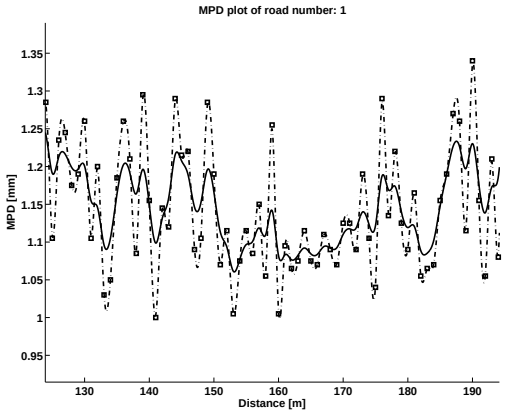

Figure 2: Data (squares) with two functional data fits (solid and dash-dotted lines) of MPD with different values of λ: Solid line $\lambda = 1$ and dash-dotted line $\lambda = 0.1$. As λ increases the fitted curve gets smoother.

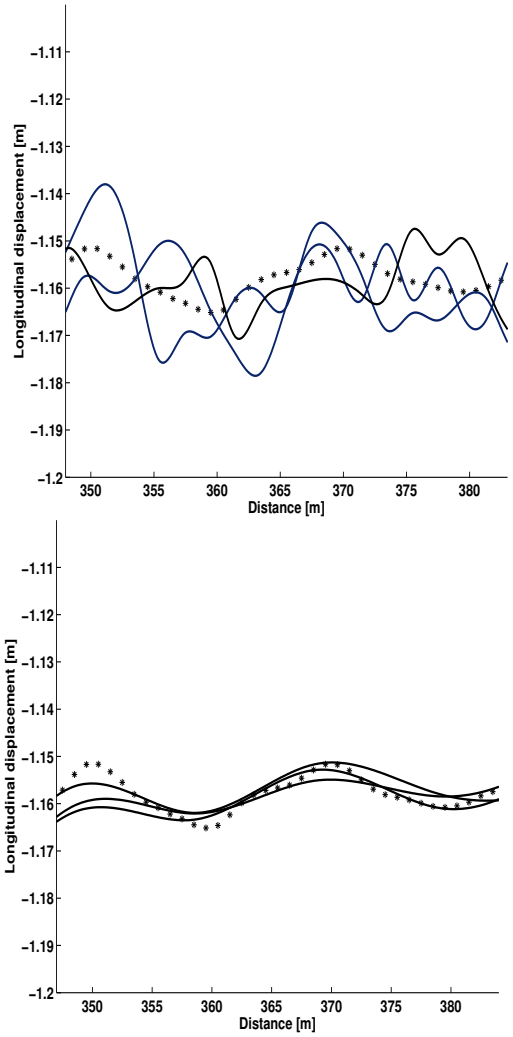

Figure 4: Different ways of incorporating random noise into the road elevation data. Solid lines are perturbed functional data and stars are measurements. Too many knots (left) will cause fluctuations in the functional data curve which does not reflect the behavior of the underlying measurements. By using fewer knots (right) the noise introduced to the data causes fluctuations that reflects the qualitative behavior of data.

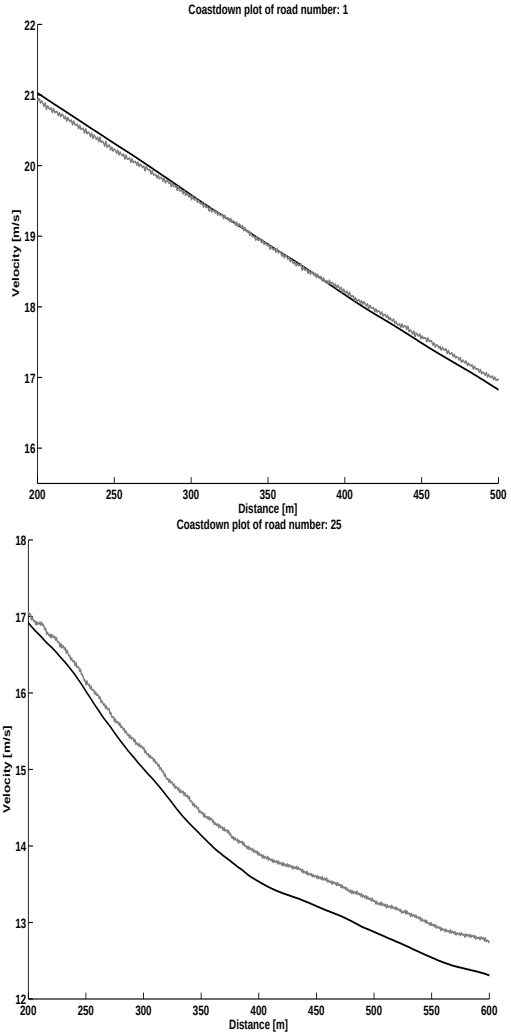

Figure 5: Two different simulation results to exemplify difference in estimation fit. The black lines are simulations based on eq. 11 with input data in functional form. The grey lines are measurements.

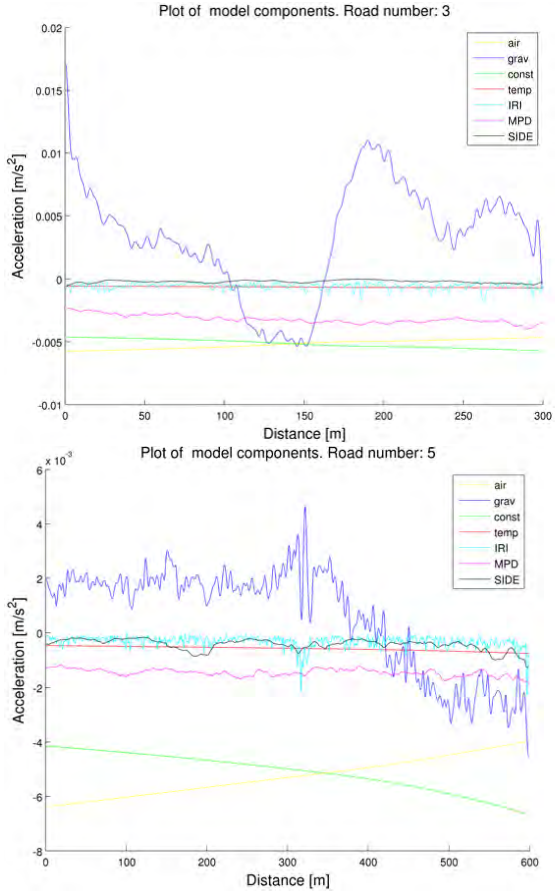

Figure 6: Plot of the different terms from eq. 11 for two different cost-downs.

Table 2: List of parameters in coast-down model

Parameter	unit	description
v	$[m/s]$	Velocity of vehicle
IRI	$[mm/m]$	Roughness measure
MPD	$[mm]$	Macrotexture measure
$\rho(T,p)$	$[kg/m^3]$	Air density
p	$mbar$	Pressure
A_{yz}	$[m^2]$	Projected frontal area of the vehicle
C_L	[#]	Air dynamic coefficient
α	$[rad]$	Angle between wind and driving direction
w	$[m/s]$	Wind speed
T	$[^\circ C]$	Temperature
T_0	$[^\circ C]$	Temperature
C_A	$[N/radians]$	Tire stiffness
m	$[kg]$	Vehicle mass
g	$[m/s^2]$	Earths gravitational acceleration
β	$[radians]$	Longitudinal slope
γ	$[radians]$	Road crossfall
K_J	[#]	Correction factor
K_ρ	$[kg^\circ Km^{-3}mbar^{-1}]$	Conversion constant
n_{wh}	[#]	Number of wheels
J	$[kgm^2]$	Inertial moment per wheel
r_{wh}	$[m]$	Wheel radius
m_{rot}	$[kg]$	Inertial mass of rotating parts

Table 3: Overview of bootstrap results. Number of samples: 2000

μ_n	Estimate value	Reduction Bootstrap 3×28	Reduction Bootstrap 5×28	Reduction Bootstrap 7×28	Classical Bootstrap
0 Const.	-0.0807	[0.96 , 1.04]	[0.94 , 1.06]	[0.92 , 1.07]	[0.93 , 1.08]
1 T	-5.5383e-04	[0.69 , 1.32]	[0.58 , 1.47]	[0.44 , 1.66]	[0.41 , 1.63]
2 IRI	-0.0043	[0.95 , 1.07]	[0.93 , 1.09]	[0.91 , 1.12]	[0.91 , 1.12]
3 IRI$(v-20)$	-1.7600e-04	[0.78 , 1.29]	[0.67 , 1.37]	[0.56 , 1.52]	[0.53 , 1.48]
4 MPD	-0.0197	[0.97 , 1.04]	[0.96 , 1.06]	[0.95 , 1.08]	[0.94 , 1.08]
5 MPD$(v-20)$	-6.9376e-04	[0.85 , 1.23]	[0.79 , 1.31]	[0.72 , 1.37]	[0.72 , 1.41]
6 F_{Air1}	-3.2016e-04	[0.94 , 1.06]	[0.91 , 1.09]	[0.88 , 1.12]	[0.88 , 1.12]
7 F_{Air2}	-4.4371e-05	[0.95 , 1.04]	[0.92 , 1.06]	[0.89 , 1.07]	[0.91 , 1.10]
8 F_{Side}	-2.6755e-04	[0.98 , 1.02]	[0.97 , 1.02]	[0.96 , 1.03]	[0.96 , 1.03]

Table 4: Systematic gradient stability test $[\sigma^2] = mm/m$. Number of samples: 2000

μ_n	Estimate value	Systematic Noise Intensity: $\sigma^2 = 1$	Systematic Noise Intensity: $\sigma^2 = 2$
0 Const.	-0.0807	[0.92 , 1.08]	[0.83 , 1.17]
1 T	-5.5383e-04	[0.20 , 1.81]	[0.60 , 2.71]
2 IRI	-0.0043	[0.86 , 1.16]	[0.70 , 1.30]
3 IRI$(v-20)$	-1.7600e-04	[0.38 , 1.62]	[0.24 , 2.24]
4 MPD	-0.0197	[0.98 , 1.02]	[0.96 , 1.04]
5 MPD$(v-20)$	-6.9376e-04	[0.55 , 1.44]	[0.11 , 1.87]
6 F_{Air1}	-3.2016e-04	[0.29 , 1.70]	[0.42 , 2.41]
7 F_{Air2}	-4.4371e-05	[0.85 , 1.15]	[0.70 , 1.31]
8 F_{Side}	-2.6755e-04	[0.99 , 1.01]	[0.99 , 1.01]

Table 5: Random gradient stability test $[\sigma^2] = cm$. Number of samples: 1500

Parameter μ_n	Estimate value	Random Noise Intensity: $\sigma^2 = 1$	Random Noise Intensity: $\sigma^2 = 2$	Random Noise Intensity: $\sigma^2 = 5$	Random Noise Intensity: $\sigma^2 = 10$
0 Const.	-0.0807	[1.00 , 1.01]	[0.99 , 1.02]	[0.96 , 1.04]	[0.92 , 1.08]
1 T	-5.5383e-04	[0.99 , 1.06]	[0.95 , 1.10]	[0.83 , 1.21]	[0.64 , 1.40]
2 IRI	-0.0043	[1.02 , 1.07]	[1.02 , 1.09]	[0.95 , 1.16]	[0.84 , 1.28]
3 $\mathrm{IRI}(v-20)$	-1.7600e-04	[1.11 , 1.36]	[0.98 , 1.49]	[0.60 , 1.86]	[0.03 , 2.49]
4 MPD	-0.0197	[0.97 , 1.01]	[0.95 , 1.02]	[0.90 , 1.07]	[0.82 , 1.16]
5 $\mathrm{MPD}(v-20)$	-6.9376e-04	[0.86 , 1.07]	[0.75 , 1.17]	[0.44 , 1.44]	[0.07 , 2.02]
6 F_{Air1}	-3.2016e-04	[0.99 , 1.01]	[0.99 , 1.02]	[0.96 , 1.04]	[0.93 , 1.08]
7 F_{Air2}	-4.4371e-05	[0.97 , 1.05]	[0.93 , 1.09]	[0.81 , 1.20]	[0.61 , 1.39]
8 F_{Side}	-2.6755e-04	[0.99 , 1.00]	[0.98 , 1.01]	[0.96 , 1.03]	[0.92 , 1.07]

REFERENCES

[1] J. Barrand and J. Bokar. Reducing tire rolling resistance to save fuel and lower emissions. *SAE International Journal of Passenger Cars - Mechanical Systems*, 1(1):9–17, 2009.

[2] Frank T. Buckley. Abcd - an improved coast down test and analysis method. *SAE Technical Paper*, 950626, 1995.

[3] Carl de Boor. *A Practical Guide to Splines*. New York: Springer, 2001.

[4] Guy Descornet. Road-surface influence on tire rolling resistance. In *Surface Characteristics of Roadways: International Research and Technologies STP 1031*. American Society for Testing and Materials, 1990.

[5] Bradly Efron and Robert J. Tibshirani. *An Introduction to the Bootstrap*. Chapman & Hall, 1993.

[6] K. Hamabe, K. Kitoh, H. Ogata, and T. Kobayashi. An estimation of aerodynamic drag coefficient of a passenger car by coastdown tests in windy environments. *JSAE REV.*, (16 , Apr. 1985):114–120, 1985.

[7] Ulf Hammarström, Rune Karlsson, and Harry Sörensen. *Road surface effects on rolling resistance coastdown measurements with uncertainty analysis in focus.* Energy Conservation in Road Pavement Design, Maintenance and Utilisation (ECRPD), 2009.

[8] S.W. Hunt, A.M.C. Odhams, R.L. Roebuck, and D. Cebon. Parameter measurement for heavy-vehicle fuel consumption modelling. *Proceedings of the Institution of Mechanical Engineers, Part D: Journal of Automobile Engineering*, 225(5):567–589, 2011.

[9] Rune Karlsson, Ulf Hammarström, Harry Sörensen, and Olle Eriksson. *Road surface influence on rolling resistance - Coastdown measurements for a car and HGV - VTI notat 24A*. Swedish Road Administration (VTI), 2011.

[10] A. G. Kokkalis, G. H. Tsohos, and O. K. Panagouli. Consideration of fractals potential in pavement skid resistance evaluation. *Journal of Transportation Engineering*, 128:591–595, 2002.

[11] H. Korst and R. White. Coastdown tests: Determining road loads versus drag component evaluation. *SAE Technical Paper*, 901767, 1990.

[12] V. Petrushov. Coast down method in time-distance variables. *SAE Technical Paper*, 970408, 1997.

[13] Roger J. Pinnington. A particle-envelope surface model for road-tyre interaction. *International Journal of Solids and Structure*, 49:546–555, 2012.

[14] J. O. Ramsay, G. Hooker, D. Campbell, and J. Cao. Parameter estimation for differential equations: A generalized smoothing approach. *Journal of the Royal Statistical Society*, 69:741 – 796, 2007.

[15] J.O. Ramsay and B. W. Silverman. *Applied Functional Data Analysis*. Springer, 2002.

[16] J.O. Ramsay and B.W. Silverman. *Functional Data Analysis*. Springer Series in Statistics, 2005.

[17] Ulf Sandberg. Road macro- and megatexture influence on fuel consumption. In *Surface Characteristics of Roadways: International Research and Technologies STP 1031*. American Society for Testing and Materials, 1990.

[18] Ulf Sandberg, Manfred Haider, , Luc Goubert, Anneleen Bergiers, Marek Zöller, Rune Karlsson, and Jerzy A. Ejsmont. *Road surface influence on tyre/road rolling resistance*. Models for rolling resistance In Road Infrastructure Asset Management systems (MIRIAM), 2011.

[19] Ulf Sandberg, Manfred Haider, Marco Conter, Luc Goubert, Anneleen Bergiers, Gernot Schwalbe Klaus-Peter Glaeser, Marek Zöller, Olivier Boujard, Ulf Hammarström, Rune Karlsson, Jerzy A. Ejsmont, T. Wang, and J.T. Harvey. *Rolling Resistance Basic Information and State-of-the-Art on Measurement methods*. Models for rolling resistance In Road Infrastructure Asset Management systems (MIRIAM), 2011.

[20] A. Swift. Calculation of vehicle aerodynamic drag coefficients from velocity fitting of coast-down data. *Journal of Wind Engineering and Industrial Aerodynamics*, 37(2):167–185, 1991.

[21] Peter Taylor, Michel Francoeur, Olivier Lavagne dOrtigue, Cecilia Tam, and Nathalie Trudeau. *Worldwide Trends in Energy Use and Efficiency - Key Insights from IEA Indicator Analysis*. International Energy Agency, 2008.

[22] M. Saeed Varziri, Kim B. McAuley, and P. James McLellan. Parameter estimation in continuous-time dynamic models in the pressence of unmeasured states and nonstationary disturbances. *Ind. Eng. Chem. Res.*, 47:380–393, 2008.

[23] R. Wozniak, S. Taryma, and G. Ronowski. Modernization of the trailer for tyre/road rolling resistance measurements. *Key Engineering Materials*, 490:179–186, 2011.

[24] R. Wozniak, S. Taryma, and G. Ronowski. Relieving the measuring system of the trailer for tyre/road rolling resistance measurements from the inertia force. *Key Engineering Materials*, 490:265–272, 2011.